Experimental and Finite Element Modelling of Ultrasonic Cutting of Food

By

Euan McCulloch BEng AMIMechE

Department of Mechanical Engineering
University of Glasgow

A doctoral thesis submitted in fulfilment of the requirements for the award of Doctor of Philosophy (PhD) of the University of Glasgow

I. Abstract

In recent years ultrasonic cutting has become an established technology in a variety of industries including the food processing industry to cut a variety of materials. An ultrasonic cutting system consists of a generator, transducer and either a single or multiple blade cutting devices tuned to a specific mode of vibration, commonly the longitudinal mode, between 20 and 100 kHz. High power ultrasonic cutting device design has traditionally relied on the cut requirements of the product, the use of empirical approaches where ultrasonic cutting system parameters such as cutting speed, frequency of vibration, mode of vibration, blade tip amplitude, gain and cutting orientation are determined from experimental and experience of the tool designers. Finite element (FE) models have also been used to predict the vibrational behaviour of the cutting tool. However, the performance of an ultrasonic device critically relies on the interaction of the cutting tool and material to be cut. Currently the interaction between the resonant blade and the material to be cut is neglected but the cutting mechanism at the interface is of significant importance and knowledge of this mechanism would be of considerable benefit to designers when developing ultrasonic cutting blade concepts and processing requirements. Simulations of the cutting process would also enable designers to conduct parametric studies quickly using computational methods instead of conducting lengthy, laborious experimental tests.

The research reported in this thesis provides an insight into the requirements of the tool-material interaction to allow optimal cutting parameters to be estimated as an integral part of designing cutting blades for use in the food industry. A methodology is proposed for modelling the interaction between the resonant blade and the material to be cut using the finite element method, to gain an understanding of the cutting mechanism. The effect of ultrasonic cutting parameters, such as resonant frequency, mode of vibration, blade tip sharpness, cutting force, cutting speed, blade tip amplitude and are also investigated. Knowledge of the temperature distribution at the interface between the resonant blade and the substrate material would also be of benefit as currently experimental determination of the temperature at the interface is impractical using current measuring systems. Two thermo-mechanical FE models of ultrasonic cutting are developed which simulate the cutting tool and material interaction to allow cutting parameters to be derived numerically to enhance cutting blade design. The FE models incorporate experimentally derived mechanical and thermal properties of the common engineering thermoset

Perspex and also of the following food materials; toffee, cheese, chocolate and jelly. The combined thermo-stress FE model allows the temperature at the cut interface to be determined under various loading conditions and provides a method for investigating the effects of blade design on temperature at the blade-material interface. Estimations of accurate mechanical and thermal properties of foodstuffs for inclusion in the FE models are determined experimentally using materials testing techniques such as tension and compression tests. Ultrasonic cutting blades are designed using finite element analysis and experimental investigations are performed on an ultrasonic cutting rig to validate the FE models.

Two different generic 2D modelling approaches to simulate ultrasonic cutting are presented. One uses the debond method in ABAQUS standard and the alternative uses the element erosion method in ABAQUS explicit. Progression of the element erosion method into a 3D model is also presented with the intension of improving the accuracy of the modelling technique and to offer the flexibility to model complex geometries or cutting orientations. The models are presented and validated experimentally against a common engineering material, Perspex, and parametric studies are presented and discussed for the food materials; toffee, cheese, chocolate and jelly. For accurate modelling of any process, accurate material data is required and for common engineering materials such as Perspex accurate data is readily available in the literature. For food products however, the mechanical and thermal properties are not readily available and are often batch dependent. Methodologies for testing and determining the mechanical and thermal properties of two selected food materials, toffee and cheese, are also presented and the results from these experimental tests are incorporated in the finite element models to simulate the food materials during ultrasonic cutting. Models of ultrasonic cutting are for both single layer materials and also for multi layer material architectures.

II. Acknowledgements

I would like to give special recognition to the following colleagues and friends who have contributed their advice, criticisms, ideas and support towards the development of this project. Most of this was highly constructive and very much appreciated.

Professor Margaret Lucas, for allowing me the opportunity to join her highly regarded and respected ultrasonics research group to study for a PhD under her expert guidance. Margaret's supervision, direction, support and encouragement throughout this project was exemplary and it was an honour to work for a highly respected, professional engineer who is undoubtedly one of the leading names in high power ultrasonics in the world.

Dr Alan MacBeath, who worked closely with me on this project providing his input, time and expertise to many aspects of this research. We suffered some long days and nights battering our heads off each other with both the experimental and modelling work contained in this thesis but we had many laughs in the process which made the pain we suffered at the time memorable in a good way. There is no doubt without your continued patience, support and assistance the research work undertaken would not have been as successful.

Margot Cacchia and Sophie Thompson, two final year students who investigated food modelling of jelly and chocolate respectively and performed the materials tests to allow extraction of each foods material properties for inclusion in FEA. Your help and assistance in this area of the research was fundamental to producing food material data which can be used by many future researchers for a variety of purposes including investigating ultrasonic cutting numerically using FEA.

Mr Graham Hunter, a fellow colleague and friend in the ultrasonics group who not only shared an office with me but many lunches and social beverages after work. We had many laughs in and out of the office throughout the years which made the research experience very enjoyable and unforgettable. Your assistance in various aspects of the research work in this thesis and your continued support and motivation throughout this project have been truly appreciated and will be very well remembered.

Mr Kenny Stevenson and Mr Walter Robinson, for their continued support, help and troubleshooting skills of the many computer packages I used, computers I burned out and the many complicated ABAQUS jobs I ran on many computers and servers for months on end. Thanks for accommodating my demanding needs on the computing resources throughout this research as there is no way I could have completed this research without your assistance.

Mr Brian Robb, for his technical assistance and expertise in manufacturing the tuned ultrasonic cutting blades used in this thesis and for incorporating my demanding needs for technician time and assistance throughout this project.

Mr John Davidson and his predecessor Mr Alex Tory for their extensive help and assistance in the material lab and their patience and dedication to the challenging experimental testing configurations and testing techniques demanded of them over the past 3 years.

All the additional technical staff in the department who spared their time in the simplest of ways to assist manufacturing components, test rigs, specimens, animations and in countless other jobs to allow the research in this thesis to be possible.

All my fellow postgrads and academic staff in the department who had to put up with me over the last three years and who I enjoyed having countless conversations with and who made this PhD sentence memorable.

My Family and friends who supported me through this challenging degree and who had to listen to me talk about the research work in this thesis in countless number of occasions throughout the years. Thanks for taking the time to listen to me rant on about FE models, materials testing, test rigs etc especially when I really know you didn't really understand a word I was talking about.

Thank You All!

III. Contents

IV. Figure and Table Captions

Table of Figures

Table of Tables

V. Nomenclature and Abbreviations

Nomenclature

U : Displacement

x : Position

t : Time

dx : Small element of the rod

P : Applied force

σ : Stress

ε : Strain

E : Young's modulus

A : Cross:sectional area

ρ : Density

c^2 : Velocity of the stress wave in the rod

n : Mode order

l : Tuned length

f_n : Natural frequency

F : Force

m : Mass

$\frac{\partial^2 u_z}{\partial t^2}$: Acceleration

∂z : Element length

z : Longitudinal axis

r : Radial axis

u_z : Displacement in the z:axis

S : Cross sectional area

C : Constant

f_{cur} : Current natural frequency

f_{des} : Desired natural frequency

A : Amplitude of the transducer

ω : Natural frequency

t : Time

σ_1 : Principal stress in the 1 direction

σ_2 :Principal stress in the 2 direction

σ_3 : Principal stress in the 3 direction

σ_0 : Yield stress

σ_{max} : Maximum allowable stress

Q : Quality factor

φ : Acoustic loss

z : Acoustic impedance

c : Speed of sound

E : Young's modulus

σ_{yp} : Yield stress

σ_{uts} : Ultimate tensile strength,

σ_n : Nominal stress

σ_t : True stress

σ_{bp} : Break point

ε_n : Nominal strain

ε_t : True strain

Δh : Absolute deformation of the specimen

h_0 : Initial sample height

A_0 : Initial cross:sectional area

A : Original cross:sectional area

l : Deformed length

l_0 : Gauge length of the specimen

ε_0 : True strain at the yield point

σ_0 : True stress at the yield point

ε : Strain

σ : Stress

n : Curve fitting exponent

I_1 : 1st strain invariant

I_2 : 2nd strain invariant

I_3 : 3rd strain invariant

λ_1 : Principal stretch ratio in the 1 direction

λ_2 : Principal stretch ratio in the 2 direction

λ_3 : Principal stretch ratio in the 3 direction

L : Deformed length of the specimen

L_0 : Original length of the specimen

Δu : Extension of the specimen

λ_B : Biaxial stretch ratio

λ_u : Uniaxial stretch ratio

λ_S : Shear stretch ratio

λ_v : Volumetric stretch ratio

κ_0 : Initial bulk modulus

μ_0 : Initial shear modulus

υ : Poisons ratio

J_{el} : Elastic volume ratio

J_{tot} : Total volume ratio

J_{th} : Thermal volume ratio

ε_{th} : Linear thermal expansion strain

W : Strain energy potential

μ : Initial shear modulus

λ_m : Locking stretch

β : Invariant mixture parameter

D : Compressibility constant

ΔT : Temperature change

E : Energy applied

C_P : Specific heat capacity

Q : Heat

t : Thickness of the specimen

k : Thermal conductivity

μ_s : Coefficients of static friction

μ_d : Coefficient of dynamic friction

F_P : Weight attached to the pulley

F_S : Static load carried by the specimen

m : Mass of the specimen

v_{tran} : Translational velocity of the blade

U_T : Total energy

A : Area of the crack surface

W : External work

W : Energy required to make a new surfaces

R : Resistance to crack growth

a : Crack length

B : Breadth of the specimen

γ_s : Surface energy density

G_C : Energy release rate

υ : Poisson's ratio

σ_f : Critical fracture stress

W : External work

P : Applied load

Δ : Displacement

γ_P : Surface energy density in plasticity

r : Distance ahead of the crack tip

k : Scaling factor

$f_{ij}(\theta)$: Stress field about the crack tip

K : Stress intensity factor

K_I : Stress intensity factor in mode I

K_{II} : Stress intensity factor in mode II

K_{III} : Stress intensity factor in mode III

Y : The geometric correction factor

θ : Angle

Abbreviations

FE : Finite Element

FEA : Finite Element Analysis

EMA : Experimental Modal Analysis

USM : Ultrasonic Machining

RUSM : Rotary Ultrasonic Machining

EDM : Electrical Discharge Machining

HIFU : High Intensity Focused Ultrasound

ECM : Electrical Chemical Machining

MRR : Material Removal Rate

ASTM : American Society of Testing and Materials

DSC : Differential Scanning Calorimeter

DMTA : Dynamic Mechanical Thermal Analyser

HPP : High Pressure Processing

DMA : Dynamic Thermal Analyser

FEM : Finite Element Modelling

FRF : Frequency Response Function

FFT : Fast Fourier Transform

ESPI : Electronic Speckle Pattern Interferometry

DFT : Digital Fourier Transform

UTS : Ultimate Tensile Strength

CAM : Computer Aided Manufacture

SENB : Single Edge Notch Bend

Chapter 1

Introduction

Ultrasonic cutting is where a blade, or system of blades, tuned to a resonant frequency in the low ultrasonic range between 20-100 kHz causes material separation when the blade interacts with a substrate material. The blade or blades are often stimulated by mechanical vibrations provided by a piezoelectric transducer or through coupling to other tuned components. A schematic diagram illustrating the ultrasonic cutting system and also a detailed representation of the piezoelectric transducer is shown in Figure 1.1.

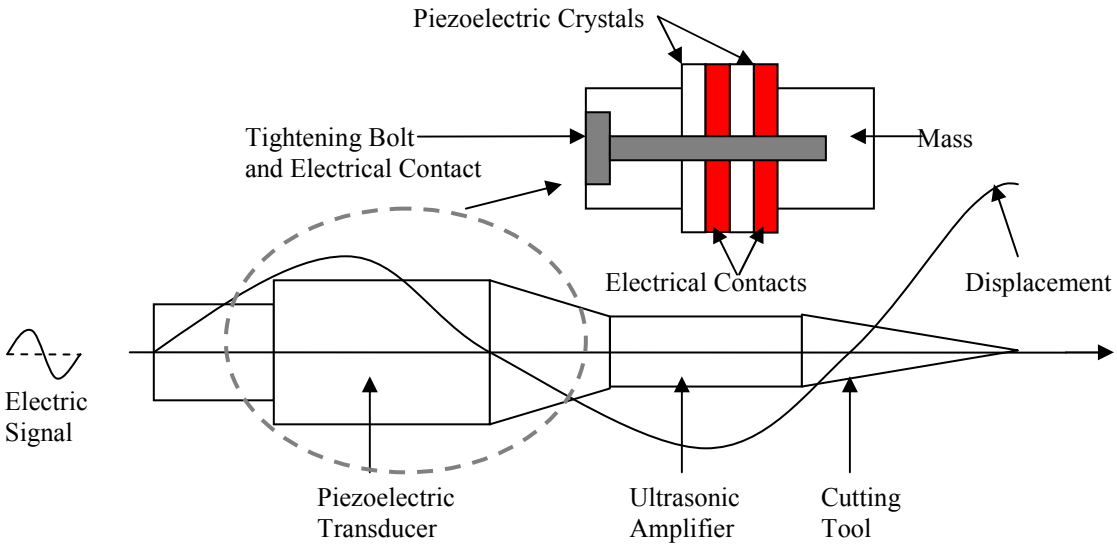

Fig. 1.1: Schematic diagram of the ultrasonic cutting system.

This thesis reports two novel generic thermo-mechanical finite element (FE) models of ultrasonic cutting developed to give an insight into the interaction between the cutting tool and material to be cut. This allows for predictions of optimal cutting parameters to be estimated as part of the design process. The main aim of any ultrasonic cutting tool is to give a successful, precise cut at the exact cut location, which produces a high quality surface finish without inflicting damage to the neighbouring material surrounding the cut zone. However, the determination of the cutting parameters required depends on the material to be cut and these parameters are usually determined from extensive experimental tests and from user experience. Currently material properties data for food is not abundant in the literature; as such the

mechanical and thermal properties for the engineering material Perspex and the foods toffee, cheese, chocolate and jelly were derived from experimental tests using adapted materials testing techniques for inclusion in the FE models using curve fitting techniques. An experimental cutting rig was also designed to perform cutting tests on Perspex and the food materials to validate the FE models and allow the user to have confidence in the modelling procedure and the simulated results.

The aims of this research were to:

(1) Design, manufacture and validate ultrasonic cutting blades using Finite Element Analysis (FEA) and Experimental Modal Analysis (EMA) for use in experimental cutting tests.

(2) Derive mechanical and thermal properties of Perspex, toffee, cheese, chocolate and jelly for inclusion in FE models from experimental materials tests.

(3) Create novel FE models of ultrasonic cutting.

(4) Design and manufacture an ultrasonic cutting rig.

(5) Validate the FE models of ultrasonic cutting against experimental cutting tests by varying ultrasonic cutting parameters.

(6) Develop an approach for determining optimum cutting parameters for various materials.

1.1 The definition and categorisation of ultrasound

Sound is vibrations that occur with a variation in pressure and propagate through mediums such as solids, liquids or gases as waves. Waves have characteristics such as frequency, amplitude, wavelength, period and speed that characterise the sound. Sound is perceived by animals such as humans by their sense of hearing but the levels of hearing vary in different animals and also depend on their age, gender and exposure to noise. Humans typically hear sound between 20 Hz and 20 kHz. Sound vibrations transmitted below the audible range of human hearing are described as infrasound and above the audible range of human hearing are classified as ultrasound [1]. Ultrasonics considers the application of vibrations above the lower ultrasonic of 20 kHz up to frequencies in the range of GHz which are currently limited only by signal generation capabilities.

Ultrasonics is divided into two distinct categories, low power and high power applications. Low power applications are usually categorised in the region of 0 – 10 W at frequencies typically above 1 MHz and are often non-invasive scanning procedures where no permanent physical

change occurs. High power applications utilise mechanical vibrations usually in the region of 20 – 100 kHz and from a few tens of Watts to several thousand Watts and invoke permanent physical changes to the structure or work-piece in either a solid, liquid or gaseous state [2].

1.2 Applications of ultrasonic technology using frequencies above 100 kHz

Low power ultrasonics is used in various industrial applications in engineering, medicine and the food industry mainly concentrating on diagnostic applications that are non-invasive and are used to investigate materials or systems by propagating sound waves through the medium under investigation. Ultrasonic waves travel through a solid, liquid or gas medium until an impedance change occurs. The size of the impedance change causes the entire wave or part of a wave to be reflected back to the transducer generating the signal. If there is no reflection the signal will pass through a component until it reaches the far wall or if the component is too thick the signal will be attenuated. Impedance changes occur between components of dissimilar materials or by changes in boundary conditions such as reaching a boundary wall, phases such as interacting with gas bubbles in a fluid or defects such as cracks in solids [2-5]. For effective use, the substrate should be impedance matched to the transducer and system prior to use to ensure that sound waves are propagated effectively throughout the material under investigation.

There are three main techniques used to measure sound waves in different media, through transmission, pulse echo and interferometry [3]. Through transmission, sometimes called the pitch and catch technique, uses a transducer to generate the wave at one side of the medium and a receiver at the other to pick up the signal. The velocity is calculated by measuring the distances between transducers and timing the wave between transmission and acceptance. Using the pulse echo technique a sound wave is generated and received from the same transducer by allowing the wave to pass into a container encasing the material and then to reflect off the other side and bounce back to the receiver. Interferometry is where the wave is passed through the medium and is reflected off from a removable reflective plate within a cell and picked up again by the receiver. The plate can move nearer or further away from the source, which allows the receiver to pick up different amplitudes in the signal. This range of amplitudes can allow the determination of maximum and minimum amplitudes in a signal and the distance between successive maximums or minima is a half wavelength. From this, the velocity in the sample can be calculated.

1.2.1 Engineering applications

In engineering the use of low power ultrasonics to test components non-destructively while in, or prior to, service has been a great technological achievement. This technique allows the detection of surface or sub-surface flaws embedded within a material to be detected without removing the component from service, or in the post-manufacturing stage without breaking the material. The information gathered from this technique, such as flaw length and depth, can be used in fracture mechanics calculations to determine if the component is safe for use within the loading environment. If safe, it allows the component to be continually used and monitored until it reaches an unsafe limit, which would require it to be fixed or replaced. This technique has allowed components to be used longer in service than previously, which has obvious cost saving benefits. In addition, ultrasonic thickness gauges can characterise the thickness of components during manufacture by determining the position of the outer surface due to a change in impedance when a boundary wall is reached. However, this technique is limited by the thickness of the component and is effective only for thin components, if they are too thick then the ultrasonic waves are attenuated through the material [7].

Sonar/Radar is a range finding technique that uses ultrasound to locate objects by generating an ultrasonic wave and propagating it in a particular direction. If an object is in the path of the projected signal the pulse or part of the pulse will be reflected back to the transmitter as an echo that can be detected by the receiver. The time delay in transmission and receiving can be measured and the distance the object is away from the transmitter can be calculated from the Doppler effect [6].

1.2.2 Medical applications

Medicine has benefited greatly from ultrasonic imaging techniques producing real time pictures, or sonograms, of internal organs to identify problems such as blockages or lesions or to monitor the development of a foetus in the womb. Blood flow measurements and cardiac problems can also be detected using an echocardiogram to allow doctors to evaluate the efficiency of heart valves or blood flow directions [6]. These techniques are non-invasive and provide quick, detailed examinations of patients. Medical processing tomography techniques produce very detailed images of the inside of the human body. This is mainly possible because the human body contains very good acoustical properties due to the majority being made up of water which transmits sound waves effectively.

1.2.3 Food industry applications

Utilisation of low power ultrasonic monitoring techniques in the food industry has provided methods for automated inspection which can improve quality control. Stringent hygiene requirements and health legislation in the food industry have driven a need for reliable non-invasive sensing technology. Non-invasive, non-destructive ultrasonic monitoring systems similar to the ones used in engineering and medical industries have been investigated and adapted for this purpose. Mason and Povey (1998) [2] amongst others have extensively reviewed ultrasonic measuring techniques for food. Applications of low power ultrasonic measuring techniques include monitoring fluid levels in containers [8], determining material properties [3] and characterising droplets within emulsions [4, 5]. The monitoring of fat thickness in meats, fat content in cheese, alcohol and sugar concentration in liquids and quality of eggs have been other topics previously researched. In the food industry one typical application of ultrasonics is in the non-destructive testing of cheese [9]. The decrease of ultrasonic attenuation during the renneting process can be used to determine the optimum cut time for cheese. In addition, the ultrasonic velocity increases during the maturity stage so it can determine the degree of maturity. This method has also been used to determine quality attributes of avocados, mangos and melons, as well as the composition of chicken, cod and pork meat. Instantaneous changes can be measured by the production and detection of sound waves in self-standing or automated production lines.

Determining food characteristics can be a very lengthy time consuming process due to the complexity of the food structure and expensive specialised instrumentation is required to characterise the foodstuff accurately and reliably [2, 3]. Determining molecular properties and monitoring the crystallisation of food products have been two of the main advancements in the food industry with the aid of ultrasonics. The application and amendment of the Wood (1964) equation for fluids by Ulrich to characterise solid and visco-elastic materials allowed the compressibility of sound in multiphase food materials to be developed. This provided a simple technique to determine mechanical properties such as Young's Modulus in food products by characterising the compressibility of the material and combining it with material density to fully describe the wave propagation in complex multiphase food structures. However, this technique was prone to errors by thermal scattering, which occurred by the expansion and compression of the wave heating or cooling of the material. Thermal scattering is a phenomenon that occurs when the centre of the material is heated or cooled differently from the external boundary. This occurs when a temperature gradient exists between the periphery of the particle and the surroundings caused by the heat capacity or volume expansivity at the boundary of the particle.

Other sound scattering phenomenon exists such as visco-scattering or differences in density and viscosity between the surroundings and the particle. Previous research into characterising mechanical properties of cheese and milk by using low power ultrasonics was studied by Orlandini and Annibaldi and Winder respectively [2, 3].

Emulsions are usually a mixture of oil and water droplets that exist in a solution. Usually in the food industry a small concentration of oil droplets exist within water. Oil and water are immiscible liquids and if initially mixed then left at rest the oil and water layers will separate into two distinct phases. Physical and chemical processes that occur within the mixture can be depicted by oil concentration within emulsions. In addition, the shelf lives of products are usually determined by the overall appearance of the food emulsion. However, emulsions are not easy to characterise. Most emulsions are murky solutions that do not allow light to transmit through which can cause difficult problems in determining droplet distribution and concentration within the solution. Although emulsions are cloudy, ultrasonic waves can pass through without hindrance. Due to this phenomenon ultrasonics has been researched for characterising droplet distribution and concentration within a solution [4, 5].

Products within the food industry rely on appearance, texture and taste to determine their success in the retail market. Droplet sizes within food emulsions have been shown to determine these characteristics, and information regarding their presence within foodstuffs can be advantageous to the food industry. Extensive tests on foodstuffs using electron and optical microscopy have been used to characterise these droplets within emulsions accurately. However, these testing techniques are time consuming and can alter the microstructure of the material. Other lab based testing regimes include light scattering and electrical conductivity experiments, which are fast to perform. These tests provide very accurate information on the droplet arrangement within the food however, they require that very concentrated samples be diluted prior to analysis, which can change the droplet distribution and cause inaccurate results. Previous research has indicated a relationship between the size and concentration of droplets and ultrasonic wave scattering [2, 4]. Ultrasonic spectrometry is a particle sizing technique that has been employed to characterise droplets in food emulsions [2, 4]. The main advantage of this technique is that it is non-invasive and dense, coloured emulsions can be examined quickly and even automated into the production process. These low power ultrasonic monitoring devices can provide significant savings in cost and time in measuring droplet distributions in emulsions due to them being tested in situ.

1.3 Ultrasonic cutting

Ultrasonic cutting systems consist typically of three parts; a generator, a transducer and a horn as shown in Fig. 1.2 but can have any number of ultrasonic components connected together if required. The generator uses mains electricity to generate a high frequency ultrasonic signal to drive the transducer which, is tuned to a specific frequency in the range 20-100 kHz and typically provides an axial vibration of between 2 - 10µm amplitude. The vibrations can be amplified using a device known as a horn or sonotrode by varying the cross-section [2, 28].

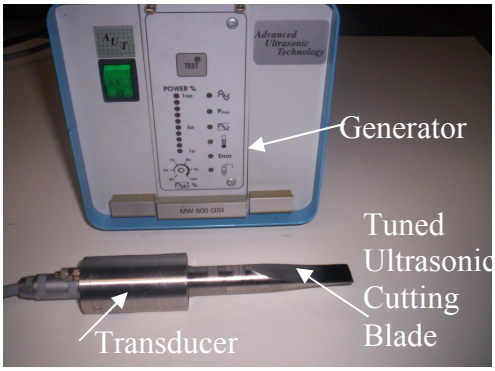

Fig. 1.2: Ultrasonic cutting system.

Ultrasonic generators have electronic circuitry incorporated in the system which can track the exact resonance frequency and amplitude of vibration to allow efficient operation of the ultrasonic cutting system. This results in low heat generation due to minimum acoustic losses in the system. Modern generators also have built in safety features such as automatic switch off in case of fracture in the horn or failure in the connections.

There are three different types of transducers, liquid driven transducers, magnetostrictive transducers or piezoelectric transducers. Liquid whistles are an alternative name given to liquid driven transducers and operate by driving a fluid through an orifice and over a thin blade, which causes the blade to vibrate. Cavitation occurs in the fluid at the trailing edge of the blade and at the leading edge a pressure wave is generated for every vibrational movement of the blade. This transducer is very robust but limited to mixing liquid solutions and is typically effective for homogenising solutions. Magnetostrictive transducers are electromechanical and utilise the principal of magnetostriction. Magnetostriction is the term given to the change in dimensions of magnetic materials on application of a magnetic field. A simple magnetostrictive transducer is a

closed square made of steel wound with a coil around two opposite sides. When current passes through the coil the square core contracts and when turned off expands again back to its original shape. Switching the current on and off rapidly can cause the core to expand and contract very quickly which can cause the mechanical vibrations. The frequency of vibration required can be generated by tuning the core to allow resonance at a particular frequency. These transducers are generally inefficient due to high heat losses and external cooling systems are often required. These transducers are also large, but can generate large driving forces if required. Piezoelectric transducers are the most common, having high efficiency, typically over 95%, smaller dimensions than the magnetostrictive counterparts and the ability to operate over a very large frequency range. Ceramic discs such as barium titanate or lead metaniobate are sandwiched between metal blocks which act as heat sinks to reduce heat losses and protect the brittle crystalline material. Current is passed through the piezoelectric ceramic discs, which causes the piezoelectric ceramic crystals to vibrate at a specific frequency, which causes the generation of ultrasonic waves. The electrical signal supplied to the discs is changed due to the piezoelectric effect into mechanical vibration and can vibrate the disc axially causing movement. The power varies with the inverse of the square of the frequency so for high power applications utilising the lower frequency range is preferred. The transducer is attached to a fixed booster horn to which additional horns can be attached to amplify the vibration if required.

For high power applications, the transducer is either attached directly to the cutting tool or via a tuned horn or booster. The amplitude of vibration at the base of the transducer is typically a few microns and the horn is used to amplify the vibration and focus the energy onto the tool. The horn requires specific tuning and the material should possess a high mechanical Q factor, be corrosion resistant, have high wear resistance, good acoustic transmission properties and high resistance to fatigue. Aluminium, titanium, monel and stainless steel are commonly used materials in horn manufacture. The cutting tool is connected to the horn by brazing, soldering, screwing or directly machined to the base of the horn during manufacture. Threaded screws are commonly used because of the ability to change the tool easily, but problems can occur such as self-loosening and loss of acoustic power [100]. The horn and the transducer should ideally be acoustically matched with similar mechanical impedance. For ultrasonic cutting applications operating in a fluid the tip of the horn can be eroded due to cavitation after sufficient operating time but replaceable screw thread tips can be reattached to extend the lifespan of the tool. Horn design varies from a uniform cylinder where there is no amplitude gain, to a tapered, stepped or exponential profiles where there is an amplitude gain. A stepped horn profile provides high gain

but results in high internal stresses and therefore the profile must be designed carefully to remain within safe operating limits of the horn material. Typical gains for linear, conical, exponential and catenoidal profiles are 1, 4, 8 and 14 respectively.

1.4 Ultrasonic applications in the frequency range between 20-100 kHz

High power ultrasonic technology has many applications and is prominent in many engineering, medical and food industries. The main generic applications include surface cleaning, welding, machining and cutting [10-22]. In engineering, high power ultrasonic technology has been used for a wide range of applications including welding thermoplastics and metals, machining brittle and hard materials and cutting plastics and composites. In medicine and dentistry high power ultrasonic applications include destruction of tumours and kidney stones, cutting tissue in surgical procedures, dental operations and descaling and cleaning teeth. More recently in the food industry newer high power ultrasonic applications have been used and include food preservation [23], degassing foams [24, 25], filtration, drying [26] and cutting foodstuffs [27, 28]. In the high power operating range ultrasonics can cause permanent changes in materials. Different phenomena are present in different mediums and common effects include fatiguing, friction and temperature changes in solids, cavitation and micro-streaming in liquids and surface instabilities in liquid-liquid and liquid-gas interfaces. Depending on the phase of the material when the ultrasound is applied, these phenomena can cause desired or undesired effects. For example, cavitation is only present in liquids and not in solids or gases due to the oscillation, expansion and collapse of bubbles in the fluid which can aid effluent treatment or sterilisation of equipment due to the destruction of bacteria, but conversely can also cause surface erosion of the horn, transducer or casings which can render the device inoperative. Also, if ultrasound is applied to suspended solids in liquid, particles separate whereas in a gas they join or agglomerate, together [29-33].

1.4.1 Engineering applications

The cavitation effect can be used to cause the destruction of bacteria due to bubble oscillation, expansion and collapse. The high frequency oscillations produced in the fluid by ultrasound cause voids in the liquid which grow, oscillate and collapse causing extremely high localised temperatures and pressures which cause cell disruption or kill bacteria. Ultrasonic cleaning utilises the cavitation effect found in fluids by causing the disruption of aggregates from the materials surface. This technique has been applied in industry to clean many pieces of equipment

from beakers and test tubes in a chemistry lab to sterilisation and cleaning of shackles in the food industry. Ultrasonic cleaning is usually used in the low ultrasonics frequency range between 20 and 50 kHz where the cavitation effect is greater and more effective as the bubbles have more time to expand and contract compared to those oscillating at higher frequencies. Ultrasonic cleaning has the ability to simplify cleaning tasks and provide a fast, efficient cleaning technique that has a lower probability of cross contamination and is more sterile than the manual cleaning method. Ultrasonic cleaning can also clean and sterilise inaccessible locations that traditional manual cleaning are unable to reach [29-33].

The plastic welding technique commonly operates at approximately 20 kHz at power levels below 1kW and can be considered to be fast, clean and easily automated. Common applications include the production of plastic toys, sealing plastic bottle caps and joining of thermoplastic components. The technique utilises an ultrasonic horn attached to a transducer and impedance matched as close as possible to the work-piece which produces an efficient energy transfer mechanism between the horn and the work-piece. The oscillatory movement of the horn produces a highly localised temperature rise at the interface between the horn and plastic work-piece which causes the work-piece to melt locally at the weld zone with little heat transfer to the surrounding material due to the low thermal conductivity of plastic. When the welding horn is removed from the welding zone the plastic solidifies and joins the materials together [73].

Ultrasonic machining (USM) is a process, which converts electrical energy to mechanical vibrations through a machining assembly consisting of a transducer, booster, horn and a tool. The horn focuses and often magnifies the mechanical vibrations onto the tool producing tool tip amplitudes in the range from 2 – 100 microns at a tuned frequency from 20 – 100 kHz. The applied mechanical vibrations stimulate the mode shape at the tuned frequency causing controlled movement of the tool. The most common mode shape excited historically is the longitudinal mode. Power ratings in the machines usually range from 50 W to 4 kW. Loads are applied to the base of the assembly and abrasive slurry consisting of water or oil with particles of silicon carbide suspended in solution are applied to the interface between the tool and work-piece. The mechanical vibration transmitted to the tool tip smashes the abrasive particles in the slurry into the work-piece resulting in micro-cracking and material removal. USM has various configurations such as rotary ultrasonic machining (RUSM), combined USM and electrical discharge machining (EDM) and traditional machining such as turning or milling assisted by ultrasonics. Applications include machining and drilling of fibre reinforced ceramic disc brakes,

gearwheels, engine block components in the automotive industry, machining silicon, silicon carbide for use in creation of semiconductors and the manufacture of lenses, mirrors and ligaments from ceramics, glass or corundum in the optical industry [45-53, 55-64].

Volkov *et al* [73] utilised ultrasonic cutting technology for cutting polymeric materials and preferred this technology over traditional mechanical cutting methods and processes such as laser, plasma, gas heat carrier and high frequency currents. Mechanical cutting technologies for plastics have several disadvantages including the requirement of various cutting tools depending on the shape required, type of plastic or mechanical process. The surface finish of the product is also of a low quality and is usually charred because of the friction between the tool and work-piece and usually requires further surface treatment. Thermal methods such as laser and plasma require no contact between a tool and work-piece and simply melt the plastic at the focal point on the work-piece to separate the material and create the required size and shape of the plastic. The set up cost of these methods is high and the quality of the product at the cutting edge is usually low with a poor appearance and surface finish which usually requires further treatment to be of an acceptable standard. The use of high frequency currents can only be adapted to certain polymers and usually result in high dielectric loses during operation. Ultrasonic operations usually operate in the low ultrasound range, typically 20 – 35 kHz, and use cutting tools directly attached to piezoelectric transducers or through a combination of booster or tuning sections to propagate and amplify the vibrations of the transducer to the cut interface between the tool and plastic. Fig. 1.3 (a) shows a typical ultrasonic cutting system and (b) shows an ultrasonic horn with interchangeable cutting tools.

(a) (b)

Fig. 1.3: (a) Ultrasonic cutting system and (b) ultrasonic cutting horn with various cutting attachments [17].

1.4.2 Medical applications

The application of high power ultrasound to treat benign and malignant tumours or cancerous tissue using a non invasive technique called high intensity focused ultrasound (HIFU) has gained popularity in the medical community in recent years [20]. The technique was originally used to treat prostate cancer and has since been adapted for destruction of other types of cancer and diseased tissue. The technique focuses ultrasound on the diseased tissue or tumour and at the focal point the ultrasonic energy is absorbed which causes a localised temperature rise in the tissue that can destroy the diseased tissue or ablate the tumour. Cavitation can also occur at the focal point that can assist in the destruction of a tumour or tissue due to the micro-bubbles collapsing and causing localised temperature increases due to the implosion of the bubbles and local jetting effects destroying the neighbouring tissues. Cavitation is used cautiously in medical applications due to the uncertainty of the tissue damage that could be caused by the imploding bubbles and the distribution around the focal area.

Applications of high power ultrasound in medicine have advanced surgical procedures by harnessing and focussing ultrasonic energy to cut tissue and coagulate blood at the incision site. Several cutting devices are currently available on the market today and are divided into two distinct groups, ultrasonic cavitational aspirators and ultrasonic cutting and coagulation devices. Figure 1.4 shows the Harmonic cutting and coagulation scalpel developed by Ethicon Endo-Surgery [19]. Operations for removing cataracts and rectal tumours are possible with the use of ultrasonic cavitational aspirators. Commercially there are several devices available to make shallow incisions and coagulate tissue during operations. Current research at the University of Glasgow has focussed on ultrasonic devices to cut hard biomaterials such as bone to provide orthopaedic surgeons with new devices for deep incisions.

Fig. 1.4: Ultrasonic cutting and coagulation surgical device [19].

High power ultrasonics has been used extensively in dentistry from the early 1950s to perform cutting operations but was superseded by the introduction of the rotary drill in the late 1950s. However, adaptation of the cutting instruments proved effective in the removal of plaque and scale from teeth in the early 1960s and were an effective alternative to hand scaling instruments. Dental scaling instruments typically use longitudinal vibrations of the tool at frequencies between 20 and 50 kHz and current research is investigating adding water at the tool tip to research if cavitation of the fluid spray aids descaling and cleaning of teeth [22].

1.4.3 Food industry applications

Power ultrasonics can be used for food preservation due to the bombardment of ultrasonic waves breaking down bacterial cell walls to aid moisture removal from cells by causing the material to expand and contract and expel water like a sponge. Currently the preservation of food in industry uses chemicals or heat treatment. The application of ultrasonics to food processing could reduce the quantity of chemicals or heat added in processing or eradicate it completely. This could improve the quality of the product, texture, taste and provide cost benefits. Care has to be taken when applying ultrasonics to food materials as foodstuffs are very complex materials that can exist as a mixture of solid, liquids and gasses and the effects of ultrasound in each food are very different and difficult to predict [2, 23].

Degassing of foams and dehydrating foods in the food industry can be achieved by using air-borne ultrasonic technology which causes ultrasonic waves to pass through air to cause removal of moisture in food, to aid preservation or to cause destruction of bubbles in the froth of fluid [25]. Dehydration of foods is extremely important as the food product life can be extended if moisture can be removed without damaging the product and is typically done by hot air drying, freeze drying or mechanical pressing. Froth removal or degassing foams can be accomplished by heating or adding chemicals or by using mechanical systems such as air or liquid jets. The basis of this technology is to impedance match the generator to air. This has been achieved historically by using whistles such as the Hartman whistle in 1939 [285] or sirens such as the rotary siren designed by Allen in 1947 [286]. These ultrasonic transducers produce gas jets which generate the acoustic energy but these instruments have low efficiency, are susceptible to noise and are confined to low ultrasonic frequencies. More recently a flexural vibrating plate driven by piezoelectric ceramics designed by Galleo-Juarez in 1989 [25], has provided an excellent impedance match with air and can generate high power through a novel stepped plate design. The large surface area of the plate is passed over the meniscus of the liquid or applied directly to

the medium and has successfully destroyed or removed the froth or the moisture in the food product. Froth formation on top of liquid mediums in manufacturing processes can cause difficulties during processing and in handling. A typical problem is in the brewing industry where yeast fermentation causes froth formation on top of alcohol. In the food and beverage industry the addition of chemicals can contaminate the product, heating can be expensive and the application of electricity is seldom used. The use of air or liquid jets and ultrasonic vibration to degas foams on beverages has proved successful. Research using the stepped plate transducer to destroy foams and gasses in the beverage industry has been successful. Adaptation to other applications in the food industry to separate solid, liquids and gasses or to cause gas sterilisation has also been proved successful.

High power ultrasonics can also be used to cause emulsification by cavitation near immiscible layers such as oil and water by using liquid whistles. This technology has been highly effective in emulsifying food products such as fruit juices, ketchup, mayonnaise and cheese. Addition of ultrasonics to enhance oxidation processes such as fermentation of wines and spirits have also been successful in producing aged products in less time. Protein extraction in meat products occurs when ultrasonic vibrations are applied to the product, which results in improved strength and tenderness of the meat with a more favourable taste. An increased yield in yoghurt production was found through the application of ultrasound because of stimulation of the living cells which also yielded improved texture and consistency of the product [2, 4, 24, 27].

Sterilisation by application of ultrasound has been extremely effective in many industries through micro-jet formation near surfaces caused by collapsing bubbles during cavitation that can penetrate crevices where manual cleaning techniques are difficult or even impossible to perform. There are numerous applications in the food industry from cleaning shackles that hang meat to cleaning food surfaces. Decontamination of bacteria in food products, cleaning and pasteurising containers are other known applications. One main application in the food industry is the cleaning of egg surfaces. Bacteria are present and breed on the surface of eggs and often absorb through the solid, porous membrane surface of the egg and kill the embryo inside. Sterilisation of liquid foodstuffs such as milk or fruit juices in either a batch process or by a flow through system using ultrasonics also has many advantages in the food industry by removing the need to heat, pasteurise or further treat the food to kill the bacteria [29-33].

There are many industrial applications where the separation of suspended solid particles from a solution is required. This process is usually accomplished by sucking the fluid solution through a semi-permeable membrane, either directly using high pressure or by using a cross-flow configuration. However, if a high concentration of suspended solids is in the solution the membranes can become fouled and fluid flow is reduced which often requires the process to be suspended and the membranes changed. This problem can be overcome by using high power ultrasonics to aid the process by attaching transducers to the unit holding the membrane, which agitate the particles on the membrane and allows fluid to flow. This technology has been used separately or with assistance to reduce the fouling process in separating coal and sewage from water [26]. After filtering the suspended solid solution, the filtrate remaining on the membrane is still moist and, if required, the filtrate is usually dried by hot air. Ultrasonics can also aid the drying process, by attaching transducers to a rigid plate and then compressing the plate on top of the moist filtrate. This process can be used in assistance with hot air or as a stand alone application.

High power ultrasonic cutting systems revolutionised the food industry in the 1990s by producing high quality cuts with minimal wastage of food material. Large volumes of food products could be cut swiftly and with ease under automated conditions in either a batch or continuous process using ultrasonic cutting knives in either a slicing or guillotining configuration. Mason and Povey [2] have extensively reviewed ultrasonic cutting in the food industry and discussed the main advantages of the process such as improving cut quality especially of brittle products, reducing cut debris and wastage, self-cleaning blades and longer tool life. Fig. 1.5 (a) shows a typical ultrasonic cutting system designed by Branson Ultrasonics with a guillotine blade attached to three transducers to cut a slab of cake. Figure 1.3 (b) and (c) depict a smaller guillotine system and a small slicing system respectively [16].

(a)

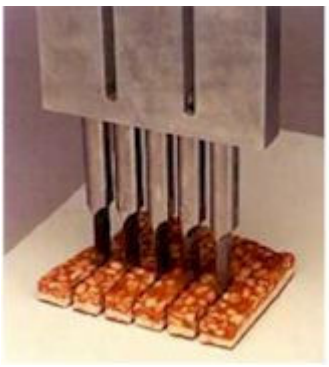

(b) (c)

Fig. 1.5: (a) Large batch ultrasonic food cutting device in guillotine orientation, (b) small batch ultrasonic food cutting device in guillotine orientation, (c) small batch ultrasonic food cutting device in slicing orientation [16 - 18]

1.5 Simulating ultrasonic cutting using FE

Currently ultrasonic cutting simulations are restricted to very fast cutting speeds (greater than 300mm/s) and small cut depths (up to 0.1mm) due to computer power, processor requirements and the large number of iteration required to solve the models [245, 247, 249, 251]. Currently there are no generic ultrasonic cutting models known to this author for simulating the ultrasonic cutting process. There is scope for developing new generic thermo-mechanical modelling techniques for ultrasonic cutting that can simulate ultrasonic cutting at lower cutting speeds and also to larger cut depths. This will allow a more detailed analysis and hence a more realistic representation of the ultrasonic cutting process to be conducted. Integration of the FE simulation into the ultrasonic cutting blade design process would allow optimum cutting parameters to be determined for a material prior to blade manufacture. Various combinations of cutting speeds,

ultrasonic amplitudes, blade tip geometries and cutting orientations could be simulated to predict optimum cutting requirements for any substrate material. At present there are no known ultrasonic cutting simulations explicitly tailored for modelling ultrasonic cutting of food products. With increased use of this process in industry it would be advantageous to model the process and predict optimum cutting parameters for ultrasonic cutting of specific food materials. Food material data for use in computational modelling packages such as FE are not widely available in the literature due to testing difficulties, complex material architecture and batch dependence. There is scope for investigating testing techniques required to predict the mechanical and thermal properties of food and conduct experimental tests on a variety of food products for use in the FE simulations. A modelling process is only useful if it correlates with the actual physical process. For simulating ultrasonic cutting there is also a requirement for developing an experimental cutting rig to conduct experimental cutting tests with variable cutting parameters to compare to the simulated results with the experimental results and validate the FE models. A validated model would allow predictions of the performance of various cutting blades and new novel designs of cutting tool to be studied faster and inexpensively compared to the costly iterative experimental methods currently used.

Chapter 2

Literature Review

2.1 Early developments in ultrasound

The term ultrasound is given to sound above the frequency of human hearing, 20 kHz. Animals such as whales and dolphins have used ultrasound for millions of years to communicate over very large distances by transmitting and receiving acoustic waves through water.

In 1830 Felix Savart [34, 35] invented the very first ultrasonic generator, the Savart wheel, which worked up to 24 kHz. Savart was one of the first investigators of high-frequency applications. The Galton whistle was designed in 1876 [36] to study the threshold of animal hearing and worked in the range of 3 – 30 kHz. Tuning forks that could operate up to 90 kHz were designed by Koenig [37] in the late 19th century. Other investigations into the velocity of sound in different media, in air by Paris in 1783, in iron by Biot in 1808 and in water by Calladon and Strum in 1826, complemented the understanding of acoustic wave propagation [39]. The discovery of the piezoelectric effect in 1880 by Pierre and Paul-Jacques Curie [34, 38] was a significant milestone in the development of ultrasonics. In the early 20th century Lord Rayleigh pioneered discoveries in optics and acoustics where fundamental understanding of bubble collapse, acoustic pressure and acoustic surface waves (Rayleigh waves) was born [34]. Research into using ultrasonics as an underwater detection system were instigated in 1912 after RMS Titanic collided with an iceberg on her maiden voyage and were given further impetus a few years later when World War 1 began.

In 1915 experiments by Langevin for the joint U.S., British and French investigation into adapting Chilowski's ultrasonic transducer design, which had weak acoustic intensity, produced piezoelectric transducers operating at resonance with high ultrasonic intensities [39]. At that time, initial pulse echo investigations at frequencies of 150 kHz were found to kill fish that were in line with the ultrasonic pulse. Also, the first practical and efficient piezoelectric transducers were made from quartz and then steel-quartz-steel combinations [40]. From the end of World War 1 to the start of World War 2, sodium potassium tartrate tetrahydrate, also known as

Rochelle salt, was the underwater transducer single crystal that was used for the U.S. navy and was superseded by the ceramic barium titanate in the early 1950s because of its excellent piezoelectric properties [41, 42]. There have been many developments in piezoelectric transducer materials since then and developments and applications of piezoelectric transducers are continuing [43].

Ultrasonics evolved after the two world wars and then divided into two distinct directions, large scale techniques and small scale applications. Large scale techniques, such as non-destructive testing by Sokolov [44] in 1920 who investigated the possibility of using ultrasound to detect flaws in manufactured components, and the evolution of sonar for use in antisubmarine warfare, were two of the main applications. Work by Wood and Loomis [45], who invented a high power oscillator tube which operated at frequencies from 200 – 500 kHz, investigated the possibility of applying the oscillator to various high power applications such as drilling, etching and cutting. They also observed modal patterns in rods, tubes and plates and manufactured an ultrasonic horn by tapering a glass tube to a point to concentrate the ultrasonic energy at the point of application. The first high power ultrasonic systems were used in industry between 1940 and 1955.

2.2 History of the design of ultrasonic tooling

The theory for designing acoustic horns has been researched extensively following pioneering work by Merkulov [117]. Merkulov [117] analysed ultrasonic concentrators, or sonotrodes, and calculated equations to compute the resonant dimensions of the horns and gain coefficients, the magnification factor of the ratio of the input to output amplitude, based on theory from the longitudinal vibration of rods with a variable cross section. Horns with a range of profiles, such as conical, exponential and catenoidal, were investigated in the study and findings proved that horns with a catenoidal profile produced the highest gain and gain was only limited by the strength of the material. Ensminger [118] produced equations for particle velocity, particle velocity amplification, stresses, length and mechanical impedance for horns excited in the longitudinal mode with solid conical profiles. The author's research was based on the assumptions that the system is lossless, Poisson's ratio may be neglected and the lateral dimensions are small compared to the length of the horn. Ensminger compared calculations based on his equations for gain from Merkulov's previous predictions of a conical steel half-wavelength resonant horn tuned to 20 kHz and found that his equations predicted a gain of 4.61 compared to Merkulov's 4.6. Neppiras [119] compared horns with various geometric profiles

such as cylindrical, exponential and Gaussian and discussed the suitability of the material for construction of the horn and concluded that titanium alloys were the most suitable due to low internal losses and high stress threshold. Belford [120] studied the ability of a solid stepped horn, that could be machined more easily than catenoidal or exponential profiles, to produce very large amplitudes of vibration for an applied force. Belford's findings predicted that for predetermined end diameters of the horn the stepped horn produced a higher gain than exponential or catenoidal horns.

Amza and Drimer [121] determined experimentally that in the vicinity of the longitudinal mode of vibration for exponential, catenoidal or conical shaped horns there often exist other modes of vibrations in the torsional or flexural mode that are excited from dissipation of some of the ultrasonic energy. As gain is increased these modes become more noticeable when the horn is excited. The authors also realised that the catenoidal shaped horn produces the largest gain between two given diameters of bar and their actual calculated resonant frequency was always higher than the frequency predicted from the actual experiment. To correct the frequency variation the authors derived a length correction factor which could be used with the original equations to allow the computation of effective working lengths of the horns. Satyanarayana *et al* [122] discussed various ultrasonic concentrators used for ultrasonic machining, including rods, conical, stepped and exponential concentrators. Findings concluded that the exponential concentrator provides the highest gain factor but is the most difficult to machine. Formulae were also derived to calculate the resonant length, gain, displacement and maximum stress nodes of the horns. Horn design and choice of horn for a particular application were discussed by Muhlen [123]. One of the main conclusions was that selecting a very slender horn design should be avoided due to manufacturing difficulties and excitation of lateral modes of vibration in the component that could cause damage during operation. Muhlen also stated that stepped horns transmit low energy due to the extremely high stresses at the step between cylinders that can instigate horn failure.

Commonly now, ultrasonic concentrators can be designed quickly and accurately using the finite element method. This has also allowed shapes of ultrasonic components to be more complex. The design of plastic welding horns using finite element analysis was explored by Derks [124] who attempted to excite longitudinal modes of vibration in cylindrical and rectangular concentrators whose dimension perpendicular to the longitudinal axis was greater than a quarter wavelength. Pis *et al* [125] calculated the concentrator design parameters using the

computational package 'derive' and verified previous concentrator horn findings. He also stated that horns with higher vibrational magnification have higher maximum stress conditions. Amin *et al* [126] explored using finite element analysis to tune to resonance a cylindrical, stepped, conical and exponential horn and compared the finite element predictions for the natural frequency, gain, and resonant length to analytical methods which involve solving the principal horn design equations. The error between the two methods for all the horns was never greater than 2%. Amin *et al* also commented that for design of a stepped horn the junction between adjoining cylinders should be at the nodal point where there is no displacement as this is also the maximum stress location and is often the location of failure in the device. Amin also discussed the use of a threaded connection instead of brazing or cementing the horn to the transducer and offered finite element analysis as a tool to model the threaded connection accurately, which was not possible using analytical horn design equations. The authors concluded by designing a horn with two conical profiles tapering to a cylindrical section, using an optimisation procedure to obtain maximum gain. Sherrit *et al* [134] presented a variety of novel horn designs including inverted, folded and flipped geometries designed using finite element analysis. Wakako *et al* [135] adapted an ultrasonic scalpel for endoscopic surgery to produce a curve in the tool using a super elastic alloy for surgical procedures. The horn was designed and tuned using FEA and verified using a laser vibrometer and an impedance analyser and experimentally tested on chicken.

Finite element analysis is an effective design tool for modelling basic ultrasonic components but as the design of the ultrasonic components increases in complexity the process becomes less accurate and validation of the manufactured components from FE predictions is required. Lucas *et al* [113-115] used non-contact measuring techniques, such as 1D and 3D laser Doppler vibrometers which measure vibrational velocities normal to the surface of the components, and electronic speckle interferometry which detects in-plane and out-of-plane surface vibrations, to validate finite element models of ultrasonic components. After the models had been validated the authors proposed redesign strategies [99-112] to alter the structural geometry to improve the system response and resonance condition. These strategies were used successfully in characterising single and multi-component ultrasonic tools for various ultrasonic cutting applications.

Recently, research into tuning ultrasonic components to flexural and torsional modes of vibration has been investigated. The development of the torsional transducer and the combined sandwich

torsional and longitudinal transducer allowed ultrasonic components to be excited and driven at modes of vibration other than the longitudinal mode. Lin [127] tuned an exponential horn to a longitudinal-torsional mode of vibration for use in an ultrasonic welding system. The incorporation of using longitudinal-flexural and torsional-flexural complex modes of vibration in an ultrasonic system using a sandwich transducer and a horn was studied theoretically and experimentally by Zhou *et al* [128]. The utilisation of complex modes of vibration for ultrasonic welding has been investigated deeply by Tsujino *et al* [129-133].

2.3 Ultrasonic machining

Ultrasonic machining (USM) is a mechanical process for manufacturing components from metallic and non-metallic materials preferably of a brittle nature with low ductility and with a Rockwell hardness greater than 40 HRC. In 1927 work by Wood and Loomis developed the concept of ultrasonic machining and the first patent was granted in 1945 to Balamuth [53]. USM has been given various names throughout the years from ultrasonic cutting, ultrasonic drilling, ultrasonic abrasive machining and ultrasonic impact grinding [46-52].

Manufacturing components and complex shapes economically and precisely from hard brittle ceramics, silicon nitride, various types of corundum: sapphire or ruby, glasses and composites have become increasingly important in recent times due to demand from the electronic, optical, semiconductor, medical, aviation and automotive industries [51-70]. These materials are preferred over metals for various applications due to their chemical stability, ability to be used as electrical insulators, hardness and ability to operate at higher temperatures. However, traditional machining processes sometimes leave these materials impossible to shape and fabricate, as the conventional cutting approach is fracture dominated in the material at the tip of the cutting tool. In brittle materials a fracture dominated process causes cracks to propagate quickly through the material in uncontrollable directions at the tool tip. This uncontrollable crack propagation causes chipping and fracture, which often results in poor surface finish on the material. Ductile materials do not exhibit this behaviour due to the localised plasticity in the material around the tool tip at the cut interface, which causes the material to separate at a very small distance ahead of the crack tip. This speed of separation is governed by the speed dictated by the tool tip as it translates through the material. Few machining options are available to fabricate components from brittle materials with diamond grinding usually the preferred option. However, this method is usually only feasible for geometrically simple components which are flat or cylindrical and the

process can inflict damage to the surface and sub-surface of the material, which is undesirable for more complex components such as turbine blades which are highly stressed in operation. Other manufacturing alternatives available to machine complex geometric shapes such as electrical discharge machining (EDM) or electrical chemical machining (ECM) are usually preferred, but only work on metallic highly conductive materials and can also cause surface and subsurface damage to a component during manufacture due to the thermal cutting mechanism. Manufacturing complex shaped components from ceramics, composites and other non-conducting materials is in demand and USM is a viable alternative that is non-thermal and has the ability to fabricate components from non-conductive materials, producing little surface and sub-surface damage to the workpiece.

2.3.1 Ultrasonic machining processes and operations

USM typically uses a guillotine configuration where a tuned ultrasonic cutting tool is moved axially into the workpiece by a static force using a pneumatic, hydraulic or solenoid feed system with the option of applying abrasive slurry simultaneously at the cut site. The system should maintain a uniform force while machining for optimum results. Cutting rates must be selected with caution as cutting too quickly can cause jamming or breakage of the tool in the machine and too slowly reduces productivity in the machining process. Abrasive slurry containing either silicon or boron carbide particles in the fluid which have a very high hardness, can be applied by pumping directly onto the work piece or through the horn, which can also serve as a coolant during operation. In addition, the abrasive slurry can be sucked through the horn by a vacuum pump to aid material removal or driven onto the cut interface. The slurry delivers abrasive particles to the material-tool interface, which complements cutting, allows cavitation to occur due to the high oscillatory movement of the tool and fluid interacting which complements material removal, flushes debris material away from the cut site and cools the tool, horn, and work piece during operation. The cutting tool vibrates quickly smashing the abrasive grains in the slurry into the material causing micro cracking and then material removal [51]. This process can be improved with the application of rotary movement to aid material removal at the interface and improve accuracy in cylindrical shaped cuts. This procedure is commonly called rotary ultrasonic machining (RUSM) [52, 55]. RUSM is a commercially recognised, low cost and reliable method for machining circular holes in hard brittle materials and was invented in 1964 by Legge [51]. Another adaptation was investigated by Pei *et al* [55] who used rotary ultrasonic face milling in the fabrication of components from ceramics.

Further investigations and adaptations of ultrasonic machining have involved turning of aviation materials. Astashev and Babitsky [46] considered the improvement of this process using superimposed ultrasonic vibration on the cutting tip which changed the process to a repetitive incremental vibro-impact process with the work-piece being rotated in a lathe. This vibro-impact process had difficulties maintaining the resonance condition whilst cutting due to the nonlinear interaction of the tool and work-piece. The incorporation of closed loop feedback control in the system to allow the tool to sustain resonance during cutting by automatically adjusting the frequency of the generator to provide the system with the ability to "self tune" during variations in dynamic loading and cutting conditions was developed to help alleviate the problem. More recently the option to maintain resonance and tip amplitude to further improve the cutting process further has also been developed [71]. The closed loop feedback control incorporated in the cutting system is used to attempt to achieve the steady state cutting process but in reality a truly optimum ultrasonic cutting performance can never be achieved as the loading is continually changing during cutting. Ultrasonic cutting using an auto-resonant control system is flexible and robust where variations of cutting tools, cutting speeds, depths of cut and the opportunity to cut many different materials using the same system are an option. Work by Astashev [46] showed that for a fixed cutting speed, applied force decreases with an increase in vibration amplitude. Also, other common traits of ultrasonic cutting were observed in his work such as reduction of residual stresses in the work-piece, strain hardening of the material, machining time, noise and surface roughness. Experimental analysis concluded that surface roughness and roundness of components had improved by 25-40% and 50% respectively in the machining trials. Also utilisation of ultrasonic vibration whilst cutting soft ductile materials such as aluminium or copper abolished the build up edge that is found in conventional cutting [70].

USM is used in many drilling processes to manufacture simple blind or through holes in a material. In the fabrication of deep holes Neugebauer *et al* [48] observed decreased cutting forces, higher removal rates, decreased friction in the tool-work piece zone, and longer tool life in addition to improved chip formation in ultrasonically assisted drilling. Many problems arise in drilling operations due to chip formation and removal, burr formation at tool exit and process reliability. However, as new materials are being developed and the needs for precision components are in demand by industry, improvement in the accuracy of deep drilling of holes is required. Conventional drilling uses a rotary movement allowing continuous contact and a continuous cut due to the tool and the material being permanently in contact at the interface. Drilling with the aid of ultrasonic vibrations superimposes a sinusoidal high frequency

oscillation onto the tool. Neugebauer *et al* [48] noticed that the cutting performance is directly related to the geometry of the cutter, the inclination and orientation of the rake angle, wedge angle and tool clearance angle. In addition, to achieve optimum performance in drilling with ultrasonic vibrations, the vibrations should be directed on the tool material interface. There are three possibilities to achieve this; excitation of the tool, excitation of the work-piece or excitation of the entire tool spindle.

Several adaptations of the USM process have been made to allow complex cut outs in the material similar to die sinking, which allows complex three dimensional shapes to be machined where depth can vary along the profile of the workpiece [49-52, 55, 60, 62]. For example graphite electrodes required for electrical discharge machining, which take typically 20 hours to machine by copy milling were manufactured in as little as 30 minutes with this process. When tools are complex shapes, non-uniform tool wear can result due to machining rates differing over the working surface and complex tools often are difficult to manufacture and tune to resonance. However, advances in FEA have assisted in the development of more complex ultrasonic cutting tools. In addition, some rotary CNC ultrasonically assisted machines are available commercially, which allow complex shapes to be manufactured [54].

The rapid expansion of the electronics industry and the need to produce smaller microchips and semiconductors has driven the development of micro-machining techniques such as micro-assisted lapping to assist in manufacturing low cost high precision non-silicone materials [56-58]. There are two common methods; the traditional sinking method where a load is applied to the base of the work-piece, traditionally used to drill blind and through holes; or the path controlled method, where the work-piece is moved in any direction to manufacture complex shapes. Micro-ultrasonic assisted lapping and ultrasonic vibration cutting [59-64] are two of the most successful processes in manufacturing small micro-components of hard brittle materials due to reduced machining force. Ultrasonic assisted lapping is similar to conventional ultrasonic machining, where an abrasive slurry is passed under a vibrating tool and the high frequencies supplied by the sonotrode repeatedly hammer the particles of slurry into the material causing micro-cracks and eventually material removal. Thoe [51] described this mechanism as mechanical abrasion, by hammering the particles into the surface, combined with cavitation from the slurry which results in micro-chips at the interface. However, micro-assisted lapping [64] has some difficulties, namely manufacturing and tuning a tool to the micro-scale, maintaining a constant depth of cut due to high tool wear, and physically aligning and connecting the tool to

the sonotrode which, if done incorrectly, could cause the tool to break or not function properly. Several advances in machine configuration to overcome these common problems have been proposed such as rotated tool, on machine tool preparation, applying ultrasonic vibration to the work-piece and compensating for tool wear by feeding the material into the tool to compensate for the worn tool.

The use of ultrasonic vibration cutting to machine particle reinforced metallic matrix composites was studied by Zhao *et al* [63]. These materials are based on a metallic matrix of a light material such as aluminium which is reinforced with particles to increase hardness. There are two different kinds of metallic matrix composite, particle reinforced which exhibits low weight, high strength, high stiffness, and whisker reinforced which has very high elastic modulus and strength. These materials are advantageous for use in many industries but provide problems in machining due to their hardness and complex material structure and often result in increased tool wear, reduced surface finish and reduced manufacturing precision. Difficulties in manufacture, and requirements for high precision components from these materials, drive the need for highly precise and efficient machining. Research is directed towards studying conventional cutting methods and improving the endurance of cutting tools, however, little research has been directed towards the study of other non-conventional techniques such as ultrasonic machining. Studies of the chip shape show that traditional cutting produces a spiral chip with a small curl radius with toothing edges on either side of the chip. In addition, there are folds on the back due to pile up of the material when the chip is highly distorted, producing a short thick chip. In vibration cutting a long thin loose spiral chip is observed with a large curl radius. This is due to the intermittent contact of the tool and work-piece at high frequency causing less cutting deformation, increased crushing at the front and side of the chip and regular ridges along the chip. Ultrasonic vibration cutting is a process where discontinuous contact between the tool and work-piece can be represented as a reduction in the coefficient of friction at the cut site. This discontinuous contact was found to produce an oxygenated flat (layer of air), which prevents bonding between the tool and work-piece, hence reducing the coefficient of friction. Tangential residual stresses in ultrasonic vibration cutting are higher than conventional cutting due to the ironing effect of the vibration cutter. This effect reduces if the speed of cutting is increased because the separation time of the tool and chip is shorter, resulting in a decrease in the residual stress. Axial stress is however related to the feed-rate of the material. It was found experimentally that the conventional cutting process produces surface burrs, built up edges and the surface finish is poor

whereas ultrasonic cutting reduces tearing, plastic deformation and build up edge and is a more stable process [59].

2.3.2 Mechanisms and considerations of ultrasonic machining

The mechanism of material removal has been studied by several authors including Miller [72] and a review of the main mechanisms of material removal and the corresponding authors who studied the mechanisms is available in Thoe *et al* [51]. The main mechanisms include mechanical abrasion, micro-chipping, cavitation and chemical effects due to the fluid in the slurry. These effects either combined or separately result in the material being removed by shear, fracture and plastic deformation. Significant cavitation effects have been noticed in the machining of porous materials such as graphite. However, Markov and others considered cavitation erosion and chemical effects to be secondary mechanisms [269]. Various studies have been carried out to observe the effects of varying several operating parameters on the material removal rate [65-70]. Various researchers have tried to compare the amplitude of tool vibration with material removal rate. There have been quite inconclusive results however, in general, as amplitude increases material removal rate increases if all other parameters are kept constant. Rozenberg *et al* [270] and Kainth *et al* [271] both showed that by increasing static load material removal rate (MRR) increased up to an optimum value then MRR reduced due to reduced slurry circulation and smaller particles reaching the tool work-piece interface. However, Kops [272] stated that for optimal performance, static load should not be increased to the optimum value because tool wear increases due to increased abrasive wear. The type of abrasive slurry has a direct influence on MRR and in general the abrasive particles should have a higher hardness than the work-piece, and the larger the size and concentration of abrasive particles the higher the MRR. Increasing the size and concentration of the abrasive particles yields a higher MRR up to an optimum level because larger particles will have greater difficulty reaching the cut site. Kazantsev [273] showed that increasing delivery rate of the slurry to the site increased MRR without the need to increase static load, grit size or concentration. Pentland *et al* [274] determined that by improving circulation of the abrasive slurry, cavitation effects, blockage and contamination were reduced. MRR is also directly related to the geometry of the tool, namely the ratio of tool area to tool perimeter. Goetze [275] compared tools with the same contact area and various perimeters and claimed that the larger the perimeter the larger the penetration rate, mainly due to the distribution of the abrasive slurry over the cut site. For RUSM the rotational movement increases MRR accuracy, reduces cutting forces and increases tool life. Komaraiah *et al* [276] claimed that RUSM was more efficient for machining than USM because there were

combined effects from indentation of the surface of the work-piece, sliding contact between the embedded grains, and rolling contact from free moving grains. For RUSM Komaraiah [276] and Prabliakar [277] stated that higher rotational speeds increased MRR.

Another significant variable in USM is tool wear. Tool wear has been shown to occur in USM, due to cavitation effects at the tool-work-piece interface, when very hard and coarse abrasive particles are used in the slurry. Venkatesh [278] and Adithan [279] stated that maximum tool wear occurs at the optimum static load for MRR. Tool wear can also be affected by the hardness and surface roughness of the work-piece. When the tool is work hardened the MRR will increase due to a decrease in penetration of abrasive particles and debris removal from the sides of the work-piece will increase, often resulting in the formation of a convex surface on the material. Tool wear also increases with increasing depth of hole and cutting time.

Surface finish is very important in machining and low thermal operation of USM reduces thermal damage and residual stresses in the material. The grain size in the slurry has a direct influence on surface finish and accuracy. A reduced grain size leads to a better surface finish and a hole with a higher accuracy. Dam *et al* [280] stated that surface finish improved when feed rates and cutting depth decreased. Kennedy [281] and Koval'chenko *et al* [282] claimed that the uneven slurry distribution at the bottom of the hole renders it difficult to machine a flat hole. Shaw [283] stated that increasing static load increases surface finish due to larger abrasive particles not being able to move into the tool – work-piece interface and also due to the reduction of lateral vibrations minimising out-of-surface roundness of holes. It has been shown that using tungsten carbide and stainless steel as tool materials, using an internal slurry system and tools with tapering walls, reduces conicity. Kremer [284] stated that graphite machining by USM produced a rough surface finish due to cavitation and blockage and contamination of the slurry by debris. The use of machine oil in the slurry instead of water led to an increase in the surface finish of the materials but reduced the cutting rate.

2.4 Ultrasonic cutting

Ultrasonics has enhanced the cutting of various materials and products in a variety of different industries. Ultrasonic cutting has been used in the creation of components from wood, plastics and glass. In 2005 Sinn *et al* [73, 74] compared the reaction forces and chip thicknesses in conventional and ultrasonic cutting of spruce, beech and MDF in the wet and dry states.

Dependencies between the cutting force and blade tip amplitude were also discussed and results indicated that the use of superimposed oscillations on the blade tip reduced the cutting force in all materials in both the wet and dry states and as the blade tip amplitude increased the cutting force decreased. The results also indicated that when all the materials were wet the cutting and normal forces were lower for both ultrasonic and conventional cutting compared to the dry state. The study concluded that ultrasonic vibrations superimposed on the cutting tool reduce the friction between the blade and the wood specimens and cause the cutting force to decrease. Comparisons of the surface roughness of the three materials when cut using conventional non-oscillatory cutting techniques compared to ultrasonic cutting were also investigated using scanning electron microscopy and surface topography. Findings proved that the mean surface roughness was similar using both conventional and ultrasonic cutting operations.

An investigation of ultrasonic cutting of polymeric materials was conducted in 2001 by Volkov and Sannikov [75] and findings proved that as the frequency of oscillation of the cutting tool increased between 20 and 50 kHz there was no observable effect on cutting performance. However, increasing pressure applied to the cutting tool and higher blade tip amplitude were found to improve cutting performance and later discussions involved increasing these parameters simultaneously to further improve the process. Kuriyama [76] successfully received his first patent in 2004 for creating a cutting device for wood and plastic using a resonant ultrasonic cutting tool.

Optical technology has advanced dramatically in recent years due to highly accurate precision technologies for manufacturing precision lenses or other optical components using plastics or glasses. Kim *et al* [77] investigated the use of ultrasonic cutting to machine precisely optical lenses from optical plastics to produce a mirror finish and remove any requirement for finishing using other processes such as grinding or polishing. Findings proved that ultrasonic cutting decreased brittle fracture and irregular crack formation in the work-piece compared to conventional cutting techniques and subsequently decreases the waviness and roughness of the surface of the work-piece. Zhou *et al* [78] further researched ultrasonic cutting of optical glass using superimposed ultrasonic vibration on a diamond tool. The research proved the critical depths of cut was dependent on the ratio of cutting speed of the work-piece to vibration speed of tool. The cutting force was significantly reduced and this was believed to be due to dynamic friction and lubrication between the tool and work-piece, which the authors believed to be two of the main reasons for the increase in the critical depth of cut.

Osteotomes such as tools, chisels or other primitive surgical tools date from the 17th century and were adapted from instruments used for cutting wood [79]. Several devices are currently used in surgery at present, including mechanical knives, high frequency electric knives and laser knives to name but a few. Further, research has adopted ultrasonic tools as surgical instruments. This technology has significant advantages for several medical procedures such as the ability to minimise bleeding, cut bone and tissues and minimise possible damage, trauma and pain to patients [85]. There are extensive applications of ultrasonics in medicine, such as dental devices [86, 87], brain surgery, nerve surgery and ocular surgery [88].

Technological advancements in surgical instruments have included motorised cutting devices such as rotary, oscillating or rectilinear motion saws or non conventional techniques such as laser, water jet or ultrasonic cutting techniques. Using oscillatory motion in surgical procedures was established in 1955 when Vang *et al* designed a surgical scalpel which oscillated in the longitudinal mode at frequencies between 6 and 12 kHz. Further improvements of this original design were made by Shafer in 1958, when a piezo-electric crystal was substituted for the solenoid-magnet transducer assembly, and by Sawer in 1974 who had a patent granted for an electronically powered knife based on the original concept by Vang [89]. Many further investigations occurred comparing ultrasonic cutting devices to alternative cutting technologies and these were reviewed by various authors all discussed by Giraud *et al* [79]. Conclusions proved that ultrasonic cutting could be a viable alternative to conventional cutting techniques however, several issues needed to be addressed. Namely, designing ultrasonic cutting tools for cutting bone and tissue, addressing the problem of very highly localised temperature increases at the cut site to levels above the necrosis value and possible fatigue failures of the cutting tools during surgery that could damage neighbouring tissues or bone. Scaling down the ultrasonic cutting tools into micro-cutters for delicate surgical procedures has been reported by several authors [80-84].

2.5 Ultrasonic cutting of food

The introduction of ultrasonic cutting in the food industry is very recent and dates from the middle of the 1990s. The process was adapted from ultrasonic welding technology and was found to have several benefits in the cutting of food products. High quality food manufacture requires cutting tools that produce minimum waste and produce high cut quality. Often food

products cut with conventional cutting tools require specialised processing prior to cutting such as freezing. The cut quality of the food product is governed by blade shape, cutting force, sharpness, cleanliness, blade motion, orientation and speed through the product [2, 90, 94]. Alternative technologies such as high pressure water jet cutting or laser cutting are extremely effective in producing precise cuts, but have limitations [95-98]. Laser cutting is expensive to operate and can chemically react with the product being cut, and water jet cutting can form sludge with food waste that can add to the plant's waste water. Both processes have difficulties controlling the depth of cut. Traditional rotational disc cutters are inexpensive but food adheres to the blade and fouls the cutting tip which reduces the cutting performance of the blade and often requires the process to be shut down for cleaning. Poor cutting performance can affect the product's shape, size and appearance. Often the product shatters or deforms with smeared, burned or melted edges at the cut site. Multilayered materials can often become separated, smeared or crumbled during cutting, resulting in high material wastage. Food materials are extremely complex and their material properties change over time and with temperature. Temperature and aging can have a significant impact on the texture of the food product and on their ability to be cut. Freezing or semi-freezing, commonly known as tempering, the food material prior to being cut is a common method for improving the cut quality of food products that are easily smeared or are sticky, but this additional process increases operational costs. Removal of these processes could therefore have considerable time, energy and cost savings/benefits for the manufacturer. The main aim for food cutting in industry is to minimise product damage and waste whilst maximising productivity.

Commercial production of food products is usually accomplished by making large bulk quantities which are produced in blocks or sheets, which need to be reduced in size by cutting to enable them to be made available to the consumer in convenient sizes through the retail market. On a commercial scale, custom made machines are specifically designed to cut a particular food product effectively based on size requirements. Several commercial systems are available, from suppliers including Branson and Dukane [16-18], that offer the ability to cut soft, sticky food products without pre-processing. Various sizes and styles of machines are available and they can be installed as stand-alone machines or in automated production lines in guillotine or slicing configurations, a mixture of either configurations or several different arrangements on custom designed lines. Guillotine rotary ultrasonic cutting machines are available and are usually extremely flexible with a range of click stops on the table to allow accurate positioning of the product or the cutting tool which allows for a large variation of cutting arrangements depending

on what material is being cut or what shape is required. Manual machines or profile cutting machines are also available and are usually customised to a specific operation but supply a lower throughput of product and sometimes can have an increased cost of operation due to an operator being required. Various simple or complex cutting shapes can be made by manipulation and repositioning of other cutting blades in the production line which allows the system to be extremely flexible.

The visual appearance of a food product is of paramount importance as this factor is one of the main driving forces behind a consumer buying the product. For this reason, food products have a requirement that the cut surfaces of the product have to be visually attractive and have high quality with good surface finish. Ultrasonic cutting complies with stringent food hygiene requirements in industry and has been found to produce food products that are visually appealing with reduced smearing, crumbling and melting at the cut interface between the blade and material. The high quality of cut produced during ultrasonic cutting ensures there is little debris associated with the cut and that no trimming is required, which ensures high throughput with minimum waste. Benefits of the process also include reduced cutting force, simplicity of automation, low running costs, low tool wear and consequently increased tool life, self cleaning blades due to the high surface accelerations on the blade and low chance of shatter in brittle products. Ultrasonic cutting can be applied to a wide and diverse range of products. Multilayered products are cut easily resulting in less separation and even hard pieces such as nuts in soft products can be cut effectively. Schneider *et al* [136] reported that when the ultrasonically excited cutting tool interacts with food of high fat content, secondary mechanisms such as cavitation occur at the cut site which may initiate chemical reactions and food degradation. The ultrasonic cutting process is simple to operate and operators can monitor or adjust parameters at any time such as cutting speed or set up the process to change automatically during cutting. Many foodstuffs are suitable for cutting by ultrasonic cutting such as frozen foods, hot bread or difficult to cut sticky foods such as confectionary. Material parameters attributing to cutting performance include temperature, stickiness, toughness, moisture content and material consistency. Improved cut quality and reduced waste by eliminating uncontrollable fracture at the cut interface of many food products, including brittle confectionary products, have been widely documented [2, 16-18, 90-94].

Research by Cardoni and Lucas [91] has proved blade breakages during cutting can be reduced by improved design of the ultrasonic blades where consideration of the linear and non-linear

dynamic responses are analysed at the design stage. Lucas *et al* [99-116] has published several research papers to provide methods for characterising the dynamic interactions of ultrasonic cutting systems and provide practical design solutions for ultrasonic cutting blades. The main research and development of ultrasonic cutting technology focuses directly on the operation of the ultrasonic cutting system comprising of the generator, transducer and cutting tool whilst neglecting the cutting operation or investigation into the interaction between the cutting tool and the material to be cut. At present ultrasonic cutting systems are being adapted from existing systems currently available to provide a method for separating new materials using new blade designs based on empirical approaches. Resulting ultrasonic cutting products are often restricted in their performance during operation and produce cuts in products, especially multi layered products, of a low quality. In the food industry very few food materials or products consist of one homogeneous material but usually of several combined. Often when cutting multi-layered products the cutting tool will cut one layer effectively and produce a low quality of cut to the others or sometimes not cut them at all. Investigating the interaction of the ultrasonically excited cutting tool with the food material during cutting could increase the cutting performance of the ultrasonic cutting tool. Knowledge of the ultrasonic cutting parameters prior to cutting would allow the ultrasonic cutting system to be set up to optimise cutting of a particular product and produce a high quality cut.

2.6 The mechanical properties of foodstuffs

Food products behave very differently from metallic, plastic or composite materials and many researchers have attempted to characterise mechanical properties of various food materials for a wide range of applications. Nesvadba *et al* [137, 138] discuss the requirements of physical mechanical and thermal data and standards for testing foodstuffs for use in the food industry. Knowledge of these properties in the literature or stored on a database would offer food technologists, the food industry or other industrial companies access to accurate data which could allow modelling of manufacturing processes and provide an opportunity to develop more sophisticated processing machinery more cost effectively. Due to the economic importance of nuts and seeds, used as food additives, medicines or for export in countries such as Nigeria, India and Turkey, many researchers [139-145] have studied their mechanical properties with the aim of developing handling, transport and processing machines to improve the quality of the final product, reduce labour intensity and reduce processing times. Mechanical properties such as seed

rupture force, deformation and seed orientation are derived from simple quasi-static compression loading.

Research has been performed to try and correlate the mechanical properties of food with sensory evaluation. Sensory evaluation is important to the food processing industry, as food texture is of paramount importance to the way consumers enjoy food products. Sensory evaluation is labour intensive, expensive and is thought by many as ineffective for quality checks. However, if mechanical test data such as fracture toughness, Young's modulus and hardness could be correlated to texture, crunchiness and crispness, this would mean that food quality could be cheaply and easily assessed. Eves *et al* [146] described the existing tests used to determine the stickiness of toffee, by determining the force required to pull apart two plates stuck together with toffee, and the snap test for chocolate. Various investigations have been performed to try and characterise the texture of food products. Aguilera [147] discussed extensively the importance of applying concepts and methods from materials science to food products to explore their structure and composition and relate the findings to perceptions of texture. Air pockets, microstructure and fibres were all discussed with reference to the food structure. Possible adaptation of the food structure to give the desired product texture to the consumer were proposed. Ross *et al* [148] performed tension tests on fried potato crust to generate fracture toughness values using both the generalised fracture mechanics approach and the brittle fracture approach to correlate fry time with mechanical properties. As fry time increased the material changed from a ductile to brittle material. Vincent *et al*. [149-151] measured the critical stress intensity factor for various fruits and vegetables using three point bend tests and compared the results to a team of panellists' sensory results. The hardness and crunchiness of the material are very closely related to the stress required to cause crack propagation through the sample. Crispiness could be related to the sudden drop of force on the load-displacement curve which is associated with the rapid propagation of fracture such as a brittle fracture process. This parameter was tested on crisps, which were not viscoelastic in nature. An alternative method used by Vincent [149] relates the sound produced when a material is broken to the acoustic sound produced by a fracture event that can also quantify crispiness.

Various authors [152-159] have characterised gels and films using mechanical testing techniques such as the compression and tension test. The mechanical properties of Alginate gels were studied by Mancini *et al* [152] who used the compression test and stress relaxation test to characterise the viscoelastic properties of the gel materials. These testing configurations provide

a means for characterising the gelling ability of commercial alginates used in the manufacturing process and offer the possibility to guarantee the gel strength of the material with minimum alginate concentration and minimum cost to the manufacturers. Tang *et al* [153] studied the stress-strain relationships of gels with different gellan polymer and calcium concentrations in tension, compression and torsion. This gave a deeper insight into the gel's mechanical behaviour compared with using compression tests alone. The stress-strain diagram for each gel in each testing configuration was considered and the results showed that for gels containing 1% gellan polymer had identical tensile and compressive moduli at small strains, <0.04. The tensile, compressive and torsion data were curve fitted using the Mooney-Rivlin strain energy potential, and three other adaptations of this equation, to characterise the best fit to represent the material data accurately for modelling purposes. Protein films were investigated mechanically in tension by Liu [154] *et al*. to characterise the effect of different treatment methods, such as chemical, ultrasound, heat and ultraviolet radiation, on the films and their suitability to create bio polymeric films for packaging. The mechanical properties of β-lactoglobulin films formulated with different plasticisers were researched by Sothornvit [155] in tension to evaluate the mechanical properties of the films and determine the most suitable plasticiser and the concentration of the plasticiser against the desired mechanical properties of the films. Jagannath *et al* [156] studied the effect of starch concentration on the mechanical and thermal properties of low density polyethylene film for use as a biodegradable plastic for food storage. The mechanical properties were determined from simple tension tests using the American Society of Testing and Materials (ASTM) methods and the thermal properties, such as the glass transition temperature, were measured with a differential scanning calorimeter (DSC) and a dynamic mechanical thermal analyser (DMTA). Both thermal methods used to calculate the glass transition temperature were similar, as glass transition determination depends on testing conditions and sample preparation. Caner *et al* [157] also used the tensile test to determine the modulus of elasticity, percentage elongation and tensile strength for various multi-layer films and scanning electron microscopy to determine the damage of the film before and after high pressure processing (HPP) for food storage requirements. Ettelaie [158] reviewed various literature on mathematical modelling and computer simulation of food colloids and concluded that currently models of food system behaviour are not advanced enough to predict colloid behaviour.

Boakye *et al* [159] studied the textural properties of beef from slaughter to 16 days after slaughter and investigated the mechanical properties of the meat using hardness tests. The study

included detailed discussions of hardness, cohesiveness, gumminess, springiness and chewiness of the meat as it aged. This study proved that packaging and storage conditions of the meat such as temperature and humidity could age the meat during transportation. The rheological and mechanical properties of smoked sausage and the effect that composition of fresh and frozen broiler chicken, B-vitamins and processing conditions had on the shear force, hardness, cohesiveness, springiness and chewiness of the meat were studied by Awonorin [160, 161]. Findings proved that compressive stress, hardness and cohesiveness of the meat reduced as the percentage guinea fowl in the sausage decreased. Tocci *et al* [162, 163] investigated the thermophysical properties of various meats, including thermal conductivity, specific heat capacity and enthalpy using differential scanning calorimetry and the transient probe method to calculate the cooling or freezing times of various meats to allow for advanced design of refrigerator equipment.

Various authors [164-168] have investigated how food materials fracture. Investigations on how particle shapes and air holes within the material cause stresses and propagation of cracks along fracture paths using gelatinised starch [164, 165] have been researched. Fracture toughness and examination of the fracture surfaces of Sephadex/protein gel has also been studied [166]. Stress fields and cracking of spherical foods during freezing [167] and measuring fracture stress in compression of soybean curd at low temperatures have also been researched [168].

Mango maturity was studied and predicted by Jha *et al* [169] using parameters such as sphericity, firmness, colour and size. Chiralt *et al* [170] investigated how osmotic dehydration of fruits using sucrose solution affected the textural properties and appearance of kiwi fruits, mangos and strawberries using the uniaxial compression test. Similarly, the mechanical properties of dried apples and the effect temperature and water retention had on the apples was investigated by Lewicki *et al* [171] using uniaxial compression relaxation tests. Other mechanical properties such as fracture toughness and failure paths of apples, carrots, lollipops, chocolate, rice treats and Tootsies rolls were investigated by Pepi [172]. Schantz [173] investigated the effect common emulsifiers had on the rheological properties of milk and dark chocolate. Brunllo [174] studied the mechanical properties and microstructure of cocoa butter using a rheometer to determine viscosity measurements and micrographs. These were used to allow processors to develop processing parameters specifically required to produce a specific product for market. Other researchers [175-178] have investigated mechanical properties of fruit and vegetables. Bananas were researched to gain knowledge of the force required to cut bananas

at different sections of the fruit [175] to aid the design of processing equipment to peel and cut bananas. Physical dimensions of different grades of Egyptian onions and different mechanical properties such as coefficient of friction and crushing load were also studied to aid the design of processing and transportation equipment [176]. Research into comparing the mechanical properties of different types of apples [177] and lettuce [178] to quantify the mechanical properties to peoples perceptions of texture were also actively studied. The mechanical properties of spaghetti and pasta were studied by Akiyama [179] and Cuq [180] in tension using a simple tensile test and by using a rheometer to determine the fracture stress and strength of the products at different temperatures and moisture contents.

Bread dough, tortillas and biscuits have been studied [181-190] to determine the mechanical and thermal properties of the materials and to model the material behaviour computationally. Charalambides *et al* [183-185] studied the mechanical properties of bread dough using the simple uniaxial compression test and the bubble inflation technique. The first test represents the uniaxial stress-strain response of the bread dough and the latter test represents the stress-strain data of the material in the equi-biaxial testing configuration. The uniaxial compression test is influenced by the friction condition at the interface between the platens and the sample being compressed. The lubrication condition can cause the specimen to deform into a barrel shape or an hourglass shape so it is important that the correct quantity of lubricant is used between the platens and the specimen to ensure the specimen deforms with straight sides. Specimen dimensions also have an influence on the stress-strain response of the material. The authors studied the effect of lubrication and specimen dimensions, such as diameter and height of the specimen, on the stress-strain response in compression for various lubricants and ratios of height to diameter of sample. The stress-strain response of the material was verified mathematically and also by finite element analysis of the uni-axial compression test. The bubble inflation technique is a method to determine the equi-biaxial stress-strain data of dough or other soft materials and has been used extensively for rubbers. A disc of the material under investigation is clamped around its perimeter and is then placed above an air inlet, controlled by a piston and cylinder configuration. When the piston is compressed, the air inflates the dough and the pressure, height of the bubble, thickness and strain of the sample during inflation is measured. The investigation found that the bubble shape was only spherical at small strains and as strain increased the bubble shape became elliptical. Also, the thickness of the bubble was non uniform, thinner at the top than at the clamping locations, and the specimen is not incompressible with a Poisson's ratio of 0.5 but is slightly compressible due to air pockets within the mixture and a Poisson's ratio of

0.46 represents the data more accurately. By combining the uniaxial and biaxial data the authors could represent dough using a hyperelastic constitutive equation incorporating time dependent and either incompressible or compressible behaviour to characterise the material for modelling purposes. Zhang *et al* [181] also studied the modelling of bread baking using the finite element method to investigate transport mechanisms such as temperature, heat flow and shape changes of the bread during baking. Matuda [182] and Clubb [186] studied the influence that emulsifiers and vegetable shortening had on the mechanical properties of French bread dough and the influence that glycerol and salt had on the mechanical properties of corn tortillas, using a differential scanning calorimeter (DSC) and a dynamic thermal analyser (DMA). The mechanical properties of biscuit dough was studied by Maache-Rezzoug *et al* [187] using the uniaxial compression test and conical penetrometry. Saleem *et al* [188] and Kim *et al* [189] determined the mechanical and transport properties of crackers and rich tea biscuits. The mechanical properties were used to model biscuit cracking for use in the food industry. Gormley [190] devised a simple 3 point bend test to measure the resistance to fracture of cream cracker biscuits and he compared the resistance to fracture of several leading brands and orientations of cream crackers and found that oven baked cream crackers were more resistant to fracture than under cooked ones.

Cheese has been extensively researched [191-207] in an attempt to characterise sensory perceptions of food texture by people to fundamental mechanical properties. This research is attempting to produce a more scientific approach to developing foodstuffs that are of a desirable, optimal texture and consistency that consumers want to buy. Currently in the food industry, panellists are used to decide if a food product is of correct texture and consistency and to check for quality, but each person's pallet differs slightly and a consensus between panellists is often difficult to achieve. A more scientific approach would enable manufacturers to target their product within a range of desirable mechanical properties and offer a more precise and cost effective method of determining the quality of their product. Cheese has been characterised by several researchers [194-206] using the uniaxial compression and tensile tests, the indentation test, stress relaxation test and the three point bend test. When conducting the uniaxial compression test between two platens, the cheese behaviour and stress-strain response is dependent on the sample dimensions, the frictional behaviour at the interface between the platens and the sample, the speed of compression and the age of the sample. The difficulty with using the compression test to characterise cheese behaviour is that there is no clear failure point of the material in compression, and failure is therefore often assumed to occur at the macroscopic

fracture point that is visible with the human eye or at the plateau region of the stress-strain diagram. Also, as the specimen is compressed, natural fats within the material ooze out and further lubricate the platens. This can cause over-lubrication and the specimen deforms in an hourglass shape. Fife *et al* [197] investigated pulling melted cheese in tension using a three pronged hook in order to characterise the mechanical behaviour and give an indication of how the cheese would melt and stretch on a pizza when it was baked and eaten. Usually testing food materials in tension is extremely difficult due to problems with gripping the specimen. Gripping soft food materials in tension can often induce failures in the material prior to testing or cause microscopic failures near the grips. Goh *et al* [198] used compression and indentation tests with a spherical indenter to determine the non-linear viscoelastic material properties of cheese. The viscoelastic behaviour was modelled using separable strain and time dependent behaviour. The strain dependant section is either linear or non-linear elastic and was modelled using the van der Waals hyperelastic function. The time dependent section was modelled using the Prony series, where the time dependent constants were found from relaxation tests. The authors also studied the fracture properties of cheese using the three point bend test and correlated the energy release rate from the test with an extrapolated energy release rate from wire and blade cutting tests. Atkins *et al* [207] also conducted simple cutting experiments on cheddar cheese and salami and offered an engineering solution as to why it is easier to cut when you push and slide the knife through the food material rather than just pushing the blade through the material alone.

2.7 Finite element modelling of conventional and ultrasonic cutting

Cutting or machining are the most common techniques used to generate components of a specific size and surface finish. The use of FEA to simulate cutting and machining processes without the requirement of experimental testing, has been explored over the last 10 years.

2.7.1 FE modelling of conventional cutting

Several authors [208-241] have simulated the machining of materials using FEA. Simulations developed by Tay *et al* [233, 234] and Lin *et al* [235] were initially concerned with the temperature distribution in the tool and work-piece and not with the actual separation of the work-piece due to the tool during cutting. Further research [238, 239] accounted for a separation of the cut material in chip formation by detaching the chip from the work-piece by separating the nodes along the cut path when a pre-determined failure criterion was achieved. Further enhancements of the separation process in chip formation were conducted by Strenkowski *et al*

[238], Konvopoulos *et al* [239] and Camacho *et al* [226] who incorporated the adaptive meshing or remeshing technique into their Lagrangian FE codes in order to avoid excessive distortion of elements. Marusich *et al* [221] further developed the chip formation model using a thermo-mechanically coupled approach using an explicit solver. An explicit solver is generally more robust than the implicit solver and is preferred for modelling of contact problems. The simulation accounts for the dynamic response of multiple bodies in contact, in addition to interfacial heat transfer using a continuous re-meshing technique. The cutting tool was represented as an elastic deformable body which improved on previous models which considered only a rigid body representation. The author accurately predicted the tool temperature and stresses during high speed cutting at a speed of 30 m/s. Knowledge of the temperature and stresses in the tool allowed evaluation of tool performance. Other authors then used this thermo-mechanical modelling approach, which is based on crack propagation modelled as node separation when the maximum critical stress and maximum critical shear stress is reached to model chip breaking processes. A variety of similar modelling configurations were researched based on other materials to be cut, element types, contact conditions and failure mechanisms to predict residual stresses, cutting force and power in an attempt to validate their FE modelling approaches with experimental tests to achieve optimum cutting parameters numerically opposed to experimental testing [213, 219, 224, 225,239].

Further work by Shirakashi and Obikawa [223] used an FE simulation to predict chip formation, distribution of residual stress in the machined material and also to investigate tool wear. Their modelling approach was based on a non-linear, plastic deformation analysis with time dependent heat flows, in which a large geometry change updated Lagrangian method was used. They used an iterative convergence method, where a separation of the nodes directly ahead of the tool tip is realised when suitable failure criteria are achieved such as stress or strain in the material and this allows the tool to advance in the material simulating cutting. But the authors stressed that this may not be the best method to model the machining process as tool advancement does not rely on the machinability of the work material. The contact condition between the tool face and the chip was modelled assuming non-linear friction using a non-linear stress equation.

The machining of two phase alloys of Ferrite and Pearlite with different material properties and compositions was investigated by Sasahara and Obikawa [240], to investigate the effects of ferrite on chip formation and compare simulation results to experimental tests. Sandstrom *et al* [220] used 2D FE models to investigate chip formation in the high speed machining of aviation

materials, especially to investigate the temperature and plastic strain in the material to be cut. Other authors [208-211, 215, 216, 223, 231] also investigated orthogonal or oblique cutting using 2D fully coupled models to investigate the effect of cutting parameters such as tool geometry, orientation and cutting speed on temperature, contact conditions, tool wear, stress and strain in the material using material representations, failure criterion such as debonding nodes using critical stress strain or strain energy density or element deletion.

McCarthy *et al* [250] investigated experimentally and numerically, the sharpness of surgical blades during cutting of an elastomer. A 2D FE modelling approach was developed utilising the symmetry of the cutting configuration. The elastomer was modelled using the Ogden hyperelastic strain energy density function and the scalpel blade was modelled as a rigid body. Cut initiation is determined from experimental tests by driving a scalpel blade at constant velocity into an elastomer substrate and photographing the deformation using a high speed camera. Comparisons between the experiments and FE model were then made for the deformation in the material at the point of cut initiation. Plotting the resulting von Mises stress distribution ahead of the blade tip indicated that the failure stress was maximum a small distance ahead of the blade tip indicating that failure would occur below the surface of the substrate.

2.7.2 FE modelling of ultrasonic cutting

Although FEA has been used extensively to simulate conventional machining processes, simulations of ultrasonic machining or cutting processes are limited. Smith *et al* [242] explored the possibility of representing ultrasonic cutting of a brittle material using a fracture mechanics approach where a crack propagates in a controlled mode 1 manner when the stress distribution around the crack tip increases and reaches a critical limit where the stress intensity factor K_{IC} of the material is achieved which causes material failure. Displacement boundary conditions at the crack tip corresponding to ultrasonic cutting blade vibrational amplitudes simulated the blade cutting the material.

Smith *et al's* [242] approach was adapted by Smith and Lucas [243] for ultrasonic cutting of bone. Bovine compact tension specimens were experimentally investigated to correlate with the fractures mechanics FE modelling approach. Prescribed vibration displacements were applied to the crack flanks of the compact tension specimens to simulate ultrasonic cutting. Findings showed that the critical load required to cause mode 1 failure in a compact tension specimen was

reduced with superposition of ultrasonic vibrations on the crack flanks and was also further reduced with increased amplitude of vibration.

Astashev and Babitsky [244] proposed that the ultrasonic cutting mechanism was that of a non-linear vibro-impact process. The authors investigated autoresonant control which used a closed loop feedback system to maintain the cutting system at resonance during cutting. The closed loop feedback allowed constant updating of the resonance condition which allowed the ultrasonically excited tool to be optimised during cutting to maintain the desired cutting parameters as the ultrasonic cutting blade progressed into the material. Babitsky *et al* [246] continued development of the autoresonant control of ultrasonically assisted cutting by using computer control to regulate the piezoelectric transducer during ultrasonically assisted turning, which ensured that the excitation of the vibrating system was maintained at a stable level under varying dynamic loads.

Mitrofanov *et al* [245] conducted the first finite element simulations of the ultrasonic turning process. Compared to conventional turning, advantages include a decrease in cutting force, improved surface finish, increased tool life and noise reduction. The ultrasonic turning process, where cutting is in the tangential direction, was modelled using a thermo-mechanical coupled model of the chip formation. The deformation at the cut site was compared to real time observations of chip formation at the cut site recorded using a high speed digital camera. Preliminary models considered the tool to remain static for conventional cutting and to oscillate for ultrasonic cutting, both with the material travelling at a constant speed into the tool. The material properties were considered not to be dependent on temperature and to be strain-rate independent. The initial model assumed that the friction at the interface was negligible due to the tool intermittently being in contact with the material. Automatic remeshing was used to overcome convergence difficulties that could arise with highly distorted elements, and the critical stress failure criterion was implemented to allow the material to fail when the nodes on the cutting path reach a critical stress value.

Babitsky *et al* [247-249] continued investigating experimental ultrasonic turning of aviation materials using an autoresonant control system, comparing the results with simulated turning using FEA. Findings suggested that the surface finish and roundness was greatly improved with ultrasonic vibration of the cutting tool. Improvements ranged from 25-40% for surface roughness and up to 40% for roundness. FEA results suggested that there is a comparison between

ultrasonic and conventional turning of Inconnel 718 in relation to the contact conditions at the interface of the tool and material to be cut, stress/strain in the tool and workpiece and in relation to the cutting forces.

Mitrofanov *et al* [249] further extended the FE model of ultrasonically assisted turning of Inconnel 718 to incorporate heat generation due to friction at the interface in the cutting zone. By using a fully coupled thermo-mechanical modelling technique, the temperature of the ultrasonically excited tool and work piece could be determined for conventional and ultrasonic machining. The cutting speed considered was 300 mm/s, frequency of excitation was 20 kHz and the tip amplitude was 13 μm. The contact condition at the interface was assumed to be a shear friction model which depends on the fraction of equivalent stress in the material and not on the normal contact force as in the Coulombic model. The material failure and separation criteria were based on the deformation method where plastic flow of the material was considered under the applied force of the ultrasonically excited tool. This failure method was preferred to element deletion or separation of nodes due to fewer convergence problems which allowed greater computational efficiency. The development of the chip and its shape during cutting, for a very short time period of 6 milliseconds, was investigated. The temperature and stress and strain distribution in the work-piece and the tool were also calculated. FE simulations with and without friction were developed and findings indicated that the chip formation neglecting friction at the interface had approximately 4 times less radius of curvature than with friction. Other effects common in ultrasonic cutting are reduced cutting forces during operation. These were considered to be reduced as the average stresses created in the material are lower as the tool only contacts with the material a fraction of the time thus reducing the applied cutting force during cutting. Temperature in the material and the tool decreased with ultrasonic excitation due to the reduced contact in the cutting zone. Mitrofanov *et al* [279] extended this work further to investigate the influence that several friction conditions and heat transfer coefficients have on the mechanical and thermal properties of the work-piece and the tool in the cut zone. Findings indicated as the heat transfer coefficients and the coefficient of friction increases the tool temperature increases during cutting.

A finite element model of rotary ultrasonic machining of ceramics was created by Jiao *et al* [227] and simulations were compared with experiments to improve understanding of the rotary ultrasonic machining method. Experiments considered the spindle speed of the ultrasonically excited tool, power supplied by the ultrasonic generator, feed rate of the cutting tool into the

material and the grit size in the abrasive slurry. Experimental findings showed that as spindle speed increased, the chipping thickness and the cutting force decreased. With increased feed-rate the cutting force and the chipping thickness increased. Other comparisons considering two or more parameters and their relationship to cutting force and chipping thickness were also investigated. The FEM was a 2D axi-symmetric model and considered the rotary ultrasonic machining process initially as a static (neglecting inertial effects) rather than that of a dynamic (including inertial effects) problem. Further simplifications of the process included using degree-of-freedom constraints rather than contact elements in the FE model. Cutting force was modelled as a uniform pressure on the ultrasonically excited tool. The failure criterion for the work-piece material was the maximum normal stress criterion at a distance from the crack tip. Cutting force and chip thickness were compared for both the FEM simulation and the experimental cutting tests and conclusions were drawn that chipping thickness was proportional to cutting force and the experimental scatter could be attributed to other influencing parameters. Further investigations on rotary ultrasonic machining using FEM was conducted by Li *et al* [228] who explored edge chipping reduction further that extended the preliminary work done by Jiao *et al* [229]. The process was again modelled as a 2D axi-symmetric problem where the failure criterion was assumed to be the maximum normal stress criterion and the von-Mises stress criterion. Three parameters were investigated in the study; cutting depth, support length and pre tightening load and the influence each had on the maximum normal stress and the von Mises stress where edge chipping initiates were also investigated. Findings indicated that as cutting depth increases the normal and von Mises stress increase nonlinearly. As pretightening load increases the normal and von Mises stress increases slightly. But as support length increases the normal and von Mises stress decrease which could delay edge chip initiation in the material.

Ahmed *et al* [217] investigated the surface layer formed on Inconnel 718 using a combination of experiments and FEA. Comparisons were made between the experiments and FEA with and without ultrasonic vibrations on the tool during turning. The FEM investigation considered mainly the temperature distribution, residual stresses and thermal stresses in the cut zone, with the experimental study focussing on using nanoindentation, light microscopy and scanning electron microscopy to investigate residual stresses, material hardness and microstructure of the material being cut. The modelling technique used was a 3D fully thermo-mechanically coupled finite element simulation that used previous modelling considerations and parameters as previously explained in Mitrofanov *et al* [249]. Numerical results prove increased thermal strains and residual stresses in the cut zone when Inconnel is turned with superimposed ultrasonic

vibrations compared to conventional turning. Further work by Ahmed [251] explored the stress, strain, temperature and cutting force distribution in both the work-piece and the tool for both conventional and ultrasonic turning of Inconnel with and without friction. Results proved that average cutting forces using ultrasonic turning were up to three times smaller compared to the conventional counterpart and the chip thickness ratio and radius of curvature of the chip are approximately four times larger with friction rather than the frictionless, lubricated, conditions.

The ultrasonic cutting models currently developed which are presented in this literature review using FEA are at the early stage and currently consider very small cut depths and cut initiation at very fast cutting speeds due to computational limitations. However, the FEM approaches allow tool design to be improved as discussed in section 1.5 of chapter 1 of this thesis. Further investigations could include adjusting cutting speed, frequency, vibration amplitude, cutting force, blade geometry and blade orientation, and investigate the relationship between these parameters and temperature in the cut zone. Currently there are no FEM simulations that consider ultrasonic cutting of food products or multi-layered products in the guillotine or slicing cutting configuration. The literature presented indicates that there is scope for simulating ultrasonic cutting techniques using finite element modelling in order to improve tool design for the food processing industry or even to develop generic ultrasonic cutting models that can be adapted to a variety of industrial cutting applications. Knowledge of accurate material representations of food materials for FE purposes is also in the primitive stage and creating new specimen preparation and testing techniques would also be advantageous to develop accurate material representations that are the basis for any FE modelling technique. The literature indicates testing food products in tension is at a very basic stage where reproducible accurate representations of the materials are extremely difficult to produce and there is also scope for developing novel gripping and testing arrangements for testing food products in tension. Testing food products in tension in particular is extremely difficult and food material characteristics are often based on the uni-axial compression test. However, the material response in tension can be significantly different than in compression and for modelling cutting processes where failure directly in front of the cutting tip is in tension and not compression tensile test data is advantageous for capturing the process accurately. FE modelling is only beneficial if the modelling technique can replicate the actual real life process accurately. As such there is also scope for design and manufacture of an experimental cutting rig where experimental cutting tests can be done on a known reproducible material for validation purposes and also on various food materials to validate the FE modelling technique and to provide confidence in the modelling

approach to the complex problem of ultrasonic cutting and offer postulations on the cutting parameters required for ultrasonic cutting of various materials.

Chapter 3

Cutting Blade Design

3.1 Introduction

Ultrasonic cutting devices which use a tuned blade (or blades) resonant in a longitudinal mode, have been used to cut a range of materials from confectionery, baked products and frozen foods, to wood, bone, foams and composites [102]. Although ultrasonic cutting is an established technology, computational simulations of cutting are limited [243]. The performance of cutting operations has been shown to be dependent on the cutting parameters and the geometrical design of the blades [110]. The blade design process typically uses finite element (FE) models validated by experimental modal analysis (EMA) to develop blades that are tuned to a specific mode of vibration [105]. The optimal cutting conditions for the material to be cut are then usually determined from experimental testing. This tends to be an iterative process which could be reduced or eliminated if cutting parameters such as the blade tip amplitude and cutting speed could be predicted prior to blade design and manufacture. Ultrasonic cutting has become established in the food processing industry, as the technology produces cuts of high quality and accuracy and reduces system downtime due to cleaning of the blades.

In food processing, ultrasonic cutting devices have been successfully designed and manufactured to cut a variety of food products in both the guillotine and slicing configurations as previously shown in Section 1.4 of Chapter 1 of this thesis. The guillotine cutting configuration is where the tip of the cutting tool is translated into the material in a linear action and the slicing configuration is where the side of the cutting tool is translated into the material to cause separation. In industry the cutting parameters of the ultrasonic blades are derived from experimental testing. These blades are continuously in use and are often driven at full power regardless of the food product being cut which can often result in blade fatigue and breakages. There is scope for determining the optimum vibrational cutting parameters which allow the tuned component to operate within safe stress limits but maintaining a high quality of cut through the substrate material. Simulation

of the ultrasonic cutting process using finite element analysis could therefore provide a solution to this problem numerically, reducing the number of iterations in the design process.

Currently ultrasonic cutting devices are driven by a piezoelectric transducer which converts the applied electrical signal into mechanical vibrations and, when coupled to a tuned blade, excites a predetermined mode shape at a specific natural frequency. The vibrational amplitude provided by the transducer can be amplified through a reduction in cross-sectional area from the base of the blade to the tip but care has to be taken to ensure the integrity of the component is not at risk through increased stress levels. Ultrasonic instruments designed using FEA have enabled more accurate and efficient components to be manufactured. The designs using FEA are usually validated using experimental modal analysis (EMA). These design techniques provide the opportunity to study more complex modes of vibration, than previous designs based on numerical hand calculations. The components of an ultrasonic device are designed to be resonant in either a single mode or in multiple modes of vibration. For high power systems the operating frequency range is usually between 20kHz and 100kHz. Ultrasonic systems can have a simple structure, with one transducer and horn connected together, or can have more complex structures where several horns and boosters are connected to the transducer. Complex structures are usually used to incorporate gain, to transmit vibration to other tuned components or to allow several tools to be excited by one transducer.

The current blade design process is illustrated in Fig. 3.1 where the current process is depicted by yellow boxes and the proposed inclusion of the ultrasonic cutting model to predict the operational characteristics of the ultrasonic cutting system using FEA is highlighted in grey. Currently a concept is generated by the designer, a detailed engineering drawing is produced, a frequency and steady state finite element stress analysis of the design concept is conducted then the natural frequencies and mode shapes of the blade are studied from the output of the analysis. The required mode shape and natural frequency of the blade is selected by the designer and then the ultrasonic cutting blade is tuned to the driving frequency of the transducer. Several iterations of this process can be required to ensure the blade is tuned correctly. Once this occurs the stress levels produced in the blade for a given input from the transducer are analysed to ensure they exist within critical stress limits of the material. If the stress limits are exceeded further iterations of the design process are required. Once this process is complete the final blade design can be detailed in an engineering drawing and then manufactured. Experimental modal analysis is then used to determine the mode shape and natural frequencies of the component. Other phenomena

can occur such as coupling of modes or other unwanted modes of vibration occurring at frequencies close to the driving frequency. These may warrant another design iteration. Experimental cutting tests follow, to determine if the blade can successfully cut the substrate material. If not, another iteration of the design occurs usually by incorporating more gain into the blade. Iterations continue until a blade is manufactured that can cut the product but remain within critical stress limits.

Ultrasonic components are precision manufactured within very low tolerances and, therefore a reduction of iterations in the design stage is economically desirable. This can be achieved if the ultrasonic cutting parameters are known prior to blade design to cut a particular substrate material. The addition of an ultrasonic cutting model using FEA in the design process can allow the required blade design parameters required to cut a particular material to be determined and offer design flexibility to produce optimum cutting parameters for a variety of cutting configurations. Parameters such as cutting blade material, geometry of the cutting tip, frequency of vibration, blade tip vibration, amplitude and cutting orientation can all be modified easily in the simulation. The effects of these parameters on cutting force and cutting temperature are particularly important to the designer in providing detailed knowledge of the interaction between the ultrasonic blade and the material at the cut site. Modifying these parameters in the model allows prediction of the optimum cutting parameters to be determined numerically.

This section of the thesis discusses the stages of the design process and this links to the theory of high power ultrasonic component design. Two titanium alloy guillotine blades tuned to 20 and 35 kHz are designed to resonate in the longitudinal mode. Both blades have the same blade tip geometry. The blades are designed and manufactured to allow experimental validation of the FE models by comparing experimental cutting tests to FEA predictions.

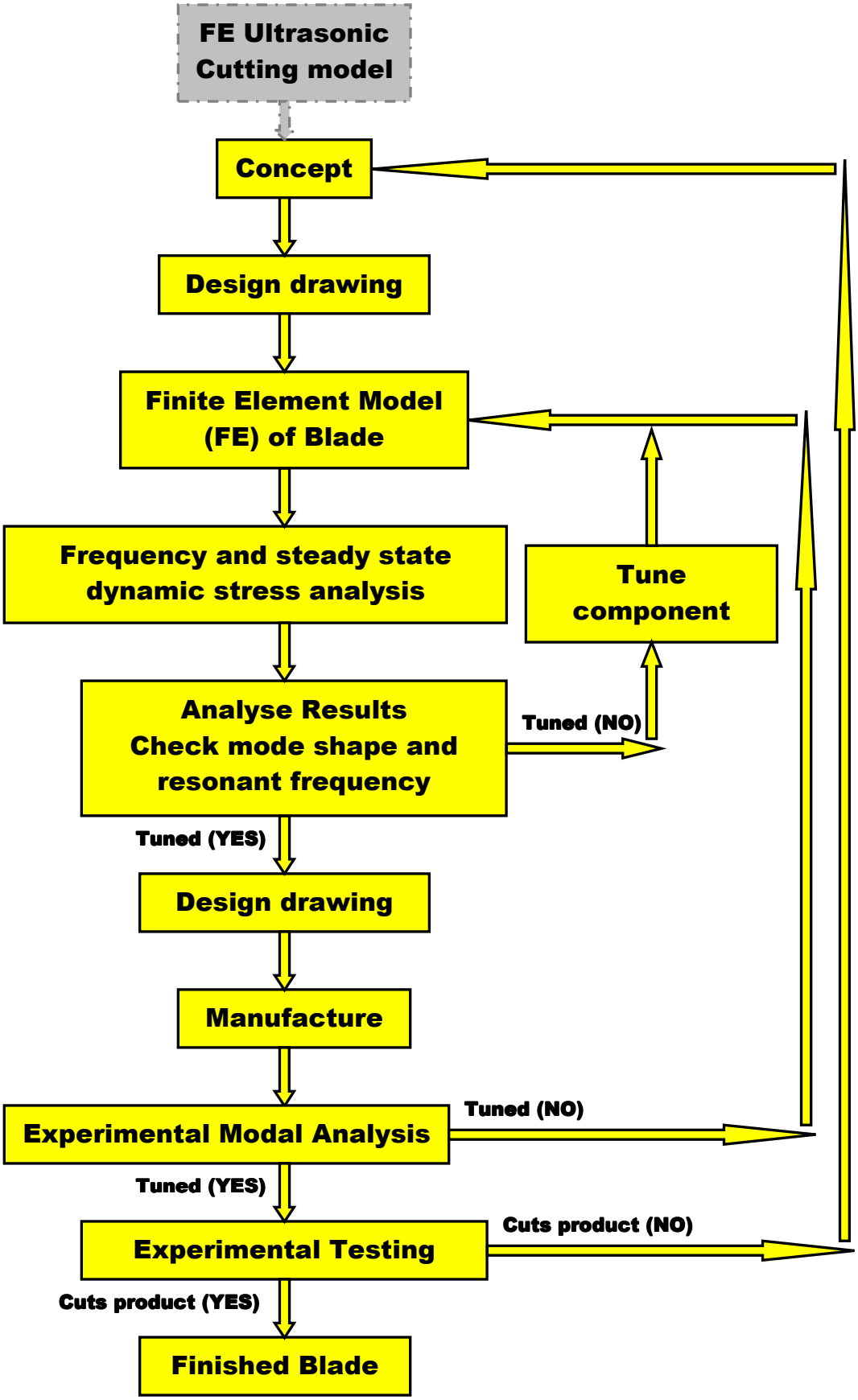

Fig. 3.1: Ultrasonic cutting blade design process.

3.2 Theoretical background to cutting blade design

Ultrasonic components can be tuned using equations based on theory derived from the longitudinal vibration of rods [287]. Simple geometric shapes can be tuned accurately using this method, but as the geometry of the blade increases in complexity analytical solutions are ineffective. Very complex component geometries can be tuned accurately using the computational FE method.

3.2.1 Longitudinal vibration of rods

When in-plane vibration displacements are excited along a profile, a uniform rod, longitudinal mode vibration occurs. The displacement, *u*, is a function of position, x , and time, t.

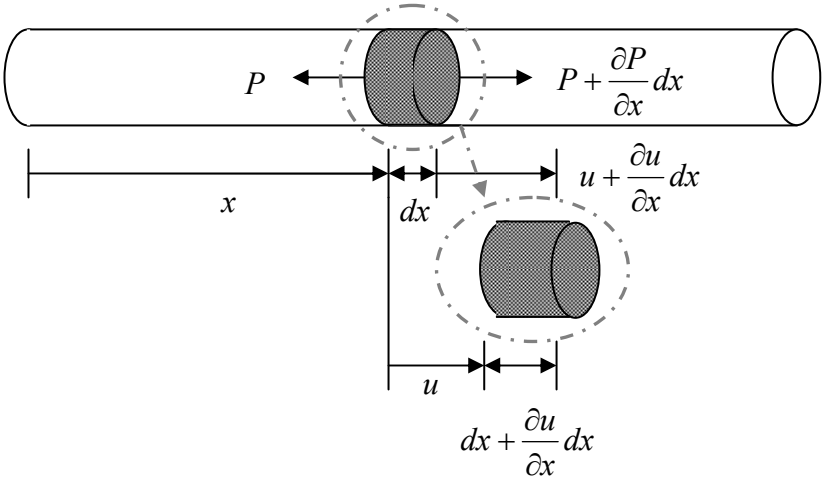

Fig. 3.2: Longitudinal motion of a uniform rod.

For an isotropic, uniform, elastic rod with free-free boundary conditions, the equation of motion can be found by considering a small element of the rod, dx , where under an applied force, *P*, the displacement at x is *u* and the displacement at $x+dx$ is $u+\frac{\partial u}{\partial x}dx$. The element dx has now increased in length by $\frac{\partial u}{\partial x}dx$ and the strain in the elongated element is $\frac{\partial u}{\partial x}$ as shown in Fig. 3.2. If $\sigma = \varepsilon E$ where σ is the stress in the element, ε is the strain and E is the Young's modulus, then for a rod with cross-sectional area *A*, and applied force *P*;

$$\varepsilon = \frac{u+\frac{\partial u}{\partial x}dx - u}{\partial x} = \frac{\partial u}{\partial x} = \frac{P}{EA} \tag{3.1}$$

Applying Newton's second law:

$$P + \frac{\partial P}{\partial x} - P = \rho A dx \frac{\partial^2 u}{\partial t^2} \tag{3.2}$$

Where ρ is the density.

Substitute (3.2) in (3.1):

$$AE \frac{\partial^2 u}{\partial x^2} dx = \rho A dx \frac{\partial^2 u}{\partial t^2} \tag{3.3}$$

$$\frac{\partial^2 u}{\partial t^2} = \frac{E}{\rho} \frac{\partial^2 u}{\partial x^2} \tag{3.4}$$

The equation of motion can be defined as:

$$\Rightarrow \frac{\partial^2 u}{\partial x^2} = \frac{1}{c^2} \frac{\partial^2 u}{\partial t^2} \tag{3.5}$$

Where $c^2 = \frac{E}{\rho}$ and is the velocity of the stress wave in the rod.

Separation of variables can be used to solve the partial differential equation and a solution is considered of the form:

$$u(x,t) = G(x)H(t) \tag{3.6}$$

Substituting (3.6) in (3.5):

$$\frac{1}{G} \frac{d^2 G}{dx^2} = \frac{1}{c^2} \frac{1}{H} \frac{d^2 H}{dt^2} \tag{3.7}$$

Each side of equation (3.7) must be a constant as the left hand side is independent of x and the right hand side is independent of t. Let the constant be $-\left(\frac{\omega}{c}\right)^2$, then two ordinary differential equations (ODE's) can be obtained.

$$\frac{d^2 G}{dx^2} + \left(\frac{\omega}{c}\right)^2 G = 0 \tag{3.8}$$

$$\frac{d^2 H}{dt^2} + \omega^2 H = 0 \tag{3.9}$$

The general solution is of the form:

$$G(x) = A\sin\frac{\omega}{c}x + B\sin\frac{\omega}{c}x \text{ and } H(t) = C\sin\omega t + D\cos\omega t \tag{3.10}$$

Where A, B, C, and D are dependant on boundary and initial conditions. The general solution for *u* is therefore:

$$u(x,t) = \left(A\sin\frac{\omega}{c}x + B\sin\frac{\omega}{c}x\right)\left(C\sin\omega t + D\cos\omega t\right) \tag{3.11}$$

For a free-free rod, the natural frequency is found to be:

$$f_n = \frac{n}{2l}\sqrt{\frac{E}{\rho}} \tag{3.12}$$

Where *n* is the mode order and *l* is the tuned length.

For a fixed resonant frequency, the tuned length can be calculated from:

$$l = \frac{n}{2f_n}\sqrt{\frac{E}{\rho}} \tag{3.13}$$

From Eq. 3.13, the natural frequency, f_n, is dependant on the length of the component and the material constants E and ρ. Eq. 3.13 is only accurate for components of low mode orders that have length much greater than the diameter of the rod.

3.2.2 Alternative non uniform geometries

In high power ultrasonic devices, non-uniform geometry horns can be used to amplify the vibration amplitude supplied by the transducer. Non-uniform profile horns incorporate gain, which is defined as the ratio of output to input vibration amplitude, by modifying the cross sectional area from the input to the output surface. The gain required in an ultrasonic component depends on the ultrasonic amplitude required for the process. Traditionally, gain has been incorporated using axisymmetric profiles.

From the theory of longitudinal vibration of rods, equations for conical, exponential and catenoidal rods were derived by Merkulov [117]. The equations were derived by assuming that the stress waves remain perfectly in-plane and that the stress is distributed evenly across the cross-section as can be seen in Fig. 3.3. Lateral out-of-plane stresses are considered to be negligible.

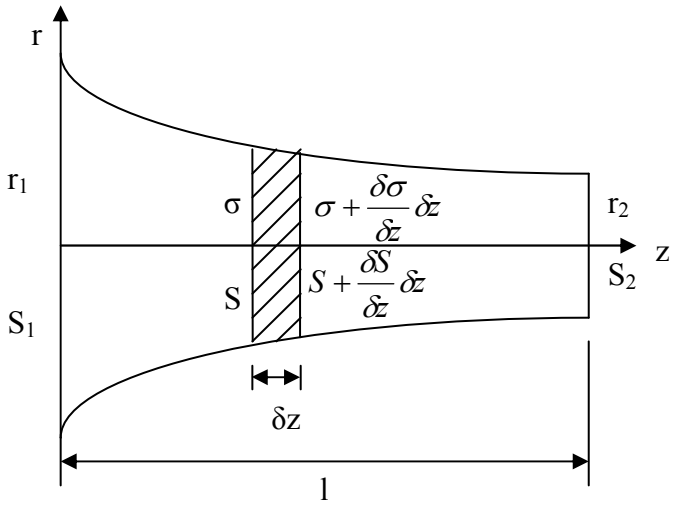

Fig. 3.3: Axially-symmetric horn profile depicting stress distribution.

The equation of motion for a small element of the axisymmetric profile with a cross-section S_1 with radius r_1 tapering to a cross section S_2 with radius r_2 defined in Fig. 3.3 can be determined using Newton's second law, $\sum F = m\frac{\partial^2 u_z}{\partial t^2}$ where F is the force, m the mass and $\frac{\partial^2 u_z}{\partial t^2}$ is the acceleration. The equation of motion of the small element, as indicated by the shaded area in Fig. 3.3, can be defined in Eq. 3.14 where S is the cross-sectional area, m is the mass and is the product of the density and volume of the element, ρ is the density, ∂z is the length of the element, z is longitudinal axis, r is the radial axis and u_z is the displacement in the z-axis. The volume of the element is defined in Eq.3.14 as:

$$\left(S + \frac{\partial S}{\partial z}dz\right)dz + \left(S - \left(S + \frac{\partial S}{\partial z}dz\right)\right)dz = Sdz \qquad (3.14)$$

The sum of the forces can be found from $F = \sigma S$ where F is the force, σ is the stress in the element and S is the cross sectional area. The sum of the forces is described in Eq. 3.15 as:

$$\sigma S + \frac{\partial S}{\partial z}\sigma dz + \frac{\partial \sigma}{\partial z}Sdz - \sigma S = 0 \qquad (3.15)$$

Substituting Eq.3.14 and Eq.3.15 in Newton's second law gives the equation of motion as described by Merkulov [117] as:

$$\rho S\delta z\frac{\partial^2 u_z}{\partial t^2} = \frac{\partial \sigma}{\partial z}Sdz + \frac{\partial S}{\partial z}\sigma dz \qquad (3.16)$$

Merkulov [117] derived the following equations to describe how to obtain the resonant length for several types of horn. An illustration of these common axi-symmetric horn profiles is shown in Fig. 3.4. The corresponding equations to calculate the tuned length, *l*, are:

$$l = \frac{\lambda k l}{2\pi} \tag{3.17}$$

for a conical horn, where $k = \frac{\omega}{c}$ and *kl* are the roots of the equation.

$$l = \frac{\lambda n}{2} = \frac{\lambda}{2}\sqrt{\frac{(n\pi)^2 + (\ln N)^2}{\pi^2}} \tag{3.18}$$

for an exponential horn where $N = \frac{r_1}{r_2}$, $\lambda = \frac{c}{f}$ and *n*=1, 2, 3, …..

$$l = \frac{\lambda}{2}\sqrt{\frac{(k'l)^2 + (\cos^{-1} N)^2}{\pi^2}} \tag{3.19}$$

for an exponential horn where $k' = \sqrt{k^2 - \gamma^2}$, $N = \frac{r_1}{r_2}$, $\lambda = \frac{c}{f}$ and $\gamma = \frac{1}{l}\cos^{-1}\frac{r_1}{r_2}$ and $k'l$ are the roots of the equation.

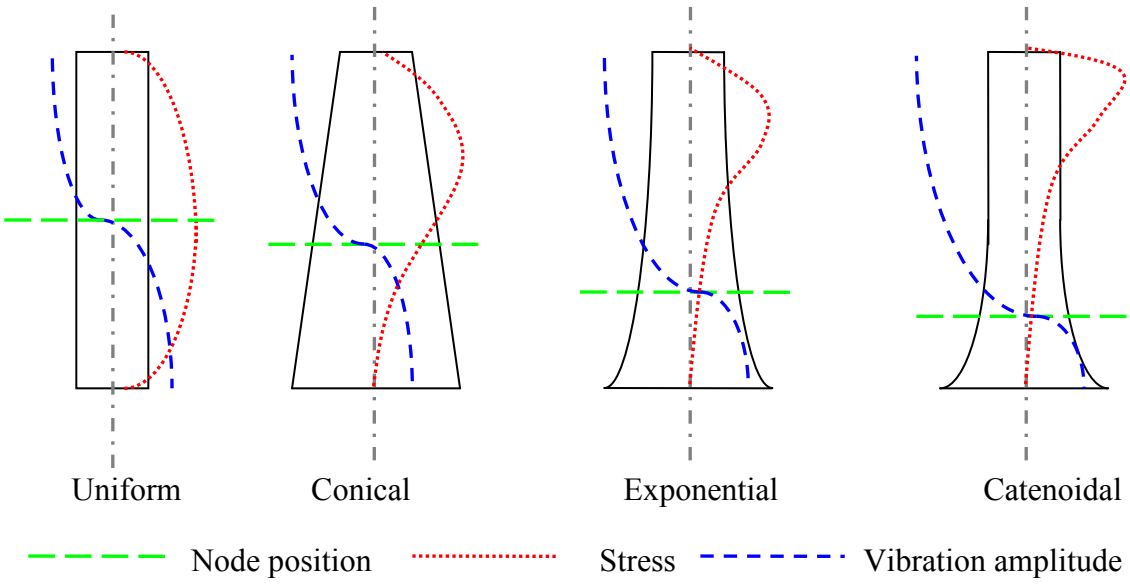

Fig. 3.4: Common axi-symmetric horn profiles illustrating node position, stress distribution and vibrational amplitude along length of ultrasonic component.

Consideration as to the most suitable horn profile to be used depends on the application and the ultrasonic amplitude required for the process. The horn profile is a compromise between

component integrity and gain. Catenoidal horns produce a larger gain than conical horns but exhibit higher stress for the same material. Manipulation of these profiles can provide increased structural integrity of the component by shifting the node position, which is the location of zero displacement, away from the maximum stress location.

3.3 Finite element modelling

The creation of the finite element method in 1943 was by Courant [288] who obtained approximate solutions to vibrating systems by utilising the Ritz method of numerical analysis and minimisation of variational calculus. Further work followed this pioneering work by Courant to establish the FE method for practical use and by the 1970s it was being used by large industries such as aerospace, automotive, defence and nuclear industries on large, mainframe computers. However, with rapid advancements in computational power and the reduced cost of FE software, FEA is now widely used. The FE method works by modelling a structure using a mesh of elements connected together using nodes. The elements can have simple or complex material properties applied to characterise the behaviour of the structure under analysis. Boundary and loading conditions can be simulated on the nodes or elements of the mesh and a variety of analytical results can be calculated depending on the type of analysis requested by the user and the parameters the user is interested in. Several modelling techniques can be used to analyse a structure in using either a 2D or 3D modelling domain, the choice of which depends on the structure under analysis. Complex problems can be solved quickly and accurately using the FE method and FEA is now considered to be an essential tool in the arsenal of an engineer especially for design or troubleshooting [288].

The FE package ABAQUS [252] was used to calculate the natural frequencies of a uniform steel rod using beam and solid elements. A mesh convergence study is also conducted by varying the element densities of the rods to provide confidence in the accuracy of the FE modelling technique. The static and dynamic responses of loaded structures can be analysed computationally using FE packages in this example using a frequency analysis to determine the natural frequencies and mode shapes of the uniform rod. Fig. 3.5 (a), (b) and (c) depicts mode shapes of the first longitudinal, bending and torsional mode of vibration respectfully for the uniform analysed using 20 noded elements with no boundary conditions. These mode shapes are simplistic and other more complex modes of vibration exist at higher harmonics which can be a

combination of these fundamental mode shapes and when stimulated provide complex movement of the rod.

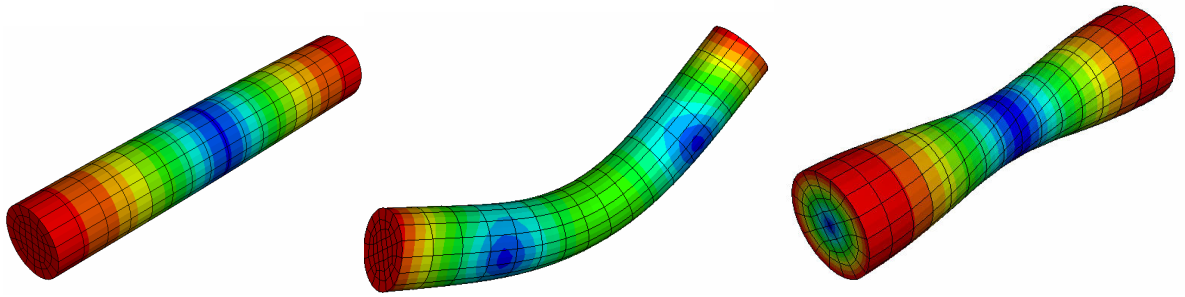

(a) (b) (c)

Fig. 3.5: Mode shape diagrams with contours of displacement for (a) 1st Longitudinal (b) 1st bending and (c) 1st torsional mode of vibration.

To conduct a vibrational analysis in ABAQUS two prescribed steps are applied; firstly a frequency step using either the Lanczos or subspace eigensolver to extract natural frequencies within the frequency range of interest, and secondly a steady-state dynamics direct step to predict the steady-state amplitude and phase of the system under a predefined loading of a harmonic excitation at a specific frequency. The frequency step allows natural frequencies and mode shapes of the system to be calculated and the steady-state dynamics direct step allows stress, strain and displacement of the system to be predicted for the applied loading condition. For computational efficiency and for solver accuracy, geometrically similar shapes such as rods, I-sections or box sections can be modelled in FEA by simplifying the uniform profile to a single line with the associated cross sectional profile assigned to it and by specifying a particular element type to the model. Truss elements consider the element to be rigid and neglect bending whereas beam elements consider bending in the element when loaded. These element types are particularly advantageous as the number of elements in the finite element model can be reduced dramatically compared to those required to define the 3D profile, saving modelling and solving time and also providing very high accuracy. Solid elements also provide very high accuracy but usually require an increased number for the same accuracy compared to beam elements which obviously increases computational time. Solid elements simplify every shape to a cubic form and for circular shapes a high number of elements is required to capture the curvature of the circular shape and even then it is still approximated, but as element density is increased, the geometry tends towards a circular shape. But for complex geometries solid elements provide a high

accuracy and are often preferred to the tetrahedral counterparts where the use of beam elements is not feasible.

Fig. 3.6 (a) illustrates a mesh density study using 2 noded linear and 3 noded quadratic beam elements by varying the number of elements along the longitudinal direction of the rod. Findings indicate the natural frequencies of the first longitudinal mode using the FE package ABAQUS to be 20 and 35 kHz and mesh convergence is achieved by using only 4 quadratic or 8 linear beam elements. Fig. 3.6 (b) shows mesh convergence is achieved using 6 solid quadratic elements along the longitudinal axis where the radial element density is negligible for any number of elements greater than 4. These solutions prove that the FE package ABAQUS is sufficiently accurate to provide a solution to frequency domain problems for components using both types of elements for a relatively low number of elements, and provides confidence in the modelling approach for determination of natural frequencies, mode shapes of low mode orders and for tuning ultrasonic components with complex geometry. This example considers convergence for a simple low mode order natural frequency but for modes with frequencies close together a higher mesh density may be required, but the process is still the same.

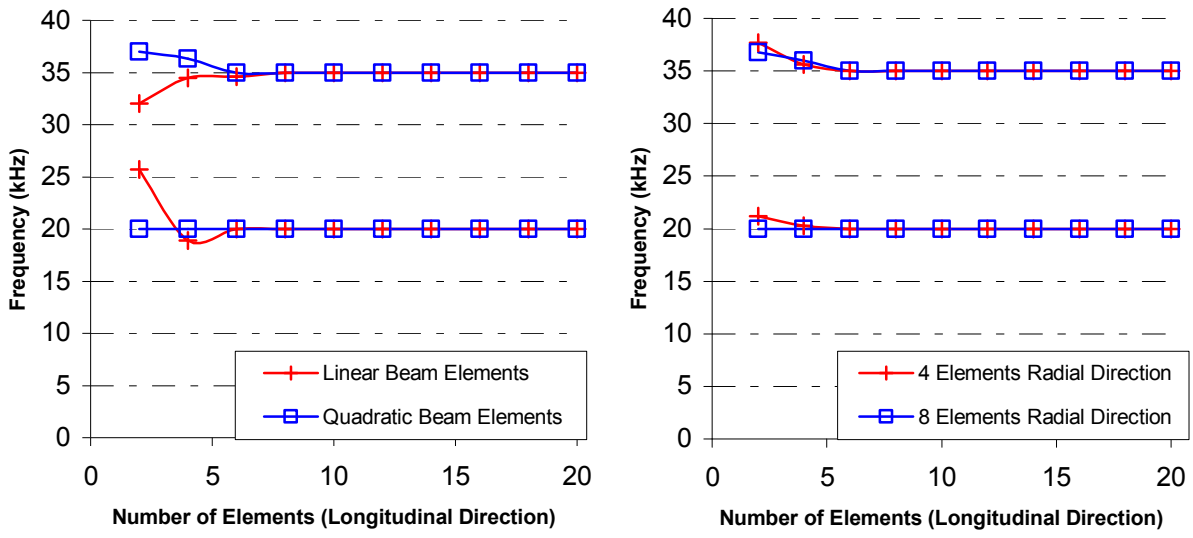

(a) (b)

Fig. 3.6: Mesh convergence study on uniform steel rods using (a) Beam elements and (b) Solid elements.

3.4 Experimental modal analysis

Experimental modal analysis (EMA) is a technique to determine the modal parameters (natural frequency, mode shapes and damping factors) of a structure using a set of frequency response function (FRF) measurements taken from a grid of points on the excited structure. Commonly the FE modelling technique is used to calculate these modal parameters but validation of the FE simulations is carried out using EMA. Experimental modal analysis is not only a validation tool but can also be a useful troubleshooting and design tool. EMA is used in this study to confirm the FE predicted modal parameters for the ultrasonic cutting blades.

3.4.1 FRF

An FRF is simply defined as a curve representing the output to input ratio of a transducer. An FRF can characterise the dynamic properties of a mechanical structure such as natural frequencies, damping and mode shapes. The applied force and the response of the structure (as either displacement, velocity or acceleration) are measured. The measurement is captured in the time domain and then converted to the frequency domain using a fast Fourier transform (FFT) algorithm. During the transformation the functions become complex and contain real and imaginary components and use both magnitude and phase to describe the FRF response.

3.4.2 EMA measurement system

The experimental testing equipment and operating configuration used in this study consists of a function generator that produces a random excitation signal, an amplifier which, amplifies the signal from the function generator, a transducer that converts the electrical signal from the amplifier to mechanical vibration through the piezoelectric effect, a tuned ultrasonic cutting blade excited by vibration supplied from the transducer, a 3D non contact laser Doppler vibrometer to measure the response of the system and a data acquisition system and modal analysis software to capture the measured data and interpret the experimental data using FFT analysis respectively. A flow diagram of the experimental testing configuration is shown in Fig. 3.7.

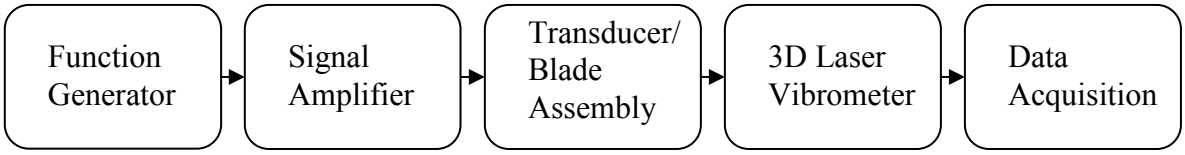

Fig. 3.7: Flow diagram of EMA experimental configuration.

3.4.3 Excitation device

Several excitation devices are available to excite the structure and cause vibration of the system. Devices include shakers, impact hammers and transducers [258-260]. Various shakers are available, from mechanical shakers that use out-of-balance rotating masses connected to the structure by stingers, electromagnetic shakers where a coil is moved in a magnetic field to electro hydraulic shakers where substantial static and dynamic forces can be applied to the structure by hydraulics.

The most common ultrasonic transducers in use are those utilising piezoelectric technology. Piezoelectric transducers can stimulate vibrations at higher frequency levels than electromagnetic shakers. The transducers work by passing an electric current to piezoelectric crystals which cause the piezoelectric material to expand or contract, usually at high frequency as shown in Fig 1.1 in Chapter 1 of this thesis.

3.4.4 Response measurement

For a FFT analysis to be performed to develop the vibrational characteristics of a system the force applied to a structure and the surface acceleration at a known point on the structure needs to be measured. To measure the force, force transducers are used which measure the applied load in compression or tension using piezoelectric crystals by creating a charge proportional to force when a transmitted load is applied. The piezoelectric crystals are encapsulated in a casing and the measurement device is usually attached to the structure by using either a stud, wax or a magnet. A simple stud is usually the most preferable. An accelerometer works by utilising a seismic mass attached to piezoelectric crystals within a casing. The acceleration is measured by considering the inertia force supplied to the crystals by the seismic mass which creates a charge proportional to the applied load, and using Newton's second law the acceleration can be determined. The seismic mass and the body are assumed to move together so the acceleration of the body and the acceleration of the seismic mass are identical. Transducers that incorporates both an accelerometer and a force transducer in a single casing are also available and are called impedance heads. Various ranges of accelerometers, force transducers and impedance heads are available on the market and several operating ranges are available for each depending on the application. Care has to be taken when using these devices as the weight of the measuring devices can affect the natural frequencies and mode shapes of the system and can often shift the natural frequencies of the structure. Minimising added weight to the system should always be

considered but for large structures such as bridges the weight of the measuring devices will be negligible but as the size of the measuring device approaches the size of the system larger errors will be encountered. Alternative measuring devices that do not add any weight to the system are also available such as non-contact laser Doppler vibrometers or electronic speckle pattern interferometry (ESPI) which have high accuracy and minimise errors but are very expensive devices. ESPI systems give a real time visual display of fringe patterns which allow the vibration response of the system and mode shapes to be deduced.

Non-contact laser Doppler vibrometers [289] are optical devices that are able to detect the instantaneous velocity of a surface of a structure. The measurement is deduced by shining a direct laser beam at a target on the structure and measuring the Doppler shifted wavelength of the reflected beam using an interferometer. For these devices to work accurately a direct line of sight to the target point on the structure is required with the target point having a shiny reflective surface if possible. The Doppler shift is a phenomenon that describes how light wave frequency changes if the source translates relative the point of observation. So the wavelength of the reflected light is different from the wavelength of the incident beam, if moving towards the incident light the wavelength decreases as the distance is shorter and vice versa. If the wavelength of the incident light is known then the velocity of the object can be determined from the change in wavelength of the light. But due to the very high frequency of the light beam direct demodulation is impossible and optical interferometry is used where two waves are superimposed to detect differences between them. This technique is very sensitive and can detect changes of wavelength up to a half wavelength of the type of light used.

3.4.5 Signal processing

When the measurement signals have been gathered at various target locations on the structure by the response measuring devices the data is collected and processed using a spectrum analyser. To extract the natural frequencies and mode shapes of the system FRF's are calculated from Fast Fourier transforms (FFT's). Fourier transforms convert response signals from the measurement devices in the time domain to spectral properties in the frequency domain using digital Fourier transform (DFT) analysis a form of the FFT algorithm developed by Cooley and Tukey in the 1960s [258]. Erroneous results can be produced using digital Fourier analysis by aliasing. Aliasing is a problem where the discretisation of the continuous time history is misinterpreted if the sampling rate is too slow, and high frequency signals can be misinterpreted as low frequency signals and can cause a distortion of the measured spectrum using DFT. This phenomenon can

be avoided by using anti-aliasing filters where the original time signal is subjected to a low-pass sharp cut-off filter. Leakage is a problem where a sample of the signal is taken using a finite length of time history coupled with the Periodicity Principle. The Periodicity Principle considers all signals to be periodic but unfortunately signals such as random excitation are not. If the signal sampled is ideal and is precisely periodic the resulting spectrum will display a single line at the frequency of the sine wave but if the signal is not ideally periodic several lines will appear surrounding the single frequency and as such the spectrum produced does not indicate the single frequency which the time signal possessed. This problem can be minimised or avoided by changing the duration of the measurement sample, increasing the duration of the measurement period, using zero padding where zeros are added to the end of the measured sample and by using the windowing technique where a prescribed profile, such as hanning, cosine taper, hamming or exponential is used on the time signal. Filtering is also a solution that can be used on its own or alongside the windowing technique on the sample in the frequency domain instead of the time domain. Common filters include high-pass, band limited, narrow band and notch.

The FRF's of the manufactured blades were generated in this study using a hanning window and also a high pass sharp cut off filter to minimise leakage and aliasing. The FRF results during the EMA of the ultrasonic blades were also improved by collecting 20 responses during the analysis for each measurement point and averaging the FRF results to improve the final FRF.

3.5 Design process for ultrasonic cutting blades

To validate the FE model of ultrasonic cutting two tuned ultrasonic cutting blades are required to compare force and temperature measurements from experimental cutting tests to equivalent FE predictions. The literature on ultrasonic component design indicates that for uniform cylinders the gain of the tuned component is 1. I.e. theoretically if 1 micron amplitude is supplied by the transducer at on end of the rod then the displacement at the other end is 1 micron. This however in reality never occurs due to slight internal losses. Also, gain is dependent on the rate of change in cross-sectional area from the base of the component, where the input is supplied, to the tip. A reduction in cross-sectional area from the base to the tip increases gain and an increase in cross-sectional area reduces gain. Many component profiles exist such as conical, exponential, catenoidal or stepped or combinations of each to magnify or reduce amplitude at the tip of the component [89, 99-126].

3.5.1 Cutting blade requirements and design concepts

For the experimental cutting tests two blades tuned to the longitudinal mode of vibration are required, one resonating at 20 kHz and the other at 35 kHz. It was advantageous to build gain into the blades by reducing the profile from the base to the tip to allow a study of the effect tip displacement had on cutting parameters and as both of the transducers only outputs a maximum of 8 microns when operating on full power an increase in gain would allow a larger range of amplitudes to be investigated. To increase the vibrational amplitude of the blade and for simplicity for tuning and comparison studies two symmetric circular cuts were taken from both sides of a uniform rod along the longitudinal axis to reduce the cross sectional area from the base to the tip as shown in Fig. 3.8. The geometry of the cutting tip for both the tuned blades was designed specifically to be the same for both the 20 and 35 kHz blades to investigate the effect frequency had on temperature at the cut site and cutting force applied. The longitudinal mode of vibration was selected as it is simple to model in 2D and also because both the transducers stimulate vibrations in the longitudinal mode.

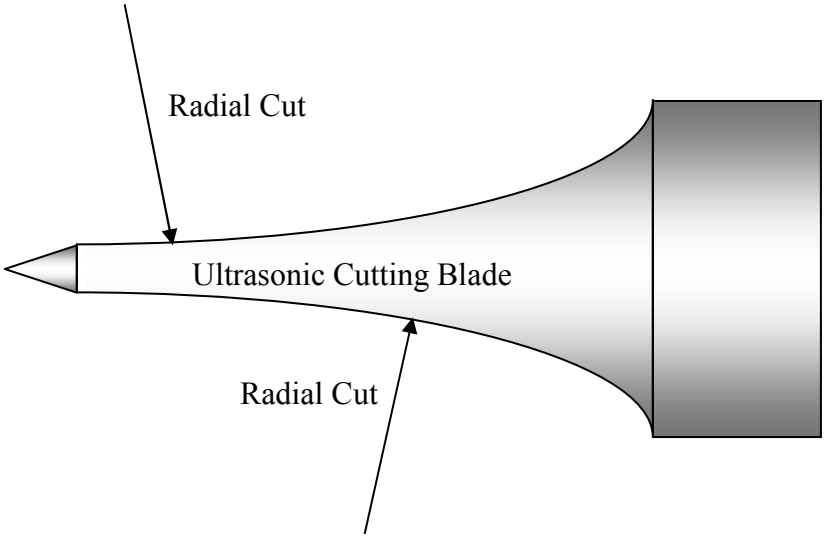

Fig. 3.8: Symmetric circular cuts through a uniform rod.

3.5.2 Tuning the ultrasonic cutting blades

From basic elementary vibration equations it is standard to tune the waveguide to resonance by scaling the geometry of the blade by a constant. This can be determined by Eq. 3.20 where *C* is the constant, f_{cur} is the current natural frequency of the required mode shape and f_{des} is the desired natural frequency the component will be driven at by the transducer.

$$C = \frac{f_{cur}}{f_{des}} \tag{3.20}$$

To ensure the geometry of the blade tip was the same for both blades where one resonated at 20 kHz and the other at 35 kHz only the longitudinal length was multiplied by the constant to tune the blade whilst the radial dimensions remained constant. To tune the ultrasonic cutting blades the geometry of the blade was created in ABAQUS and then the program executed to determine natural frequencies. The longitudinal mode of the cutting blade was identified and the resonant frequency recorded. Afterwards the length of the blade was rescaled by multiplying the length by the constant as calculated in Eq. 3.20 which was the ratio of the calculated output frequency to the desired frequency. In this case the driving frequencies are 20 and 35 kHz as these are the operating frequencies of the transducers. The analysis was then resubmitted and the longitudinal mode identified to determine if it was operating at the driving frequency. Further iterations of this process were conducted if required until the longitudinal mode of vibration occurred at the required driving frequency.

3.5.3 Stress analysis using FEA

After the blade had been tuned to resonance a forcing function was applied to the base of the blade as indicated in Eq. 3.21 where F is the force, A the amplitude of the transducer (8 microns), ω the natural frequency and t the time..

$$F = A\sin\omega t \tag{3.21}$$

A steady state dynamics direct step was included in the FE analysis after the frequency step to analyse stress and displacement of the blade due to the applied loading at the longitudinal mode of vibration. The stress distribution in the blade can be plotted using the von-mises and Hencky criteria [261] as shown in Eq. 3.22 below where σ_1, σ_2, σ_3 are the principal stresses and σ_0 is the yield stress.

$$(\sigma_1-\sigma_2)^2+(\sigma_2-\sigma_3)^2+(\sigma_3-\sigma_1)^2=2\sigma_0^2 \tag{3.22}$$

Assuming the stress distribution lies in-plane along the cross-section of the blade where no traverse movement exists implies that there is only one principal stress, σ_2, acting in one direction always and no shear stress and using Eq. 3.23:

$$\sigma_1,\sigma_3=0$$

$$(0-\sigma_2)^2+(\sigma_2-0)^2+0=2\sigma_0^2$$

$$2{\sigma_2}^2=2\sigma_0^2$$

$$\sigma_2=\sigma_0 \tag{3.23}$$

As shown in Eq. 3.23 the von Mises stress will be the same as the maximum principal stress in the longitudinal direction in the waveguides when excited in the longitudinal mode. Maximum stress limits in components must always be considered in any design and for ultrasonic cutting blades ideally the maximum stresses must lie in the elastic region of the material at a safety factor typically of 4 or greater for operational safety. The maximum allowable stress in an ultrasonic component when designed can therefore be considered to be the yield stress of the material divided by the safety factor as denoted in Eq. 3.24.

$$\sigma_{\max}=\frac{\sigma_{Yield}}{SafetyFactor} \tag{3.24}$$

3.5.4 Material selection for ultrasonic cutting blades

Material selection for ultrasonic components is critical to ensure the blades operate correctly. Material factors such as high strength and high toughness are usually specified for the design of ultrasonic components especially ultrasonic cutting blades where the components experience extreme loading conditions. Minimising heat generation during operation is often a design specification for ultrasonic cutting to restrict burning at the cut interface that can ruin the substrate material, and materials with low internal friction coefficients are required to minimise temperature rises during operation. However, in some processes such as ultrasonic cutting of food products a slight temperature increase is sometimes an advantage and for soft materials can locally melt the material at the interface which can often produce a cut surface that is visually appealing to the eye. Ideally during operation an acoustic loss factor of zero is perfect as there will be no energy losses due to heat or noise and all energy supplied will be transformed into mechanical vibration but in reality every ultrasonic component will experience acoustic losses and energy will be lost in the system. Often the quality factor is used to characterise the effectiveness of the ultrasonic components and a high mechanical Q is often advantageous for ultrasonic component design. The mechanical Q or quality factor can be calculated using Eq.3.25 where Q is the quality factor and φ is the acoustic loss avaliable from materials tables.

$$Q=\frac{1}{\varphi} \tag{3.25}$$

Many materials have high quality factors but it is also critical when selecting a material for component design to consider the acoustic impedance, z, of the material which can be determined from Eq. 3.26 where c is the speed of sound in the material and ρ is the density.

$$z = c\rho \tag{3.26}$$

When several ultrasonic components are connected, usually by using threaded studs where one component is tightened against another, the acoustic impedance should be matched as closely as possible to ensure energy transfer is maximised between joining components and to ensure the vibration is transferred effectively between one component and the next.

3.5.5 Experimental ultrasonic cutting blades

In this investigation grade 5 Titanium alloy ($Ti_{90}Al_6V_4$) is used for the two ultrasonic cutting blades used in the experimental cutting trials due to its high strength, high toughness, corrosion resistance, durability and low acoustic loss (or high mechanical Q). The material properties for Titanium alloy ($Ti_{90}Al_6V_4$) are tabulated in Table 3.1. Two tuned ultrasonic cutting blades were designed using the FE package ABAQUS using the procedure described previously to resonate in the longitudinal mode at 20 and 35 kHz. Fig. 3.9 (a) and (b) depicts the undeformed and deformed vibration response of the tuned blades excited in the longitudinal mode at 20 and 35 kHz respectively.

Titanium alloy (Ti90Al6V4)	
Density	4430 kg/m^3
Hardness (Vicker's)	349
Ultimate Tensile Strength	950 MPa
Yield Strength	850 MPa
Young's Modulus	113.8 GPa
Poisson's Ratio	0.342
Fatiague Strength @1e+7cycles	240 MPa
Specific Heat Capacity	0.5263 KJ/Kg°C
Thermal Conductivity	6.7 W/mK

Table 3.1: Material properties of titanium ($Ti_{90}Al_6V_4$).

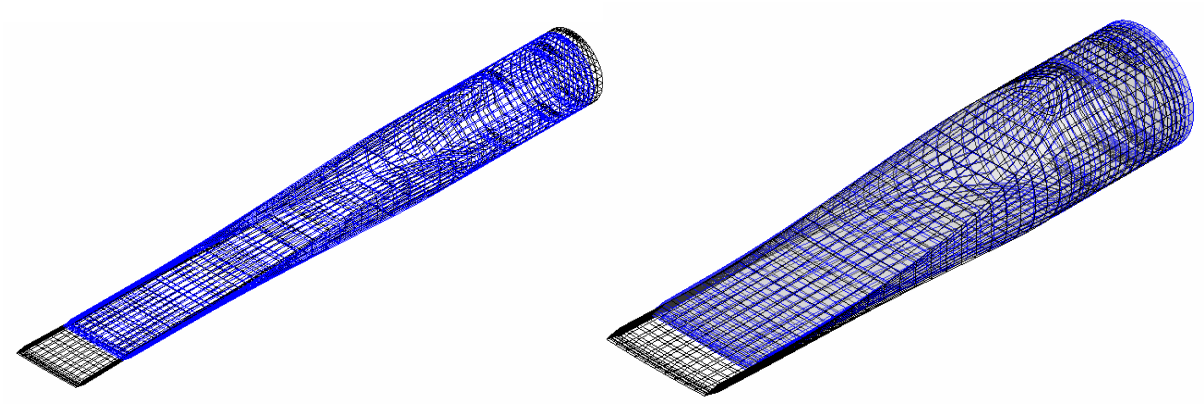

(a) (b)

Fig. 3.9: Graphical representation of the deformed and undeformed shape for the tuned ultrasonic cutting blades excited at (a) 20 kHz and (b) 35 kHz.

By analysing the results of the steady state dynamics direct step of the analysis, where the maximum output displacement of the transducer was represented using a sinusoidal forcing function as explained using Eq.27, the maximum stress, blade displacement and gain could be determined. Fig. 3.10 (a) and (b) illustrate using contour plots, the locations of maximum stress and displacement for the 20 kHz cutting blade when excited in the longitudinal mode using a base input vibration displacement of 8 microns. Similar illustrations are depicted in Fig. 3.11 (a) and (b) for the 35 kHz blade.

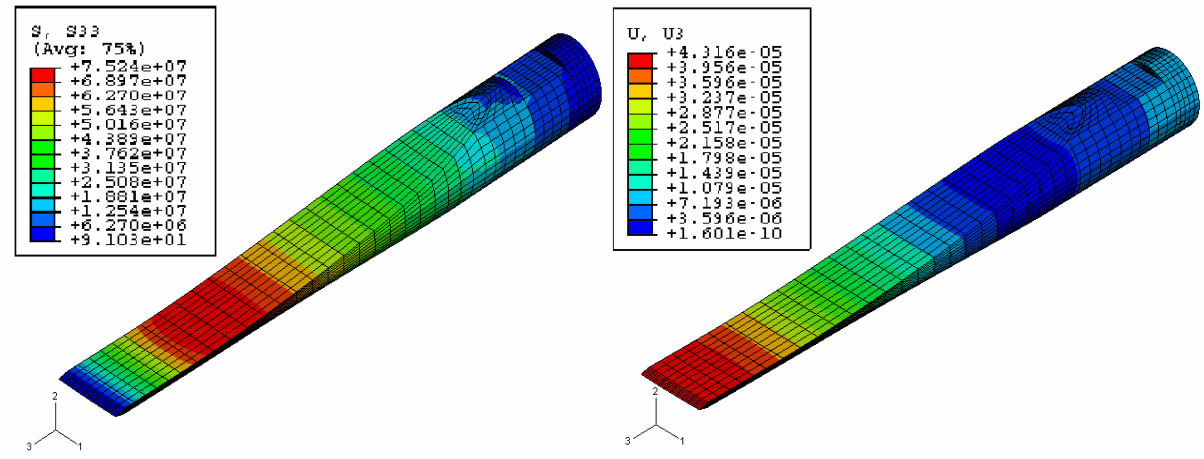

(a) (b)

Fig. 3.10: Contour plot of the deformed shape for the tuned 20 kHz ultrasonic cutting blade illustrating (a) maximum principal stress in the longitudinal direction and (b) maximum displacement in the longitudinal direction.

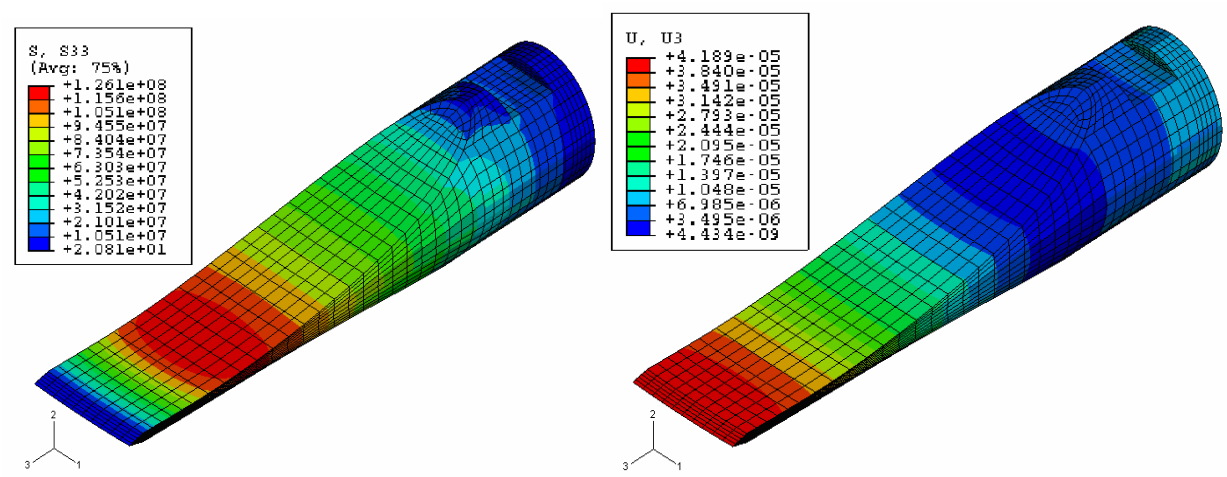

Fig. 3.11: Contour plot of the deformed shape for the tuned 35 kHz ultrasonic cutting blade illustrating (a) maximum principal stress in the longitudinal direction and (b) maximum displacement in the longitudinal direction.

From the FE analysis, the maximum stress location along the longitudinal axis of the ultrasonic cutting blades was predicted by plotting the principal stress in the longitudinal direction or the Mises stress along a path of nodes along the centre of the blade at the excited natural frequency. Similarly, the nodal displacement can also be determined along the same nodal path. Fig. 3.12 (a) and (b) present the nodal displacement, principal stress in the longitudinal direction and Mises stress for the 20 and 35 kHz blades respectively.

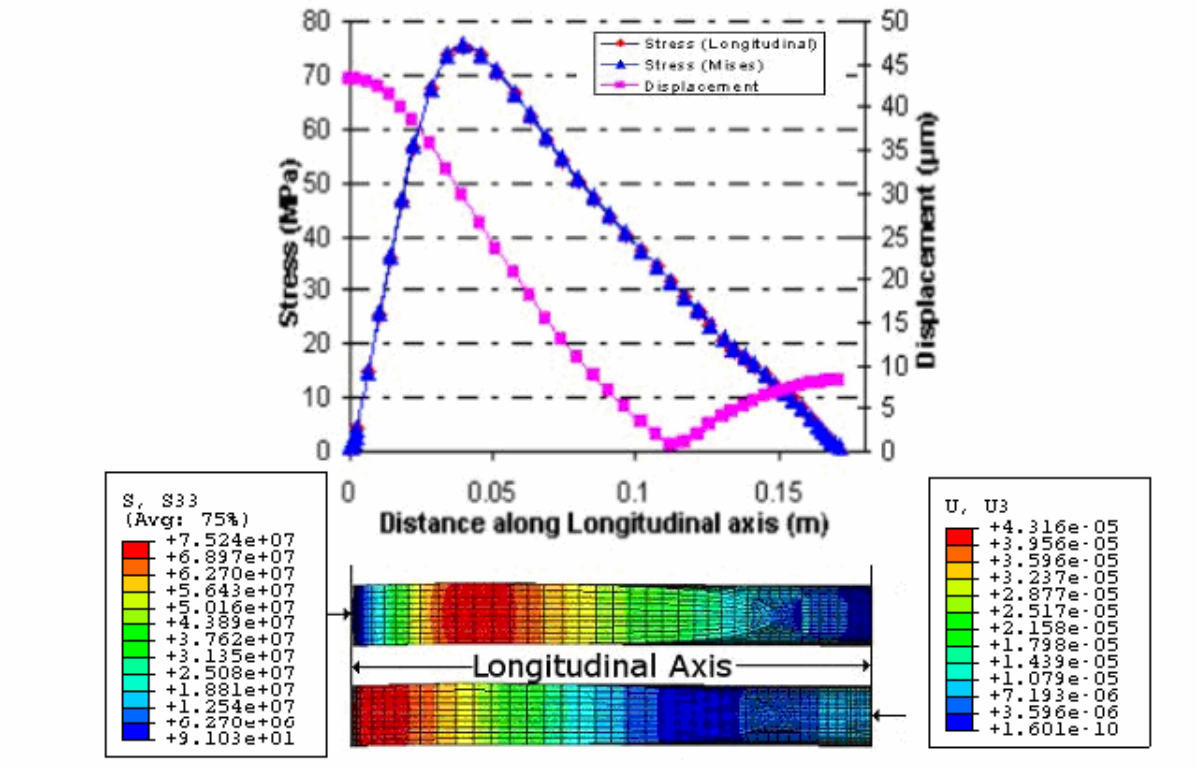

(a)

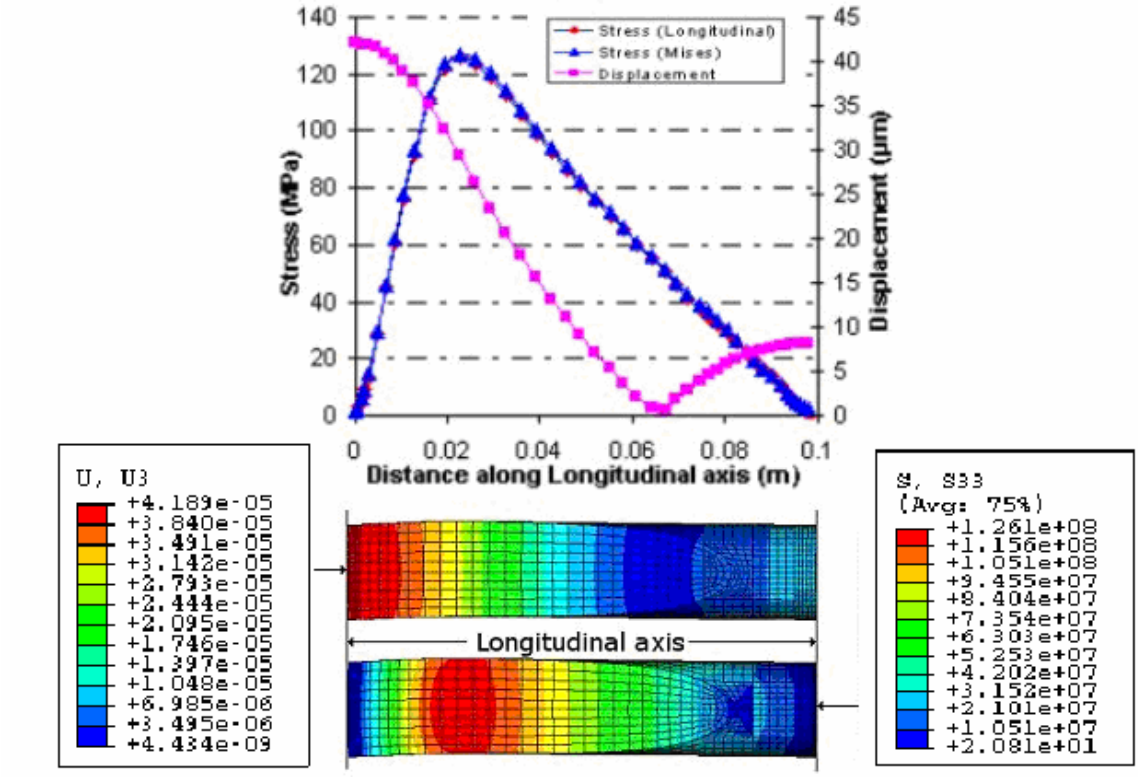

(b)

Fig. 3.12: FE stress and displacement results for (a) 20kHz and (b) 35 kHz ultrasonic cutting blades.

Fig. 3.12 (a) and (b) shows the maximum principal stress and Mises stress in both of the ultrasonic cutting blades are nearly identical as predicted in Eq. 3.23. In Eq. 3.23 it was assumed the out-of-plane stresses were zero as there was no transverse movement, only movement in the longitudinal axis but in reality there are very slight out-of-plane stresses but these are small enough to be considered negligible. The FE program calculates these small out of plane stresses when calculating the Mises stress and as such when comparing the maximum principal stress in the longitudinal axis and the Mises stress in the blade they are not perfectly identical but are very similar. The maximum principal stress for a base displacement of 8 microns, which is the output displacement from the 20 and 35 kHz ultrasonic transducers, was calculated to be 75.16 MPa at a distance of 39.95 mm from the tip of the cutting blade and 125.7 MPa at a distance of 22.71 mm from the tip of the cutting blade for the 20 and 35 kHz cutting blades respectively. The gain was calculated for the 20 and 35 kHz blades and was 5.39 for the 20 kHz blade and 5.23 for the 35 kHz blade. Thus the tip amplitude for each of the cutting blades when the transducer is operating at full power and providing a base displacement of 8 microns is 43.2 μm for the 20 kHz blade and 41.9 μm for the 35 kHz blade. For the 20 kHz blade, the nodal plane lies at a distance of approximately 114 mm from the cutting tip along the longitudinal axis of the cutting blade and at 68 mm for the 35 kHz blade. From the results we can see that the maximum stress in both of the cutting blades is significantly lower than the yield point of the Titanium alloy which is considered to be 850 MPa. It is safe to assume from the FE analysis that the ultrasonic cutting blades operate within a safe operating regime in terms of stress levels and even considering a safety factor of 4 still remain well within safe operating limits of the material.

3.6 Manufacture

Tuned ultrasonic cutting blades and other ultrasonic components use precision engineering equipment to manufacture accurately the ultrasonic components to the required size to ensure the component is tuned precisely. For the ultrasonic cutting blades used for the experimental cutting trials in this thesis, the blades were manufactured using a four axis CNC machine using computer aided manufacture (CAM) technology.

Fig. 3.13 depicts the manufactured 20 and 35 kHz blades machined to the predicted sizes using CAD/CAM technology for use on the experimental cutting rig to conduct cutting trials on food materials and to allow validation of the FE models of ultrasonic cutting.

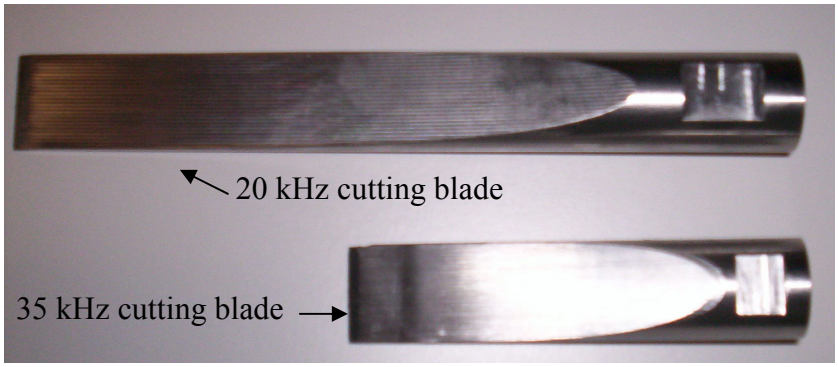

Fig. 3.13: Manufactured 20 and 35 kHz titanium ultrasonic cutting blades.

3.7 Validation

To validate the FE modelling approach to ultrasonic cutting blade design, the longitudinal mode shape from the FE analysis was analysed for both of the designed ultrasonic cutting blades and compared to the mode shapes from the EMA analysis on both blades. The EMA was conducted on both of the ultrasonic cutting blades by considering only one side of the blade geometry and creating a mesh of points along the face which should be sufficient to capture the movement of the blade at any mode shape. The FE and EMA mode shape results for the 20 kHz and the 35 kHz cutting blade are shown in Fig. 3.14 (a) and (b) respectively. From both Fig. 3.14 (a) and (b) it is evident both the 20 and 35 kHz FE and EMA modal responses for the designed ultrasonic cutting blades show movement in the longitudinal mode at both of these frequencies. The predicted modal frequencies using FEA are 2.743% and 1.29% away from the measured natural frequencies using EMA for the 20 and 35 kHz ultrasonic cutting blades respectively. Additionally to compare the accuracy of the modelling approach a normalised displacement from the FE modelling package ABAQUS where a sinusoidal forcing function is applied to base of the blade at the driving frequency of the transducer and one using the EMA software is compared in Fig. 3.15 (a) and (b) for the 20 and 35 kHz blades respectively where the frequency response of the FE analysis of the blades are measured from a single point on each of the blades. The slight variation in the natural frequency of the manufactured blades to the theoretically designed blades using FE could be attributed to the accuracy of the material properties such as Young's modulus and Poisson's ratio for the titanium used in the FE analysis, errors in machining such as the final surface finish of the component, tool wear or slight movement of the work-piece during machining of the component using the CAD/CAM system and errors in the measurement of the natural frequencies using the EMA system such as the accuracy of the laser Doppler vibrometer which is dependent on the surface finish and the geometry of the component and also in the calculation of the FRF using the FFT method. Modelling the transducer and the connection to the

ultrasonic cutting blade using FEA may reduce the error, especially in multi-blade systems driving off of one transducer but for a single blade system can be considered negligible when taking into account the other errors. The small percentage difference in the predicted modal responses compared to the measured response is sufficient to assume the FE modelling procedure for blade design can be considered accurate and is suitable for design of simplistic or complex precision ultrasonic components.

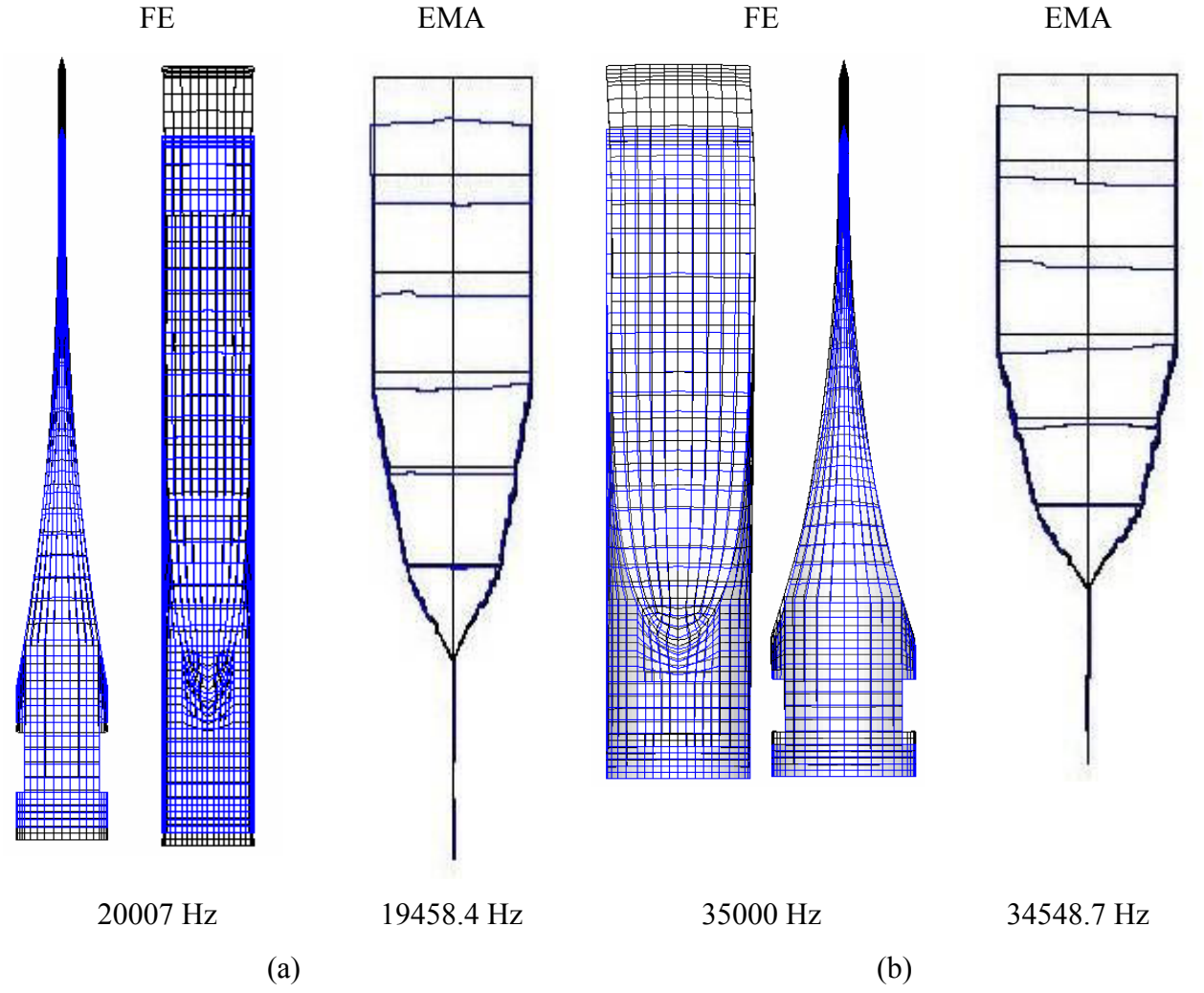

Fig. 3.14: Validation of the manufactured and theoretical ultrasonic cutting blades using FEA and EMA for the ultrasonic cutting blades tuned to (a) 20 kHz and (b) 35 kHz.

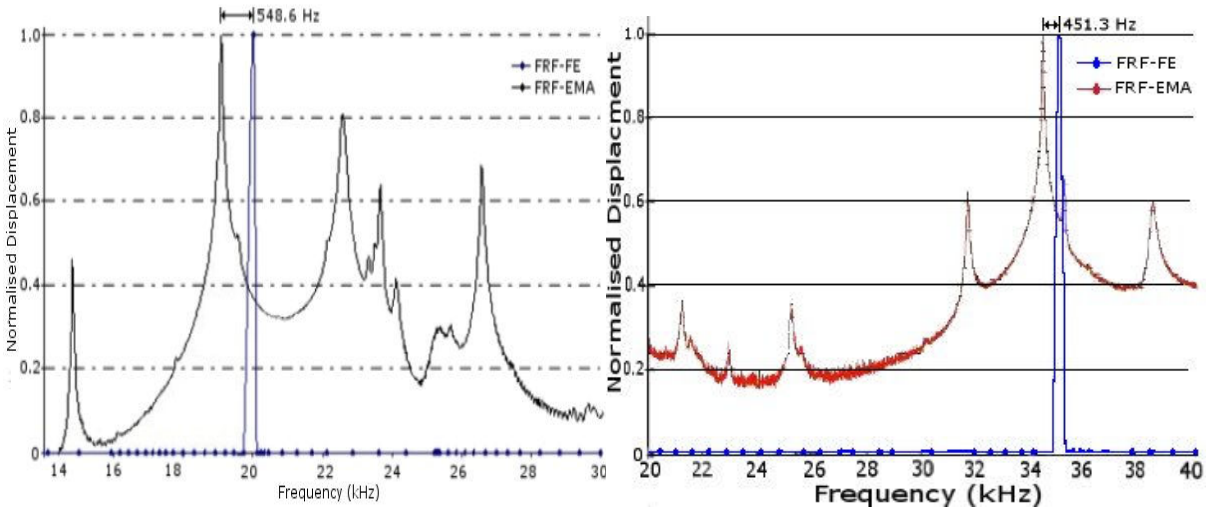

(a) (b)

Fig. 3.15: Superimposed normalised displacement for (a) the 20 kHz and (b) the 35 kHz ultrasonic cutting blades measured using FE and EMA.

3.8 Conclusions

The cutting blade design process has been introduced and explained in detail in this section and an introduction to the idea of including a FEA ultrasonic cutting simulation into the design process has been discussed with the aim of refining the design process and predict the ultrasonic cutting parameters of optimum cutting velocity, blade tip geometry, ultrasonic amplitude, cutting orientation, ultrasonic cutting blade material prior to blade manufacture. FEA was used to design two ultrasonic cutting blades resonant in the longitudinal mode at 20 and 35 kHz for use in experimental cutting tests.

The theory of the longitudinal vibration of uniform rods used to calculate the tuned length of a 20 and 35 kHz uniform steel rod has been discussed. The calculated lengths of the uniform steel rods were then modelled using the FE modelling package ABAQUS using linear and quadratic beam elements and solid quadratic elements to determine the resonant natural frequency of the longitudinal mode and also provide a mesh convergence study to provide confidence in the accuracy of the modelling approach for predicting the longitudinal mode of vibration. Results indicated that mesh convergence was achieved quicker using quadratic elements rather than linear counterparts. Convergence was achieved using only 4 quadratic and 8 linear beam elements and 6 solid quadratic elements along the longitudinal axis of the rod.

A 20 and 35 kHz titanium blade for experimental cutting trials was designed and tuned using FEA. A frequency and steady state dynamic analysis was performed on both of the ultrasonic

cutting blades from the initial design concept and tuned to the driving frequency of the transducers to resonate in the longitudinal mode of vibration. The tip displacement, gain, maximum stress and its location along the longitudinal axis and the nodal position along the longitudinal axis in both of the ultrasonic cutting blades were determined using the FE procedure for a sinusoidal base displacement of 8 microns simulated at the longitudinal driving frequency which considers the maximum output displacement of the transducers. The stress results were analysed for the maximum vibrational output of the transducers considering a safety factor of 4 during operation to ensure the stress levels did not exceed the yield point of the blade material to ensure the operational condition of the material always resided in the elastic region. The final designs were manufactured using CAD-CAM technology and then EMA was used to validate the dynamic response of the manufactured ultrasonic blades and compare the findings with those of FEA. This chapter has investigated the use of FEA for ultrasonic component design and illustrated how the versatile modelling process can be used for sophisticated ultrasonic blade design.

Chapter 4

Characterisation of the mechanical and thermal properties of food products

4.1 Introduction

There is a growing interest in deriving mechanical and thermal properties data of food products in order to model food processing applications and also to characterise food texture, mastication or storage. For most food products, such data is not readily available and there is also therefore a growing interest in assessing the applicability of standard materials testing techniques in the characterisation of foods. Research to derive accurate mechanical and thermal properties of food products for use in the food processing, packaging and storage industries has been gathering momentum in recent years [137]. Several studies have also reported research which tries to relate the mechanical properties of food to the consumers' perception of texture, crispness, crunchiness and mastication [149-151, 193-206]. Also, the food processing industry is increasingly interested in improving the throughput of their production lines while increasing the quality of their final product. Typical food processing operations will involve cutting, shredding or rolling of a product into a final product shape for packaging. In order to optimise these processes, there is significant value in creating food process models, but these rely on the availability of accurate mechanical and thermal properties data of the foods. Developing accurate and reliable material data for use in finite element analysis programs such as ABAQUS [252] or for engineering calculations is of paramount importance and for FE modelling can be the distinctive factor determining if a simulation gives accurate and realistic results.

In this study, food properties data is required in order to develop finite element models of food cutting processes and in particular ultrasonic cutting, which is a technology gaining popularity in the food industries. Modelling the interaction of a cutting blade and a food product relies critically on an accurate description of the food material and, for ultrasonic cutting, also relies on an accurate determination of the temperature dependent material properties.

This investigation uses four materials, namely cheese, toffee, chocolate and jelly, to determine the mechanical and thermal properties of these foods from experimental tests for implementation in FEA, especially simulations of the ultrasonic cutting process. The food materials selected were considered to be general representations of each food material and are not considered to accurately represent the full spectrum of toffee, cheeses, chocolates or jellies available in the market. The methodology presented however, allows specific types or brands of food products to be tested but consideration should still be given to the batch dependency of food products in addition to age, storage and transportation during testing. The common food materials cheese, toffee, chocolate and jelly were selected because these materials have very different mechanical and thermal behaviours, they are readily available, and their batch dependency can be somewhat controlled.

4.2 Introduction to the stress-strain diagram

Tensile and compression tests are conducted by pulling or pressing a specimen with a predefined geometry along an axis until failure occurs in the specimen. The two measurable quantities are force required to pull or compress the specimen and displacement of the specimen under load. Corresponding stress-strain curves for the materials can then be plotted and mechanical properties such as Young's modulus, E, yield stress, σ_{yp}, ultimate tensile strength, σ_{uts}, nominal stress, σ_n, true stress, σ_t and break point, σ_{bp}, can be determined for use in engineering calculations or for FEA as shown in Fig. 4.1, which represents typical behaviour of an elastic-plastic material.

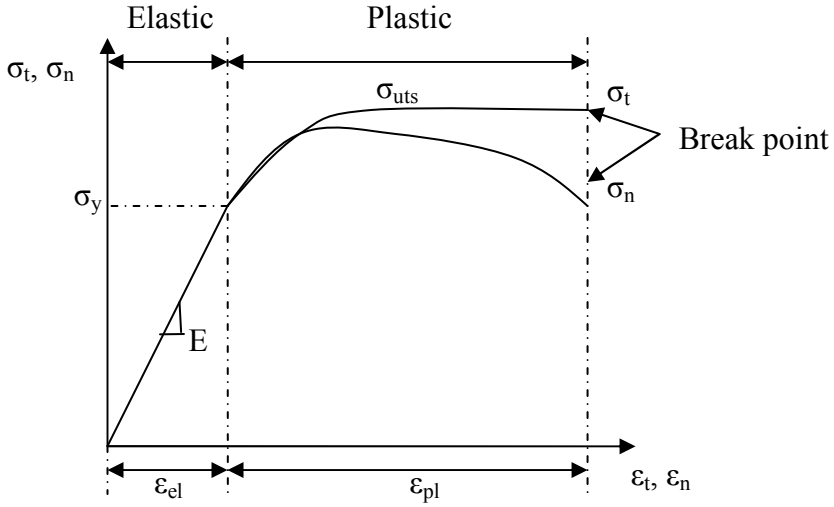

Fig. 4.1: Stress-strain diagram showing typical mechanical properties of interest.

Two different types of strain can be calculated, nominal strain sometimes called Cauchy strain, ε_n, or true strain sometimes called Hencky or logarithmic strain, ε_t. Nominal strain is calculated by dividing the absolute extension or compression of the specimen against the original length of the specimen using Eq. 4.1 and true strain, which accounts for the change in cross sectional area as the specimen is being deformed, can be calculated using Eq. 4.2, where ε_n is the Cauchy strain or nominal strain which is dimensionless, ε_t is the Hencky strain or true strain, again dimensionless, Δh is the absolute deformation of the specimen and h_0 is the initial sample height. Nominal strain is a small strain measure and is only usually recommended to be used up to 5% strain. For larger strain values true strain should be used as there is a large geometry change in the specimen and the area reduction is usually large which incorporates higher inaccuracies in the solution. Volume is assumed to be conserved while the material is deformed.

$$\varepsilon_n = \Delta h/h_0 \tag{4.1}$$

$$\varepsilon_t = \ln[(1+ \Delta h/ h_0] \tag{4.2}$$

There are several techniques used to measure the extension of a specimen or component when an external load is applied in either tension or compression, the most common being a strain gauge or an extensometer. Strain gauges work by adhering a linear or rosette foil gauge to a specimen using a thin layer of adhesive. As the specimen is elongated the resistance of the wire in the strain gauge changes and is proportional to a change in voltage which can be correlated to the strain. Strain gauges are very accurate but bonding to various materials can be difficult or impossible as in the case for foods due to the soft nature of the material or its oily surface. The adhesive can also chemically change the material which can affect the measurements and cause errors in mechanical properties estimations. Extensometers vary in sizes and types, they can be contact or non-contact and are usually used to measure strain over a predefined distance. Fig. 4.2 depicts a jelly tensile specimen pulled in tension, where the laser extensometer directs a narrow laser beam along the central vertical axis of the specimen. The laser beam is reflected by two thin reflective strips adhered to the specimen at a predefined distance apart, usually the gauge length of the specimen. As the specimen elongates, the reflective strips move and their position is recorded. This technique is a more accurate displacement measurement for the specimen than the internal extensometer fitted to the tensile testing machine as the displacement is calculated over the gauge length explicitly whereas the internal extensometer calculates displacement of the specimen and the internal fittings of the machine to the crosshead and accounts for a change in length of the grips, specimen and fixtures.

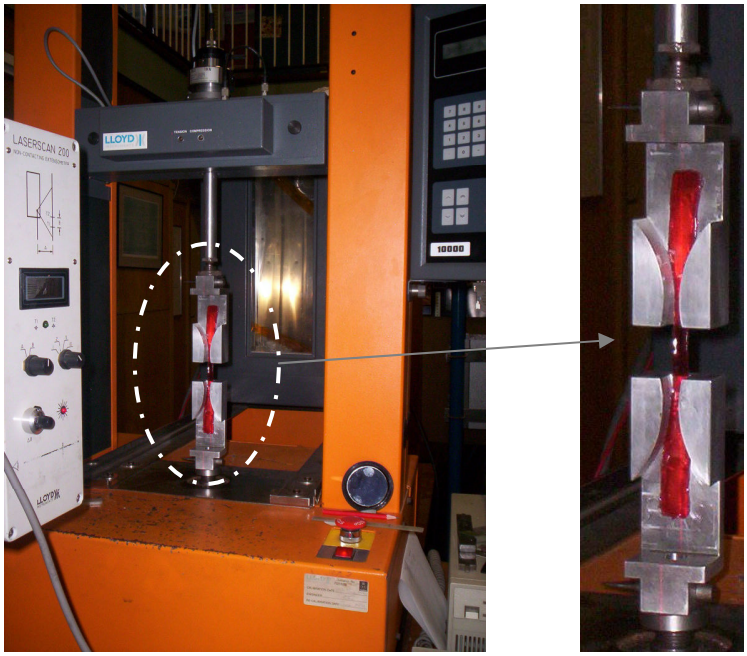

(a) (b)

Fig. 4.2: (a) Tensile testing configuration with laser extensometer and (b) Exploded view of gripping arrangement.

Two different types of stress can be calculated, nominal stress, σ_n, and true stress, σ_t. Nominal stress is calculated using Eq. 4.3. True stress can then be calculated using Eq. 4.4, which accounts for the change in cross-sectional area as the specimen is being deformed. In Eq. 4.3 and Eq. 4.4 A_0 is the initial cross-sectional area, F is the Force, σ_n is the engineering stress or nominal stress and σ_t is the true stress. Again true stress should not be used for anything exceeding 5% strain of the specimen as large deformation occurs and hence a large geometry change but nominal stress is suitable up to this value and the volume is assumed to be conserved during deformation of the specimen.

$$\sigma_n = F / A_0 \tag{4.3}$$

$$\sigma_t = \sigma_n(1- \varepsilon_n) \tag{4.4}$$

The Young's modulus, E, is specified as the gradient of the linear region of the nominal stress – nominal strain curve where the material exhibits elastic behaviour and conforms to Hooke's Law. For materials such as steels this region is linear with a distinct yield point. However, not all materials behave in a truly linear fashion and are often characterised as exhibiting non-linear

behaviour with no distinct yield point. However, the Young's modulus is an important parameter in defining a material's characteristics and obtaining this parameter from uniaxial tests is advantageous in design as many structures or components are required to exist in the elastic region and this one parameter can define the elastic region of a material. Several methods have been developed to define the Young's modulus from uniaxial tests, such as the 0.2% offset method where the linear region is approximated from the nominal stress–nominal strain curve and then an imaginary line is offset parallel to the approximated linear region to 0.2% of the total strain. Where the imaginary line intersects the nominal stress–nominal strain curve the yield point of the material is defined as shown in Fig. 4.3. The yield stress is the location which defines where the material ceases being elastic. If a load is applied up to this point and then removed the material would be considered to return to its original length. However if the material is loading up to and exceeding this point it is considered that the material would not return to it's original length, simply remaining deformed in a state of plasticity.

The ultimate tensile strength, σ_{uts}, is the greatest stress a material can withstand prior to significant deformation of a material occurring and catastrophic failure following at the break point, σ_{bp}. This is shown in Fig. 4.1 and Fig. 4.3.

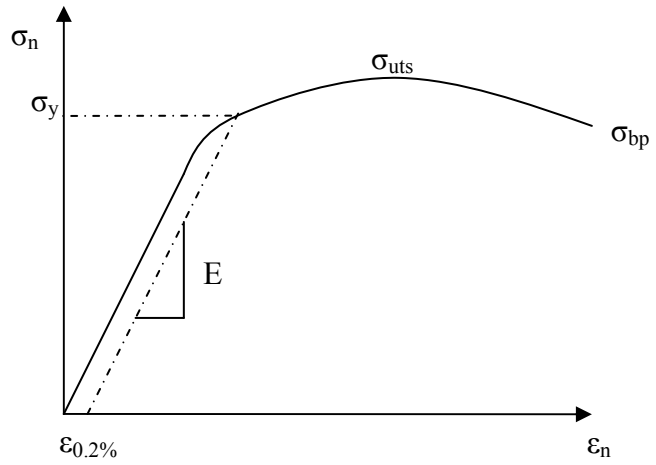

Fig. 4.3: Stress-strain diagram showing 0.2% offset method.

4.3 Uni-axial testing techniques

Currently the majority of food material testing utilises the uniaxial compression test, where a sample of food is pressed between two platens at a fixed speed and the measured load and

displacement data is used to derive the stress-strain relationship. This method is chosen over the tensile test due to the simplicity of the testing configuration and specimen shape [193, 195]. Tensile tests require dog-bone specimens to be produced, with a requirement that the specimen can be gripped at its extremities by clamps and that the specimen tapers to a uniform cross-section for a given gauge length. Tensile tests are difficult to perform on most foods, as specimens are very difficult to cut exactly to size without creating flaws and are extremely difficult to grip without inducing failure in the specimen. However, compression tests have inherent problems due to the contact surfaces, where friction between the platens and the sample can cause the specimen to deform non-uniformly. This either results in barrelling, where the specimen deformation at the central cross-section is greater than at the surfaces in contact with the platens, or hour-glassing, where material deformation is greater at the surfaces in contact with the platens than at the centre. These effects can be reduced with the application of a lubricant between the platens and the specimen to reduce barrelling, but over-lubrication can cause the specimen to deform into an hourglass shape [195]. In addition, it has been found that certain food materials, such as cheese, will leak oils and fats which can adjust the lubrication condition between the specimens and platens. Also, the characterisation of failure from the measured data is difficult to quantify and is usually determined from the fall-off in the measured force-displacement curve or at the plateau region [194]. The plateau region is where as strain increases there is no increase or decrease in stress in the material, the specimen exhibits a constant stress condition. However, many soft materials, including many foods and especially foods at higher temperatures, do not necessarily show a fall-off because the specimen continues to deform until flat. Consequently, the failure location on the stress-strain curve is difficult to identify. Generally, compression tests are simple to perform but the derived mechanical properties are not representative of those derived from tension tests. In food processing applications such as cutting, failure can occur either in tension or in shear at the interface between the blade and the material, so it would be advantageous to be able to characterise the material from tensile test data as well as compression test data.

The mechanical properties of foods are highly temperature dependent and therefore the temperature dependent material properties are required for modelling processes such as cutting, shredding and rolling. Food materials also often change temperature through the production process so that for accurate modelling, temperature data is essential to try to encapsulate the complete process. In the case of ultrasonic cutting, the temperature at the cutting surface is governed by a combination of the cutting parameters (such as frequency, ultrasonic amplitude

and cutting speed) and the cut material, and therefore temperature dependent material properties must be included in any cutting model.

4.3.1 Specimen Preparation

4.3.1.1 Tensile test specimens

A diagram illustrating the sizes of the tensile specimens used for each material are shown in Fig. 4.4. The thickness of the specimens varies depending on the material being tested and manufactured.

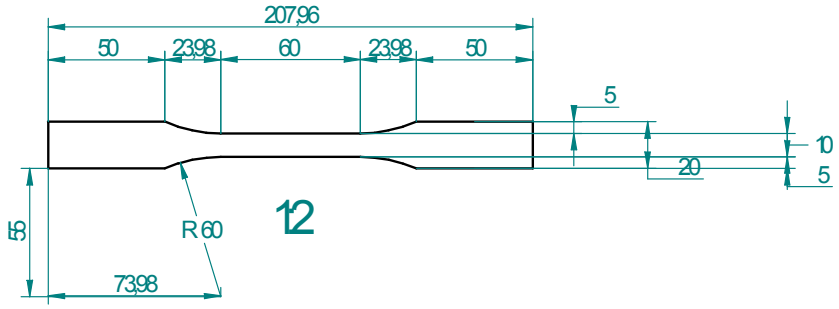

Fig. 4.4: Tensile specimen dimensions in mm.

Toffee was cooked using a standard recipe and chocolate was heated in a saucepan. The mixture was then carefully poured into specially designed moulds that were pre-greased with butter to ensure that the mixture did not adhere to the sides. The tensile test specimen moulds were manufactured by machining a pocket in the shape of a tensile test specimen in a sheet of aluminium and drilling and tapping 6 screw holes in the top and bottom faces of the machined pocket to allow flat aluminium plates to be screwed onto the faces. The moulds were designed to be open at the top that allowed the mixture to be easily poured and excess air to be removed. The base of the moulds had a small opening to allow the molten toffee or chocolate to flow to the base and push excess air out at the bottom. This ensured no air was trapped in the specimen when it set. The specimens were allowed to set for 1 hour and were then carefully removed from the moulds. The final dog bone specimens and moulds are shown in Fig. 4.5.

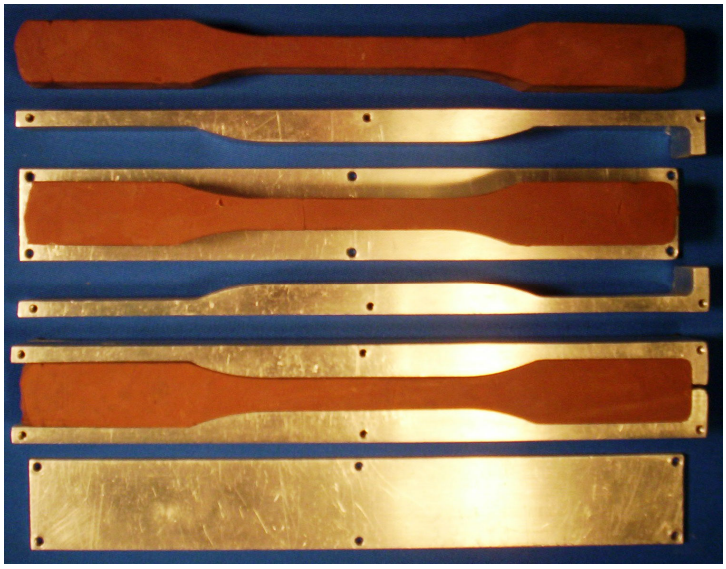

Fig. 4.5: Tensile test specimen moulds and chocolate specimens.

To prepare cheese specimens a large block of cheese was sliced in a band saw to a uniform thickness of 10 mm. A steel dog bone template was placed on the cheese slice and a scalpel was used to cut around the template in one continuous movement to produce the final dog bone shape. Care had to be taken when cutting around the template with a scalpel to prevent tearing. Optimum results were obtained by ensuring the scalpel remained vertical and cutting was performed in one continuous movement around the template, as shown in Fig. 4.6.

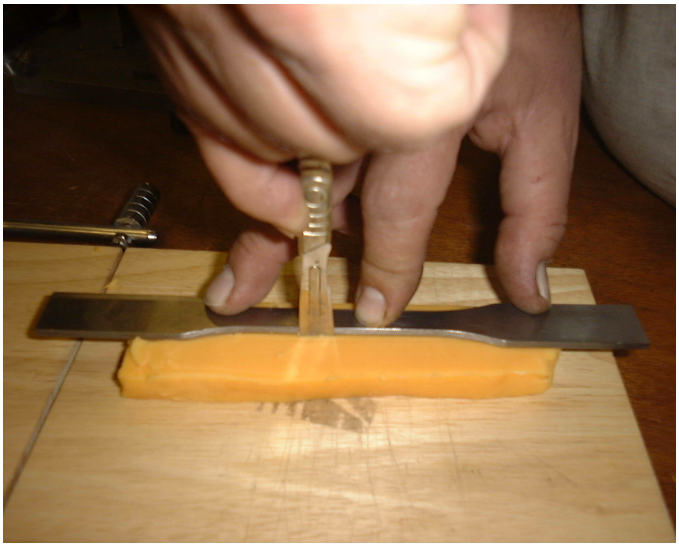

Fig. 4.6: Cheese tensile specimens and manufacturing technique.

Jelly dog bone specimens were created by pouring a liquid jelly mixture, made from solid gelatine and a spoonful of water, into dog bone moulds. The moulds used for jelly differ from the ones described previously as the opening for pouring is created along the length of the specimen and not at the top. The sides of the moulds are secured to a flat plate by screws prior to pouring. To aid removal of the specimen it was determined that sticking of the specimen to the moulds

could be prevented by thoroughly cleaning the moulds prior to pouring. This moulding configuration can be shown in Fig. 4.7. This moulding configuration is preferred over the one explained previously for toffee and chocolate as the jelly has a significantly lower viscosity than the molten chocolate or toffee and flows much better when poured.

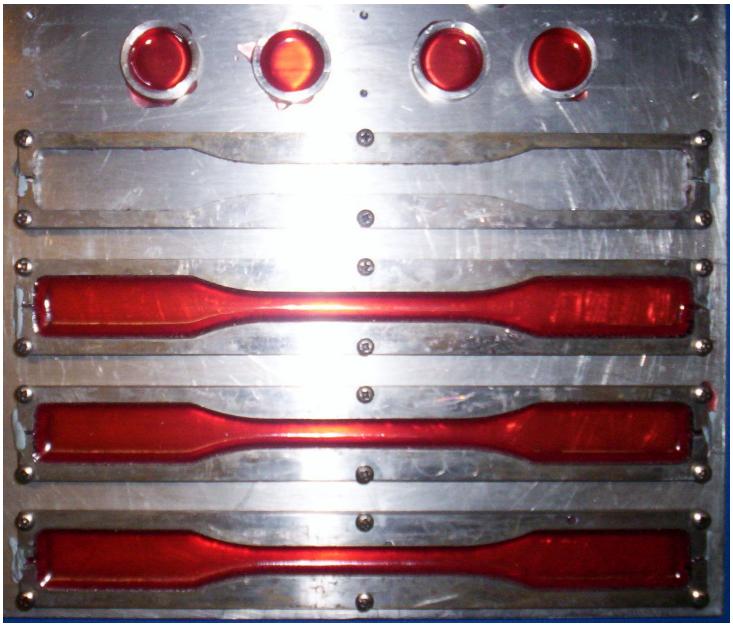

Fig. 4.7: Moulding configuration for jelly.

The moulds depicted in Fig. 4.5 have been found to be more effective in producing dog bone specimens where the flowing mixture is a higher viscosity. The material takes a long time to flow from the poured region to the extremities of the mould. Findings indicated if the material has to flow a long distance the specimen is usually formed unevenly as pouring is difficult to control in addition to the material often setting before reaching the extremities of the mould which is prevented in this configuration. The mould opening as shown in Fig. 4.5 has a low surface area at the pouring location but is large enough to ensure pouring the molten material into the opening without touching the sides is easy. The high viscosity material can then reach the extremities of the pouring location quickly forming the specimen shape and gravity and an accurate eye and steady hand can ensure the material reaches the bottom of the mould. An indication the material has also reached the bottom of the mould is the material starts to slightly flow out of the base through the slight opening deliberately designed to expel air out of the specimen. The high viscosity ensures minimum material flows through the slight void and setting results quickly on the cold moulds again ensuring minimum material loss. When the pouring location is located at the top of the dog bone specimen the unevenness of the surface is not as important as no measurements are taken for cross-sectional area or gauge length from that surface so stress-strain determination is unaffected. This moulding configuration is not as useful

or as efficient for low viscosity molten materials as the material flows quickly through the small void at the base of the moulds and through any small gap in the moulds. Material loss moulding using this method is extremely high when moulding a high viscosity molten material, and the configuration described in Fig. 4.7 is more efficient.

The configuration in Fig. 4.7 allows the material to be poured easily into the largest side of the mould. When poured the low viscosity of the material means it reaches the extremities of the mould quickly and the material does not set before it reaches the sides of the moulds. The thickness of the material can be controlled accurately by pouring, no air is trapped in the specimen as the pouring location is extremely large in relation to the specimen and can be vented easily into the air and material loss is minimal as the splits in the moulds are plugged using a soft removable material. When the specimen sets the material slightly contracts at the pouring surface but for low viscosity materials this has been found to be negligible during measuring the specimen thickness. However, this is not the case for materials with a high viscosity, studies have found the material contracts significantly at the interface between the specimen and the moulds. The surface at the pouring location experiences a significant curvature and when measuring the thickness of the specimen the curvature can incorporate significant errors when calculating cross sectional area.

Two methods were attempted to remove this curvature when manufacturing specimens using a high viscosity material. Firstly, the toffee specimens with a high viscosity were allowed to set in the moulds then the curved side of the specimen produced after moulding was dissolved using water by initially lightly running the curved side under a tap and then latterly by rubbing the surface with a wet cloth. This technique did remove the curvature in the specimens but the method was very laborious and time consuming and could often either dissolve too much of the specimen in the case when using the flowing water from the tap, or induce failure in the specimens prior to removal from the moulds in the case with rubbing the surface. The second technique considered skimming the top of the moulds with an ultrasonic knife initially when the mixture was still warm and once it had set. Cutting using an ultrasonic knife in the food industry is extremely advantageous as the high oscillatory movement of the blade prevents material adhering to the surface and also causes the material to melt locally at the cutting interface which could be useful in removing the curvature of the specimens in the moulds. When the excess material was removed with the ultrasonic knife when the mixture was warm the tacky surface tended to pull all the material located in the mould out as well as removing the excess material.

When the material was set the initial contact between the ultrasonic knife and the moulds/specimen often shattered the specimen or caused hairline cracks in the specimens and when removed from the moulds they were often completely destroyed. The moulding arrangement in Fig. 4.5 is the preferred option for moulding high viscosity molten materials.

4.3.1.2 Compression test specimens

Dog bone specimens of toffee were moulded and manufactured as previously discussed. To create compression test specimens the ends of the dog bone specimens were cut using a hacksaw to 20mm and the rough uneven edges on the surface were dissolved in water and smoothed using a surface polisher, which created the cube specimens. Cube specimens were used instead of circular specimens due to ease of manufacture. For cheese, a block of cheese was sliced to 5.5 mm thick on a bandsaw. Specimens were then pressed out of the cheese slice using a 22 mm circular cutter. Care had to be taken when pressing out the specimens as the sides would slightly deform due to the soft nature of the cheese. For this reason the specimens were cut out of the cheese slice after having been placed in a refridgerator for 1 hour at 4 °C, which reduced the uneven edges. Jelly and chocolate compression test specimens were manufactured by pouring the material into circular moulds of diameter 20 mm and thickness 5 mm. The specimens were then carefully pressed out of the moulds ready for testing.

4.3.2 Tensile Tests

Tension tests of toffee and cheese were conducted on a Lloyd's testing machine at crosshead velocities of 5, 15 and 25 mm/min and at temperatures of 20, 25, 30 and 35 °C for toffee, 4, 24, 30 and 35 °C for cheese. Jelly and chocolate were tested in tension at temperatures of 4 and 20 °C on a Lloyd's testing machine at crosshead velocities of 20, 40 and 60 mm/min for jelly and at 0.25, 1, 2 and 4 mm/min for chocolate. All dog bone specimens were measured using a micrometer for accurate measurement of cross sectional area and then placed in specially designed grips that allowed the specimens to be pulled under the radii of the dog bone specimens to overcome gripping difficulties. The novel grips are shown in Fig. 4.8. The grips are made from aluminium to minimise weight on the test machine and are connected to the test machine by passing a pin through location holes at the top of the grips. They have two radii of 60 mm diameter (the same as the dog bone specimens) machined to allow the dog bone specimens to reside on the grips and allow an equal pressure distribution to be placed on the radii of the grips during testing. This ensures no failure occurs at the gripping locations. Special attention was

given to the alignment of the grips in the testing machine to ensure they were perfectly in plane to remove any possibility of a bending moment or rotation being produced, which could cause the specimen to fail prematurely.

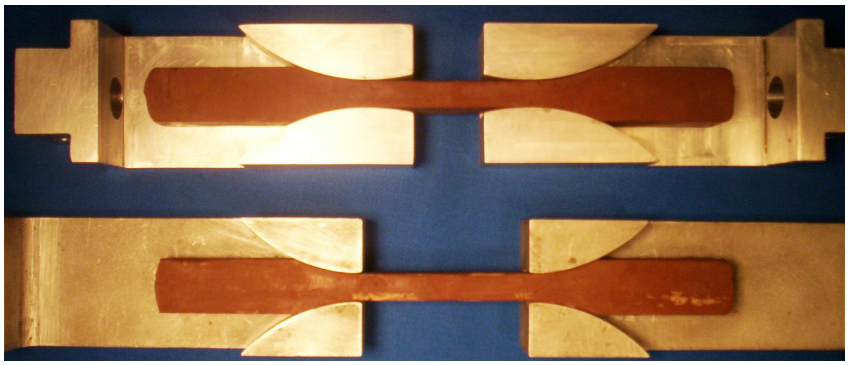

(a)

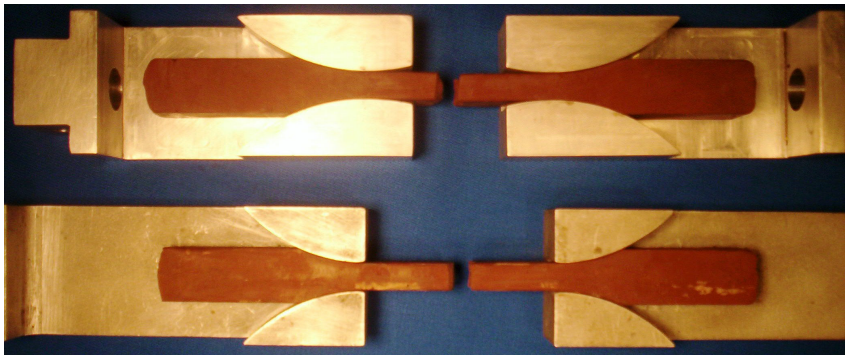

(b)

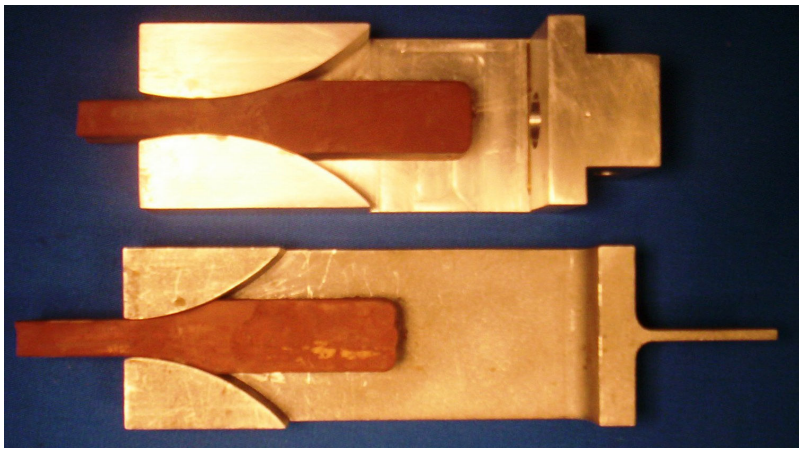

(c)

Fig. 4.8: Custom designed novel tensile testing grips where (a) Specimens are set up prior to testing (b) specimens have been pulled in tension and failed (c) attachment to the test machine can be either by a pin and a lock nut or by gripping a thin plate.

For jelly, the ends of each dog bone specimen were placed between two small plastic plates and clamped to the grips using tool maker's clamps because of the very flexible nature of the

material and to ensure that the specimen remained aligned in the grips during testing. This procedure was performed prior to testing on the specially designed grips to ensure a uniform pressure was placed across the specimen and to avoid tearing the sample when the clamps were tightened. As the specimen was placed on the radii of the grips it was very difficult to keep the specimen vertical and in-line as the specimen tended to adhere to the grips at various locations along the radii of the dog bones and at the surface at the back of the specimen. To avoid this, oil or water was used to lubricate the sides of the grips and on the specimen but testing indicated that lubrication with water or oil dissolved part of the specimen and often rendered the specimen fragile for testing. It was found that when the main constituent of the jelly, gelatine, interacted with a fluid, the viscosity of the specimen was altered and the mechanical properties of the material changed.

When placing the specimens in the grips care was taken to avoid cracking or scratching the specimens, which could induce failure prior to or during testing. This could be avoided by careful preparation and handling of the samples. Each specimen was placed in a controlled environmental chamber at the test temperature for 1 hour to allow the heat to soak through the specimen and the specimen to equilibrate at the test temperature. A control specimen with a thermocouple embedded at the centre of the gauge length was placed on a duplicate set of grips on a clamp stand at the back of the chamber and used to monitor the temperature on a digital display. This duplicate specimen was used to ensure the correct test temperature was obtained in the centre of the specimen. During the heat soaking period prior to testing, the specimens elongate slightly. The slack was taken up in the grips carefully before the test at a very slow crosshead velocity to ensure that the specimen did not break prior to testing. The specimen was then pulled at the appropriate crosshead velocity until failure.

The only exceptions were cheese, chocolate and jelly tests at 4 °C. For these tests the specimens were refrigerated for one hour and then placed immediately in the test machine. This eliminated the need for liquid nitrogen to be used in the testing chamber for cooling. The very small time delay between removing the specimen from the refridgerator and testing meant that the specimen temperature did not rise above 4 °C and the temperature change was negligible.

4.3.3 Compression tests

Toffee and cheese were tested in a Lloyd's uni-axial testing machine in compression at temperatures of 20, 25, 30 and 35 °C for toffee and temperatures of 4, 24, 30 and 35 °C for cheese at crosshead velocities of 5, 15 and 25 mm/min. Jelly and chocolate were tested in compression at temperatures of 4 and 20 °C on a Lloyd's tensile testing machine at crosshead velocities of 20, 40 and 60 mm/min for jelly and at 0.25, 1, 2 and 4 mm/min for chocolate. A set of digital callipers was used to measure each of the specimens prior to testing to ensure the cross sectional area of the specimen was calculated accurately. Each specimen was positioned between two platens which were lubricated with two drops of silicone grease on each side to eliminate the barrelling and hour glassing effect in the specimen during testing. The centre of each specimen was carefully positioned below the plunger of the testing machine to ensure that the compression force was being applied axially. Each specimen was placed in the environmentally controlled temperature chamber and allowed to equilibriate for 1 hour to ensure that the specimen was at the correct testing temperature. Again a duplicate specimen was placed at the back of the cabinet and the temperature inside the material was monitored on a digital display. For cheese at 4 °C the tests were again conducted by removing the specimen from the fridge and placing it immediately in the testing machine. The specimens were then compressed to failure. This procedure was repeated for each food material, temperature and crosshead speed three times.

4.4 Extracting Material Properties for Finite Element Modelling

Once a material's stress-strain behaviour has been characterised it is important to determine the material response and identify the elastic and plastic regions of the material and the fundamental mechanical properties such as Young's modulus, yield stress, ultimate tensile stress and break stress. Several material models exist within finite element packages to represent experimental data in a convenient form that can be used in the solution to finite element problems. Two of the material models available in the commercial finite element code ABAQUS will be used in studies involving food materials, namely the elastic-plastic and hyperelastic material models [252-253]. The elastic-plastic material model will describe the material behaviour using fundamental engineering properties such as Young's modulus and yield stress at different temperatures and crosshead velocities. The hyperelastic material model allows a non-linear description of the tensile and compressive response of the material to be represented as one strain energy density function. For materials with differing tensile and compressive behaviour it can be advantageous to model both types of behaviour for certain processes such as cutting.

4.4.1 Elastic-plastic curve fitting technique

The elastic-plastic material model assumes that the material is categorised into two distinct regions, the elastic region and the plastic region. The elastic region is perfectly linear and is represented using Young's modulus and Poisson's ratio for each test temperature. The plastic region is defined in terms of true stress and corresponding plastic strain values, ε_p, at each temperature and the yield stress is defined where the plastic strain is zero. This is shown in Fig. 4.1. The measured force-displacement data from the experimental tests on the food materials (toffee, cheese, chocolate and jelly) was converted to nominal stress-nominal strain using Eq. 4.5 and Eq. 4.6 where σ_n is the nominal stress, F is the force, A is the original cross-sectional area, ε_n is the nominal strain, l is the deformed length and l_0 is the gauge length of the specimen. The experimental data was then converted to true stress and true strain using Eq. 4.7 and Eq. 4.8 where σ_t is the true stress, σ_n is the nominal stress, ε_n is the nominal strain and ε_t is the true strain.

The elastic properties used in the material model were Young's modulus and poisons ratio at different test temperatures and crosshead velocities. The Young's modulus was calculated from the linear region of each of the nominal stress-nominal strain diagrams for all food materials in tension and compression and at each temperature and crosshead velocity tested. The Poisson's ratio for each food material, testing configuration and test temperature was assumed to be 0.49, which has been typically used to represent most food materials [201-203]. The plastic region of the true stress against plastic strain from the yield stress of the material to the UTS was defined for all materials, again in both testing configurations where applicable and at the tested crosshead velocities and temperatures, using a power law curve as described in Eq. 4.9 where ε_0 is the true strain at the yield point, σ_0 is the true stress at the yield point, ε is the strain, σ is the stress and n is the curve fitting exponent.

$$\sigma_n = \frac{F}{A} \tag{4.5}$$

$$\varepsilon_n = \frac{l - l_0}{l_0} \tag{4.6}$$

$$\sigma_t = \sigma_n\left(1 + \varepsilon_n\right) \tag{4.7}$$

$$\varepsilon_t = \ln(1 + \varepsilon_n) \tag{4.8}$$

$$\frac{\varepsilon}{\varepsilon_0} = \left(\frac{\sigma}{\sigma_0}\right)^n \tag{4.9}$$

4.4.2 Hyperelastic curve fitting technique

Hyperelasticity is the general term given to materials such as rubber that can experience large deformations in the order of 100 – 700 %, usually due to the untwisting of cross linked molecular chains. The material is nearly incompressible as there is little volume change under applied load and can usually be modelled as incompressible unless in confined spaces where volumetric data is essential for accuracy. The hyperelastic curve-fitting procedure is typically used to model isotropic, large strain, nearly incompressible, elastic, non-linear rubbers exhibiting S-shaped behaviour in the stress-strain diagram, or J-shaped behaviour for biological materials, in the form of strain energy density functions [252-254]. These materials are susceptible to elastic instabilities which do not conform to Hooke's Law. Often their stiffness decreases with increasing load at some regions of the S-shaped curve. For J-shaped curves, initially a small increase in stress results in large strain, but at larger extensions the material becomes increasingly stiff. Very rarely food materials exhibit classical linear elastic behaviour that conforms to Hooke's law, more often the stress-strain response is non-linear where the response in the stress strain diagram is often in the form of S or J shaped curves.

ABAQUS [252], as with other finite element packages, offers curve fitting procedures to characterise the response of a material exhibiting S or J shaped curves from nominal stress-strain data from uni-axial tension or compression, bi-axial tension or compression, planar shear or volumetric compression tests or combinations of all of these. The curve fitting procedures generalise the nominal stress-strain response using elastic strain energy potentials of the experimental data. The curve fitting procedure is extremely sensitive to the test data input and can often cause material instabilities if not properly applied to the model. Many of the strain energy potentials require a minimum of uni-axial tension or compression data to produce stable results. For the first order models such as the Arruda-Boyce [252] or the Mooney-Rivlin [252] the strain energy potential can be determined from one set of test data but the accuracy of the response is compromised with insufficient material data and often can cause strain hardening effects at high strain rates. Due to the sensitivity of this fitting procedure to test data input, steps can be taken to reduce the fitting errors by approximating the stress-strain response to a

polynomial equation prior to including in the fitting procedure and generating equally spaced data points using the polynomial function [202].

Hyperelasticity models are assumed to be isotropic, isothermal and elastic resulting in the strain energy potential being created as a function of the strain invariants. There are three strain invariants denoted I_1, I_2, I_3 as defined in Eq. 4.10, 4.11 and 4.12 from the principal stretch ratios, $\lambda_1, \lambda_2, \lambda_3$,which are commonly used to define the strain energy density function, W [253].

$$I_1 = \lambda_1^2 + \lambda_2^2 + \lambda_3^2 \tag{4.10}$$

$$I_2 = \lambda_1^2\lambda_2^2 + \lambda_2^2\lambda_3^2 + \lambda_3^2\lambda_1^2 \tag{4.11}$$

$$I_3 = \lambda_1^2\lambda_2^2\lambda_3^2 \tag{4.12}$$

I_3 =1, for fully incompressible materials.

The three principal stretch ratios, $\lambda_1, \lambda_2, \lambda_3$, can be defined by using the expression for uniaxial tension as shown in Eq. 4.13:

$$\lambda = \frac{L}{L_0} = \frac{L_0 + \Delta u}{L_0} = 1 + \varepsilon_E \tag{4.13}$$

Where L is the deformed length of the specimen, L_0 is the original length of the specimen, Δu is the extension of the specimen and ε_E, is engineering strain. The principal stretch ratio's can be described graphically in Fig. 4.9 where $\lambda_B, \lambda_u, \lambda_S, \lambda_v$ are the stretch ratios in the biaxial, uniaxial, shear and volumetric configurations respectively.

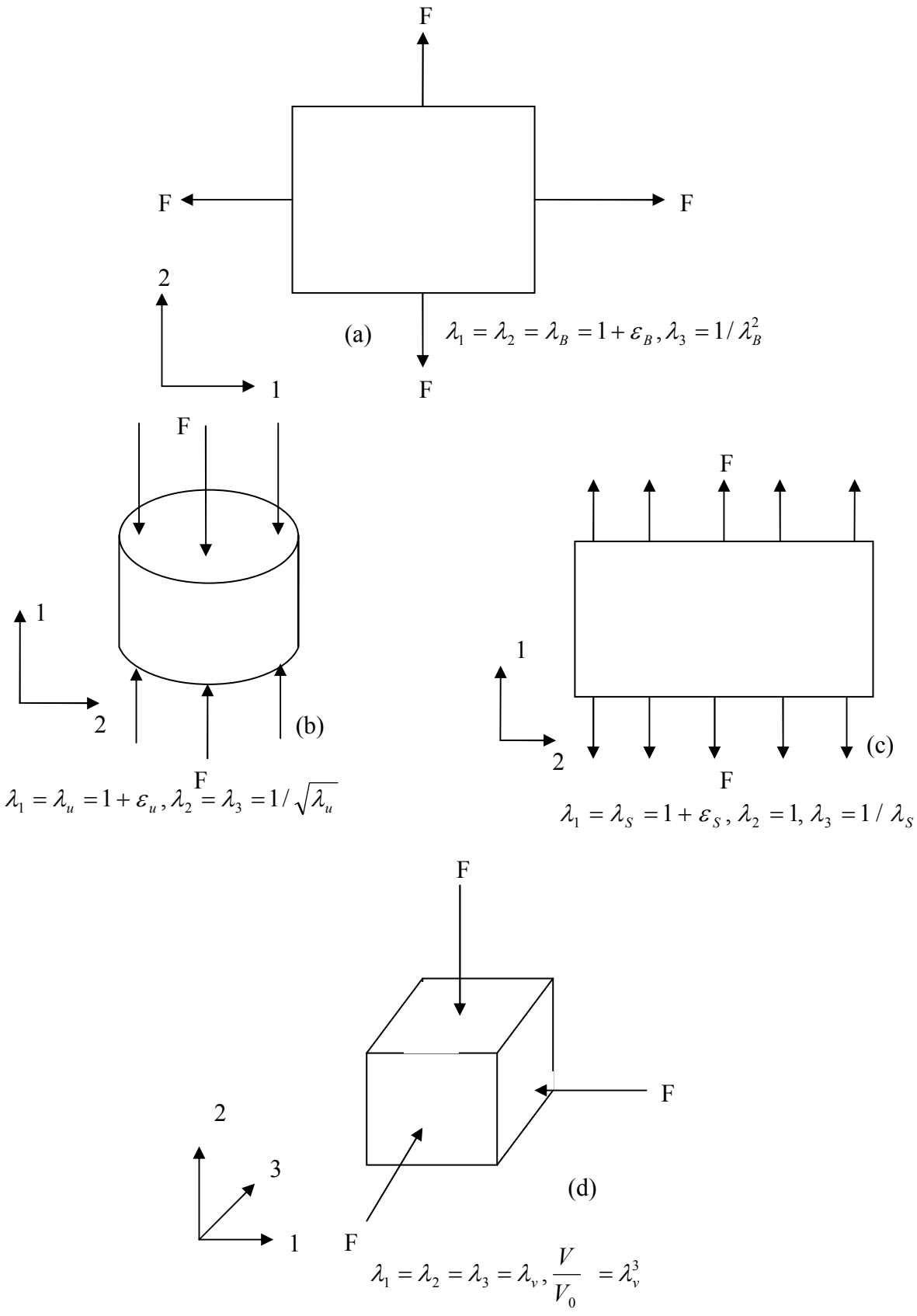

Fig. 4.9: Deformation modes with associated principal stretch ratios (a) biaxial tension, (b) uni-axial compression, (c) planar shear and (d) volumetric compression.

Compressibility can be defined by the ratio of the initial bulk modulus, κ_0, to the initial shear modulus, μ_0, or through poisons ratio, υ as expressed in Eq. 4.14.

$$\upsilon = \frac{3(\kappa_0 / \mu_0 - 2)}{6(\kappa_0 / \mu_0 + 2)} \tag{4.14}$$

Isotropic thermal expansion is allowed within the material model where the elastic volume ratio, J_{el}, is related to the total volume ratio, J_{tot}, and thermal volume ratio, J_{th}, by Eq. 4.15 and Eq. 4.16 where ε_{th} is the linear thermal expansion strain obtained from the temperature and the isotropic thermal expansion coefficient.

$$J_{el} = \frac{J_{tot}}{J_{th}} \tag{4.15}$$

$$J_{th} = (1 + \varepsilon_{th})^3 \tag{4.16}$$

The strain energy potential, W, can either be defined by a function of the strain invariants or the principal stretch ratios as shown in Eq. 4.17.

$$W = W(I_1, I_2, I_3), W(\lambda_1, \lambda_2, \lambda_3) \tag{4.17}$$

Strain energy potentials are usually written in terms of a deviatoric and a volumetric component due to material incompressibility as shown in Eq. 4.18.

$$W = W_{dev}(\bar{I}_1, \bar{I}_2) + W_{vol}(J_{el}) \tag{4.18}$$

There are many different strain energy potentials available to fit material test data from uniaxial, biaxial, planar and volumetric tests, some based on the strain invariants and some on the principal stretch ratios. Some of these are discussed below.

Arruda-Boyce

$$W = \mu \sum_{i=1}^{5} \frac{c_i}{\lambda_m^{2i-2}} (\bar{I}_1^i - 3^i) + \frac{1}{d} \left(\frac{J_{el}^2 - 1}{2} - \ln J_{el} \right) \tag{4.19}$$

Where, $c_1 = \frac{1}{2}, c_2 = \frac{1}{20}, c_3 = \frac{11}{1050}, c_4 = \frac{19}{7000}, c_5 = \frac{519}{673750}$ and are derived from a series expansion of the inverse Langavin function, μ is the initial shear modulus and λ_m, is the locking stretch, at which value the gradient of the stress-strain curve will rise sharply. This model is also recognised as the eight chain model due to its derivation from a single volumetric element with

eight springs attached at its centre to its corners. It behaves on the principal that the eight chains are stretched equally under the action of a deformed state.

Marlow [254]

$$W = W_{dev}(\bar{I}_1) + W_{vol}(J_{el}) \tag{4.20}$$

$$I_1 = \lambda_1^2 + \lambda_2^2 + \lambda_3^2 \tag{4.21}$$

This considers that the strain energy potential is independent of the second deviatoric invariant, $\bar{I}_2$, and reproduces the experimental data exactly, but care has to be taken to ensure that enough data points are provided to reproduce the material data accurately.

Mooney-Rivlin

$$W = c_{10}(\bar{I}_1 - 3) + c_{01}(\bar{I}_2 - 3) + \frac{1}{d}(J_{el} - 1)^2 \tag{4.22}$$

This first order hyperelastic model is also the same as the polynomial form when N=1 [described below]. This function only provides a sufficiently accurate representation of the material up to 100 % nominal strain and does not allow for upturn at high strain rates.

Neo-Hookean

$$W = \sum_{i=1}^{1} c_{i0}(\bar{I}_1 - 3)^i + \sum_{k=1}^{1} \frac{1}{d_k}(J_{el} - 1)^{2k} \tag{4.23}$$

This strain energy potential represents the simplest first order form using the first deviatoric strain invariant and is generally used for nominal strains up to 100 %.

Ogden

$$W = \sum_{i=1}^{N} \frac{2\mu_i}{\alpha_i^2}(\bar{\lambda}_1^{\alpha_i} + \bar{\lambda}_2^{\alpha_i} + \bar{\lambda}_3^{\alpha_i} - 3)^i + \sum_{k=1}^{N} \frac{1}{d_k}(J_{el} - 1)^{2k} \tag{4.24}$$

Ogden's strain energy potential is based solely on the principal stretch ratios and not on the strain invariants thus it is usually more accurate but computationally more expensive. The bulk modulus can be written as $\kappa_0 = \frac{2}{D_1}$, N = 1-6 and the shear modulus depends on all coefficients $\mu_0 = \sum_{i=1}^{N} \mu_i$. If N=2 the Mooney-Rivlin model is obtained with $\alpha_1 = 2, \alpha_2 = -2$ and if N = 1 the Neo-Hookean form is obtained with $\alpha_1 = 1$.

Polynomial

$$W = \sum_{i+j=1}^{N} c_{ij}(\bar{I}_1 - 3)^i(\bar{I}_2 - 3)^j + \sum_{k=1}^{N} \frac{1}{d_k}(J_{el} - 1)^{2k} \qquad (4.25)$$

This model is based on the first and second deviatoric strain invariants. For low strains up to 100% nominal strain lower order polynomials represent the material sufficiently but for high strains higher order polynomial descriptions are advisable. In the mathematical description N = 1-6, but it is rarely used above N = 2. Also, c and d are temperature dependent parameters, Bulk modulus, κ_0 ,and shear modulus, μ_0 ,depend only on polynomial coefficients when N = 1 and can be related by: $\kappa_0 = \frac{2}{D_1}$, $\mu_0 = 2(C_{10} + C_{01})$.

Reduced polynomial

$$W = \sum_{i=1}^{N} c_{i0}(\bar{I}_1 - 3)^i + \sum_{k=1}^{N} \frac{1}{d_k}(J_{el} - 1)^{2k} \qquad (4.26)$$

This model is similar to the polynomial model is simplified as it only considers the first deviatoric strain invariant. Similarly, for small strains up to 100 % the lower order models will represent the data sufficiently accurately but for larger strains higher order representations are advisable.

Van Der Waals (Kilian)

$$W = \mu\{-(\lambda_m^2 - 3)[\ln(1-\eta) + \eta] - \frac{2}{3}a(\frac{\tilde{I} - 3}{2})^{\frac{3}{2}}\} + \frac{1}{D}(\frac{J_{el}^2 - 1}{2}) - \ln J_{el}) \qquad (4.27)$$

Where, $\tilde{I} = (1-\beta)\bar{I}_1 + \beta\bar{I}_2$ and $\eta = \sqrt{\frac{\tilde{I} - 3}{\lambda_m^2 - 3}}$. This model uses the first two strain invarients and a global interaction parameter, a, which models the reactions between the chains and the locking stretch, λ_m. β is an invariant mixture parameter and D describes the compressibility.

Yeoh

$$W = \sum_{i=1}^{3} c_{i0}(\bar{I}_1 - 3)^i + \sum_{k=1}^{3} \frac{1}{d_k}(J_{el} - 1)^{2k} \qquad (4.28)$$

This is a special case of the reduced polynomial form with N=3 and can create the typical S shape of the stress-strain behaviour of a rubber material.

Each of these models is defined in terms of the principal stretch ratios or the strain invariants. ABAQUS can derive material constants for the different strain energy functions by evaluating the experimental nominal stress–nominal strain data input into the curve fitting section of the ABAQUS programme for each of the strain energy functions to correctly define the material response. The user can then decide, based on the curve fits or whether the strain energy density function is stable or unstable for the material data used, what is the most appropriate strain energy density function to represent the material in the finite element analysis.

4.4.3 Thermal testing techniques

Dynamic mechanical thermal analysis (DMTA) and differential scanning calorimetry (DSC) are thermal testing methods that measure the response of materials through a temperature range. The techniques can be used to predict the glass transition temperature and also the elastic or viscoelastic response of the material as temperature is increased. The specific heat capacity and thermal conductivity can also be determined using DSC and a fox 50 thermal conductivity machine respectively.

4.4.3.1 Dynamic mechanical thermal analysis

DMTA of toffee and cheese was performed using a Tritec 2000 DMTA with a material pocket in a single cantilever bend mode at a frequency of 1 Hz. Material pockets are commonly used as holding devices for powders or food materials in a DMTA. The storage modulus and tan δ were plotted against temperature for both materials. Tan δ is the ratio of the loss modulus to the storage modulus. By measuring the difference in phase due to the oscillating force damping properties can be determined. A peak in the tan δ against temperature curve gives the glass transition temperature. Energy is absorbed through the glass transition temperature and subsequently the storage modulus is reduced as the material is less stiff. Glass transition is sensitive to moisture content and testing frequency. The tests conducted on toffee and cheese in this study therefore give only an approximate value of glass transition because the tests are batch dependent, depend on the recipe and the tests were not conducted in a humidity controlled chamber or at different frequencies.

4.4.3.2 Differential scanning calorimetry

DSC allows the energy absorbed or dissipated by a material to be monitored when subjected to a preset temperature profile. Two aluminium pans were used, one a reference pan and one

containing the cheese or toffee sample. Each pan is subjected to the same temperature profile and the difference in heat flow is measured. Heat flow is measured against temperature and the corresponding endothermic heat absorbed by the material and exothermic heat expelled by the material is determined. Modulated differential scanning calorimetry is used to determine the heat capacity of the sample at different temperatures by measuring the heat absorbed in the sample according to Eq. 4.29 where ΔT is the temperature change, E is the energy applied and C_P is the specific heat capacity. The specific heat can then be calculated by dividing the heat capacity by the mass of the sample in the reference pan.

$$E = C_P \Delta T \tag{4.29}$$

4.4.3.3 Thermal conductivity

The thermal conductivity of toffee and cheese was determined using a Fox 50 thermal conductivity instrument. A specimen is placed between two platens. The upper platen is stationary and the bottom platen is driven by pneumatics to ensure good contact between the sample and the platens. The sample is subjected to a temperature profile and the thermal conductivity is calculated using Eq. 4.30 where Q is the heat, t is the thickness of the specimen, A is the cross sectional area, ΔT is the temperature change and L is the length of the specimen and k is the thermal conductivity.

$$\frac{Q}{tA} = \frac{k\Delta T}{L} \tag{4.30}$$

4.5 Results

4.5.1 Mechanical and thermal testing results and material properties of toffee

Toffee at temperatures of 20 and 25°C exhibits brittle behaviour but at 30 and 35 °C it is very ductile. The brittle nature of the toffee is captured in Fig. 4.10 (a) and (b) where there is very little strain at the maximum stress and the curves are nearly linear with no distinct plastic region. The specimens break suddenly in tension with little reduction in cross-sectional area and the failure surfaces are smooth and are created by a clean break. Brittle materials are extremely difficult to test in a reproducible way and measurement data is often scattered. Toffee is no exception and the failure stress is quite varied between tests at temperatures of 20 and 25 °C. Sources of variability occur from moulding the toffee specimens due to the material cooling on the surface of the moulds quickly and trapping air in the specimen, a poor pouring technique, small stresses being induced in the specimen when removing them from the moulds, differences in the preparation of the toffee mixture, and slight inaccuracies in the alignment of the grips in

the Lloyds uni-axial testing machine. These known problems were minimised by strict weighing and preparation of the toffee, accurate pouring into the centre of the moulds at a constant speed ensuring no toffee touched the sides, careful removal of the specimens from the moulds by ensuring they were pre-greased heavily and handled away from the gauge length carefully, and strict alignment of the grips in the Lloyds machine. If the specimen is not being pulled perfectly in line then a slight bending moment is placed across the specimen, which can cause premature failure. In addition, the surface finish of the specimens is a considerable factor and a very high surface finish is desirable to reduce the number of surface flaws within the material, which can instigate failure in the specimen. Due to the very brittle nature of the toffee, polishing the surface was not possible but a smooth surface finish was produced by rubbing the surface of the specimens lightly using warm water to dissolve any excess toffee or fill in any hairline cracks prior to testing.

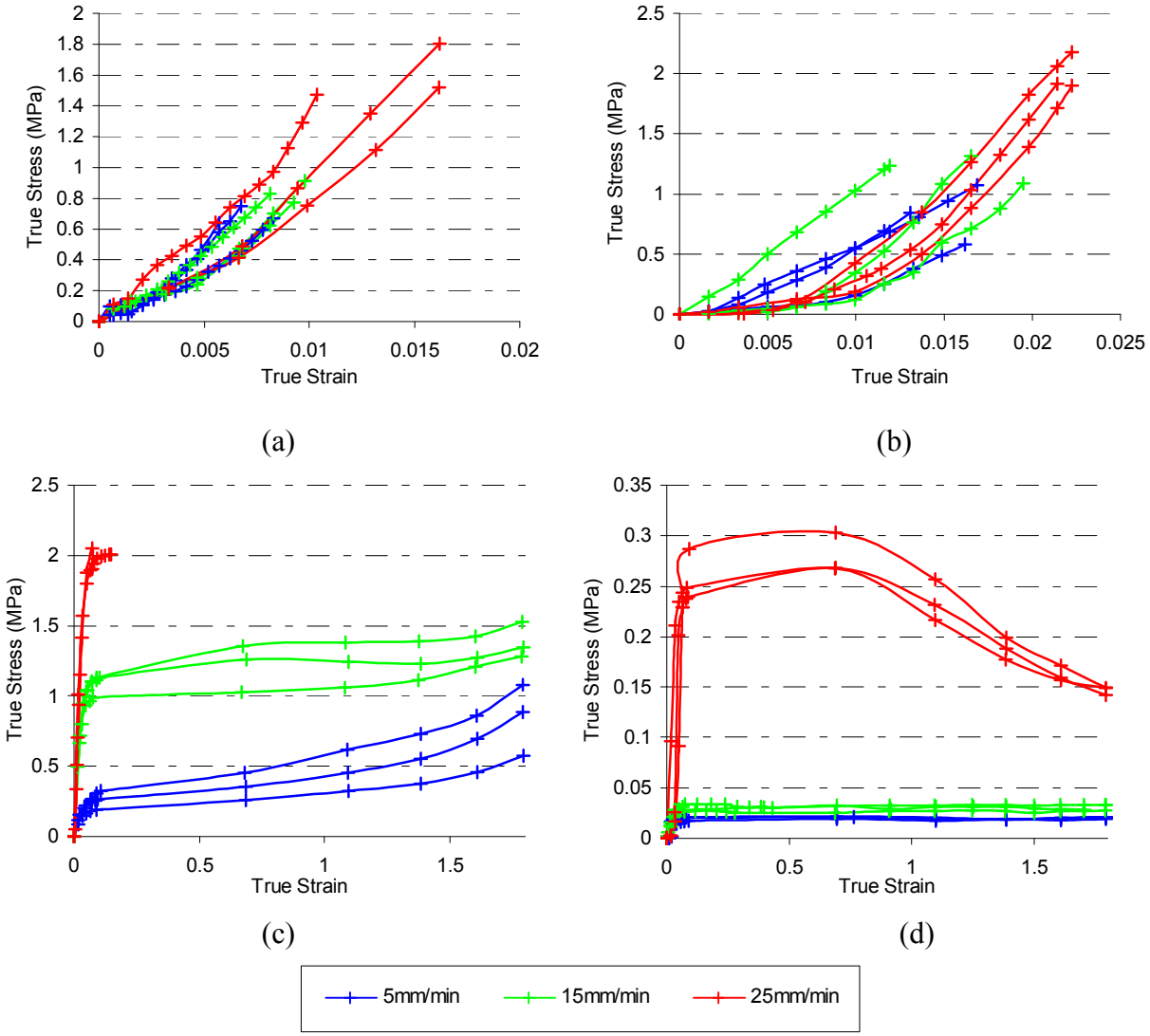

Fig. 4.10: Experimental tensile test data for toffee at (a) 20 °C (b) 25 °C (c) 30 °C (d) 35 °C

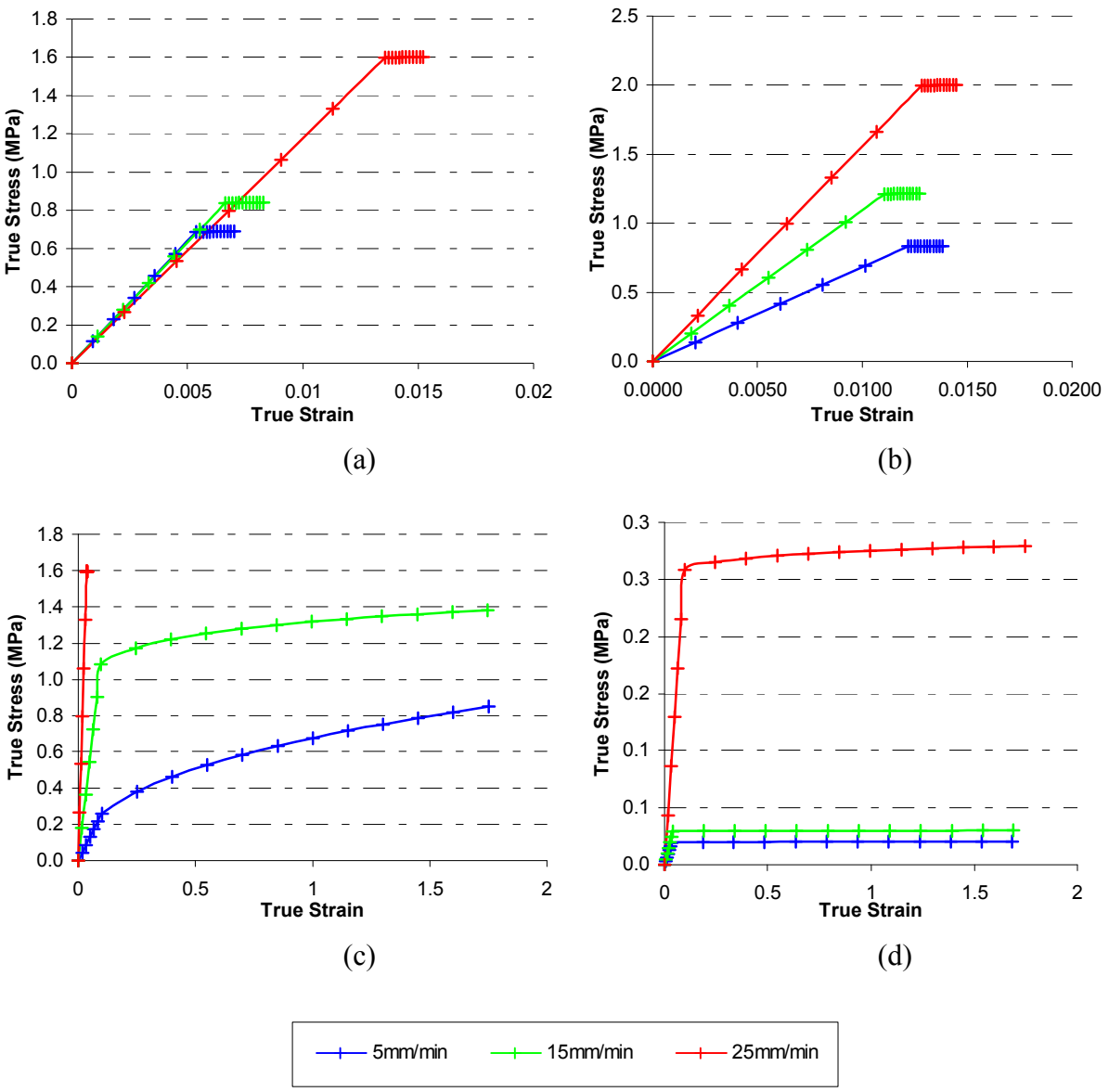

Fig. 4.11: Average curve fitted tension test results for toffee at (a) 20 °C (b) 25 °C (c) 30 °C (d) 35 °C.

At temperatures of 30 and 35 °C in Fig. 4.10 (c) and (d) the material is ductile with a distinct yield point and large plastic region after the material yields. The specimen can withstand very high strains without failing in tension and the cross-sectional area at the gauge length of the material reduces until it is extremely small before failure occurs. At these temperatures the three samples used for each strain rate produced more consistent stress-strain data than those at the lower temperatures. The results show distinctive material behaviour compared to the lower temperatures as shown in Fig. 4.10 (b) and (c). Specimen variability occurs due to inaccuracies in specimen preparation, including different consistencies of mixture and batch dependency of the material. When the crosshead velocity is increased in tension the stresses increase due to the

strain rate dependence of the material. This dependence is consistent across all temperatures for toffee and is more pronounced at higher temperatures as can be seen in Fig. 4.10 (c) and (d). As the temperature increases the Young's modulus decreases. Toffee at temperatures of 20 and 25 °C has no distinct yield point, which is common in brittle materials. In this study, at temperatures of 20 and 25 °C the yield point and UTS are considered to be the same. Between these two temperatures as crosshead velocity increases the yield point and UTS both increase. This could be due to the material nearing the glass transition of the material and the toffee beginning to become slightly ductile allowing the material to elongate slightly more and withstand slightly higher stresses. At temperatures of 30 and 35 °C there are distinct yield points in the stress-strain curves and the yield point of the toffee increases with increasing crosshead velocity and decreases with increasing temperature as the material becomes softer and less stiff. The multiple measured tensile test data at each crosshead velocity and temperature was averaged and then an average curve fit created for use in FEA. Average curve fitted tension results are depicted in Fig. 4.11 and tabulated in Table 4.1 for toffee tested in tension at crosshead velocities of 5, 15 and 25 mm/min at temperatures of 20, 25, 30 and 35 °C.

	Temperature 20 °C		
Test Speed (mm/min)	5	15	25
E (N/m^2)	1.27E+08	1.26E+08	1.18E+08
Yield Stress (MPa)	0.6853	0.8379	1.5981
UTS (MPa)	0.6853	0.8379	1.5981
Fail Strain	0.0069	0.0091	0.0142
Fail Stress (MPa)	0.6853	0.8379	1.5981

	Temperature 25 °C		
Test Speed (mm/min)	5	15	25
E (N/m^2)	6.83E+07	1.10E+08	1.56E+08
Yield Stress (MPa)	0.8317	1.2126	1.9972
UTS (MPa)	0.8317	1.2126	1.9972
Fail Strain	0.0154	0.0160	0.0220
Fail Stress (MPa)	0.8317	1.2126	1.9972

	Temperature 30 °C		
Test Speed (mm/min)	5	15	25
E (N/m^2)	2.57E+06	1.13E+07	4.46E+07
Yield Stress (MPa)	0.2590	1.0851	1.5937
UTS (MPa)	0.8455	1.3862	1.6888
Fail Strain	1.7912	1.7881	0.0824
Fail Stress (MPa)	0.8455	1.3862	1.6888

	Temperature 35 °C		
Test Speed (mm/min)	5	15	25
E (N/m^2)	5.39E+05	7.19E+05	2.67E+06
Yield Stress (MPa)	0.0192	0.0293	0.2584
UTS (MPa)	0.0203	0.0296	0.2798
Fail Strain	1.7918	1.7619	1.7918
Fail Stress (MPa)	0.0203	0.0296	0.1467

Table 4.1: Mean tension data for toffee

In compression toffee exhibits the same temperature dependencies as in tension. For temperatures of 20 and 25 °C toffee is brittle and the stress strain curve is nearly linear with no distinct plastic region as shown in Fig. 4.12. As temperature increases between 20 and 25 °C, the Young's modulus increases slightly but the UTS decreases slightly when temperature is increased. At temperatures of 30 and 35 °C, Young's modulus is lower at 35 °C as the material is less stiff. The UTS increases as the test temperature increases from 25°C to 30 °C and then falls when temperature is increased to 35 °C as shown in Fig. 4.12 (c) and (d). The average measured data for toffee in compression at temperatures of 20, 25, 30 and 35 °C and at crosshead velocities of 5, 15 and 25 mm/min are depicted in Fig. 4.13 and tabulated in Table 4.2. At all temperatures, when the crosshead velocity increases the Young's modulus, Yield point and the UTS all increase. The compression tests on toffee at all temperatures show that the material can withstand higher stresses when compressed compared to being pulled in tension. The yield point and UTS are in some cases greater by a factor of 10 and the Young's modulus in compression is higher than in tension.

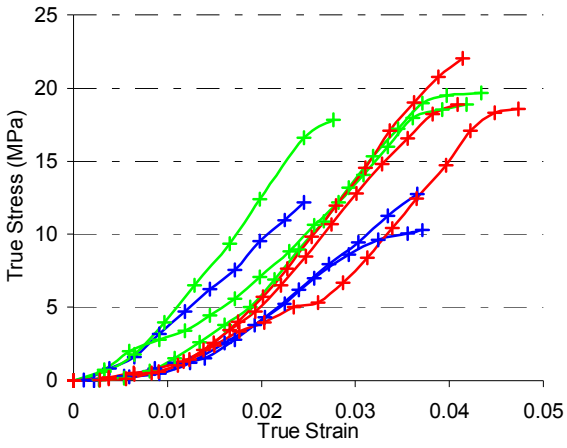

(a)

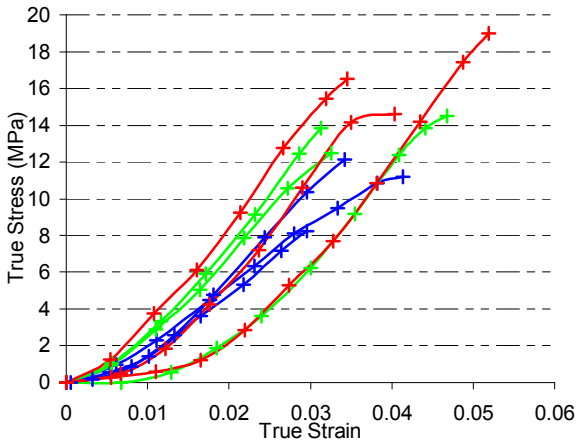

(b)

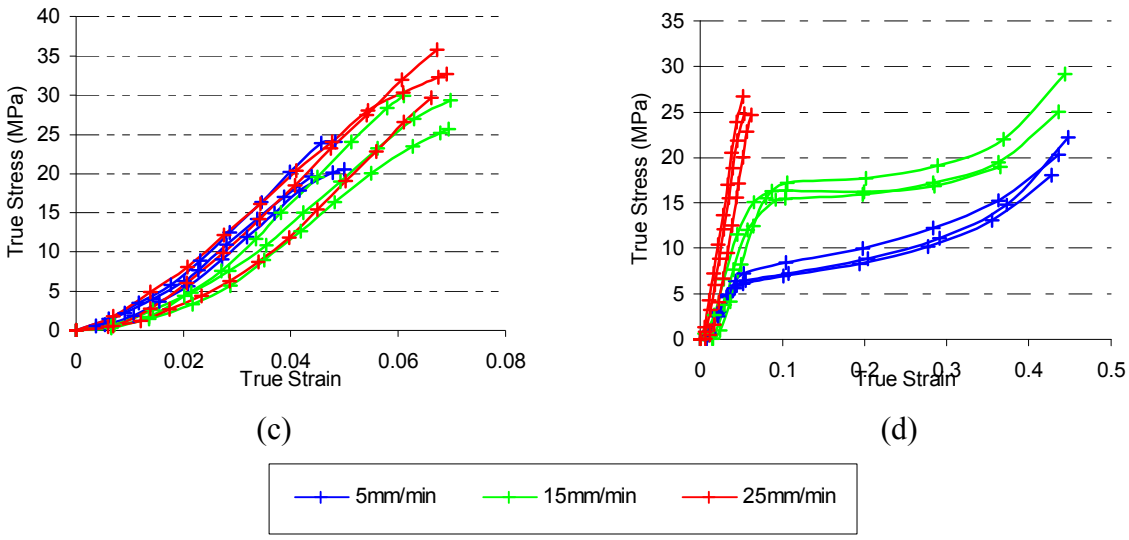

Fig. 4.12: Experimental compression test data for toffee at (a) 20 °C (b) 25 °C (c) 30 °C (d) 35°C

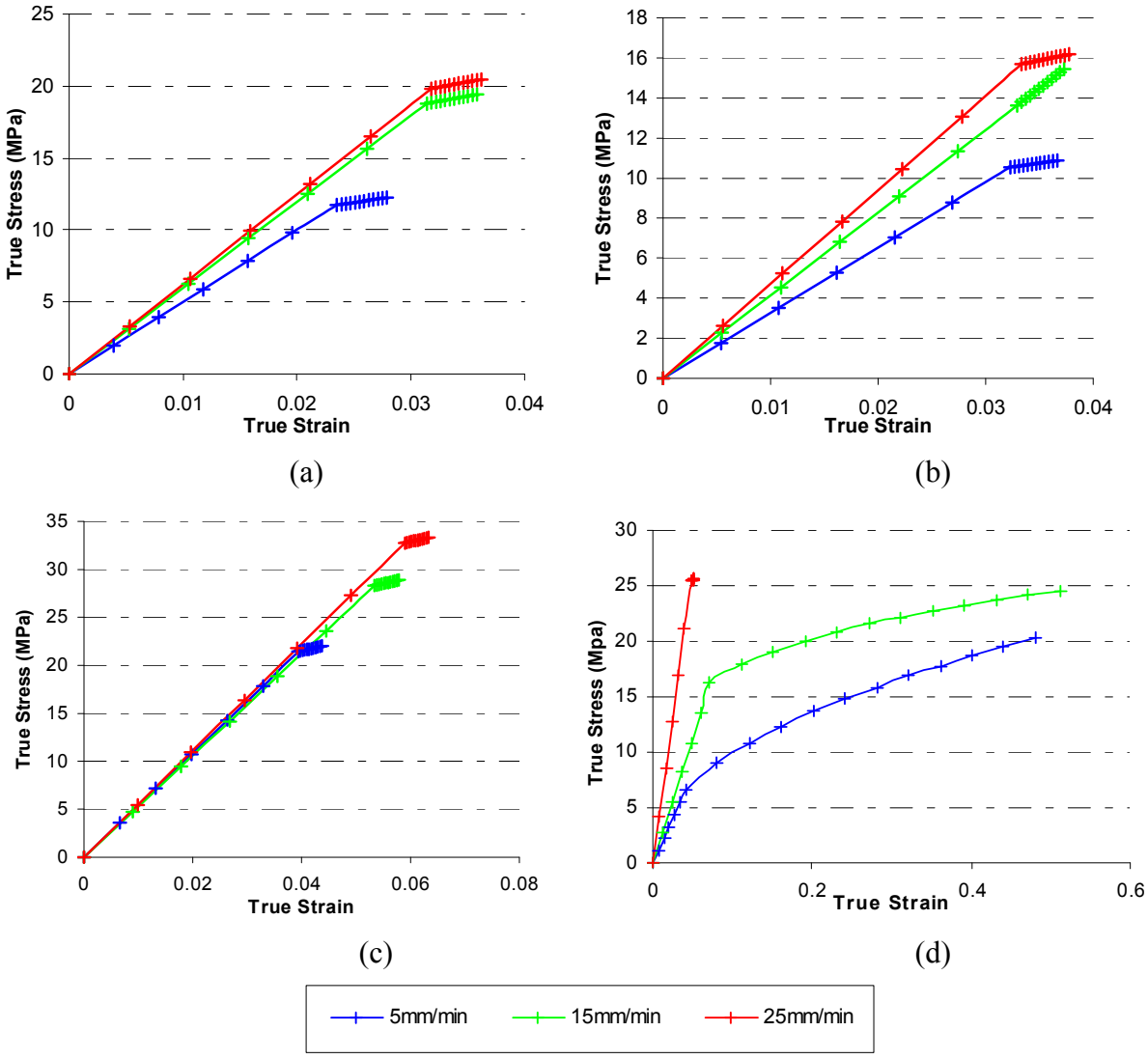

Fig. 4.13: Average curve fitted compression test results for toffee at (a) 20 °C (b) 25 °C (c) 30 °C (d) 35 °C.

	Temperature 20 °C		
Test Speed (mm/min)	5	15	25
E (N/m^2)	5.00E+08	5.98E+08	6.23E+08
Yield Stress (MPa)	11.7599	18.8050	19.8246
UTS (MPa)	11.7599	18.8050	19.8246
Fail Strain	0.0328	0.0376	0.0432
Fail Stress (MPa)	11.7599	18.8050	19.8246

	Temperature 25 °C		
Test Speed (mm/min)	5	15	25
E (N/m^2)	3.26E+08	4.14E+08	4.70E+08
Yield Stress (MPa)	10.5405	13.6283	15.6848
UTS (MPa)	10.5405	13.6283	16.7138
Fail Strain	0.0351	0.0369	0.0423
Fail Stress (MPa)	10.5405	13.6283	16.7138

	Temperature 30 °C		
Test Speed (mm/min)	5	15	25
E (N/m^2)	5.44E+08	5.29E+08	5.55E+08
Yield Stress (MPa)	21.4415	28.3195	32.7213
UTS (MPa)	21.4415	28.3195	32.7213
Fail Strain	0.0474	0.0667	0.0675
Fail Stress (MPa)	21.4415	28.3195	32.7213

	Temperature 35 °C		
Test Speed (mm/min)	5	15	25
E (N/m^2)	1.62E+08	2.28E+08	5.33E+08
Yield Stress (MPa)	6.6051	16.3199	25.4033
UTS (MPa)	20.2230	24.4031	25.4033
Fail Strain	0.4373	0.4150	0.0559
Fail Stress (MPa)	20.2230	24.4031	25.4033

Table 4.2: Mean compression data for toffee

The glass transition temperature for toffee was determined from testing using a material pocket in a DMTA. The glass transition temperature is determined as the peak in tan δ as shown in Fig. 4.14. For toffee this was measured at 18 °C. An alternative method to determine the glass transition temperature is by using a DSC. In this case, the glass transition temperature is determined by plotting heat flow against temperature and locating the region on the graph where there is a sudden drop in heat flow. Glass transition occurs over a small temperature range so that determining an exact glass transition temperature is difficult. It is usually estimated as the midpoint of the drop off of heat flow. The glass transition temperature of toffee from the DMTA measurements is close to room temperature. However in the tensile test the material characteristics change from brittle to ductile at approximately 30 °C indicating that 18 °C is a low estimation of the glass transition temperature. Food materials are very sensitive to humidity and it is expected that a better estimation requires the use of a humidity chamber in the DMTA.

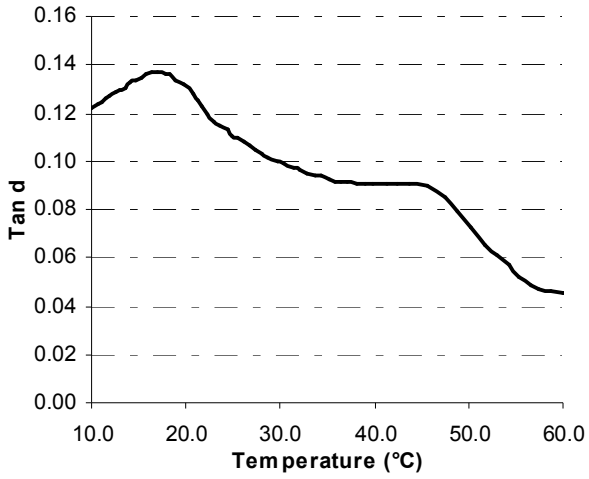

Fig. 4.14: Prediction of glass transition of toffee using DMTA.

Table 4.3 presents additional data for toffee that is required for finite element simulations of ultrasonic cutting. The density of the material was calculated by dividing the mass of the sample by the volume of a cubic specimen. Poisson's ratio was assumed to be 0.49 as this is typical for most food products from information in the literature [201-203] and the specific heat and thermal conductivity was measured using the techniques described in sections 4.4.2 and 4.4.3 respectively.

	Toffee
Density (kg/m^3)	1411
Poisson's Ratio	0.49
Specific Heat (kJ/kg°C)	1.948
Thermal Conductivity (W/mK)	0.096

Table 4.3: Mechanical and thermal data for toffee

4.5.2 Mechanical and thermal testing results and material properties of cheese

In tension cheese exhibited ductile behaviour at all four temperatures. The material is pliable and the stress-strain diagrams at each temperature and crosshead velocity tested are smooth curves until the failure point. The Young's modulus was determined from an estimated linear portion of the curve up to the estimated yield point using the 0.2 % offset method. The UTS is the highest stress on the stress-strain diagram. All specimens failed in tension by tearing from an outside surface within the gauge length. Due to the porous nature of cheese, there were slight imperfections on the surface of the specimens. These were created when the scalpel passed through small voids in the material when the dog bone shape was being produced. These imperfections result in variations between the three specimens for each test as shown in Fig. 4.15. As the temperature increases from 4 to 24 °C the Young's modulus, yield point and

ultimate tensile strength in the material decrease as expected as the cheese is becoming more ductile. Between 24 and 30 °C there is an increase in the Young's modulus, yield point and the UTS and the failure strain of the material begins to increase significantly. Between 30 and 35 °C the material is getting very soft and again with increasing temperature the Young's modulus, yield point and UTS all decrease. Also at increasing crosshead velocities for all temperatures the results showed slightly increased Young's modulii, Yield points and UTS's when the material was deforming due to the strain-rate dependence of the material. Average curve fitted tension results are illustrated in Fig. 4.16 and tabulated in Table 4.4 for cheese tested in tension at crosshead velocities of 5, 15 and 25 mm/min at temperatures of 4, 24, 30 and 35 °C.

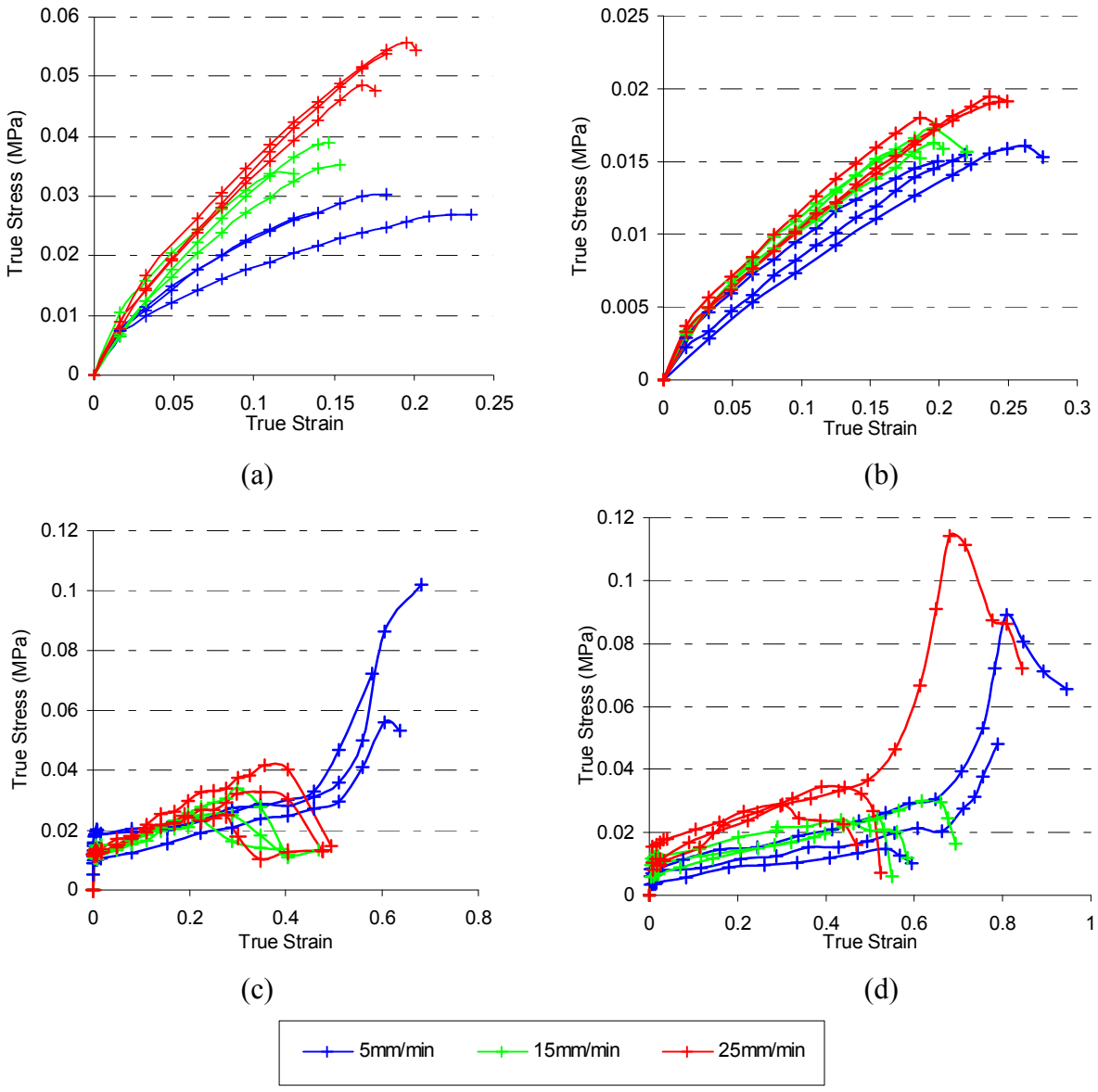

Fig. 4.15: Experimental tensile test data for cheese at (a) 4 °C (b) 24 °C (c) 30 °C (d) 35 °C

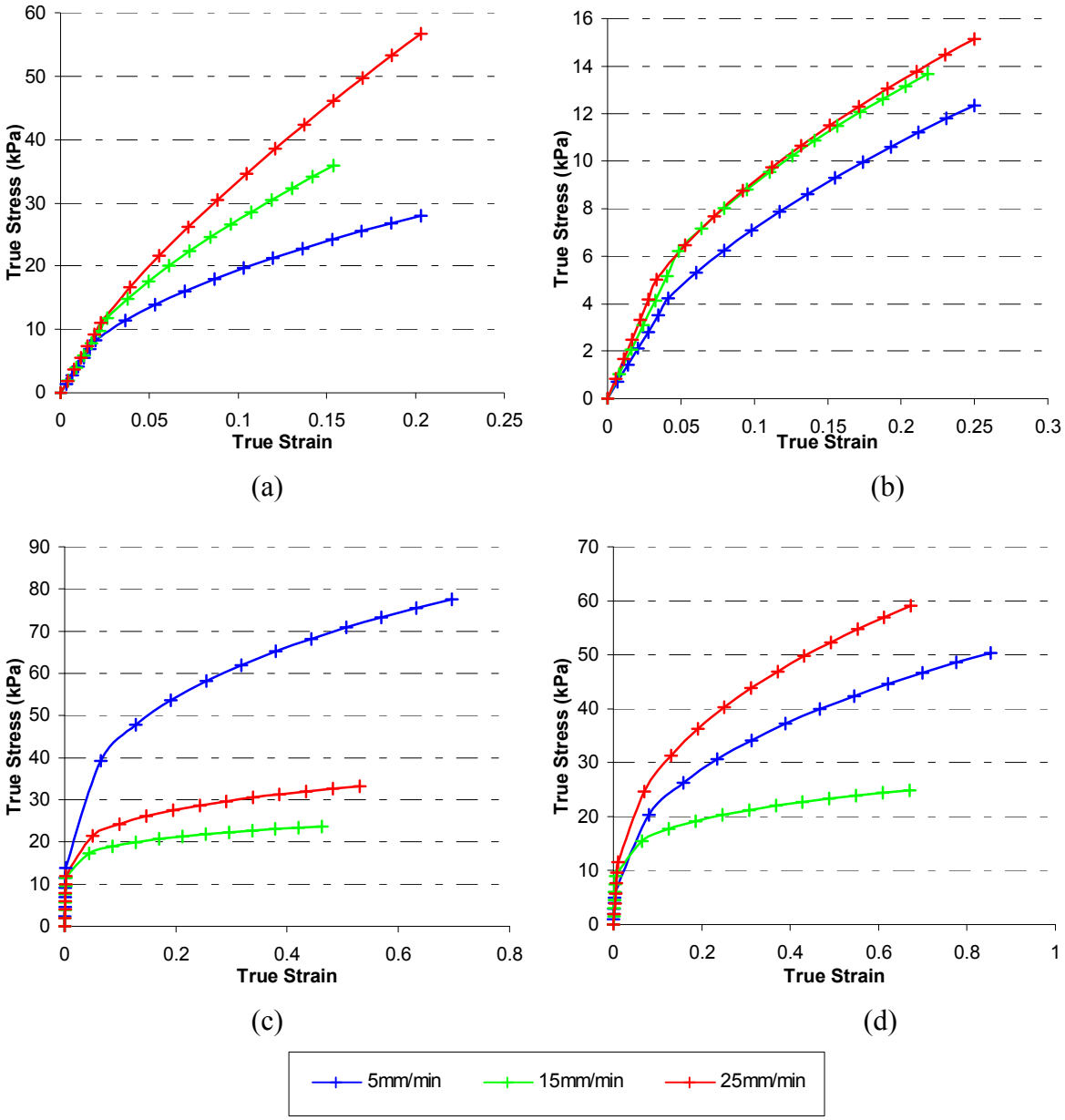

Fig. 4.16: Average curve fitted tension test results for cheese at (a) 4 °C (b) 24 °C (c) 30 °C (d) 35 °C.

	Temperature 4 °C		
Test Speed (mm/min)	5	15	25
E (N/m^2)	4.15E+05	4.47E+05	4.87E+05
Yield Stress (MPa)	0.0082	0.0117	0.0111
UTS (MPa)	0.0281	0.0360	0.0527
Fail Strain	0.1864	0.1421	0.1867
Fail Stress (MPa)	0.0281	0.0360	0.0519

	Temperature 24 °C		
Test Speed (mm/min)	5	15	25
E (N/m^2)	1.02E+05	1.27E+05	1.50E+05
Yield Stress (MPa)	0.0042	0.0062	0.0050
UTS (MPa)	0.0124	0.0136	0.0151
Fail Strain	0.2309	0.2029	0.2301
Fail Stress (MPa)	0.0153	0.0156	0.0186

	Temperature 30 °C		
Test Speed (mm/min)	5	15	25
E (N/m^2)	8.25E+06	5.72E+06	5.72E+06
Yield Stress (MPa)	0.0138	0.0115	0.0119
UTS (MPa)	0.0768	0.0238	0.0332
Fail Strain	0.6330	0.4211	0.4828
Fail Stress (MPa)	0.0759	0.0127	0.0138

	Temperature 35 °C		
Test Speed (mm/min)	5	15	25
E (N/m^2)	1.77E+06	1.94E+06	1.16E+06
Yield Stress (MPa)	0.0059	0.0090	0.0115
UTS (MPa)	0.0506	0.0249	0.0592
Fail Strain	0.7763	0.6094	0.6126
Fail Stress (MPa)	0.0412	0.0115	0.0318

Table 4.4: Mean tension data for cheese

In compression cheese displayed similar trends as in tension. The Young's modulus, Yield point and UTS decreased with increasing temperature and as crosshead velocity increased there was a slight increase in Young's modulus, yield point and UTS at all temperatures. As in tension some errors occurred in the averaging of the data for Young's modulus, yield point and UTS as can be seen in Table 4.5. These errors occurred due to the sensitivity of the testing machine as very small forces were calculated from the Lloyds machine during the experimental testing set up. The specimens also experienced moisture loss as they were tested at increased temperatures in the cabinet and absorb heat that caused some of the water in the specimens to evaporate. The experimental results are illustrated in Fig. 4.17 and Fig. 4.18 and in Table 4.5. In compression no distinct flattening of the stress-strain curve, plateau region, is noticeable and as strain increases stress increases until the cheese is squashed flat against the platens. To remove the possibility of excessive loading of the cheese and as there is no distinct, noticeable failure point each test was conducted in compression to a height of 3 mm. Tables 4.4 and 4.5 present the calculated Young's modulus, yield point and UTS from the experimental stress-strain data in compression, which are lower than that in tension at all temperatures and crosshead velocities.

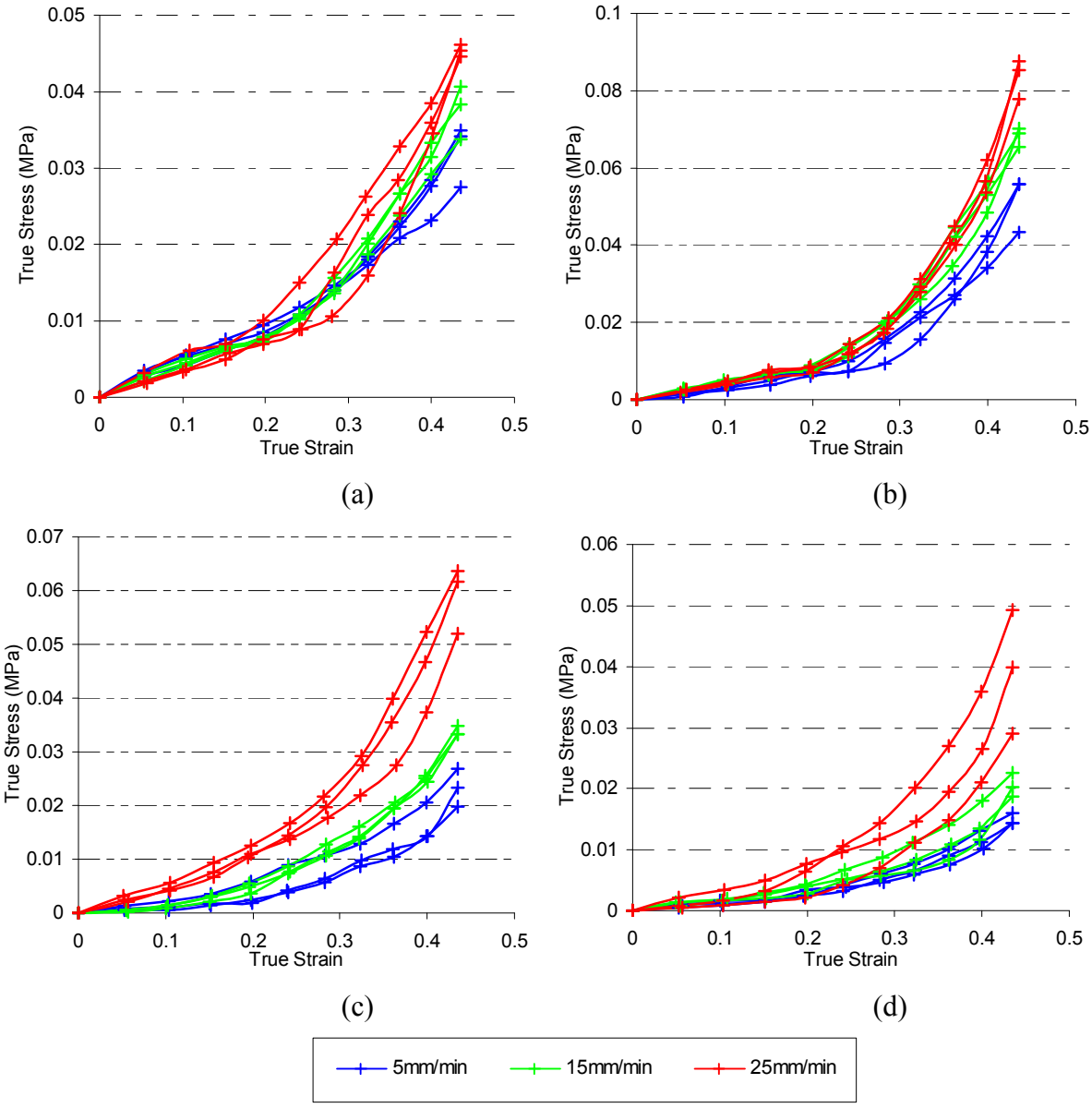

Fig. 4.17: Experimental compression test results for cheese at (a) 4 °C (b) 24 °C (c) 30 °C (d) 35 °C.

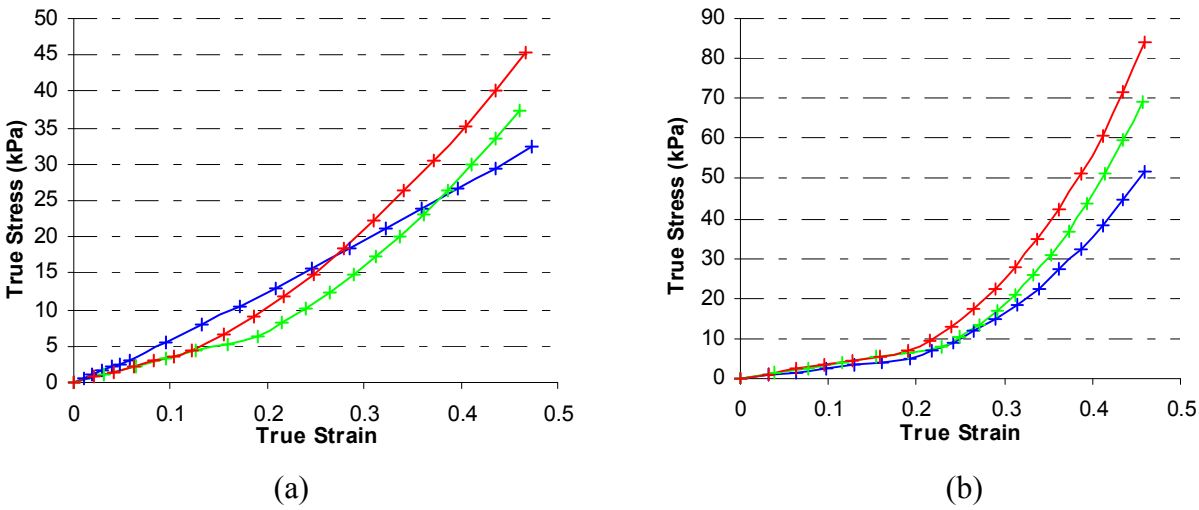

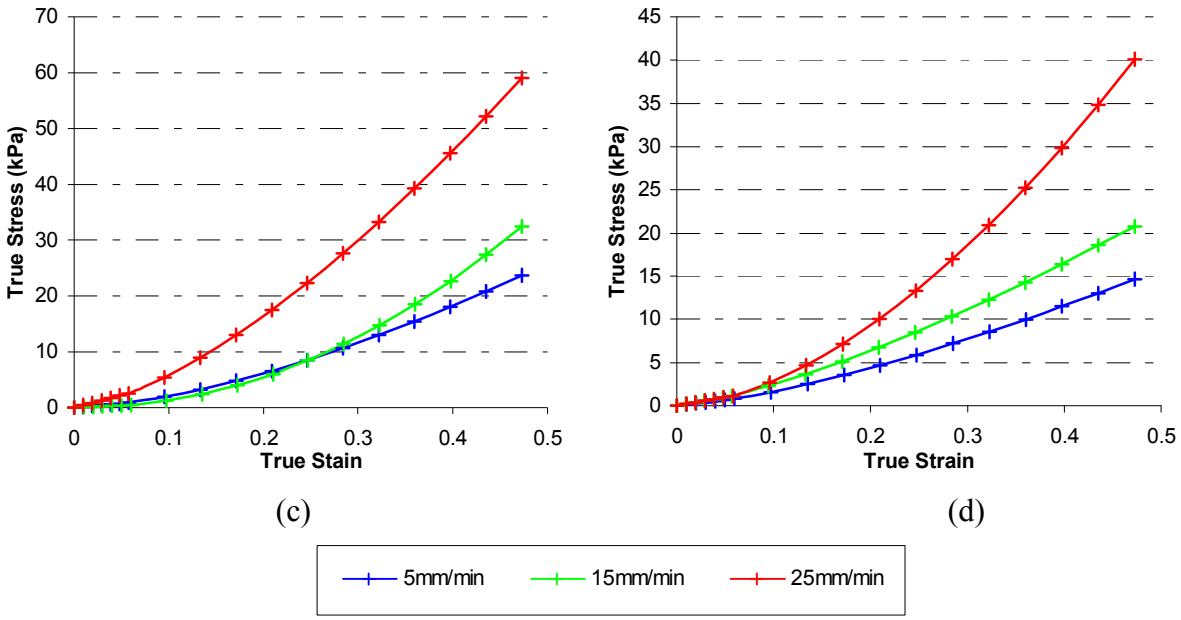

Fig. 4.18: Average curve fitted compression test results for cheese at (a) 4 °C (b) 24 °C (c) 30 °C (d) 35 °C.

	Temperature 4 °C		
Test Speed (mm/min)	5	15	25
E (N/m^2)	5.41E+04	3.37E+04	3.55E+04
Yield Stress (MPa)	0.0031	0.0064	0.0044
UTS (MPa)	0.0322	0.0376	0.0454
Fail Strain	0.4353	0.4353	0.4353
Fail Stress (MPa)	0.0322	0.0376	0.0454

	Temperature 24 °C		
Test Speed (mm/min)	5	15	25
E (N/m^2)	2.57E+04	3.51E+04	3.57E+04
Yield Stress (MPa)	0.0050	0.0080	0.0068
UTS (MPa)	0.0517	0.0682	0.0836
Fail Strain	0.4353	0.4353	0.4353
Fail Stress (MPa)	0.0517	0.0682	0.0836

	Temperature 30 °C		
Test Speed (mm/min)	5	15	25
E (N/m^2)	1.53E+04	7.34E+03	4.43E+04
Yield Stress (MPa)	0.0009	0.0004	0.0026
UTS (MPa)	0.0233	0.0339	0.0591
Fail Strain	0.4353	0.4353	0.4353
Fail Stress (MPa)	0.0233	0.0339	0.0591

	Temperature 35 °C		
Test Speed (mm/min)	5	15	25
E (N/m^2)	1.33E+04	2.01E+04	1.97E+04
Yield Stress (MPa)	0.0008	0.0011	0.0011
UTS (MPa)	0.0149	0.0204	0.0394
Fail Strain	0.4353	0.4353	0.4353
Fail Stress (MPa)	0.0149	0.0204	0.0394

Table 4.5: Mean compression data for cheese

Cheese was also modelled in ABAQUS as an incompressible hyperelastic material rather than an elastic-plastic material. This allowed the tensile and compression data to be represented as one strain energy density function that could be incorporated in the FE models of ultrasonic cutting. This strain energy density function considers both the compressive and tensile nature of the material during cutting rather than modelling cheese as either tensile data or compression data. A curve fitting procedure using a fourth order polynomial was applied to the combined tension and compression experimental nominal stress-nominal strain data to smooth the experimental data [8]. This smoothed data was then implemented in a curve fitting procedure within the FE code to obtain material constants for the strain energy density function which best described the experimental data. The reduced polynomial curve fitting expression of order 3 was chosen to represent the data in ABAQUS as shown in Fig. 4.19. This material modelling technique considers the material data to exist in the elastic region only until failure. This allows a more complex stress-strain curve to be modelled more accurately and represents the experimental data more closely than an elastic-plastic representation but assumes that the material does not exhibit plasticity. For FE simulations, a more precise representation of the material response should allow more accurate results to be obtained from the simulations however for some studies the elastic-plastic material response will model the process sufficiently.

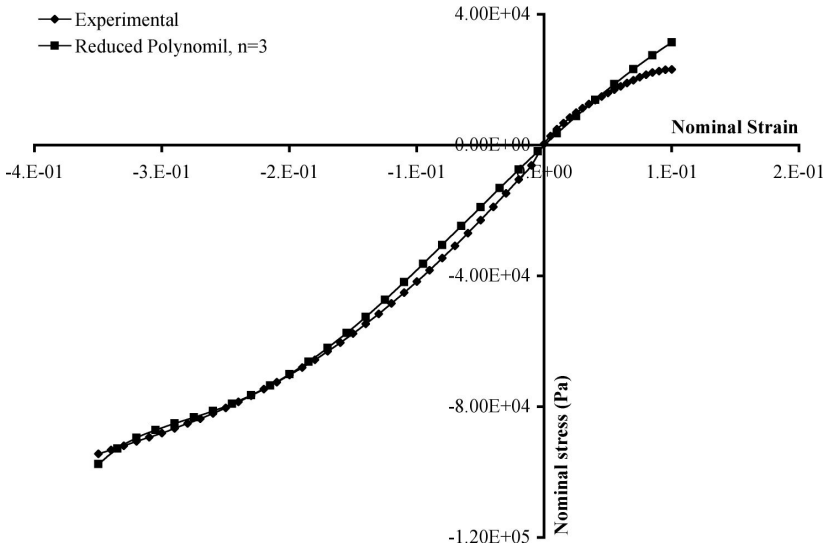

Fig. 4.19: Average combined tensile and compression hyperelastic curve fitted result for cheese at 24 °C and at a crosshead velocity of 5 mm/min.

The response of cheese measured using a DSC is presented in Fig. 4.20 (a) where the initial starting temperature of the analysis was 32 °C. The glass transition temperature, as explained previously, can be determined by locating the region on the graphs where there is a sudden drop in heat flow after the analysis settles as depicted in Fig. 4.20 (a) at 40 °C. Fig. 4.20 (b) shows the

tan δ response against temperature for cheese tested using a DMTA for comparison. In this case the glass transition temperature was determined to be 39.8 °C for cheese which is the peak on the curve. Using a DMTA the response is very faint as the material is very pliable over the temperature range but after 40 °C there is a slight decrease in tan δ.

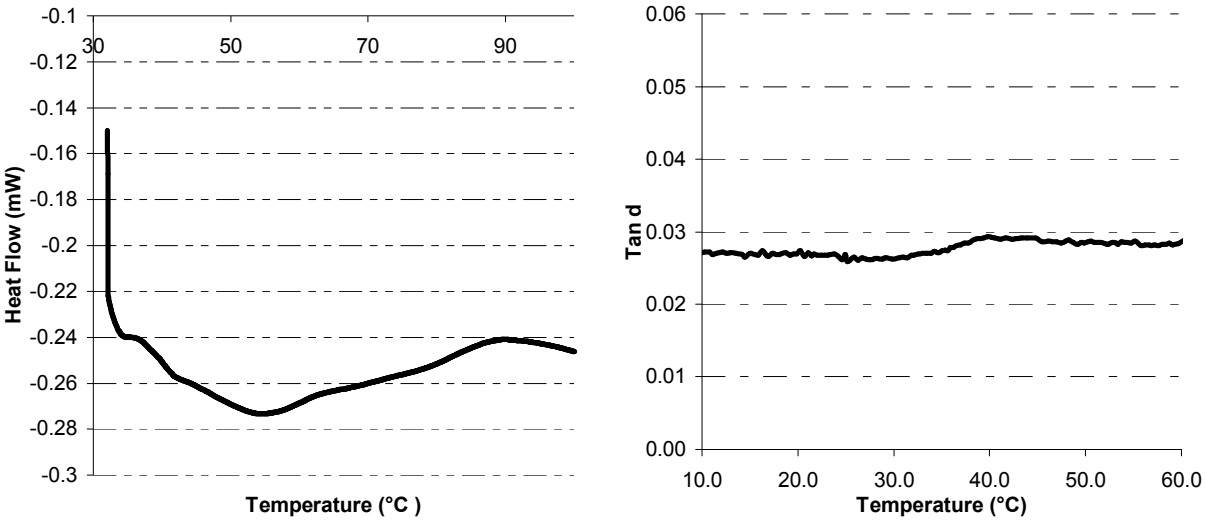

(a) (b)

Fig. 4.20: Prediction of glass transition of cheese using (a) DSC (b) DMTA.

Some additional material properties including density, Poisson's ratio, specific heat and thermal conductivity which are required for FE simulations of the ultrasonic cutting of cheese are tabulated in Table 4.6.

	Cheese
Density (kg/m^3)	4425
Poisson's Ratio	0.49
Specific Heat (kJ/kg°C)	0.91
Thermal Conductivity (W/mK)	0.164

Table 4.6: Mechanical and thermal data for cheese

4.5.3 Experimental testing results and material properties of chocolate

Similarly to toffee, chocolate at temperatures of 20 and 25 °C exhibits brittle behaviour where the tensile specimens break suddenly with little reduction in cross-sectional area. Fig. 4.21 (a) and (b) illustrates several tensile tests conducted at 4 and 20 °C respectively at crosshead velocities of 0.25, 1, 2 and 4 mm/min. Due diligence and care was taken in the preparation of the chocolate when heated and poured into the specially designed tensile moulds. Again careful removal of the specimens from the moulds by handling them away from the gauge length and strict alignment of the grips in the Lloyds machine was ensured to prevent the specimens from breaking or fracturing prior to or during testing. From Fig. 4.21 (a) and (b) it is apparent again

that there is a noticeable spread in experimental stress-strain results. This spread in results can again be attributed to the batch dependency of the material, specimen preparation and preparation of the experimental testing configuration. The effect of strain rate dependency is also apparent. As the crosshead velocity increases the Young's modulus, yield point and UTS increase and the fail strain decreases. Average curve fitting representations are shown in Fig. 4.22 (a) and (b) using the same technique as previously explained for the elastic-plastic curve fitting procedure for chocolate at 4°C and 20 °C respectively. The average data for Young's modulus, yield point, UTS, fail strain and fail stress is also tabulated in Table 4.7 for each temperature and crosshead velocity.

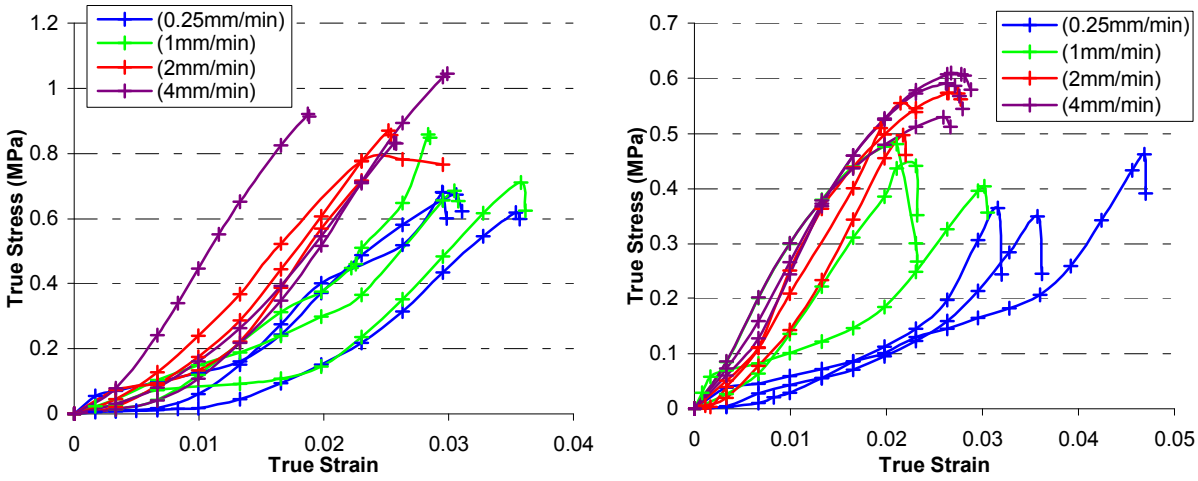

Fig. 4.21: Measured tensile test data for chocolate at (a) 4 °C and (b) 20 °C.

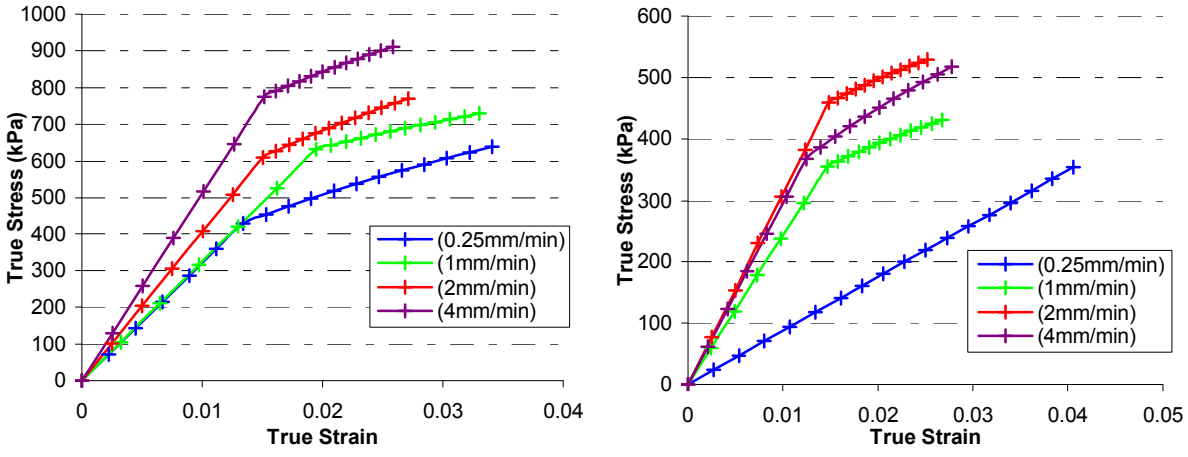

Fig. 4.22: Average tension test results for chocolate at (a) 4 °C and (b) 20 °C.

	Temperature 4 °C			
Test Speed (mm/min)	0.25	1	2	4
E (N/m^2)	3.20E+07	3.24E+07	4.06E+07	5.11E+07
Yield Stress (MPa)	0.4296	0.6318	0.6105	0.7756
UTS (MPa)	0.6382	0.7292	0.7709	0.9103
Fail Strain	0.0322	0.0318	0.0260	0.0249
Fail Stress (MPa)	0.6083	0.7101	0.7802	0.9298

	Temperature 20 °C			
Test Speed (mm/min)	0.25	1	2	4
E (N/m^2)	8.74E+06	2.42E+07	3.10E+07	2.96E+07
Yield Stress (MPa)	0.1408	0.3555	0.4596	0.3685
UTS (MPa)	0.3776	0.4314	0.5294	0.5618
Fail Strain	0.0384	0.0257	0.0243	0.0278
Fail Stress (MPa)	0.2929	0.3255	0.5208	0.5458

Table 4.7: Mean tension data for chocolate

Chocolate when tested in compression displays the same brittle behaviour as in tension at both testing temperatures but as the chocolate is compressed between the two platens there is no noticeable decrease in the stress levels on the stress-strain graph as can be seen in Fig. 4.23 (a) and (b). The stress-strain diagram exhibits the S shaped response typical of rubbers. As the platens are compressed there is no distinct failure location and the material can be compressed until flat. The stress rises continuously but large cracks are visible which indicate specimen failure. At the instant in time the visible cracks are present the material is considered to have failed in compression and the stress on the stress strain diagram for the material is considered to be at a maximum. In compression the experimental tests show a lower Young's modulus and yield point but a larger UTS, fail strain and fail stress than the equivalent tensile tests. The fail stress and fail strain locations for chocolate in compression were difficult to quantify as there was a decline in stress on the stress-strain diagram but were assumed to be when the test ended at a strain of 0.3747, where visible cracks were present in the material. Taking the failure location as such for comparison purposes the Young's modulus increased with increasing crosshead velocity, the yield stress had variable results that did not indicate any particular trend but were very similar at all crosshead velocities for each testing temperature and the fail stress decreased with increasing crosshead velocity which is the opposite effect to that in tension. Average compression curves at each crosshead velocity and at both test temperatures are indicated in Fig. 4.24 (a) and (b) and the average mechanical properties are also tabulated in Table 4.8.

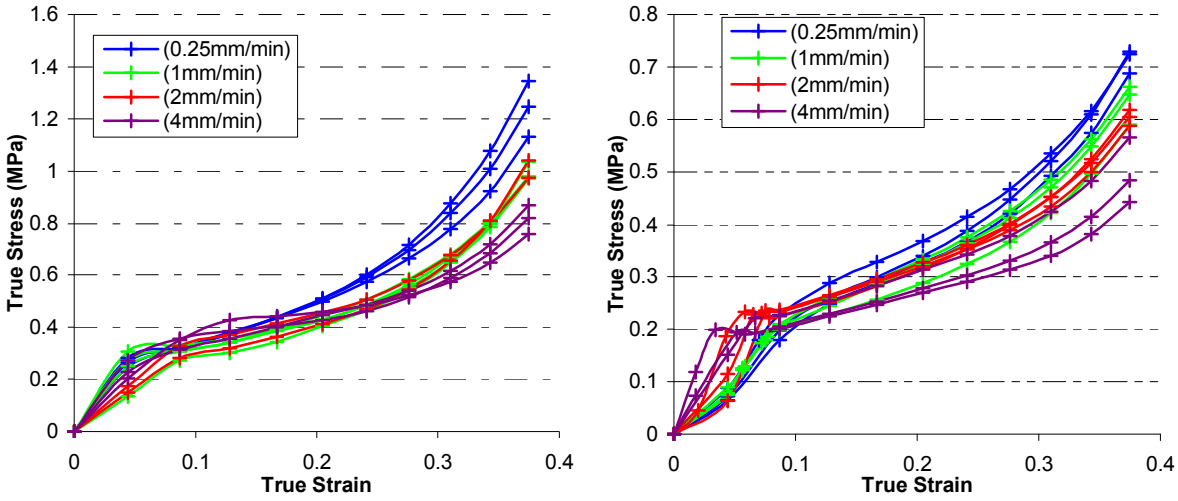

(a) (b)

Fig. 4.23: Measured compression test data for chocolate at (a) 4 °C and (b) 20 °C.

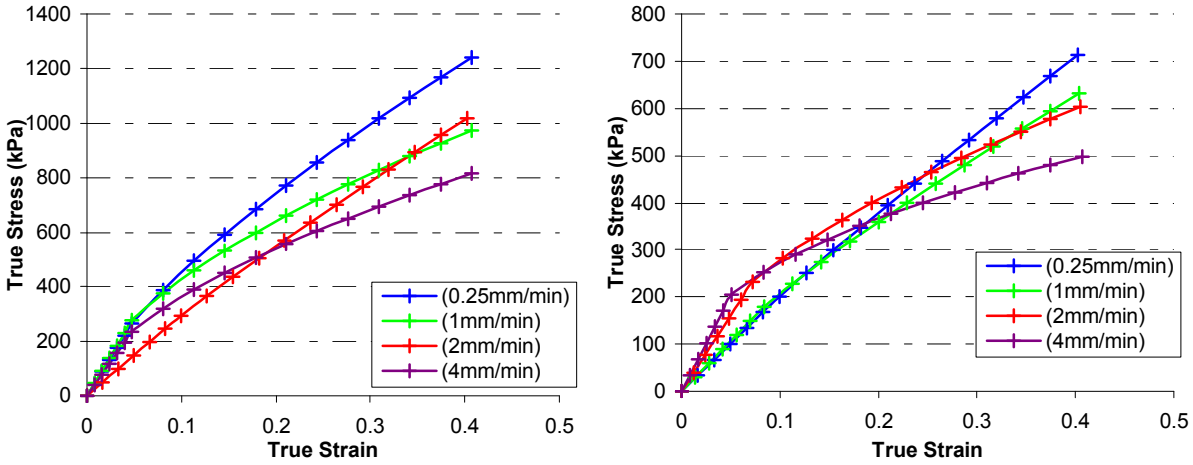

(a) (b)

Fig. 4.24: Average compression test results for chocolate at (a) 4 °C and (b) 20 °C.

	Temperature 4 °C			
Test Speed (mm/min)	0.25	1	2	4
E (N/m^2)	5.57E+06	5.80E+06	2.96E+06	4.94E+06
Yield Stress (MPa)	0.2645	0.2755	0.2936	0.2345
UTS (MPa)	1.2417	0.9772	1.0184	0.8161
Fail Strain	0.3747	0.3747	0.3747	0.3747
Fail Stress (MPa)	1.2417	0.9772	1.0184	0.8161

	Temperature 20 °C			
Test Speed (mm/min)	0.25	1	2	4
E (N/m^2)	2.03E+06	2.14E+06	3.20E+06	4.01E+06
Yield Stress (MPa)	0.2009	0.1791	0.2317	0.2041
UTS (MPa)	0.7137	0.6338	0.6040	0.4981
Fail Strain	0.3747	0.3747	0.3747	0.3747
Fail Stress (MPa)	0.7137	0.6338	0.6040	0.4981

Table 4.8: Mean compression data for chocolate

4.5.4 Mechanical and thermal testing results and material properties of jelly

Tensile tests of jelly are shown in Fig. 4.25 (a) and (b) at temperatures of 4 °C and 20 °C respectively at crosshead velocities of 20, 40 and 60 mm/min. The graphs indicate the stress-strain behaviour for different specimens are similar and show reproducible stress-strain curves at 4°C at each testing temperature and crosshead velocity. At 20 °C the results are not as reproducible at the higher crosshead velocity of 60 mm/min but are similar when tested at slower crosshead velocities of 20 and 40 mm/min as shown in Fig. 4.25 (b). The stress-strain response is a typical J shaped curve, representative of biological materials. Fig. 4.25 (a) shows that as crosshead velocity is increased the UTS of the jelly increases slightly at a temperature of 4 °C. This trend is not replicated at a temperature of 20 °C as illustrated in Fig. 4.25 (b) where the resulting stress-strain diagrams have a spread in data at each crosshead velocity tested. The experimental test data was averaged for each material at each crosshead velocity and curve fitted using the elastic-plastic curve fitting procedure and is displayed in Fig. 4.26 (a) and (b) for temperatures of 4 °C and 20 °C respectively. This method is not an ideal curve fitting method for materials that exhibit J shaped behaviour due to the very high upturn in the curve at high strain approaching failure strain and the curve fit usually has a polynomial exponent between 0 and 1. The average tensile data for jelly produced from the curve fits of the experimental data is tabulated in Table 4.9.

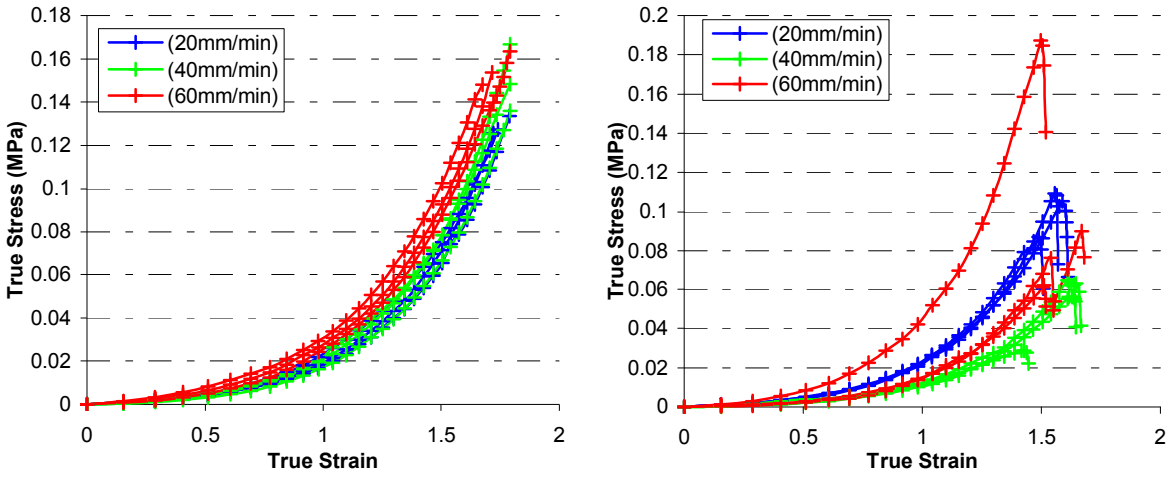

Fig. 4.25: Measured tensile test data for jelly at (a) 4 °C and (b) 20 °C

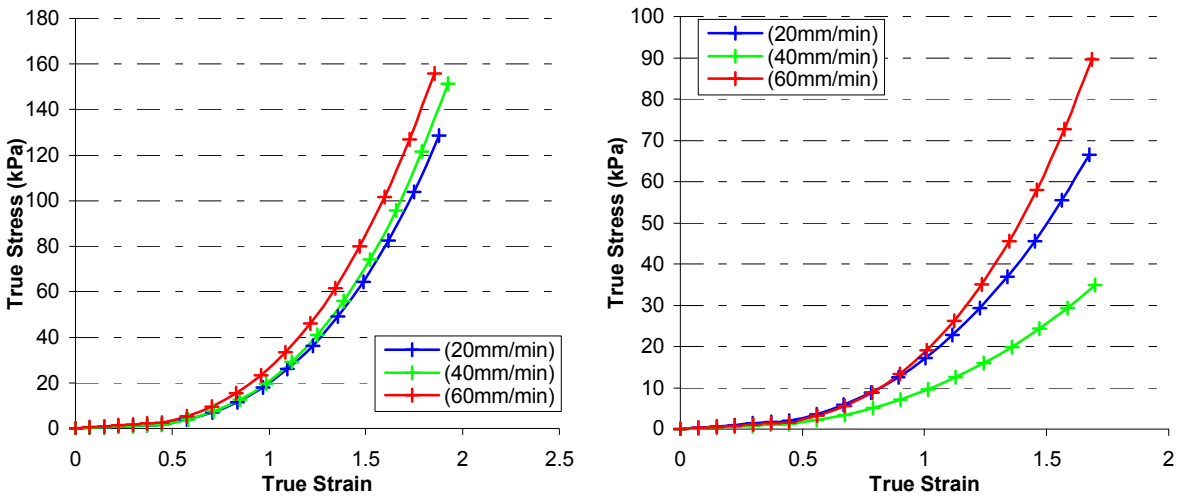

Fig. 4.26: Average tension test results for jelly at (a) 4 °C and (b) 20 °C.

	Temperature 4 °C		
Test Speed (mm/min)	20	40	60
E (N/m^2)	4.01E+03	4.02E+03	5.80E+03
Yield Stress (MPa)	0.0018	0.0018	0.0026
UTS (MPa)	0.1288	0.1503	0.1551
Fail Strain	1.7498	1.7914	1.7276
Fail Stress (MPa)	0.1288	0.1503	0.1551

	Temperature 20 °C		
Test Speed (mm/min)	20	40	60
E (N/m^2)	4.52E+03	2.74E+03	3.63E+03
Yield Stress (MPa)	0.0020	0.0012	0.0016
UTS (MPa)	0.0665	0.0349	0.0893
Fail Strain	1.5640	1.5859	1.5724
Fail Stress (MPa)	0.0665	0.0349	0.0893

Table 4.9: Average tension data for jelly

Fig. 4.27 (a) depicts tensile test results conducted at a temperature of 20 °C and at a crosshead velocity of 40 mm/min where the strain was determined using a non-contact laser extensometer instead of the displacement travelled by the crosshead of the machine. The reproducibility of the experimental technique for jelly tested using the laser extensometer measuring device is illustrated in the Fig. 4.27 (a) where the curves lie very closely to each other and provide confidence in the testing configuration. Fig. 4.27 (b) is a comparison between the average experimental tests conducted at a temperature of 20 °C and at a crosshead velocity of 40 mm/min using the laser extensometer as a measuring device and without the laser extensometer where the displacement the crosshead travelled was used to calculate strain. Findings show that both methods produce similar results at very low strains but as strain increases the results diverge due to the laser extensometer calculating the change in displacement of the gauge length of the

specimen as opposed to the displacement of the crosshead, which measures the change in length of the entire specimen, grips, fixtures and fittings. The laser extensometer provides a more accurate measurement of the strain. For the purposes of this thesis calculating strain in the materials using the change in displacement of the crosshead can be considered accurate for FE modelling purposes but future considerations of materials testing of food products should employ a non-contact measuring device such as a laser extensometer or cross-correlation thermal imaging techniques to improve the accuracy of the material testing techniques and provide a more accurate representation of the material properties of foodstuffs.

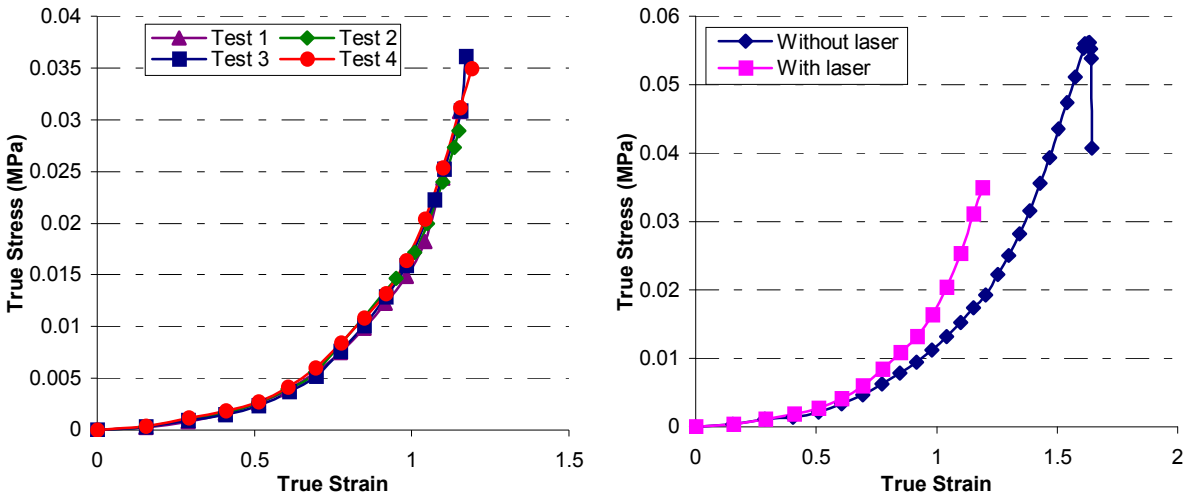

Fig. 4.27: (a) Experimental tension results for jelly tested at 20 °C and 40 mm/min using laser extensometer and (b) comparison between average experimental tension results tested without the laser and using crosshead displacement at 20 °C and 40 mm/min.

In compression the experimental stress-strain diagrams at each crosshead velocity tested exhibit a small deviation in results as shown in Fig. 4.28 (a) and (b). The stress-strain response exhibits a J-shaped curve. The Young's modulus in compression is higher at all crosshead velocities tested than in tension at 4 °C but at 20 °C the Young's modulus is lower. In compression the test was stopped at strains of 0.3747 as visible cracks were starting to appear on the compression specimen. At this location the specimen was assumed to have failed and comparisons of the UTS and fail stress were collated at this strain value. In tension the specimens endured very large strain, in the region of 200 %, and behave very differently from specimens tested in compression. Fig. 4.29 illustrates the average compressive behaviour of the jelly at each test temperature and crosshead velocity after curve fitting using the elastic-plastic technique. Both graphs show that as crosshead velocity is increased the UTS, yield point is increased for the jelly. Increasing temperature causes a reduction in the UTS and the yield point in each stress-

strain curve tested at a particular crosshead velocity. The average compression data for jelly represented as an elastic-plastic material is collated in Table 4.10.

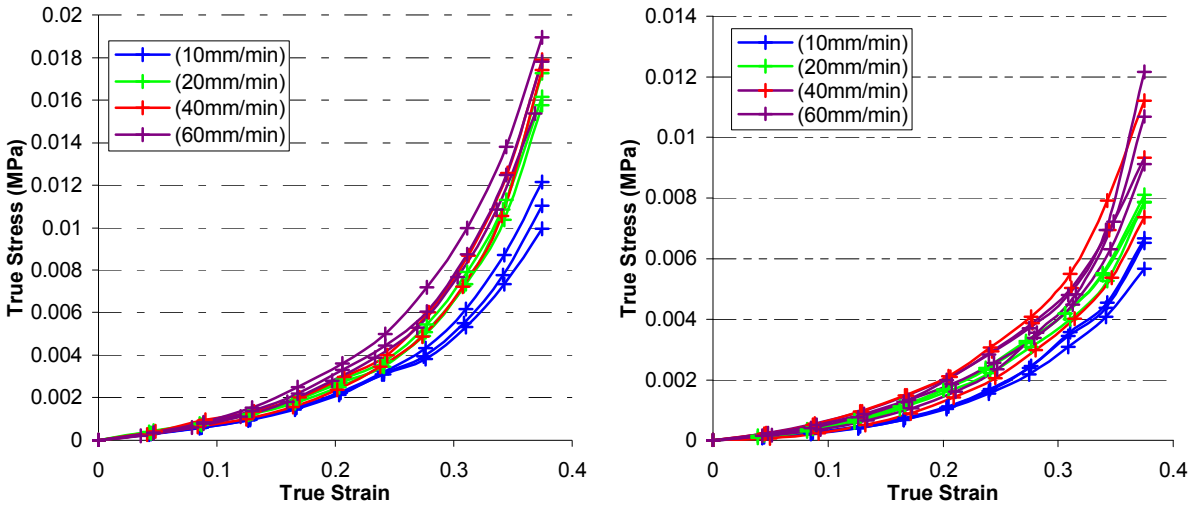

Fig. 4.28: Measured compression test data for jelly at (a) 4 °C and (b) 20 °C.

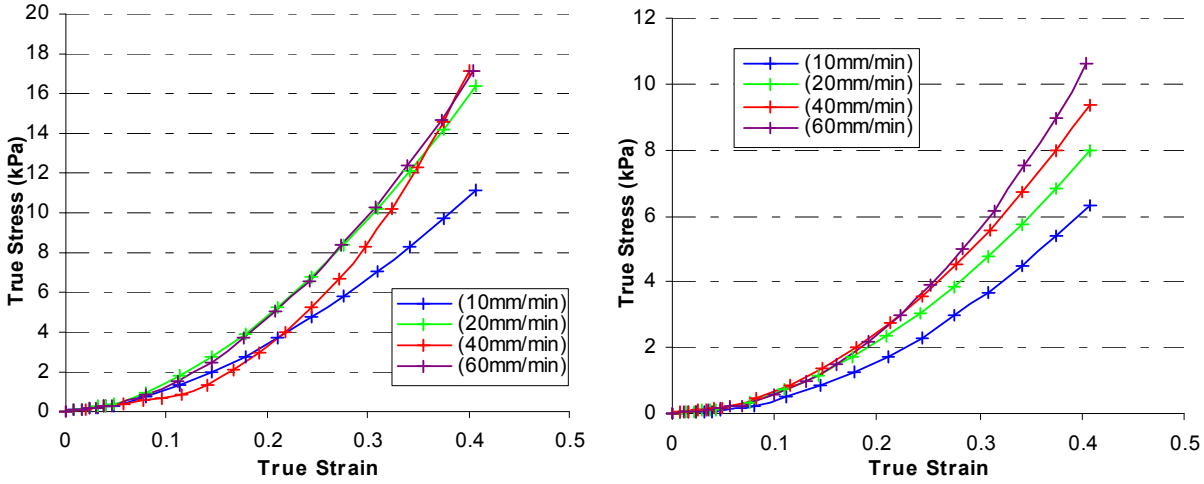

Fig. 4.29: Average compression test results for jelly at (a) 4 °C and (b) 20 °C.

	Temperature 4 °C			
Test Speed (mm/min)	10	20	40	60
E (N/m^2)	6.40E+03	8.24E+03	7.24E+03	6.57E+03
Yield Stress (MPa)	0.0003	0.0004	0.0008	0.0003
UTS (MPa)	0.0111	0.0164	0.0171	0.0174
Fail Strain	0.3747	0.3747	0.3747	0.3726
Fail Stress (MPa)	0.0111	0.0164	0.0171	0.0174

	Temperature 20 °C			
Test Speed (mm/min)	10	20	40	60
E (N/m^2)	1.93E+03	3.03E+03	3.55E+03	3.67E+03
Yield Stress (MPa)	0.0001	0.0001	0.0002	0.0003
UTS (MPa)	0.0063	0.0079	0.0093	0.0107
Fail Strain	0.3747	0.3747	0.3747	0.3747
Fail Stress (MPa)	0.0063	0.0079	0.0093	0.0107

Table 4.10: Average compression data for jelly

4.6 Conclusion

The mechanical and thermal properties of, toffee, cheese, chocolate and jelly have been investigated using a variety of different experimental testing techniques including the uni-axial tension and compression test at a variety of temperatures and crosshead velocities. Food material specimens were manufactured by using specially designed moulds or by cutting using a sharp scalpel. The specimens were manufactured to produce a smooth surface finish with few surface flaws to prevent failure emanating from the surface flaws and causing premature failure. A novel method for gripping and testing tensile specimens of food products was also presented, where specially designed grips were manufactured to grip the dog bone tensile specimens under the radii on the side of the specimens to overcome gripping difficulties. Previous researchers encountered specimen failure in tensile specimens prior to testing due to the tightening of the clamps in the conventional testing configuration that either induced failure instantly or created tears and flaws on the fracture surface in the soft or brittle materials. These problems were removed with the novel gripping technique presented in this chapter.

Experimental tensile and compression results for toffee, cheese, chocolate and jelly were presented in this chapter for repeated experimental trials at each crosshead velocity and temperature. The mechanical properties were determined for each material using conventional stress-strain relations and diagrams where useful quantifiable properties such as Young's modulus, yield point ultimate tensile stress and break point were determined. Comparisons of the mechanical properties determined in tension and compression were also included and discussed to explain the differing behaviour of each material in tension opposed to compression. The calculated mechanical properties for each material trial at each crosshead velocity and temperature were then averaged using a simple mean average to allow the experimental data for each food material to be curve fitted using an elastic-plastic material definition that could be implemented in the FE code ABAQUS. A simple mean average was used to represent the average spread of the data for the repeated tests at each crosshead velocity and temperature for each of the materials tested as the results were quite varied due to the batch dependence of the material, small differences in specimen preparation and errors attributed to experimental test set up. The average data set for each tensile and compression test at each environmental temperature and crosshead velocity tested was then curve fitted using a power law curve fitting procedure for inclusion in the FE code ABAQUS. This experimental and curve fitted data could also be used in

other engineering programmes or in engineering calculations to solve problems involving food materials.

Representing the tensile and compression stress-strain behaviour of cheese as a hyperelastic curve fit using the third order reduced polynomial curve fitting model was also studied at a temperature of 20 °C and a crosshead velocity of 5mm/min. This material modelling method allowed an enhanced representation of the material data in the FE package as both the tensile and compression data were represented by a strain energy density function which could be implemented together in the material description opposed to either one or the other. Characterising and representing the materials accurately for FE modelling of processes such as ultrasonic cutting is vital and often determines the precision of the results in the FE simulation being investigated. For modelling processes that are temperature dependent, temperature dependent material properties are essential for capturing the process accurately. In this study the thermal properties of toffee and cheese were determined using a DSC, a DMTA and a Fox 50 thermal conductivity machine to characterise the specific heat capacity, the glass transition and the thermal conductivity of the materials, all useful in FE modelling of heat transfer applications.

For toffee in tension and compression and at temperatures below 30 °C the material is brittle but at temperatures higher than 30 °C it is very ductile. Stress-strain curves produced at temperatures below 30 °C shows that the material is quite linear with a spread in results with no distinct plastic region which is typical of brittle materials. At temperatures above 30 °C the stress-strain curve illustrates typical R shaped behaviour again with a small deviation in results. As the test temperature increases for the toffee in tension and compression the material becomes less stiff and the Young's modulus decreases and the fail strain increases. The UTS and the yield point values for toffee slightly increase from 20 °C to 25 °C then start to decrease as temperature is increased. As the crosshead velocity is increased the Young's modulus, yield point, UTS and the fail stress increase at each test temperature illustrating the strain-rate dependency of the material. Toffee's mechanical properties are different in tension than compression with the material able to withstand higher stresses in compression, in excess of a magnitude of 10, and with the Young's modulus also slightly higher.

Cheese exhibits ductile behaviour at all temperatures and crosshead velocities tested where the material behaviour presents typical R shaped behaviour in tension and S shaped behaviour in

compression. In tension and compression when the test temperature increases the calculated parameters for Young's modulus, yield point and UTS decrease for cheese. Similarly to toffee as crosshead velocity is increased the Young's modulus, yield point and UTS slightly increase at each environmental test temperature. Replicated tests at each environmental test temperature and crosshead velocity indicate a slight spread in the results due to specimen inaccuracies due to the porous nature of cheese and test set up. It has been shown by experimental tensile and compression testing that the mechanical properties of cheese can be determined to a high degree of accuracy.

Experimental tensile results for chocolate indicated similar material characterisation as toffee where the material at environmental test temperatures of 4 °C and 20 °C represents typical brittle behaviour. The brittle nature of the material produces scattered results for each replicated test at each crosshead velocity and test temperature trends in calculated material properties are still apparent. In tension as the crosshead velocity increases the Young's modulus, yield point and UTS all increase at each test temperature and as the test temperature increases these properties decrease. In compression as the crosshead velocity increases the Young's modulus increased, the yield point indicated a slight spread in results illustrating no distinct trend and the UTS and fail stress decreased at each test temperature. Again as the test temperature increased when testing in compression the Young's modulus, yield point, UTS and fail stress decreased at each crosshead velocity tested.

Findings for tensile and compression tests on jelly indicated the J shaped behaviour typical of biological materials such as skin or tissue when tested in tension and compression. Findings indicate at a test temperature of 4 °C as crosshead velocity is increased the UTS and fail stress of jelly increases however at a test temperature of 20 °C this is not the case and there is no noticeable trend in behaviour. A comparison of strain measurement using a non-contact laser extensometer and the strain calculated using the displacement of the crosshead was conducted at 20 °C and at a crosshead velocity of 40 mm/min for jelly to compare the accuracy of the strain measurement. Findings indicated that using the laser extensometer the strain in the material is significantly less than that calculated using the displacement of the crosshead and can be considered more accurate as the laser extensometer only measures the strain in the gauge length of the specimen opposed to the crosshead displacement that measures the strain in the specimen and the fixtures. Further studies should incorporate using a non-contact strain measurement to

predict the stress-strain behaviour of food materials. In compression the results indicated a scatter in the replicated results at each temperature and crosshead velocity tested. The results indicated that jelly in compression has a higher Young's modulus than in tension at 4 °C and for all crosshead velocities tested. However, at 20 °C the Young's modulus is lower than that in tension. In compression as crosshead velocity is increased the UTS, yield point is increased for the jelly but as test temperature is increased the UTS and yield point decrease.

The research indicates that not only tensile tests on food materials are plausible but the mechanical properties determined in tension are different from that in compression and for some processes including ultrasonic cutting it could be beneficial in representing the material for FE purposes in tension or as a combination of tension and compression to improve the accuracy of the modelling process. The material properties calculated from the experimental tensile and compression tests can be used in the FE models of the ultrasonic cutting process to cut through these particular materials.

Chapter 5

Experimental and finite element simulation of ultrasonic cutting

5.1 Introduction

Ultrasonic cutting has become a popular technology for slicing of many difficult to cut materials including food products, especially as it avoids the product sticking to the blade and can produce a clean and accurate cut. The design of ultrasonic cutting tools has largely been based on the tuning of a single blade or multiple blade system to a selected low ultrasonic frequency, followed by trials and adaptations of the design to achieve acceptable performance. It is proposed here that a numerical simulation of ultrasonic cutting that includes a description of the product as well as a model of the cutting tool and product interaction at the cut site, offers an opportunity to conduct a parametric study of the effects of blade shape, frequency, ultrasonic amplitude and cutting speed as an integral part of the cutting tool design process. This approach can eliminate the need for repeated trialling of modified tools, can predict optimum cutting parameters and can allow novel blade designs to be proposed.

Two different approaches to the simulation of ultrasonic cutting are presented here. Both are based on fully coupled thermal-stress 2D finite element models that account for heat generation at the interface of the ultrasonic cutting tool and the material, and are developed using the finite element package ABAQUS. Both models allow detailed knowledge of the stress and temperature distribution around the cut site to be evaluated, in both the cutting tool and material to be cut. The first modelling approach represents ultrasonic cutting as a mode I fracture mechanics problem, and the second modelling approach considers ultrasonic cutting as destroying material at the cut site.

Validations of the 2D FE models are presented by comparing simulated cutting in a guillotine configuration with experimental cutting trials to provide confidence in the FE modelling approach. Parametric studies are then performed using the validated FE models to consider the

effect ultrasonic frequency, amplitude and cutting speed have on the cutting force and the temperature at the cut interface for a variety of materials. Expanding the 2D element erosion model into a 3D model that will allow more detailed results and cutting orientations to be explored is also presented in this Chapter.

5.2 Finite element models of ultrasonic cutting

Ultrasonic cutting in the guillotine configuration, Fig. 5.1(a), is represented using two different finite element models developed in the finite element package ABAQUS [252]. Both models are generic 2D fully coupled thermal-stress models that take advantage of symmetry about the cutting plane to maximise computational efficiency. The first model uses the implicit solver and the debond option and the second model uses the explicit solver and the element erosion option. Both models represent the ultrasonically excited blade and the material to be cut as elastic and elastic-plastic temperature dependent deformable bodies respectively. The elastic-plastic material model was used due to the ease of implementation of the stress-strain representation of the material in the FE code. Both models require temperature dependent material properties to be included, for both the blade and the product being cut.

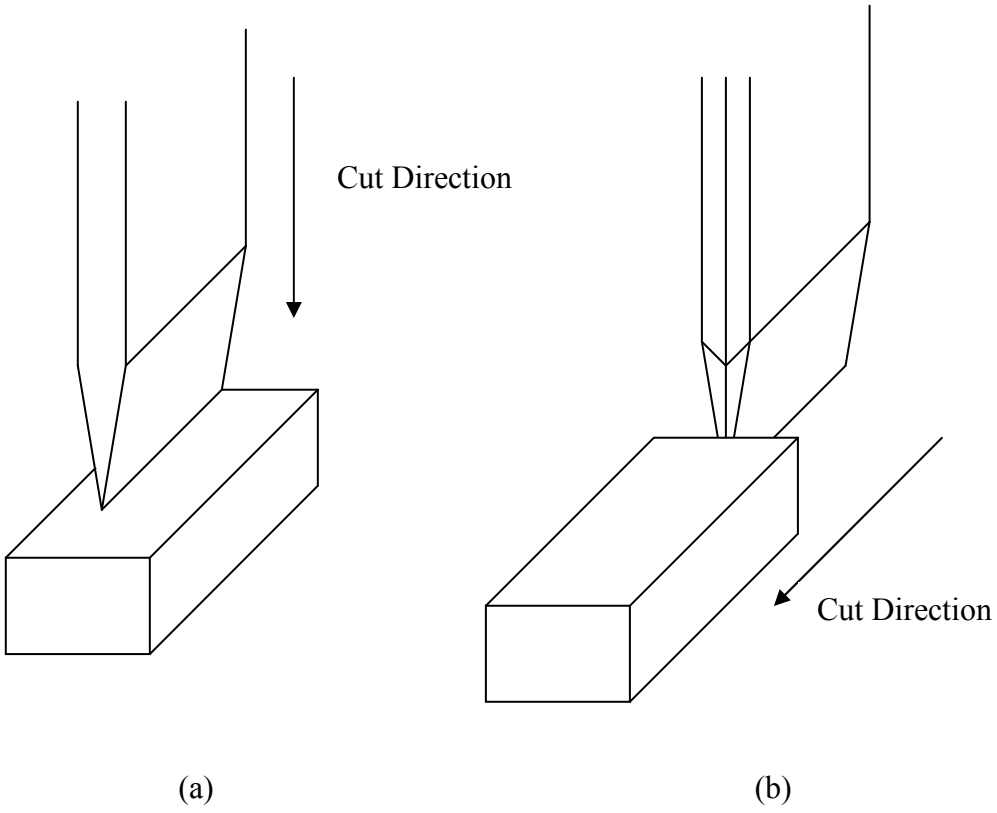

Fig. 5.1: (a) Guillotine cutting configuration (b) Slicing cutting configuration

For FE models of ultrasonic cutting, temperature dependant stress-strain relationships are required for the materials to be cut along with their strain rate dependent properties. Stress-strain curves are generated from the measured force-displacement data from standard mechanical tests. The elastic region is defined using Young's modulus and Poisson's ratio for each corresponding testing temperature and the plastic region of the curve is represented as true stress at each corresponding equivalent plastic strain value and at specific temperatures and crosshead velocities. The oscillatory movement of the cutting blade at the ultrasonic frequency is represented in both models using the predefined blade tip amplitude coupled to a periodic sinusoidal waveform. To incorporate superposition of the sinusoidal waveform on the cutting speed of the blade into the material, the blade was considered to oscillate about a fixed point at a predefined amplitude and frequency and the cutting speed was applied to the deformable specimen. Both analyses incorporate a contact definition at the interface between the food material and the blade using a Coulombic friction model combined with a model of the frictional heat generated at the interface. All the energy generated at the interface due to frictional contact is considered to be converted to heat with heat distribution also considered to be dispersed equally into the surface of the blade and material to be cut. Energy losses in the system such as noise and internal heat generation of the resonant blade are neglected for modelling purposes as they will have a negligible on the cutting mechanism at the interface compared to frictional heating, cutting force, ultrasonic amplitude, ultrasonic frequency and cutting speed. Both models are generic and easily adaptable to different cut materials, blade geometries, material properties, temperature, and other cutting parameters.

5.2.1 Material properties

The food material properties used in the FE simulations in this section of the thesis can be found in Chapter 4. For this study the material of the cutting blade was titanium $Ti_{90}Al_6V_4$ and the food materials being cut were mild cheddar cheese, toffee, chocolate and jelly. Representing materials in finite element analysis requires a description of their mechanical and thermal properties in a material model and ABAQUS has various models available to characterise material behaviour from experimental data [252].

This study represented titanium using an elastic material definition from standard material properties available in the literature [256] with Young's modulus 114 GPa, Poisson's ratio 0.3 and density 4425 kg/m^3. These properties were assumed to be constant at temperatures between

20 and 250 °C as the deviation of these properties in the materials table deviated negligibly over this temperature range. All materials being cut were represented as an elastic-plastic material model using average temperature dependent and strain-rate dependent stress-strain data derived from experimental tension test data due to the simplicity of implementation in the FE code. Averaging the temperature and strain rate dependent curves was performed by averaging the Young's modulus, yield stress, ultimate tensile stress and true strain value at break point for each experimental test conducted at each temperature and crosshead velocity. The average plastic region was curve fitted between the average yield point, average ultimate tensile stress and average true strain value at break point using a simple polynomial curve fitting representation.

Averaged and curve fitted data derived from the experimental tensile tests provided the input data for the material characterisation in the FE model at various temperatures and crosshead velocities. The ABAQUS FE model requires input of an equal number of data points in the plastic region for each stress-strain curve, for each temperature and strain rate, to allow interpolation between the curves at different temperatures. This allows ABAQUS to generate look up tables that are used by the solver during the analysis. In this investigation 12 data points in the plastic region were defined for each curve and for every material. The material model also includes characterisation of the thermal properties of titanium and the material to be cut. Specific heat capacity and thermal conductivity properties are included that are essential for fully capturing the material behaviour during ultrasonic cutting. Thermal properties for titanium are widely documented [256]. The specific heat and thermal conductivity for titanium used in the FE simulations were 598 kJ/kg°C and 6.6 W/mK respectively and both specific heat and thermal conductivity were assumed to be constant in the models due to them differing very slightly in standard tables. The specific heat capacity and thermal conductivity for the food materials was measured using a differential scanning calorimeter (DSC) and a Fox 50 thermal conductivity machine, respectively. Values for these parameters for each food material can be found in Chapter 4 of this thesis.

Perspex was used initially to validate the FE models against ultrasonic cutting trials as it is homogeneous and can allow repeatable experimental analysis. The mechanical and thermal material properties of Perspex will be included in this section to allow the FE models of ultrasonic cutting to be validated and to provide confidence in the modelling technique of ultrasonic cutting.

5.2.1.1 Experimental testing results and material properties of Perspex

Perspex dog bones were machined by milling to specified sizes as illustrated in Fig. 4.4 in Chapter 4 section 4.3.1.1. Care was taken to ensure that there was a high surface finish to minimise surface cracks and flaws.

Perspex was tested in tension and investigated at four selected temperatures in the range 20 – 110°C and at crosshead velocities of 5, 15 and 25 mm/min. Each test was conducted using three identical samples for each temperature and crosshead velocity in order to check the reproducibility of the tests. The raw data at temperatures of 20, 50, 80 and 110 °C for each crosshead velocity is depicted in Fig. 5.2. The graphs indicate there is a small spread in data for the three tests at every temperature and crosshead velocity except 110 °C where the spread is quite large due the material nearing the glass transition temperature. This is usually due to the small inaccuracies in the specimen preparation during machining, material composition and small experimental and operator errors when setting up the test due to clamping tightness and preloading. For the purpose of gaining material properties to validate the FE models of ultrasonic cutting the results are considered to be reproducible for each test temperature and crosshead velocity. Findings show that as temperature increases from 20 to 110 °C the yield point, UTS and break point all decrease and the strain and ductility of the specimen increase which are common phenomena in plastic materials.

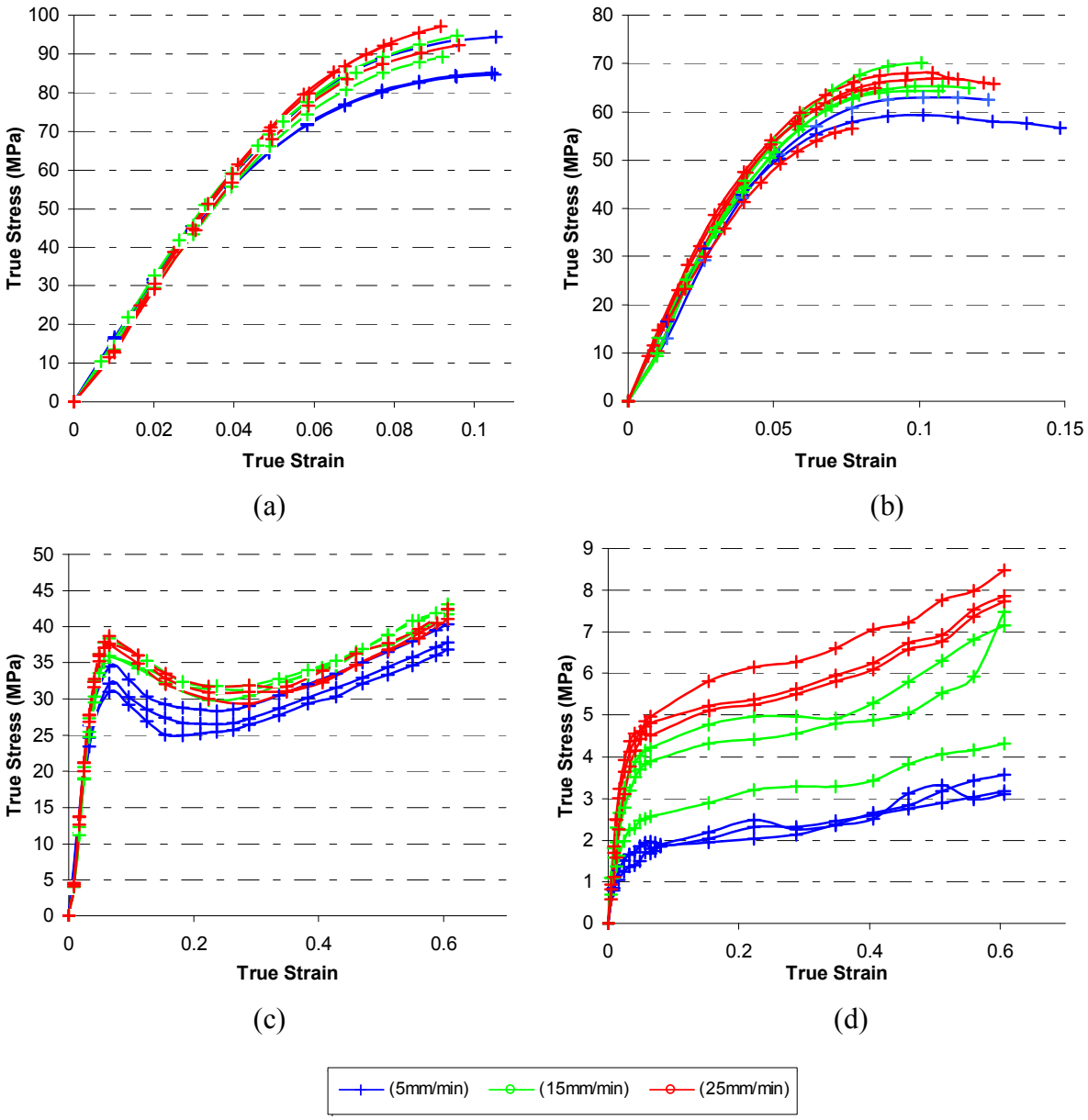

Fig. 5.2: Experimental temperature and strain rate dependent stress-strain data for Perspex at (a) 20 °C, (b) 50 °C, (c) 80 °C and (d) 110 °C.

Once the raw experimental stress-strain data is obtained from the experimental tests the data is curve fitted using the procedure described in section 4.4.1 for the elastic-plastic material model at all temperatures and crosshead velocities. The strain-rate dependent test data and curve fitted data are shown in Fig. 5.3 for Perspex at 20 °C.

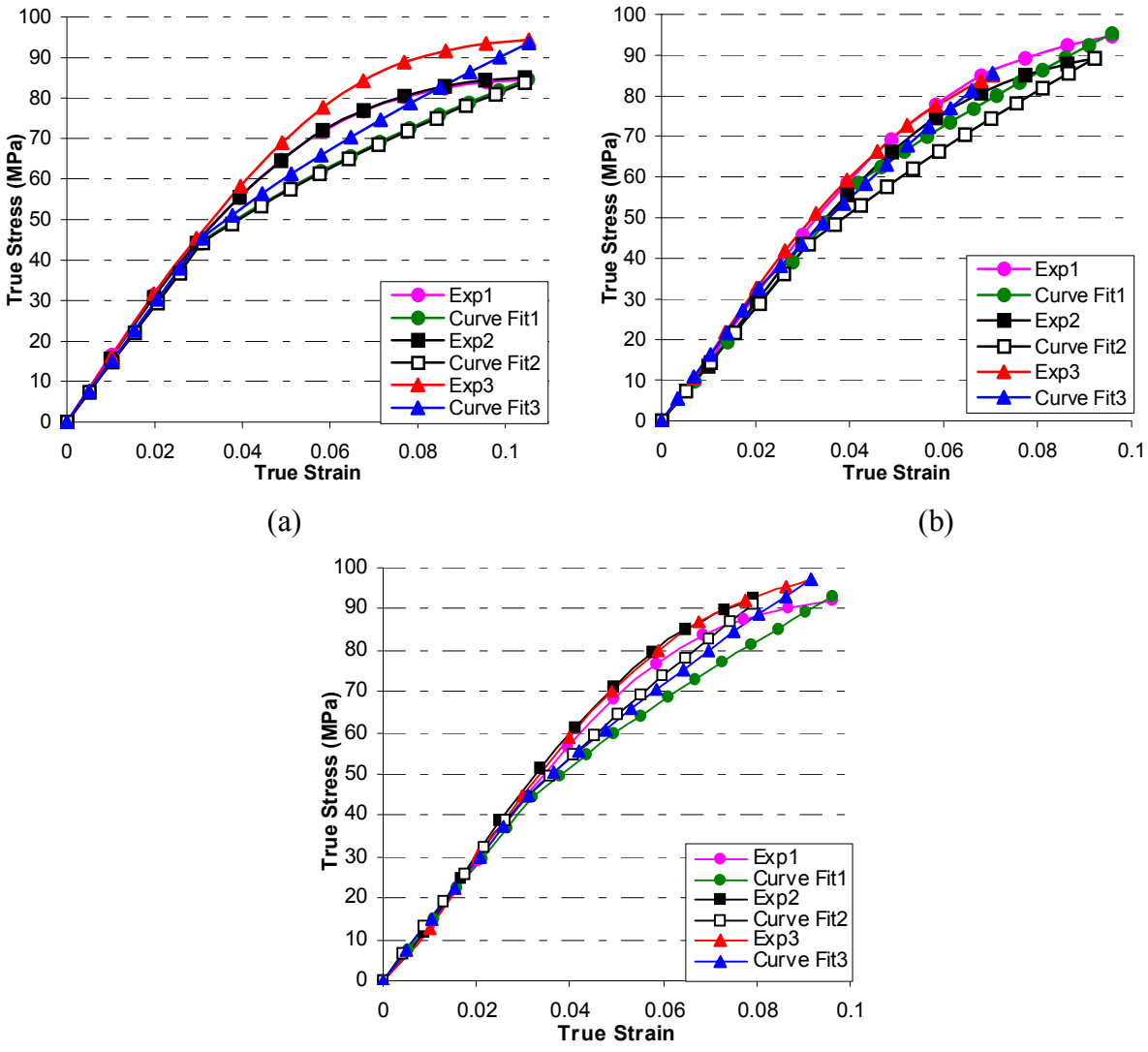

Fig. 5.3: Experimental and curve fitted stress-strain data for Perspex at 20 °C for (a) 5 mm/min, (b) 10 mm/min and (c) 15 mm/min.

After all the curve fitted data is obtained for each temperature and crosshead velocity tested, the Young's modulus, yield point, UTS, fail strain and fail stress at each temperature and crosshead velocity are calculated from these curve fitted results. An average is then calculated for Young's modulus, yield point, UTS, fail strain and fail stress from the multiple tests at each temperature and crosshead velocity and then these averaged parameters are used to generate average curve fitted data for each test temperature and crosshead velocity for use in FEA. This data is tabulated in Table 5.1. This data is represented graphically in Fig. 5.4, which illustrates the average stress-strain data for Perspex from mechanical tests which, will be implemented in FE and highlights the temperature and strain-rate dependency of this synthetic material.

	Temperature 20 °C		
Test Speed (mm/min)	5	15	25
E (N/m^2)	1.45E+09	1.45E+09	1.45E+09
Yield Stress (MPa)	44.71	44.86	42.70
UTS (MPa)	88.04	89.67	93.94
Fail Strain	0.10	0.09	0.09
Fail Stress (MPa)	88.04	89.67	93.94

	Temperature 50 °C		
Test Speed (mm/min)	5	15	25
E (N/m^2)	1.07E+09	1.13E+09	1.21E+09
Yield Stress (MPa)	40.35	35.44	31.38
UTS (MPa)	59.81	65.29	62.80
Fail Strain	0.15	0.13	0.09
Fail Stress (MPa)	59.81	65.29	62.80

	Temperature 80 °C		
Test Speed (mm/min)	5	15	25
E (N/m^2)	4.57E+08	5.84E+08	5.99E+08
Yield Stress (MPa)	32.48	36.03	37.33
UTS (MPa)	38.31	42.40	41.35
Fail Strain	0.61	0.61	0.60
Fail Stress (MPa)	38.31	42.40	41.35

	Temperature 110 °C		
Test Speed (mm/min)	5	15	25
E (N/m^2)	4.56E+07	8.22E+07	1.16E+08
Yield Stress (MPa)	1.43	3.12	4.09
UTS (MPa)	3.28	6.32	8.03
Fail Strain	0.61	0.61	0.61
Fail Stress (MPa)	3.28	6.32	8.03

Table 5.1: Average tension data for Perspex

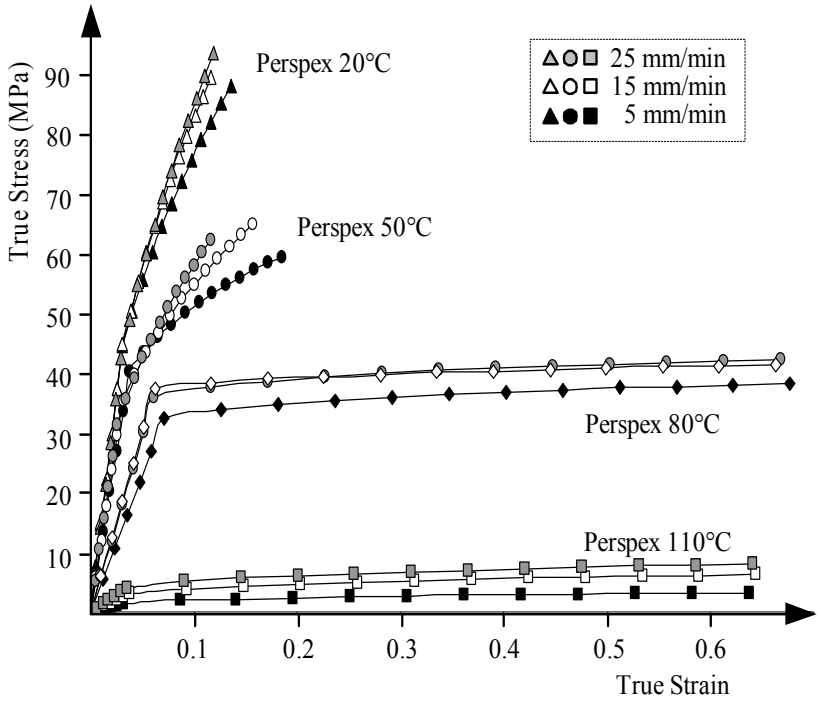

Fig. 5.4: Average temperature and strain rate dependant stress-strain data for Perspex for implementation in FE.

Table 5.2 presents other data for Perspex that is required for finite element simulations of ultrasonic cutting using a titanium blade in a Perspex sample. This data is extracted from previously published literature [256].

	Perspex
Density (kg/m^3)	1170
Poisson's Ratio	0.37
Specific Heat (kJ/kg°C)	1.47
Thermal Conductivity (W/mK)	0.19

Table 5.2: Thermal data for Perspex

5.2.2 Contact definitions

Friction is the main cause of heat generation at the interface between the ultrasonically excited blade and the material being cut, and is extremely important in defining the interface contact condition. Experiments were therefore conducted to derive the coefficient of dry friction at the interface between the cutting blade and specimen material. A titanium alloy block horn was designed using FE modelling to provide an ultrasonically excited flat surface. The titanium alloy used for the block horn is the same grade as that used for the cutting blades. The block horn was designed to resonate in its first longitudinal mode at 20 kHz. Modal frequency and mode shape

predictions from the FE model were validated by experimental modal analysis (EMA) using a 3D laser Doppler vibrometer.

Fig. 5.5 shows a schematic of the experimental rig for estimating the coefficient of friction. Specimens of Perspex, toffee and mild cheddar were moved at constant velocity across the block under an applied load and a Coulomb friction method was used to calculate the coefficients of static and dynamic friction, μ_s and μ_d using Eq. 5.1, where F_P is the weight attached to the pulley, F_S is the static load carried by the specimen, and m is the mass of the specimen. A high-speed camera sampling at 400 frames per second was used to monitor the velocity of the specimens. Tests were conducted with and without ultrasonic excitation of the block horn. As shown in Table 5.3, the coefficients of dynamic friction were significantly affected by ultrasonic excitation. The coefficients of dynamic friction under ultrasonic excitation of the test surface were used in the FE model of ultrasonic cutting to define the interface boundary condition.

$$\mu_{s,d} = \frac{F_P}{F_S + mg} \tag{5.1}$$

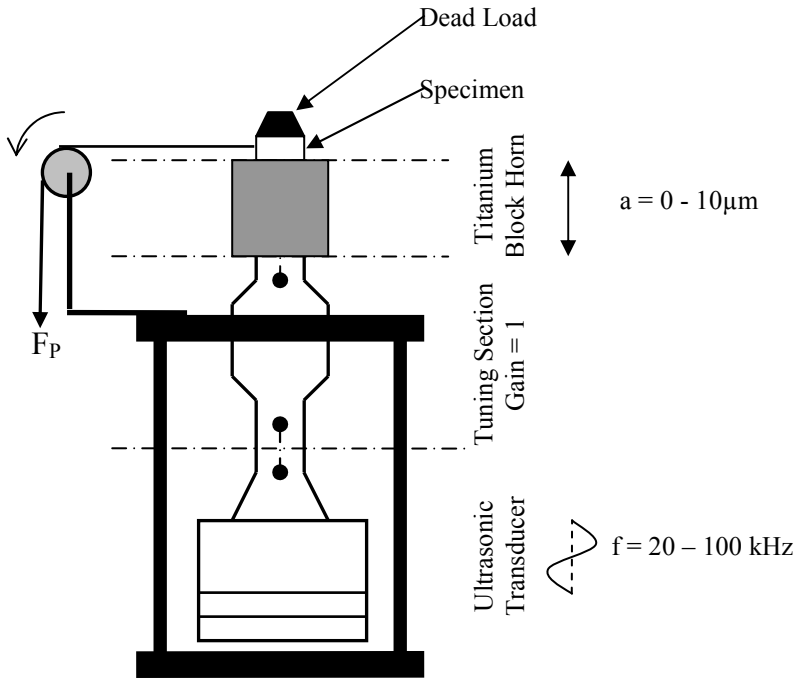

Fig. 5.5: Friction test-rig to investigate the effect of ultrasonic vibrations on dry friction occurring at blade-specimen interfaces.

Friction	Perspex	Toffee	Mild Cheddar
μ_s	0.343	0.240	0.536
$\mu_{d\ (without\ ultrasound)}$	0.282	0.116	0.457
$\mu_{d\ (with\ ultrasound)}$	0.030	0.032	0.139

Table 5.3: Coefficient of static friction and the coefficients of dynamic friction between cutting blades and material specimens of Perspex, toffee and mild cheddar cheese with and without superimposed ultrasonic vibration.

When modelling the contact between the ultrasonically excited blade and the material to be cut in the FE simulations consideration has to be given to heat generation due to friction. For all the simulations in this thesis heat generation due to friction was incorporated in the model by assuming that 50 % of the heat was passed into the blade and 50 % into the substrate material. Also, separation of the blade and the material contact surfaces can be included in the FE simulations. A contact parameter can be specified in the FE package stating whether to allow or disallow separation of the contact surfaces in the simulation once contact has been established. Separation of the blade-material surfaces will occur if the vibration velocity exceeds the cutting velocity. For a sinusoidal excitation the blade displacement can be determined from Eq. 5.2.

$$x = A\sin\omega t \tag{5.2}$$

The vibration velocity can be found by considering the first derivative of Eq. 5.2 as shown in Eq. 5.3 and the maximum amplitude of the vibration velocity is therefore $A\omega$.

$$\dot{x} = A\omega\cos\omega t \tag{5.3}$$

Considering the maximum vibration velocity and the cutting speed of the blade, it can be easily shown that separation will not occur if the velocity of the blade, $v_{tran} \geq$ amplitude of the vibration velocity, $A\omega$ and similarly separation will occur if the translational velocity of the blade, $v_{tran} \leq , A\omega$.

Table 5.4 calculates whether the contact surfaces would separate or not for a variety of ultrasonic frequencies and amplitudes considering the maximum translational speed that will be considered

in this thesis of 10 mm/s using Eq. 5.3. The rows highlighted in blue indicate the minimum blade tip amplitude required for the surfaces never to separate at each corresponding ultrasonic frequency considering the translational velocity to be 10 mm/s. Considering the blade tip amplitudes used in this thesis are in excess of the minimum amplitude required for separation, separation of the contact surfaces will be considered in this FE simulation.

$\dot{\chi}_{max}$	A (m)	ω (rad/s)	F (Hz)	v_{tran} (m/s)	Separation (Yes/No)
0	0	125663.7061	20000	0.01	No
0.01	7.95775E-08	125663.7061	20000	0.01	No
3.141592654	2.50E-05	125663.7061	20000	0.01	Yes
6.283185307	5.00E-05	125663.7061	20000	0.01	Yes
9.424777961	7.50E-05	125663.7061	20000	0.01	Yes
0	0	219911.4858	35000	0.01	No
0.01	4.54728E-08	219911.4858	35000	0.01	No
5.497787144	2.50E-05	219911.4858	35000	0.01	Yes
10.99557429	5.00E-05	219911.4858	35000	0.01	Yes
16.49336143	7.50E-05	219911.4858	35000	0.01	Yes
0	0	345575.1919	55000	0.01	No
0.01	2.89373E-08	345575.1919	55000	0.01	No
8.639379797	2.50E-05	345575.1919	55000	0.01	Yes
17.27875959	5.00E-05	345575.1919	55000	0.01	Yes
25.91813939	7.50E-05	345575.1919	55000	0.01	Yes

Table 5.4: Results tabulated to show the maximum vibration velocity required to cause the blade and specimen surface to separate during ultrasonic cutting at 10 mm/s for three ultrasonic frequencies of 20 kHz, 35 kHz and 55 kHz.

5.2.3 2D debond model

One method of simulating ultrasonic cutting as a 2D FE model is to represent the cutting mechanism as a fracture mechanics problem. Ultrasonic cutting is modelled using a fracture approach in mode I opening whereby a crack propagates at the interface of the excited ultrasonic cutting blade and the material to be cut when the critical normal stress at a pre-specified distance ahead of the crack tip is reached using Irwin's model of crack tip plasticity in an elastic-plastic material.

5.2.3.1 Fracture mechanics theory

Fracture mechanics is the study of how materials fail. This engineering field was developed in the early 20th century by fundamental work by Inglis and Griffith on an elliptical hole in a plate

[255]. Linear elastic fracture mechanics considers the material to behave in a perfectly elastic manner prior to failure and assumes the material exhibits no plasticity.

Griffith in 1920 [262] correlated the connection between fracture stress and flaw size. He further developed the work of Inglis [263] by applying a stress analysis of an elliptical hole in a plate to unstable crack propagation using either a fixed displacement or a uniformly distributed load. Griffith used an energy method for his analysis by using the first law of thermodynamics to develop a fracture criterion. This work was initially developed by studying the behaviour of glass and relates only to ideal brittle materials. Griffith postulated that crack advance occurs when there is sufficient strain energy to produce a new crack surface [255].

The Griffith energy balance is expressed in Eq. 5.4 where U_T is the total energy, A is the area of the crack surface, W is the external work and W_s is the energy required to make a new surfaces in the material.

$$\frac{dU_T}{dA} - \frac{dW}{dA} = \frac{dW_s}{dA} \tag{5.4}$$

A crack can develop or propagate if the total energy decreases or remains the same due to the application of a load or displacement. So the critical fracture condition is the situation where crack growth occurs under equilibrium conditions with no change in total energy as shown using Eq. 5.5.

$$-\frac{dW}{dA} = \frac{dW_s}{dA} \tag{5.5}$$

The formation of a crack requires two new surfaces to be created so the right hand side of Eq. 5.5 is the resistance to crack growth, R as shown in Eq. 5.6 where a is the crack length and B is the breadth of the specimen:

$$R = \frac{d}{dA}W_S = \frac{d}{dA}4aB\gamma_s \tag{5.6}$$

The resistance to crack growth is quantified as the energy necessary to break the atomic bonds in a material and this is denoted by the surface energy density, γ_s.

The left hand side of Eq. 5.4 is the difference between external work and elastic strain energy in the body and denotes the energy release rate, G_C. The energy release rate, G_C, is a measure of the available energy for an increment of crack extension.

$$\frac{d}{dA}\left(U_T - W\right) = \frac{\pi\sigma^2 a}{E'} = G_C \tag{5.7}$$

Where the Young's Modulus E' is dependent on whether the situation is plane stress or plane strain and using the tabulated Young's modulus E and Poisson's ratio υ is either,

$$E' = E \quad \text{(plane stress)} \quad \text{or} \quad E' = \frac{E}{\left(1-\nu^2\right)} \quad \text{(plane Strain)} \tag{5.8}$$

The resistance to crack extension with crack area, $2aB$, can be written as shown in Eq. 5.9 from Eq. 5.8:

$$\frac{dW_S}{dA} = 2\gamma_S \tag{5.9}$$

Equating Eq. 5.8 and Eq. 5.9 and solving for critical fracture stress σ_f gives:

$$\sigma_f = \left(\frac{2E'\gamma_S}{\pi a}\right)^{\frac{1}{2}} \tag{5.10}$$

For fracture to occur the energy stored in the body must be sufficient to overcome the surface energy of the material in the Griffith model.

The loading configuration used and the geometry of the cracked body determine the magnitude of the external work, W. Using a fixed loading configuration the work done is the integral of the applied load, P, with respect to the displacement Δ.

$$W = \int_0^{\Delta} P d\Delta = P\Delta \tag{5.11}$$

The strain energy released as the crack propagates from a to $a + da$ is:

$$U_T = \int_0^{\Delta} \frac{P}{2} d\Delta = \frac{P\Delta}{2} \tag{5.12}$$

giving the elastic energy release rate:

$$G = \frac{Pd\Delta}{2} - Pd\Delta = \frac{Pd\Delta}{2} \tag{5.13}$$

For fixed displacement there is no external work done so the energy for crack extension is the accumulated elastic strain energy in the body.

$$G = \frac{d}{da} U_T = \frac{Pd\Delta}{2} \tag{5.14}$$

Initial work by Griffith [262] correlates well for ideal brittle solids such as glass but underestimates metallic material's fracture strength. Irwin [264] and Orowan [265] modified the expression in Eq. 5.9 to allow for materials that exhibit plastic flow after realizing that the main energy absorption was a small region at the crack tip. The inclusion of a parameter to define the surface energy density in plasticity, γ_P was incorporated in the equation.

$$\sigma_f = \left(\frac{2E(\gamma_S + \gamma_P)}{\pi a} \right)^{\frac{1}{2}} \tag{5.15}$$

In a perfectly brittle solid a crack can be formed by breaking atomic bonds. However when a crack propagates in a metal, dislocations occur near the crack tip resulting in increased energy dissipation. This work was originally conducted for metals but can be adjusted to account for any type of fracture as shown in Eq. 5.16.

$$\sigma_f = \left(\frac{2Ew_f}{\pi a} \right)^{\frac{1}{2}} \tag{5.16}$$

For brittle materials:

$$w_f = \gamma_S \tag{5.17}$$

For elastic-plastic materials:

$$w_f = \gamma_S + \gamma_P \tag{5.18}$$

However this must be used with care for materials that exhibit nonlinear deformation as the Griffith model only applies to linear elastic materials. The plastic region must be confined to the crack tip and the overall response must be elastic.

Westergaard [266], Irwin [267] and Williams [268] developed expressions for stresses in an isotropic linear elastic body due to external forces. The stress field in a linear elastic body using a polar coordinate system with the origin at the crack tip can be analyses by Eq. 5.19 and can be shown in Fig. 5.6 where 2a is the crack length and r is the distance ahead of the crack tip:

$$\sigma_{ij} = \left(\frac{k}{\sqrt{r}} \right) f_{ij}(\theta) \tag{5.19}$$

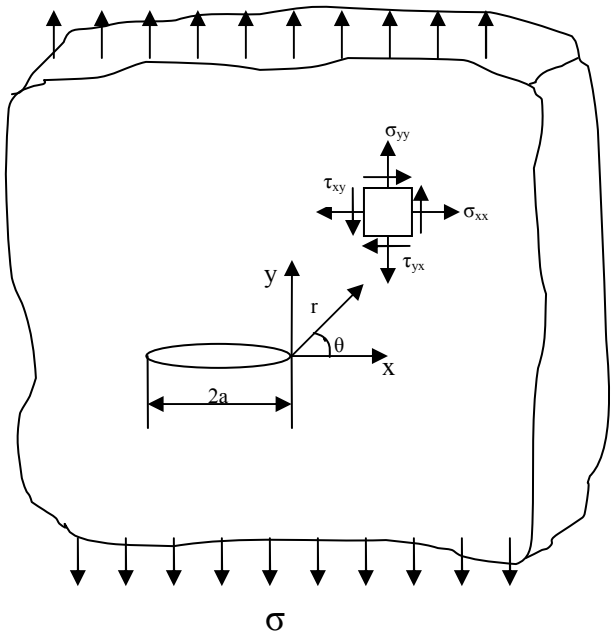

Fig. 5.6: Cracked body depicting stresses at a crack tip.

The solution of Eq. 5.19 is proportional to $1/\sqrt{r}$ and tends towards infinity as $r \to 0$. Since the resulting stress is asymptotic at r = 0 it describes a stress singularity, Fig. 5.7.

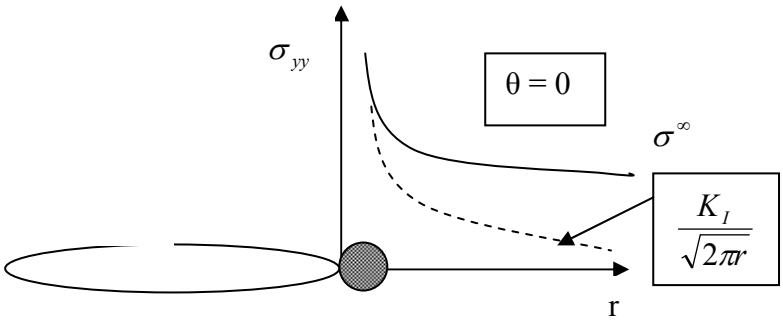

Fig. 5.7: Crack tip describing stress singularity as $r \to 0$.

A $1/\sqrt{r}$ singularity is produced at the crack tip for each of the three modes of loading. However, scaling factor, k, and the function of the rotation of the stress field about the crack tip $f_{ij}(\theta)$ depend on the mode of loading but can be related through *K*, the stress intensity factor. The stress intensity factor can be written as K_I, K_{II}, K_{III} for the three different modes of loading as shown in Fig. 5.8 using Eq. 5.20:

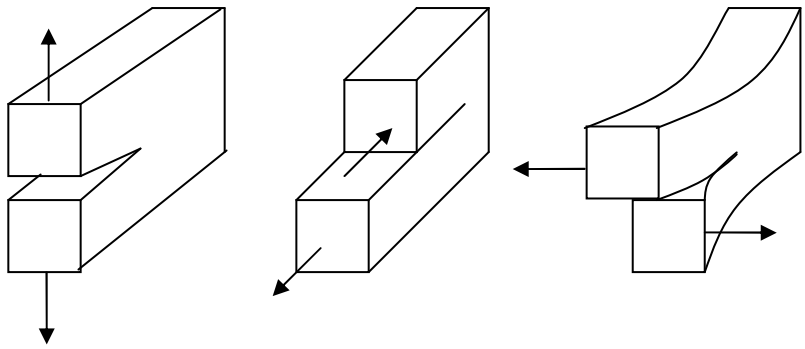

Mode I Opening | Mode II In Plane Shear | Mode III Out of plane Shear

Fig. 5.8: Three modes of loading.

$$K = k\sqrt{2\pi} \tag{5.20}$$

thus,

$$\lim_{r\to 0}\sigma_{ij}^{(I)} = \frac{K_I}{\sqrt{2\pi r}} f_{ij}^{(I)}(\theta) \tag{5.21}$$

$$\lim_{r\to 0}\sigma_{ij}^{(II)} = \frac{K_{II}}{\sqrt{2\pi r}} f_{ij}^{(II)}(\theta) \tag{5.22}$$

$$\lim_{r\to 0}\sigma_{ij}^{(III)} = \frac{K_{III}}{\sqrt{2\pi r}} f_{ij}^{(III)}(\theta) \tag{5.23}$$

The stress fields ahead of a crack tip for mode I are described using Eq's. 5.24 – 5.26:

$$\sigma_{xx} = \frac{K_I}{\sqrt{2\pi r}}\cos\left(\frac{\theta}{2}\right)\left[1-\sin\left(\frac{\theta}{2}\right)\sin\left(\frac{3\theta}{2}\right)\right] \tag{5.24}$$

$$\sigma_{yy} = \frac{K_I}{\sqrt{2\pi r}}\cos\left(\frac{\theta}{2}\right)\left[1+\sin\left(\frac{\theta}{2}\right)\sin\left(\frac{3\theta}{2}\right)\right] \tag{5.25}$$

$$\tau_{xy} = \frac{K_I}{\sqrt{2\pi r}}\cos\left(\frac{\theta}{2}\right)\sin\left(\frac{\theta}{2}\right)\cos\left(\frac{3\theta}{2}\right) \tag{5.26}$$

For $\theta = 0$, $\tau_{xy} = 0$, $\sigma_{xx} = \sigma_{yy} = \frac{K_I}{\sqrt{2\pi r}}$,

$$K = Y\sigma\sqrt{\pi a} \tag{5.27}$$

Irwin [267] considered Eq. 5.27, to be valid only where the $1/\sqrt{r}$ singularity dominates near the crack tip and the stress intensity factor, *K*, represents the amplitude of the singularity at the crack tip. Solutions for loading in modes II and III are also available for stresses and displacements

near the crack tip. The function, *Y*, is the geometric correction factor and is tabulated for many different loading geometries.

Williams [268] conducted a similar analysis for expressing the stress field in cylindrical coordinates as shown in Eq. 5.28.

$$\sigma_{ij}(r,\theta) = A_{ij}(\theta)r^{s} + B_{ij}(\theta)r^{t} + C_{ij}(\theta)r^{u} \tag{5.28}$$

where (s,t,u) = $(-\frac{1}{2},0,\frac{1}{2})$.

The elastic stress-strain relationships as shown in Eq. 5.29, 5.30, 5.31 and 5.32 can be used to derive the resulting Cartesian displacements:

$$\varepsilon_x = \frac{1}{E}\left[\sigma_x - \nu(\sigma_y + \sigma_z)\right] \tag{5.29}$$

$$\varepsilon_y = \frac{1}{E}\left[\sigma_y - \nu(\sigma_z + \sigma_x)\right] \tag{5.30}$$

$$\varepsilon_z = \frac{1}{E}\left[\sigma_z - \nu(\sigma_x + \sigma_y)\right] \tag{5.31}$$

$$\varepsilon_{xy} = \frac{\sigma_{xy}}{2\mu}, \varepsilon_{yz} = \frac{\sigma_{yz}}{2\mu}, \varepsilon_{zx} = \frac{\sigma_{zx}}{2\mu} \tag{5.32}$$

where:

$$\mu = \frac{E}{2(1+\upsilon)} \tag{5.33}$$

For a two dimensional problem the strains can be related to the displacements *u*, *v*, *w*, through the strain-displacement equations.

$$\varepsilon_x = \frac{\partial u}{\partial x}, \varepsilon_y = \frac{\partial v}{\partial y}, \varepsilon_{xy} = \frac{\partial u}{\partial y} + \frac{\partial v}{\partial x} \tag{5.34}$$

Considering the case of a thin plate or membrane, the body is subject only to in-plane stresses, as the out-of-plane stresses are zero on the surfaces and the stress gradient through the thickness is so small that it can be considered negligible, therefore:

$$\sigma_{zz} = \sigma_{zx} = \sigma_{yz} = 0, \frac{\partial \sigma_{zz}}{\partial z} = \frac{\partial \sigma_{zx}}{\partial z} = \frac{\partial \sigma_{yz}}{\partial z} = 0 \tag{5.35}$$

$$\varepsilon_z = -\frac{2(1+\nu)}{E}\nu(\sigma_x + \sigma_y) \tag{5.36}$$

However, a thin section of material at the centre of a thick plate or cylinder is restrained in the out-of-plane direction due to the material imposing out-of-plane stresses thus causing

deformation to three in-plane components of strain $(\varepsilon_x, \varepsilon_y, \varepsilon_z)$. This can be denoted the plane strain condition.

$$\sigma_{zz} = \upsilon\left(\sigma_{xx} + \sigma_{yy}\right) \tag{5.37}$$

$$\varepsilon_z = \varepsilon_{yz} = \varepsilon_{zx} = 0, \frac{\partial \varepsilon_z}{\partial z} = \frac{\partial \varepsilon_{zx}}{\partial z} = \frac{\partial \varepsilon_{yz}}{\partial z} = 0 \tag{5.38}$$

Ahead of the crack tip the displacement field (*u,v*) for plane stress and plane strain under tensile loading is given in Eq. 5.39 and Eq. 5.40:

$$u = \frac{K_I}{2\mu}\sqrt{\frac{r}{2\pi}}\cos\left(\frac{\theta}{2}\right)\left[\kappa - 1 + 2\sin^2\left(\frac{\theta}{2}\right)\right] \tag{5.39}$$

$$v = \frac{K_I}{2\mu}\sqrt{\frac{r}{2\pi}}\sin\left(\frac{\theta}{2}\right)\left[\kappa - 1 + 2\cos^2\left(\frac{\theta}{2}\right)\right] \tag{5.40}$$

where, $\kappa = 3 - 4\nu$ for plane strain, $\kappa = \frac{(3-\nu)}{(1+\nu)}$ for plane stress

Also, linear superposition can be used for mixed mode problems giving Eq. 5.41.

$$\sigma_{ij}^{(Total)} = \sigma_{ij}^{(I)} + \sigma_{ij}^{(II)} + \sigma_{ij}^{(III)} \tag{5.41}$$

Two parameters have been discussed that can be used to characterise crack tip behaviour for linear elastic materials namely the energy release rate, *G*, and the stress intensity factor, *K*. These two parameters can be related for a through crack in an infinite plate experiencing a uniform tensile stress by:

$$G = \frac{K_I^2}{E'} \tag{5.42}$$

where: $E' = E$ for plane stress or $E' = \frac{E}{(1-\upsilon^2)}$ for plane strain

Irwin's [267] model of crack tip plasticity is derived for a state of plane stress. Plane stress assumes that the stress acts on a thin plate whereas plane strain is present in thick cylinders or components. Both of these conditions cause different plastic zone shapes at the crack tip which are derived from yield criteria such as the von Mises or the Tresca yield criterion. Substituting the yield stress, σ_{YS}, for σ_Y in $\sigma_Y = \frac{K_I}{\sqrt{2\pi r}}$ along the r-axis when θ = 0 gives an estimate of the distance r_y of the plastic zone size assuming a circular plastic zone. However, this is inaccurate for plane strain as yielding will occur at a much higher stress than the yield stress as the plastic

zone size will be smaller. When defining the plastic zones for plane stress and plane strain, the calculation for r_y is over the range $-\pi \leq \theta \leq +\pi$. This is shown in Fig. 5.9 for θ=0.

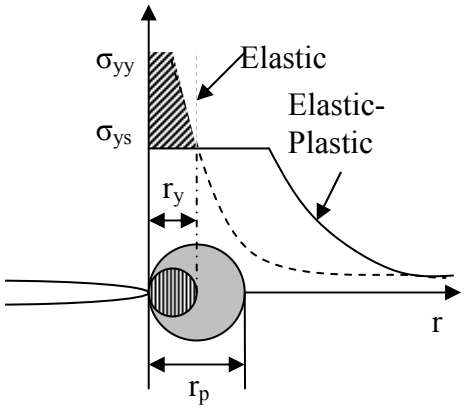

Fig. 5.9: Plastic zones in plane stress and plane strain for θ=0.

5.2.3.2 2D debond model creation

The 2D symmetric half model was developed as shown in Fig. 5.10, with the nodes on the line of symmetry considered to be the theoretical crack propagating from the cut initiation site at the tip of the cutting blade through the material. The nodes on the symmetry line are tied, using contact conditions, to an analytical rigid line but are allowed to translate in the y-direction. The failure mechanism originates from the theory from Irwin's model of crack tip plasticity. The translational and oscillatory movement of the blade into the material causes the critical stress condition to be reached at the pre-specified distance ahead of the crack tip, causing the tied node to debond from the analytical rigid line, releasing the constraints on the node and allowing it to move in any degree of freedom, simulating crack propagation and ultrasonic cutting. The critical failure stress and its location ahead of the crack tip, distance r at $\theta = 0$, for a particular material are determined from Single Edge Notch Bend (SENB) FE models using the average curve fitted material data developed from experimental tests. The model requires that the blade initially resides within the tip of the theoretical crack to allow the sharp edges of the blade to push against the walls of the crack and generate a stress normal to the crack flanks. Plane strain is assumed to represent the material and blade in the through thickness direction. The specimen is simulated to translate at either a constant velocity, set distance or applied force into the oscillating blade at a set ultrasonic amplitude between 0 and 100 μm and frequency between 20 and 100 kHz. Temperature can be determined during the analysis if required at any location in the model but for validation purposes usually at locations remote from the cut line as depicted in Fig. 5.10 where thermocouple measurements can be compared in experimental tests.

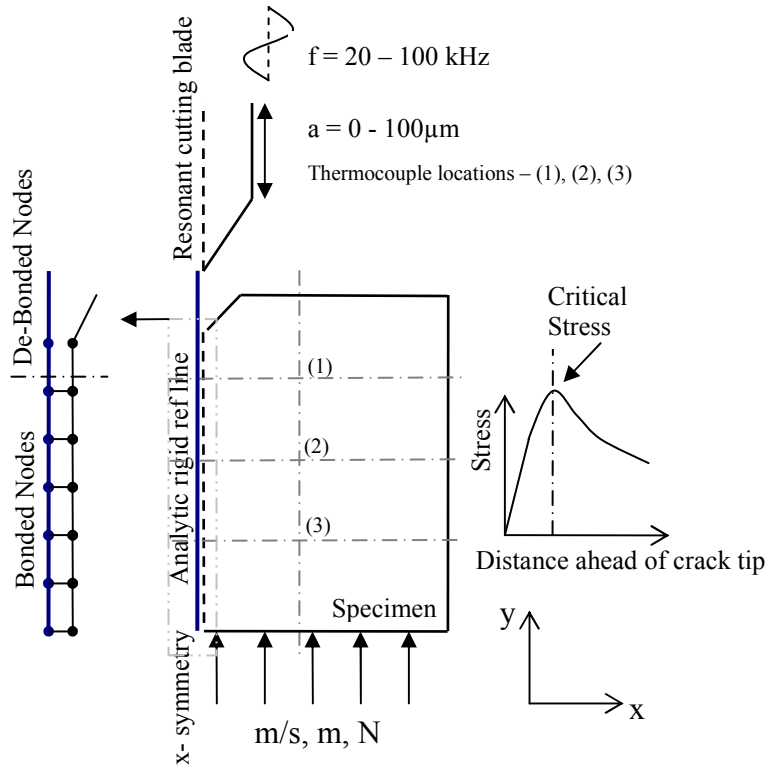

Fig. 5.10: Schematic diagram of the 2D Debond model of ultrasonic cutting.

5.2.3.2.1 2D SENB tests

Single edge notch bend tests (SENB) are used to characterise failure using a fracture mechanics approach to determine useful engineering properties, such as energy release rate, stress intensity factor and J-integral, that can be used to predict the safe loading of a component. In this study, SENB tests are primarily used to find the critical stress and its distance ahead of the crack tip, r at $\theta = 0$, to input into the debond model as a failure criterion for ultrasonic cutting. Experimental SENB tests are used to validate the FE model. The experimental force and displacement data for each material tested is useful to input as boundary conditions in the SENB FE model and using the model the failure stress at a distance ahead of the crack tip can be determined for each material using Irwin's crack tip plasticity model and used as an input into the debond modelling approach of ultrasonic cutting.

5.2.3.2.2 SENB testing technique

SENB tests, or more commonly three point bend tests, are used to determine fracture toughness of many materials and have a simple testing configuration [200, 203] compared with the more common four point bend test. The four point bend test is usually preferred due to the application of a bending moment being produced across the additional two supports opposed to the three

point bending arrangement that has a maximum bending moment directly in the centre of the specimen. However, due to the specimens of cheese sagging under their own weight, small specimens were used to minimise this problem and also to minimise handling difficulties of the specimen during experimental set up. So the three point bend option was chosen for this study. Specimens of cheese of dimensions 92 x 20 x 10 mm were tested to failure on a Lloyds testing machine for an $\frac{a}{w}$ ratio of 0.5 as shown in Fig. 5.11 (a) where loading is applied directly on the centre of the specimen exactly half way between the roller supports by a cylindrical indenter. Force-displacement data was recorded for each material and the data was used to benchmark the 2D SENB FE model by comparing the experimental data to the FE predictions.

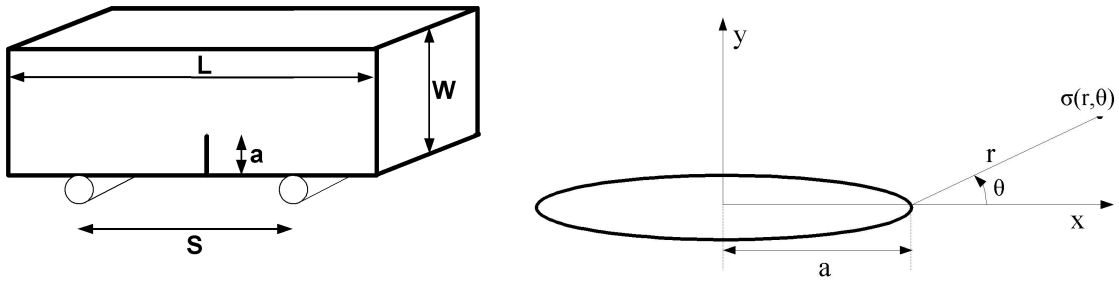

(a) (b)

Fig. 5.11: (a) Schematic of SENB specimen and (b) Irwin's crack propagation diagram defining direction of crack extension.

A 2D SENB FE model was developed using the mechanical properties from tension tests to evaluate the critical failure stress and its distance ahead of the crack tip as shown in Fig. 5.10. The critical stress and its location ahead of the crack tip were found by plotting the normal stress, σ_{22}, along r at $\theta = 0$ in the FE SENB simulation [255]. The FE results for force on the indenter against displacement of the indenter were validated against experimental SENB tests to confirm the material definition. Fig. 5.12 (a) illustrates the 2D FE SENB test, where symmetry is utilised about the crack flank in the plane of the 1 axis with boundary conditions imposed on the ligament of the specimen preventing movement in the 2 direction. The indenter and support are modelled as analytical rigid surfaces and the specimen as a deformable body. The indenter is prescribed a fixed displacement of 10 mm in the -1 direction. The deformation of the specimen after the analysis is complete is shown in Fig. 5.12 (b). An exploded view of (b) is represented in Fig. 5.12 (c) to illustrate the partitioning technique used to ensure an organised structured continuum and also highlight the density of the mesh surrounding the crack tip, which is modelled as a small root notch. Fig. 5.12 (c) also depicts the shape of the plastic zone

surrounding the crack tip and illustrates the maximum stress zones directly in front of the crack tip which are more defined in the exploded view in Fig. 5.12(d).

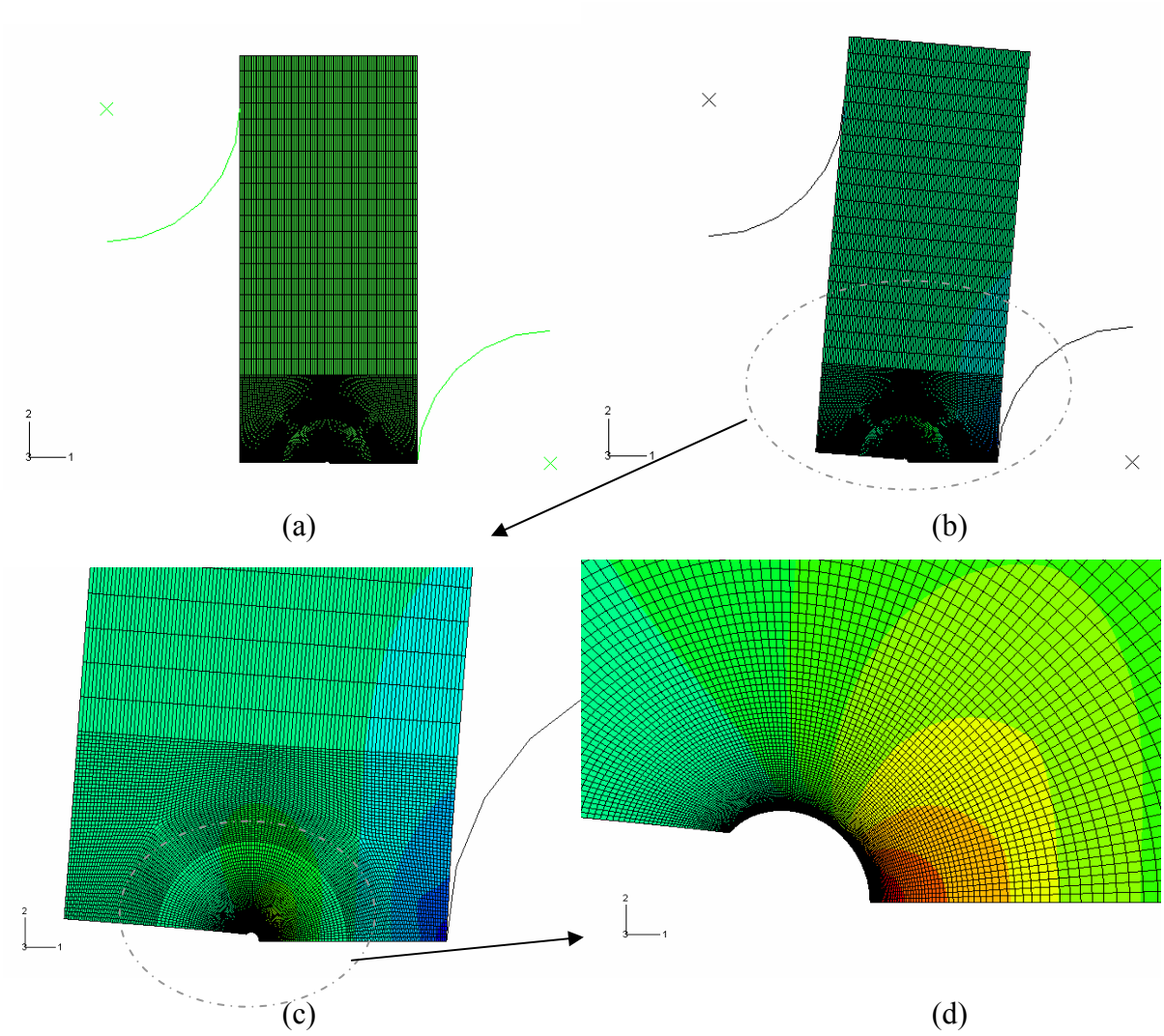

Fig. 5.12: 2D SENB FE models (a) undeformed (b) deformed illustrating contours of stress in 2 direction, σ_{22}, (c) and (d) exploded views of the crack tip also illustrating stress in 2 direction σ_{22}.

5.2.3.2.3 SENB testing results

Experimental SENB tests were conducted on cheese specimens at a crosshead velocity of 5 mm/min and at a temperature of 20 °C. Fig. 5.13 (a) shows the resulting force displacement data and depicts the variation in experimental results for cheese tests. An average experimental curve is also included in the diagram from the experimental data for comparison with the FE model due to the large amount of variation in the measured reaction force. This variation arises from the batch dependency of the material, the porous nature of the material and surfaces flaws from cutting the material. From the experimental tests it was noticed that crack propagation occurred in the experiments after approximately 1mm indentation by the indenter. As the FE model of the

SENB test doesn't consider crack propagation it was assumed that the stress produced in the specimen after 1mm displacement would cause crack propagation. Fig. 5.13 (b) shows a comparison of the average experimental reaction force with the FE predictions using both the elastic plastic and the hyperelastic material model. From the graph it is noticeable that the experimental force produced is considerably lower than the FE predictions for both the elastic-plastic and the hyperelastic material representation. This could be because of the very soft ductile nature of the cheese where the self weight of the specimen causes deformation and small crack propagation when simply sitting in the machine which isn't included in the FE model of the SENB test. Inaccuracies also occur in the experiments when preparing the specimens for testing in the machine. The accuracy of the dimensions of the specimen due to the technique of cutting with a scalpel, the cut depth created by the scalpel blade and also the handling of the specimens prior to implementation in the machine all could cause slight variations in the experimental force during testing. For FE modelling purposes at this stage to predict the critical stress at a predefined distance ahead of the crack tip for inclusion in the FE debond model the SENB simulation was considered to be sufficient to predict a preliminary critical failure stress and its corresponding distance ahead of the crack tip.

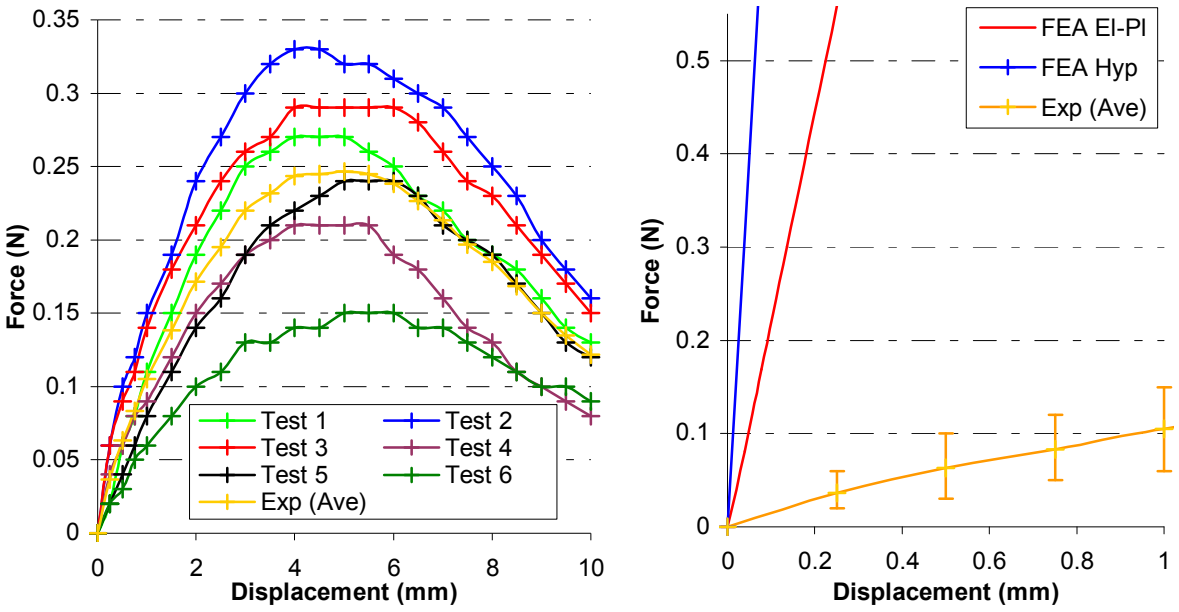

(a) (b)

Fig. 5.13: (a) Experimental and (b) FE results of SENB tests of cheese at 20 °C and at a crosshead velocity of 5 mm/min modelled as a hyperelastic and an elastic plastic material.

FE simulations of the SENB test where the specimen of cheese was represented as a hyperelastic and an elastic-plastic material were analysed to determine a failure stress at a pre-specified

distance ahead of the crack tip. This data will then be used as a failure criterion for use in the debond modelling technique for cheese where the material can be represented as either a hyperelastic or elastic-plastic model. The hyperelastic model in ABAQUS assumes a totally elastic solution which means that the critical stress is located at the tip of the notch in the SENB specimen at distance r = 0 as shown in Fig. 5.14. However, the elastic-plastic representation results in a critical stress located at a distance ahead of the crack tip, as can be seen at the peak value in Fig. 5.14 at a distance of 35 μm. Data from both the hyperelastic and elastic-plastic representations are shown in Fig. 5.14 for an indenter displacement of 1 mm. These representations correspond in the far field but as r approaches the crack tip the stress values for the hyperelastic representation and elastic-plastic representation deviate. The stress failure criterion for the elastic-plastic material representation was used in the FE cutting models for the debond criteria. The material model used, however, was hyperelastic as this provided a more accurate fit of both the compression and tension data. It is believed that this provides a more accurate representation of cheese because the experimentally derived stress-strain relationship in tension and compression are very distinct, showing that cheese is able to withstand larger stresses in compression.

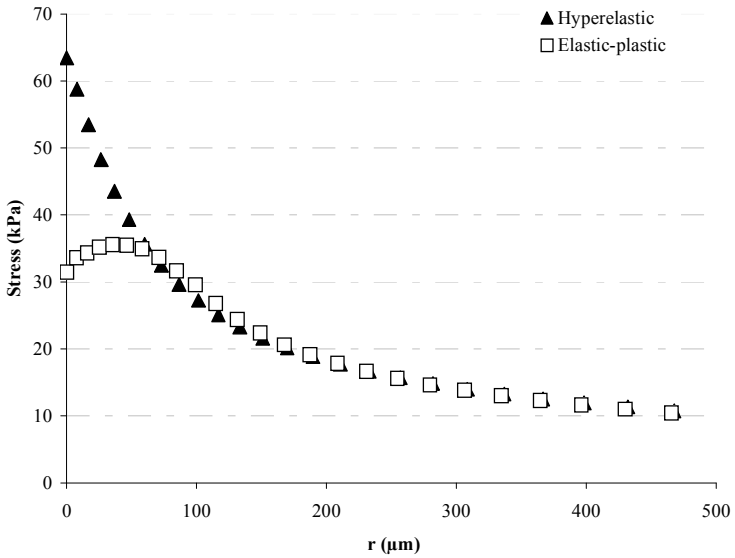

Fig. 5.14: FE SENB test result for cheese at 24 °C and at a crosshead velocity of 5mm/min using both elastic-plastic and hyperelastic curve fitting representations.

5.2.3.3 Preliminary simulation of 2D debond model

In this study, FE models of ultrasonic cutting for a single and multi-layer food product are developed. Mild cheddar cheese was chosen for the study and was represented in the FE model

using the reduced polynomial curve fitting representation of order 3 for a hyperelastic material as shown in Fig. 4.19 in Chapter 4 of this thesis. Initially a single layer finite element model was created, based on the assumption that the ultrasonic blade causes a crack to propagate in a controlled mode I opening using the debond technique where the failure criterion used is determined from three point bend fracture tests on mild cheddar cheese. Subsequently, the finite element model was developed to represent ultrasonic cutting of a multi-layered material. The multi–layer model is designed to allow incorporation of a variety of different materials representative of a multi-layer food product. The model incorporates an estimation of the friction condition between the cutting blade and the material to be cut and allows adjustment of the frequency, cutting amplitude and cutting speed.

5.2.3.3.1 Single layer material cutting model

A single layer material ultrasonic cutting model was initially developed in ABAQUS for ultrasonic cutting of mild cheddar cheese. Mild cheddar cheese was chosen due to its soft viscoelastic nature, availability and well documented material studies [191-207]. A schematic of a 3-layer cutting model was shown in Fig. 5.10(a), being a single layer model when materials 1, 2 and 3 are the same. Cutting is characterised using a 2D mode I crack opening condition using the debond modelling approach. For the preliminary model discussed in this study, the FE analysis is a simpler static stress analysis neglecting the temperature effects at the cutting interface to improve computational efficiency and allow faster convergence times. The ultrasonic cutting blade was modelled as an analytical rigid surface that oscillated at 20 kHz with a peak-peak amplitude of 100 μm, representative of a typical ultrasonic cutting blade. In this example, the material is fed into the blade at a constant velocity to a depth of 3 mm and the blade oscillates around a fixed position. A typical result showing stress contours around the debonded crack tip within a single layer specimen is depicted in Fig. 5.15.

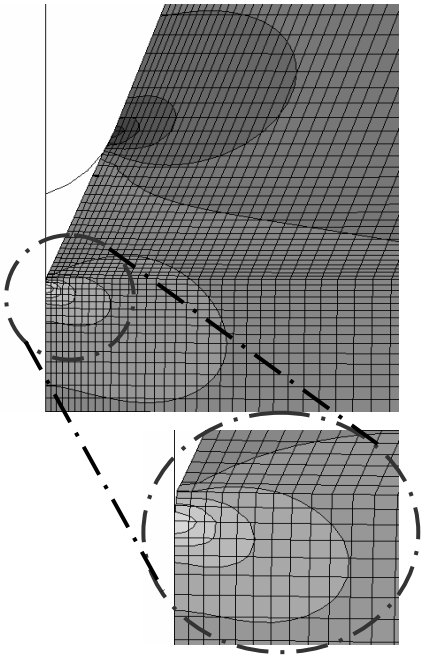

Fig. 5.15: Crack propagation in a 2D FE single material layer debond ultrasonic cutting model.

The effects of varying the blade tip amplitude and frequency were investigated. Fig. 5.16 (a) shows that increasing blade tip amplitude resulted in an increase in the peak-peak oscillating force as indicated by the dashed lines with the mean force, the solid line, staying the same. This result suggests that a higher cutting force could be achieved with a higher blade tip vibration amplitude. A blade with an ultrasonic amplitude of 50 μm was modelled at 35 kHz and 17.5 kHz and the operating frequency was found to have a negligible effect on the oscillating force as shown in Fig. 5.16(b). Both figures show an initial peak in the force before the first node debonds, termed crack initiation as shown in Fig. 5.16, and steady-state cutting occurs subsequently, at the small downturn in cutting force. These preliminary results from a single layer FE cutting model are consistent with experimental findings [89, 110].

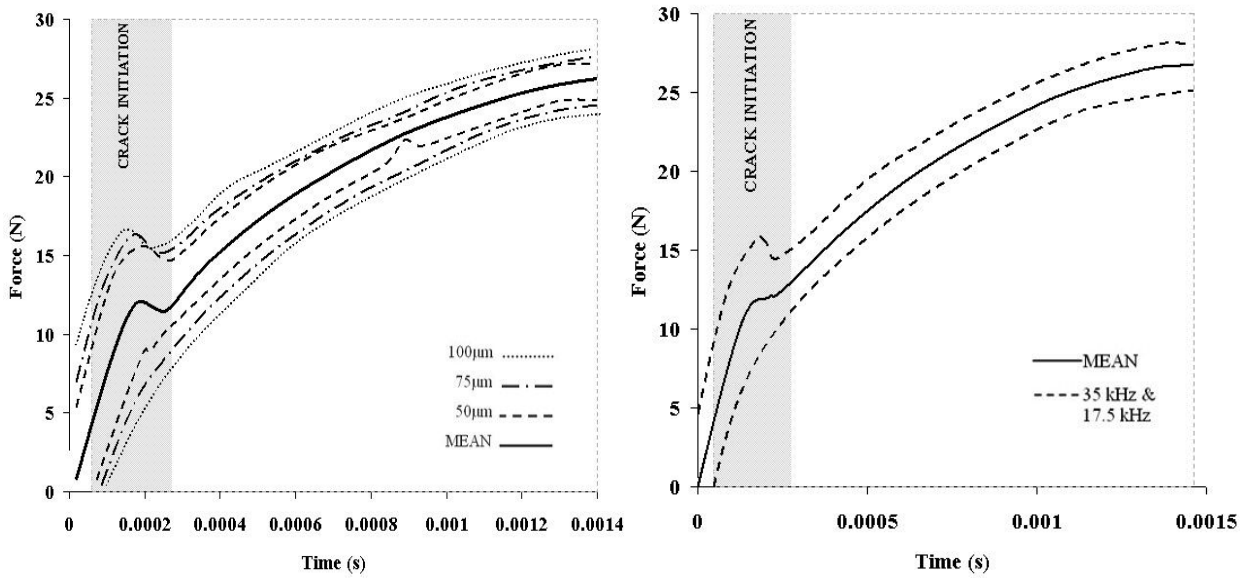

(a) (b)

Fig. 5.16: FE predicted reaction force on the cutting blade for (a) a range of blade tip vibration amplitudes at 35 kHz, showing the paths of maximum, minimum and mean force oscillations and (b) for a fixed blade tip vibration amplitude of 50 µm for two different operating frequencies, showing the paths of maximum, minimum and mean force oscillations.

5.2.3.3.2 Multi-layer material cutting model

Most food products have an architecture that combines very different materials, all with different properties. If the blade ultrasonic amplitude and blade geometry has been chosen solely for cutting one material, it may be ineffective in cutting others. The use of an FE model that predicts the cutting parameter requirements for the different materials, improves the effectiveness and design of ultrasonic cutting devices.

A multi-layer material cutting model has been proposed which adopts the same failure conditions as the single layer model. A schematic of the model is shown in Fig. 5.10. The functionality of the model is exactly as described for the single layer model, however the material has been partitioned into three material layers. Each material is separately tied to the reference analytical rigid surface and has been characterised by its mechanical properties, critical stress, coefficient of friction and pre-defined distance ahead of the crack tip.

5.2.3.3.3 Discussion

The single and multi-layered 2D models are good representations of ultrasonic cutting but rely on some critical assumptions. Temperatures that are experienced during ultrasonic cutting,

including conduction from the blade due to frictional heating at cutting interfaces and a thermal response due to ultrasonic wave propagation, are not incorporated in the model. These temperatures will influence the rate of crack propagation and the response of the material. Thermal influences will be incorporated into a coupled thermal-mechanical model. Current models also assume that specimens are pre-notched and that, after crack initiation, steady-state cutting prevails. Specimens used in typical ultrasonic cutting procedures are not pre-notched. The conditions prior to cut initiation and the mechanisms for cut initiation need to be further investigated and understood to enable cutting models to be created for specimens that are not pre-notched. The ultrasonic cutting model presented is a valuable tool that can be used to extract trends associated with blade parameters and material configurations.

5.2.3.3.4 Summary

Single layer and multi-layer material ultrasonic cutting models were developed using ABAQUS FE software using the debond modelling approach. Test materials of mild cheddar cheese have been used in FE models of ultrasonic cutting due to their availability and diversity. The material properties have been found previously using conventional material testing methods and values for critical stress and distance ahead of the crack tip have been determined from FE benchmark SENB models. The models could be used to adjust the cutting parameters, such as frequency and blade tip amplitude, to predict the excitation force or cutting speed required to cut effectively through different material layers. The validity of the models relies critically on an accurate assessment of the friction condition at the blade-material interface and accurate material models.

This initial modelling technique does not address thermal issues present during ultrasonic cutting and assumes specimens are pre-notched. Further investigations will be made to develop a coupled thermal-mechanical model to incorporate temperature effects in ultrasonic cutting. The FE models have proved to be effective in the control of cutting parameters and offer the possibility to have an insight into how blade design influences the cut of a variety of materials.

5.2.4 2D element erosion model

Element erosion is an alternative method used to define material failure within ABAQUS [252]. The model utilises the shear failure option for each stress-strain curve at every test temperature and strain rate defined in the model by the user using the elastic-plastic material representation discussed previously. ABAQUS defines the shear failure of the material as a number between 0

and 1 at each temperature and strain rate. 0 defines the stress at the yield point or where plastic strain is 0 and 1 is the stress at maximum plastic strain defined by the user in the stress-strain curve in the material representation. When the equivalent plastic strain in the material reaches the predetermined shear failure value, usually at the break point of the material, the element is eroded, which simply means that the material properties ramp down to 0. The eroded elements still remain in the model but do not participate in the analysis as they have no material properties. The adaptive mesh option is also used automatically in the element erosion model to allow the nodal coordinates of highly deformed elements that have not yet eroded, to be automatically adjusted to ensure the model remains within convergence limits until the analysis has ended or the element has been eroded from the analysis. The 2D model is represented in Fig. 5.17 with the blade and the nodes on the line of symmetry constrained from movement in the x-direction. The element erosion failure method removes the need to pre-notch specimens and removes the need to conduct FE analyses of SENB tests in order to determine the failure characteristics of the material. The ultrasonic blade simply destroys the elements within its path as it translates through the material. The element erosion method can also be used to represent the failure of material in 3D and opens up further opportunities to explore different cutting orientations, and non-symmetrical cutting tips or specimens.

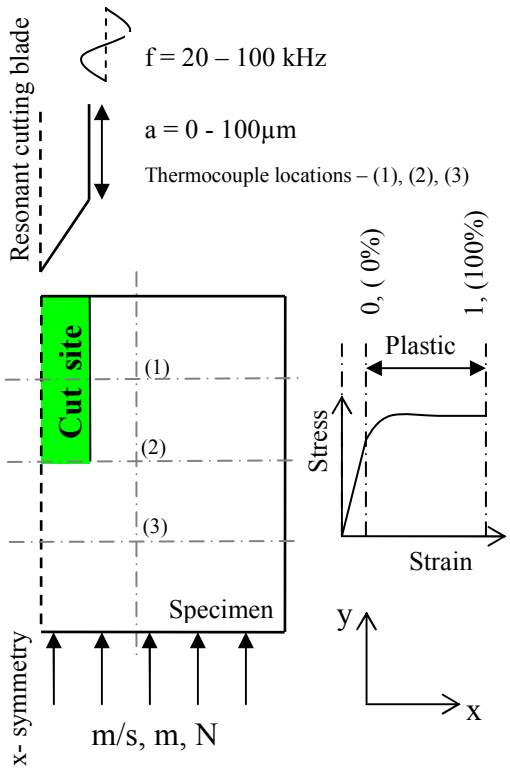

Fig. 5.17: Schematic diagram of the 2D element erosion model of ultrasonic cutting.

5.2.5 Preliminary simulation of 2D element erosion model

This study simulates ultrasonic cutting in a guillotine configuration, using the generic 2D fully coupled thermal-stress element erosion model. To demonstrate this model, the study concentrates on an analysis of ultrasonic cutting of toffee, which is sticky, brittle, highly temperature dependant and difficult to cut. In particular, the effects of ultrasonic frequency and amplitude on the temperature at the cut interface are evaluated.

5.2.5.1 FE modelling of ultrasonic cutting of toffee using the element erosion model

The element erosion model was used in this study to model ultrasonic cutting of toffee using a titanium blade. An investigation into the effect of the blade ultrasonic frequency and amplitude on the cutting temperature was explored for blade frequencies of 20, 35 and 55 kHz and ultrasonic amplitudes of 0, 25, 50 and 75 μm in the fully coupled thermal-stress element erosion model.

5.2.5.2 Material properties

For this study the material of the cutting blade was titanium $Ti_{90}Al_6V_4$ and the food material being cut was toffee. Representing materials in finite element analysis requires a description of their mechanical and thermal properties in a material model and ABAQUS has various models available to characterise material behaviour from experimental data [252]. This study represented titanium using an elastic material definition from information available in the literature [256]. The material properties used for titanium were Young's modulus, Poisson's ratio and density and were documented as 114 GPa, 0.3 and 4425 kg/m^3 respectively and assumed to be constant at temperatures between 20 and 250 °C. Toffee was represented as an elastic-plastic material model using average temperature dependent and strain-rate dependent stress-strain curves derived from experimental tension test data as documented in Chapter 4 of this thesis. Averaged and curve fitted data derived from the experimental tensile tests provided the input data for the material characterisation in the FE model at temperatures of 20, 25, 30 and 35 °C and at crosshead velocities of 5, 15, 25 mm/min. These stress-strain curves are shown in Fig. 5.18. The elastic region was defined in the FE model using the mechanical properties of Young's modulus and Poisson's ratio, which was assumed to be 0.49 and is common for most food materials, at each corresponding temperature. The density of toffee was also included for use in the analysis and was found to be 1411 kg/m^3. The plastic region was included as a curve of true

stress against corresponding plastic strain from the yield point to the ultimate tensile strength using a simple power law curve fit.

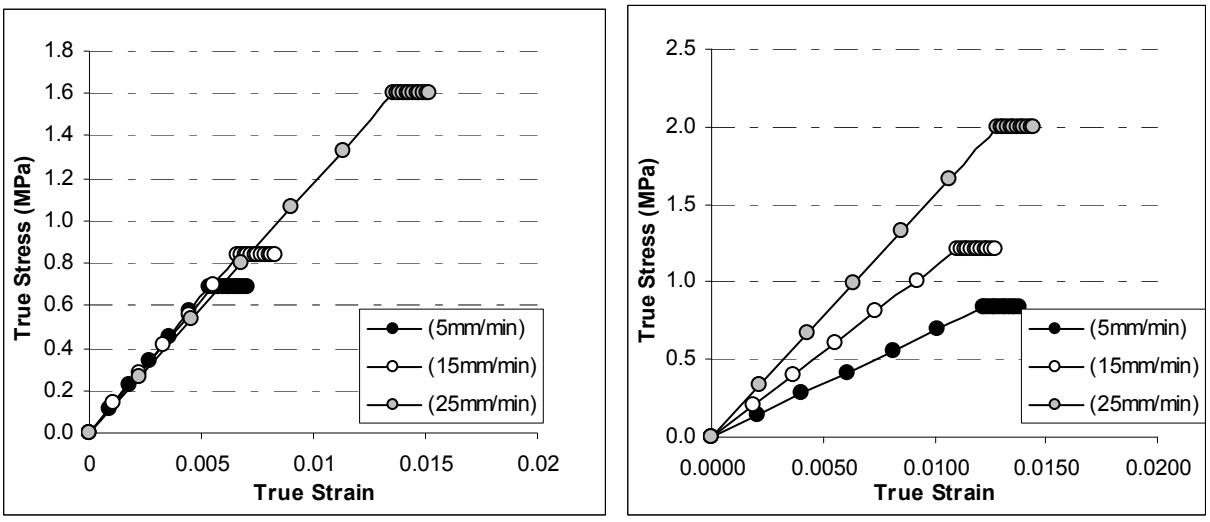

(a) (b)

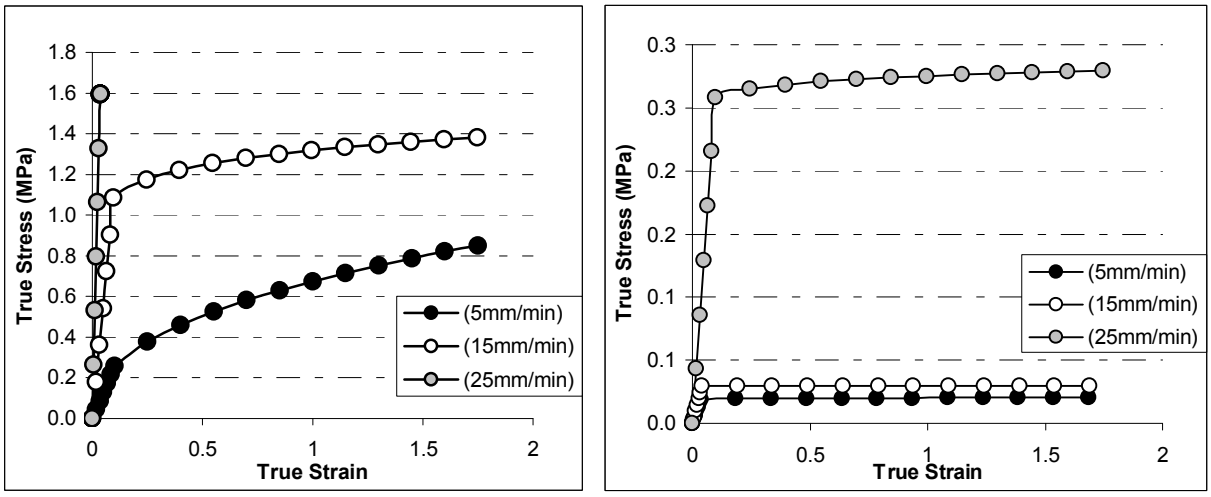

(c) (d)

Fig. 5.18: Stress-strain curves for toffee with crosshead velocities of 5, 15, 25 mm/min in tension at temperatures of (a) 20 °C (b) 25 °C (c) 30 °C (d) 35 °C.

The material model also includes characterisation of the thermal properties of titanium and toffee that are essential for fully capturing the material behaviour during ultrasonic cutting. The specific heat and thermal conductivity for toffee and titanium used in the material definitions in this study were 1.948 kJ/kg°C, 0.0964 W/m°C and 598 kJ/kg°C, 6.6 W/m°C respectively and both specific heat and thermal conductivity were assumed to be constant for both materials in the model.

5.2.5.3 Estimating friction condition

Friction is the driving mechanism in determining the heat generation at the interface between the ultrasonically excited titanium blade and the toffee, and is extremely important in defining the interface contact condition. In this study the friction at the interface between the resonant blade and the material to be cut was included from experimental friction tests as documented in an earlier section of this Chapter. The dynamic coefficient of friction determined from the experimental tests of 0.116 was used in the Coulombic friction definition to define contact between the titanium blade and the toffee. Heat generation due to friction at the interface of the ultrasonically excited blade and the toffee was also incorporated in the model by assuming that 50 % of the heat was passed into the blade and 50 % into the toffee.

5.2.5.4 Estimating cut surface temperature from FE element erosion model

Heat is generated locally at the cut site due to friction created by the oscillatory movement of the cutting blade. This can either benefit or adversely affect the food material being cut. High temperature causes many food materials to melt and this can either give the product an appealing texture and surface finish or can produce an undesirable re-solidified surface. High temperature can also result in local caramelisation of the cut surface, with an unacceptable taste, or can even cause the surface to burn. The temperature at the cut site is extremely difficult to measure during ultrasonic cutting as sensors can only be placed at a remote location i.e. to prevent them from being damaged. FE models of ultrasonic cutting, allow specific locations in the model to be probed to extract temperature data. Hence the FE model can be validated by probing the temperature data at sensor locations in the ultrasonic cutting experiments. The validated model can then allow predictions of the actual cut site temperature. The model can also be used to conduct a parametric study to investigate how cut site temperature is affected by ultrasonic and cutting parameters. The model can also be used to investigate different blade profiles and hence can be used in blade design. The validity of the model, and hence the ability to extract meaningful data from it relies on the description of the food material being accurate, the contact description being accurate, and the model material failure being accurate.

As an example, Fig. 5.19 plots the temperature predicted from the element erosion model at the tip of the ultrasonic cutting blade for (a) four different blade tip amplitudes, 0, 25, 50 and 75 μm and (b) three different ultrasonic frequencies, 20, 35 and 55 kHz. The blade translates in the model at a constant speed of 10 mm/s to a constant depth of 10 mm. Fig. 5.19 illustrates that as the ultrasonic amplitude or ultrasonic frequency of the blade increases the localised temperature

at the tip of the blade increases, which is consistent with previous experimental studies of ultrasonic cutting in a variety of different materials [110].

This method provides a modelling approach that can be used to correlate temperature and stress estimates with experimental data. The modelling technique is not limited to single layer material models, or to elastic or elastic-plastic models, but can incorporate complex multi-layered materials defined using any realistic material model representation of food materials such as hypoelasticity, hyperelasticity or anisotropy. The model can also accommodate complex blade tip geometries.

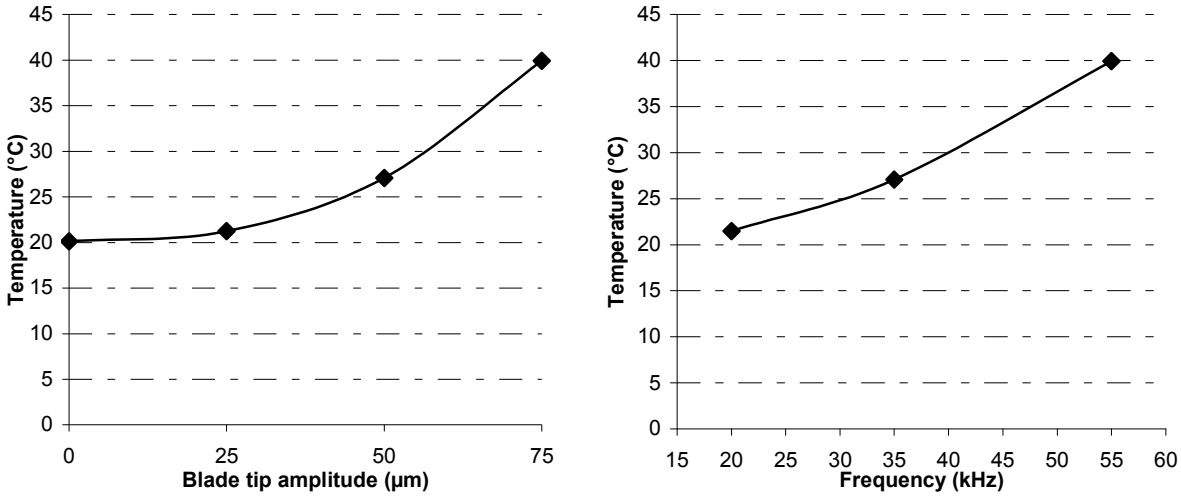

(a) (b)

Fig. 5.19: Effect of blade tip (a) amplitude and (b) frequency on the temperature at the blade tip using the element erosion FE model.

5.2.5.5 Summary

This investigation has presented an approach for representing ultrasonic cutting in the guillotine configuration using the generic 2D fully coupled thermal stress element erosion finite element model created in the finite element package ABAQUS. The modelling approach uses the element erosion option in ABAQUS explicit which removes elements during the solution when the shear criterion in the cut material is reached. The element erosion model considers the thermal issues associated with ultrasonic cutting at the blade-material interface and consider frictional heat generation and propagation through both materials due to conduction.

A study of ultrasonic cutting in the guillotine configuration of the food material toffee was conducted using the 2D element erosion model. The model illustrated how temperature at the cut site could be extracted for a range of different ultrasonic amplitudes and frequencies. Mechanical and thermal properties of toffee were included in the model from experimental mechanical and thermal tests using standard testing methods to fully characterise the food material's behaviour during cutting. The contact condition at the interface between the ultrasonically excited blade and the toffee was modelled as a Coulombic friction condition using friction data derived from experiments and this allowed heat generation at the interface between the toffee and the resonant titanium blade to be incorporated. Preliminary results from the element erosion model found that as ultrasonic frequency or amplitude of the blade was increased the temperature at the blade tip increased, agreeing with experimental findings

5.2.6 Comparison between the 2D debond and the element erosion model.

Toffee has been selected as the food material for this study because it is sticky, highly temperature dependent and often difficult to cut. Temperature dependent stress-strain data from uniaxial tensile tests on toffee were included in the FE models to characterise the material behaviour from the data in Chapter 4 of this thesis. A Coulomb friction condition at the blade-material interface is estimated from experiments, which study the change in the friction coefficient due to ultrasonic excitation of a surface, made from the same material as the blade, in contact with a specimen of toffee. A model of heat generation at the blade-toffee interface is also included to characterise contact during ultrasonic cutting. The failure criterion for the debond model assumes crack propagation will occur when the stress normal to the crack surface reaches the tensile failure stress of toffee and the element erosion model uses a shear failure criterion to initiate element removal.

5.2.6.1 Material model

Toffee was modelled as a temperature dependent elastic-plastic material by including four averaged stress-strain curves at temperatures of 20, 25, 30 and 35 °C at the lowest crosshead velocity of 5 mm/min from the data in Chapter 4. For each stress-strain curve, values for the Young's modulus and yield stress were included to define the elastic region and then a power law curve was used to smooth the plastic region.

To allow the material data to be accepted by ABAQUS, certain criteria have to be met to allow the program to interpolate between each of the temperature dependent curves. All plastic regions must have the same number of data points and be spread over approximately the same range of plastic strain [252]. This poses a problem, because toffee at 20 and 25 °C exhibits brittle behaviour with almost no plasticity whereas toffee at 30 and 35 °C exhibits high plasticity. This means that the plastic strain ranges from 0 to approximately 1.4, which is a very large range for ABAQUS to interpolate over. To overcome this problem, two dummy plastic curves were generated for toffee at 20 and 25 °C using a power law curve fit to a plastic strain of 1. These curves, along with the other two for toffee at 30 and 35 °C were then included in the FE models. Both dummy plastic regions were included only to allow the material data to be accepted in the FE program and were ignored in the analysis. This was achieved by setting the critical stress for temperatures of 20 and 25 °C to be equal to the yield stress in the debond model, and by setting the shear failure in the element erosion model to an infinitely small value close to 0. For both models this represents where the break load occurs in the experimental tensile test. The curve fitted data included in both FE models is shown for each temperature in Fig. 5.20.

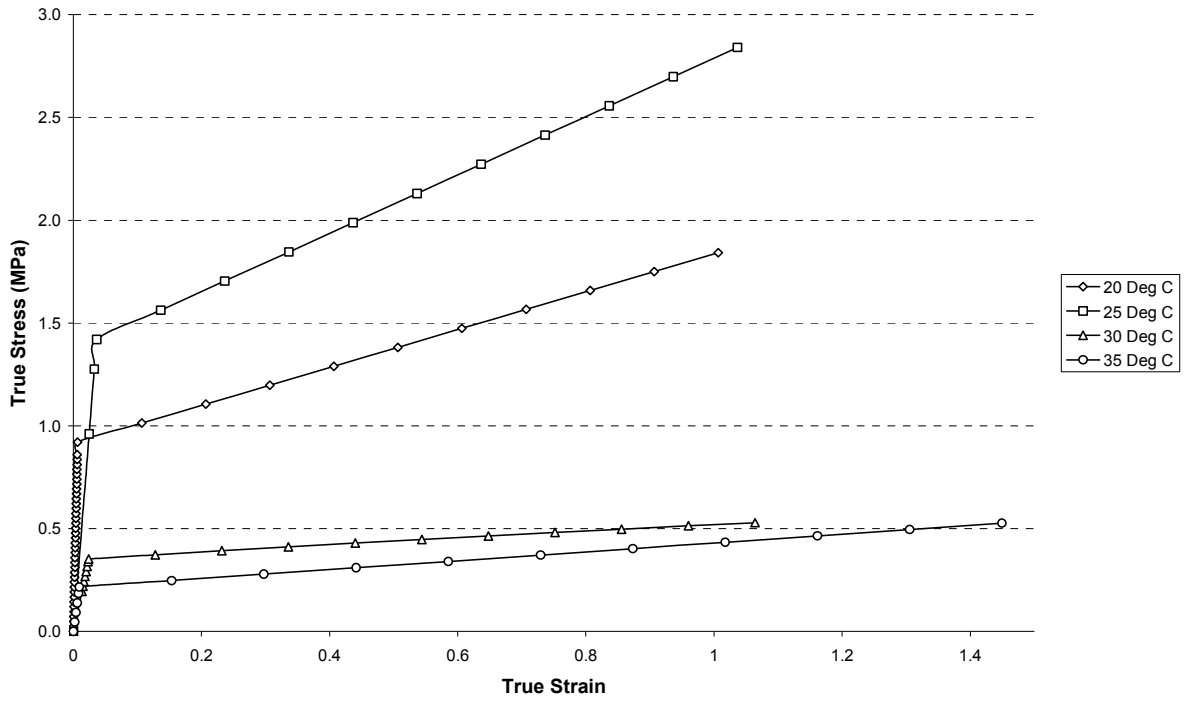

Fig. 5.20: Tension test data for toffee at 20, 25, 30 and 35 °C for inclusion in FE model.

5.2.6.2 Coupled thermal-stress models

A fully coupled thermal-stress analysis using the implicit and explicit solver in the finite element package ABAQUS was performed which allowed the influence of temperature generated by

friction at the blade-material interface to be accounted for in the modelling procedure. Two 2D FE models were developed to represent ultrasonic cutting. Both models utilised the symmetry condition about the cutting plane to enable cutting to be represented as a half model for computational efficiency.

The titanium blade was modelled as an elastic deformable body with the following material properties: Young's Modulus 114 GPa, density 4425 kg/m^3, Poisson's ratio 0.31, specific heat 586 J/Kg°C, coefficient of thermal expansion 9.0E-06 μm/m°C, and thermal conductivity 6.6 W/mK. Toffee was modelled as a temperature dependent elastic-plastic material as shown in Fig. 5.20. The initial temperature of the blade and the specimen in the model was 20 °C. The specific heat, coefficient of thermal expansion and thermal conductance of toffee is included to fully define fully the thermo-mechanical properties of the material and are documented in Chapter 4 of this thesis. A coefficient of friction of 0.032 is included from the experimental tests to define the contact condition at the interface between the blade and material. The frictional heat generation option is also used which converts all energy produced by the frictional contact into heat and distributes the heat generated due to friction at the interface equally into the blade and toffee due to conductance. A film condition is included on the blade and specimen surface representative of a heat sink to allow heat to be removed from the surfaces due to convection during cutting.

The ultrasonic blade frequency was 35 kHz and the blade tip amplitude was 50 μm. The toffee was moved into the blade at a constant velocity of 10mm/s to a constant depth of 10mm in the material.

5.2.6.3 Coupled thermal-stress debond model

The debond model simulates ultrasonic cutting as a fracture mechanics problem in mode I where a crack propagates when a critical normal stress is reached at a pre-specified distance ahead of the crack tip. A 2D half model with a defined crack tip and propagation direction was created, where the nodes defining the theoretical crack were tied to an analytical rigid reference surface using contact conditions. When the blade moves into the material, and the critical stress ahead of the theoretical crack tip is reached, the nodes debond and the crack propagates, simulating cutting. The mesh for this 2D model illustrating nodal temperature, during cutting, is shown in Fig. 5.21 (a).

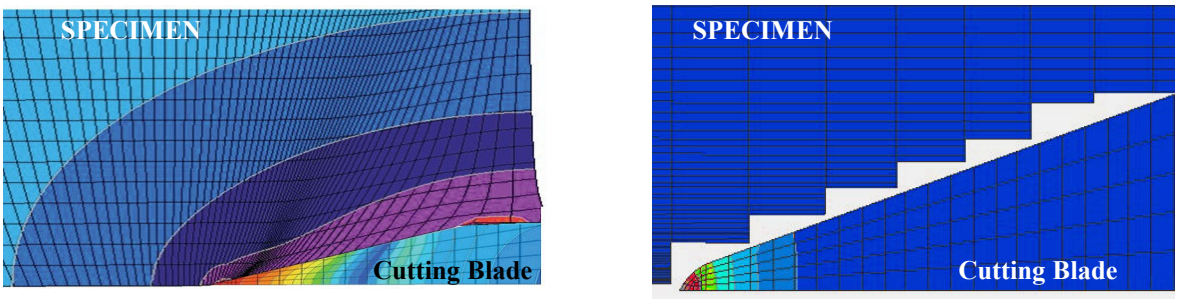

(a) (b)

Fig. 5.21: Mesh and contour plot of temperature for (a) debond model, (b) element erosion model, during ultrasonic cutting

5.2.6.4 Coupled thermal-stress element erosion model

An alternative 2D half model of ultrasonic cutting was developed in ABAQUS using the element erosion option to define failure within the material. The model used a shear failure criterion at each temperature, which corresponds to the break point at each temperature on the stress-strain curves to define the material failure condition. Due to the high deformation of the elements within the model at the blade-toffee interface, the adaptive mesh option is used which automatically adjusts the nodal coordinates of highly deformed elements ensuring they remain within convergence limits until the failure criterion is met and the element is eroded from the solution. The mesh for this 2D model illustrating nodal temperature, during cutting, is shown in Fig. 5.21 (b).

5.2.6.5 Discussion

Temperature at the cut site is difficult to measure as sensors are easily damaged by the blades during cutting. Previous experiments conducted by the author have measured temperature at various locations in a specimen and as close as 1 mm from the cut site. It is hoped that, by validating the FE models against the temperature measurement data, the models could be used to predict temperature at the actual cut site. These findings are important for customising blade designs to specific food materials, because temperature effects can be significant in the cutting process.

Fig. 5.22 plots temperature-time curves predicted from the debond FE model at a location in the toffee specimen, at a depth of 1 mm away from the cutting plane of the blade tip along the line of

cut. The FE model allows an evaluation of the effects of varying the ultrasonic cutting parameters on the temperature during cutting. For example, Fig. 5.22 shows the relationship between cutting speed and temperature in a toffee specimen. The model is run for four different feed rates with a constant depth of cut. To achieve a solution within manageable computational time, the cutting speeds are set unrealistically high in the current FE models, however the model predicts that the cutting temperature can be reduced by increasing the cutting speed, which is consistent with results from previous experimental studies of ultrasonic cutting in a variety of different materials [10].

Similar results are achievable for the debond and element erosion models. However, the element erosion model removes the need to pre-notch the specimen and allows better opportunities for convergence through adaptive meshing. Currently, the debond modelling approach has been less successful in terms of computational efficiency because it has suffered from a lack of automatic adaptive meshing. The debond model is extremely computationally intensive and difficulties often arise due to the highly distorted mesh, the very high speed oscillatory movement of the cutting blade and the translational cutting speed of the blade. The ABAQUS standard solver supports a manual re-meshing technique within the package but this is also very time consuming, complex and laborious. But recent advances within the solver, available in the newest version of ABAQUS standard, version 6.6, now incorporate an adaptive meshing option that automatically remeshes a highly distorted mesh during the analysis similar to the one offered in the ABAQUS explicit code that should increase the computational efficiency of the solution. Developments of this model are therefore continuing. The element erosion model also accommodates dynamic effects rather than adopting a quasi-static approach and removes the need to assume perfect cleavage, which is a limiting assumption of the debond model. However, the debond model offers an alternative modelling approach that can provide well-correlated estimates of temperature and stress. Both models can allow cutting parameters to be changed easily, such as blade tip vibration amplitude, frequency, cutting speed, cutting depth, blade geometry, blade material and specimen material, and can accommodate multi-layered material models.

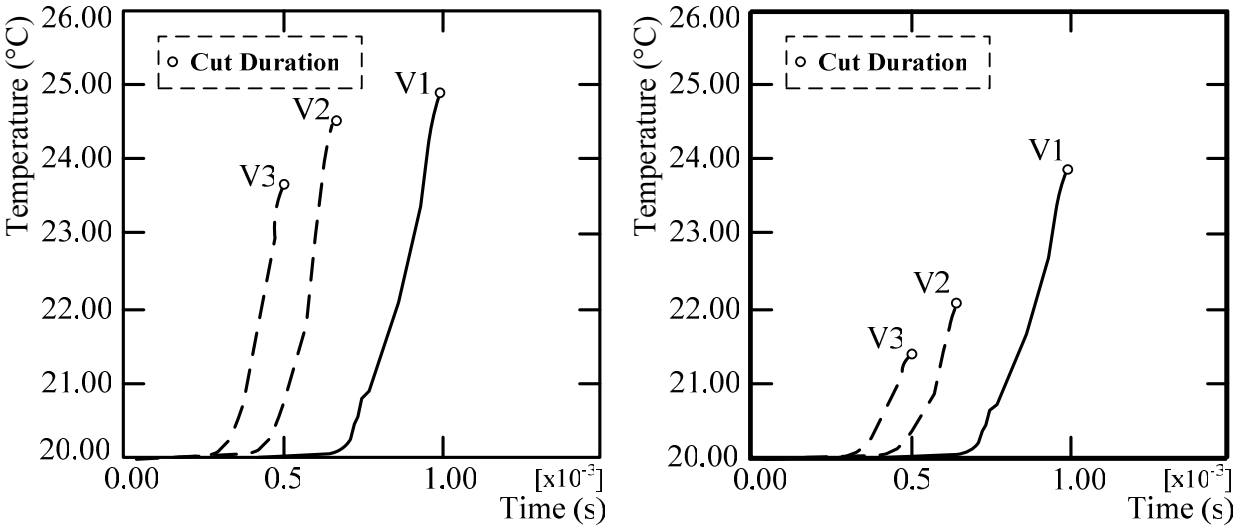

Fig. 5.22: Effect of cutting speed on temperature 1mm from cut site as predicted from (a) the element erosion FE model and (b) the debond FE model.

5.2.6.6 Summary

Two different approaches to represent ultrasonic cutting as a 2D finite element model have been presented. One uses the debond option in ABAQUS standard which represents cutting as a fracture mechanics model and one uses the element erosion option in ABAQUS explicit, where elements are removed from the solution when a shear failure criterion is reached. Both models account for thermal effects that are present during ultrasonic cutting due to friction at the blade-toffee interface. Temperature dependent material data for toffee was included in the FE model from experimental tests. The contact condition at the interface between the blade and the specimen was included in both FE models using the significantly reduced coefficient of friction determined from experimental friction tests where ultrasonic excitation was applied to a block horn.

FE models have been used to predict the effect of velocity on the temperature distribution at a distance 1mm from the cut site in material specimens of toffee. These preliminary results correlate with previous experimental investigations, which found that ultrasonic cutting temperature reduces with increased cutting velocity. Results from both FE modelling approaches correlate well with similar values attained for temperature of both models. This investigation has shown that either modelling approach is feasible for simulating ultrasonic cutting but currently the element erosion approach is more advantageous to the user. Further work will consider

ultrasonic cutting as a 3D thermal-mechanical model where blade orientation at the cut site and different blade geometries can be accommodated. In this case, only the element erosion model can be used as the debond modelling approach is unavailable in the FE package ABAQUS.

5.2.7 Mesh convergence study for 2D element erosion model.

For finite element simulations to provide accurate and meaningful results the mesh must be properly and sufficiently described in order to incorporate all of the complexities of the modelling approach. However, as the mesh density of the model increases computational time also increases so it is important to perform a mesh density study to allow the optimum mesh density to be determined that will minimise computational time but maintaining accuracy of the solution. A mesh convergence study was conducted on the 2D symmetric element erosion model to minimise computational time of this very computationally intensive modelling approach to ultrasonic cutting and to provide confidence in the results of the FE simulation.

For this study the 2D element erosion model was partitioned as shown in Fig. 5.23 and five independent simulations of ultrasonic cutting of Perspex were simulated using a cutting speed of 10 mm/s and a peak-peak blade tip amplitude of 100 μm oscillating at 35 kHz for 5 different mesh densities. A table listing the number of elements in each section of the 2D element erosion model in each corresponding mesh study is tabulated in Table 5.5.

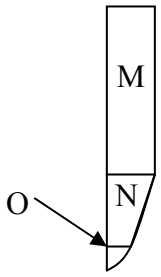

A	B	C
D	E	F
G	H	I
J	K	L

Fig. 5.23: Schematic diagram illustrating the partitioned sections for the mesh convergence study using the 2D element erosion model.

Mesh Convergence Study on Element Erosion Model					
Mesh Study 1					
Part	Area Dimensions (mm)	Area	Horizontal Elements	Vertical Elements	Total Elements
Specimen	0.75 x 2	A	2	4	8
Specimen	1 x 2	B	2	4	8
Specimen	8.25 x 2	C	2	4	8
Specimen	0.75 x 4	D	2	4	8
Specimen	1 x 4	E	2	4	8
Specimen	8.25 x 4	F	2	4	8
Specimen	0.75 x 4	G	2	4	8
Specimen	1 x 4	H	2	4	8
Specimen	8.25 x 4	I	2	4	8
Specimen	0.75 x 10	J	2	4	8
Specimen	1 x 10	K	2	4	8
Specimen	8.25 x 10	L	2	4	8
Blade	0.75 x 16	M	2	4	8
Blade	(0.1 x 1.99) + (0.5 x 1.99 x 0.65)	N	2	2	4
Blade	1/4 x PI x 0.1^2	O	2	2	3
					111
Mesh Study 2					
Part	Area Dimensions (mm)	Area	Horizontal Elements	Vertical Elements	Total Elements
Specimen	0.75 x 2	A	4	8	32
Specimen	1 x 2	B	4	8	32
Specimen	8.25 x 2	C	4	8	32
Specimen	0.75 x 4	D	4	8	32
Specimen	1 x 4	E	4	8	32
Specimen	8.25 x 4	F	4	8	32
Specimen	0.75 x 4	G	4	8	32
Specimen	1 x 4	H	4	8	32
Specimen	8.25 x 4	I	4	8	32
Specimen	0.75 x 10	J	4	8	32
Specimen	1 x 10	K	4	8	32

Specimen	8.25 x 10	L	4	8	32
Blade	0.75 x 16	M	3	6	18
Blade	(0.1 x 1.99) + (0.5 x 1.99 x 0.65)	N	3	3	9
Blade	1/4 x PI x 0.1^2	O	3	3	8
					419
Mesh Study 3					
Part	Area Dimensions (mm)	Area	Horizontal Elements	Vertical Elements	Total Elements
Specimen	0.75 x 2	A	6	12	72
Specimen	1 x 2	B	6	12	72
Specimen	8.25 x 2	C	6	12	72
Specimen	0.75 x 4	D	6	12	72
Specimen	1 x 4	E	6	12	72
Specimen	8.25 x 4	F	6	12	72
Specimen	0.75 x 4	G	6	12	72
Specimen	1 x 4	H	6	12	72
Specimen	8.25 x 4	I	6	12	72
Specimen	0.75 x 10	J	6	12	72
Specimen	1 x 10	K	6	12	72
Specimen	8.25 x 10	L	6	12	72
Blade	0.75 x 16	M	4	8	32
Blade	(0.1 x 1.99) + (0.5 x 1.99 x 0.65)	N	4	4	16
Blade	1/4 x PI x 0.1^2	O	4	4	12
					924
Mesh Study 4					
Part	Area Dimensions (mm)	Area	Horizontal Elements	Vertical Elements	Total Elements
Specimen	0.75 x 2	A	8	16	128
Specimen	1 x 2	B	8	16	128
Specimen	8.25 x 2	C	8	16	128
Specimen	0.75 x 4	D	8	16	128
Specimen	1 x 4	E	8	16	128
Specimen	8.25 x 4	F	8	16	128
Specimen	0.75 x 4	G	8	16	128
Specimen	1 x 4	H	8	16	128
Specimen	8.25 x 4	I	8	16	128
Specimen	0.75 x 10	J	8	16	128

Specimen	1 x 10	K	8	16	128
Specimen	8.25 x 10	L	8	16	128
Blade	0.75 x 16	M	5	10	50
Blade	(0.1 x 1.99) + (0.5 x 1.99 x 0.65)	N	5	5	25
Blade	1/4 x PI x 0.1^2	O	5	5	21
					1632
Mesh Study 5					
Part	Area Dimensions (mm)	Area	Horizontal Elements	Vertical Elements	Total Elements
Specimen	0.75 x 2	A	10	20	200
Specimen	1 x 2	B	10	20	200
Specimen	8.25 x 2	C	10	20	200
Specimen	0.75 x 4	D	10	20	200
Specimen	1 x 4	E	10	20	200
Specimen	8.25 x 4	F	10	20	200
Specimen	0.75 x 4	G	10	20	200
Specimen	1 x 4	H	10	20	200
Specimen	8.25 x 4	I	10	20	200
Specimen	0.75 x 10	J	10	20	200
Specimen	1 x 10	K	10	20	200
Specimen	8.25 x 10	L	10	20	200
Blade	0.75 x 16	M	6	12	72
Blade	(0.1 x 1.99) + (0.5 x 1.99 x 0.65)	N	6	6	36
Blade	1/4 x PI x 0.1^2	O	6	6	27
					2535

Table 5.5: Table containing number of elements in each section of the 2D element erosion model for five independent mesh density studies.

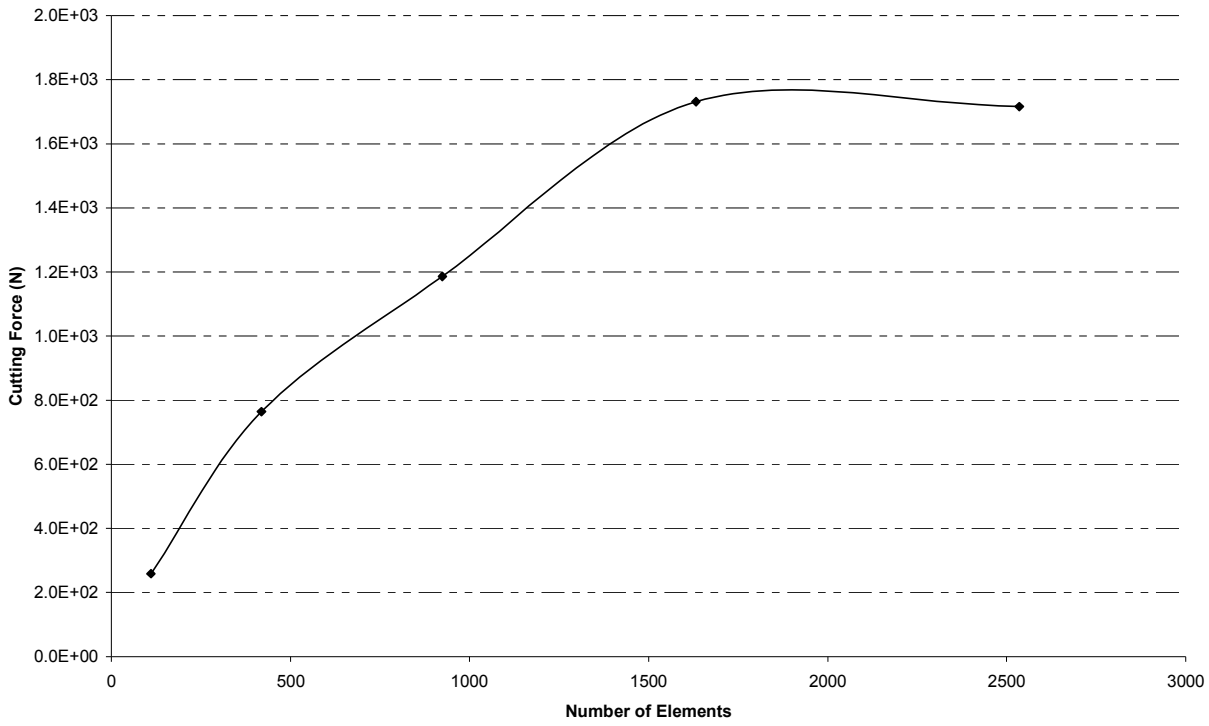

Fig. 5.24: Mesh density results for 2D element erosion model in guillotine configuration illustrating final cutting force for ultrasonic cutting of Perspex to a cut depth of 10 mm.

Fig. 5.24 illustrates the cutting force for each mesh. The graph indicates that as the mesh density increases from 1632 elements to 2535 elements the cutting force starts to plateau in the graph indicating that the optimum mesh density for the model has being reached. For the FE simulations in this thesis a mesh density of 2535 elements will be used to minimise computational time and to allow validation of the 2D element erosion model with experimental cutting trials.

5.2.8 3D element erosion model

The 3D fully coupled thermal stress analysis of ultrasonic cutting utilises the element erosion option in the FE code ABAQUS. The 3D element erosion model is developed from the 2D element erosion model by incorporating the depth of the blade and specimen. The 3D modelling approach utilises symmetry where appropriate to maximise computational efficiency. The 3D model uses a deformable body with a rigid body constraint to represent the blade and a deformable body to represent the material being cut. The rigid body constraint is applied to the deformable body for computational efficiency to assume the deformation of the blade is negligible compared to the deformation of the material to be cut. The deformable body can then

still have the ability to be meshed using the appropriate elements which allows the temperature distribution from the cut site through the blade to be calculated which cannot be done using an analytic rigid body as temperature is assumed to be constant along the blade profile.

For any analysis that incorporates temperature, mechanical properties that are temperature dependent are required to model the material fully. The main properties required are temperature dependent stress-strain curves, specific heat capacity, coefficient of thermal expansion and conductance. Contact between the blade and the interface is modelled using a Coulomb friction condition and heat generation which allows the generation of heat at the interface due to friction. In addition, conduction coefficients are specified that allows the heat to be conducted through the material away from the cutting interface. The failure of the material is modelled using the element erosion method as described in the 2D models. The failure mechanism removes elements from the model that reach a pre specified failure criterion after significant deformation has occurred. Once removed the element still exists in free space but no longer continues in the analysis. There are two types of failure criterion namely shear failure or tensile failure the same as in the 2D modelling environment. For shear failure the equivalent plastic strain from the stress-strain curve and the corresponding temperature where failure occurs is included and for tensile failure a hydrostatic cut off stress and the corresponding temperature is included from the stress strain curves. Again multiple stress-strain curves at different temperatures are included in the model to fully define the material from experimental testing. Coulomb friction and the heat generation option are included at the interface of the ultrasonic blade and the material to fully capture the interaction and to allow temperature distribution through the material and blade to be estimated.

The 3D model is very versatile and can allow different blade parameters such as materials, cutting orientation, ultrasonic amplitude, frequency, initial cutting temperature and cutting speed to be adjusted very easily. The 3D model allows the through thickness stress distribution, reaction force and temperature to be characterised for any cutting orientation. In addition, non-symmetrical cutting blade shapes can be modelled. Fig. 5.24 illustrates an example of the 3D model where the Mises stress distribution and the element temperature is depicted in Fig. 5.25 (a) and (b) respectively. The 3D element erosion model utilises symmetry about the 1-2 and 2-3 plane and in this case ultrasonic cutting in the guillotine configuration is represented as a quarter model simulation.

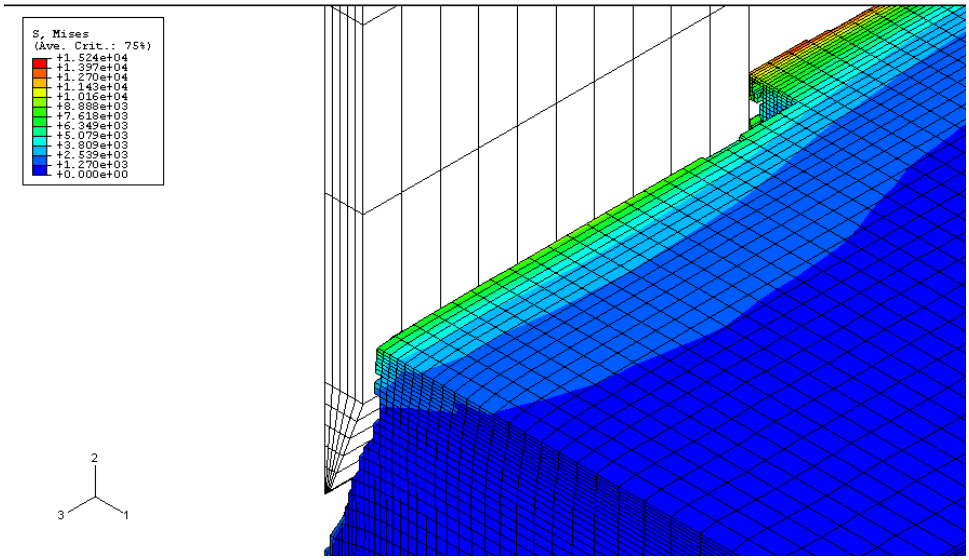

(a)

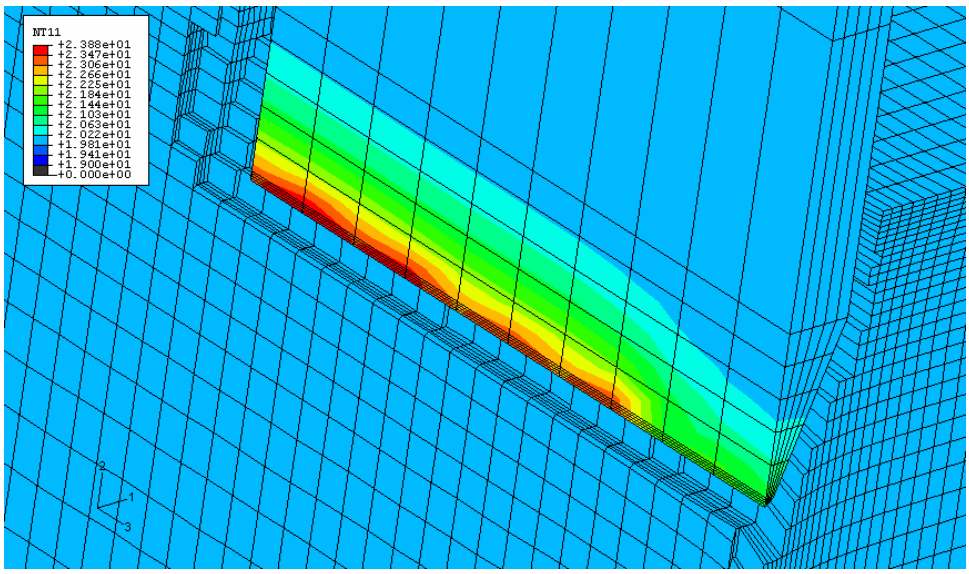

(b)

Fig. 5.25: 3D fully coupled thermal stress model of ultrasonic cutting illustrating (a) the Mises stress distribution and (b) temperature distribution.

The 3D model is extremely computationally intensive due to the large mesh density required to define the structure in 3D, the very high number of oscillations each second at ultrasonic frequencies movement of the cutting blade and the further ultrasonic cutting prediction of temperature distribution during cutting. As such, the 3D model was not be used for studies in this thesis.

5.3 Linear axis ultrasonic cutting rig

A linear translation cutting rig has been designed that enables cutting to be performed at constant velocities in the range 1 – 25 mm/s. These cutting speeds can be effectively modelled using FE models and can therefore be used to validate the fully coupled thermal-stress ultrasonic cutting models and experimentally conduct parametric studies by varying ultrasonic cutting parameters.

The test rig, Fig. 5.26, uses a motor/encoder combination that was designed to give the user the capability of predefining the cutting velocity profile prior to each cutting test and to allow the user to specify the cut depth. The encoder uses a P.I.D. controller that allows position, velocity and direction to be determined accurately for a given input. The defined velocity profile and the portion of the velocity/time curve used for the ultrasonic cutting tests are illustrated in Fig. 5.27. It can be seen that cut initiation occurs at a point on the constant velocity part of the profile. Once the required cutting depth for the tests is reached, ultrasonic cutting continues during deceleration and creep speed portions of the profile, bringing the blade to rest.

An electric motor/encoder combination which outputs 3000 revs/min is used to drive a linear screw thread by coupling with a gearbox. A translational plinth is moved linearly along two hardened steel shafts by a threaded nut that translates along the threaded shaft by rotation from the motor. Attached to the movable plinth is a lockable turntable, specified in angle of rotation, capable of clamping the ultrasonic transducer such that cutting trials can be conducted at different cutting orientations. The movable plinth has two protruding hardened steel shafts, one at either end, that were installed as a safety mechanism, whereby the electric supply to the motor is cut if either of the shafts interact with the magnetic cut-off sensors imbedded in the supports at either end of the rig. The specimen holder was designed to be locked onto the two hardened steel shafts at a distance depending on the length of the cutting blade. The specimen holder is an L-shaped bracket with four bearings embedded at each corner that slides along four hardened steel shafts and pushes onto the back of a load cell which records cutting force during cutting. The other side of the load cell is attached to another L-shaped bracket that is locked onto the two hardened steel shafts. The specimen can be clamped onto the specimen holder using a simple movable clamp. K-type thermocouple probes are used to measure temperature in the specimens at three locations along the direction of the cut, at a depth of 1 mm from the cutting axis.

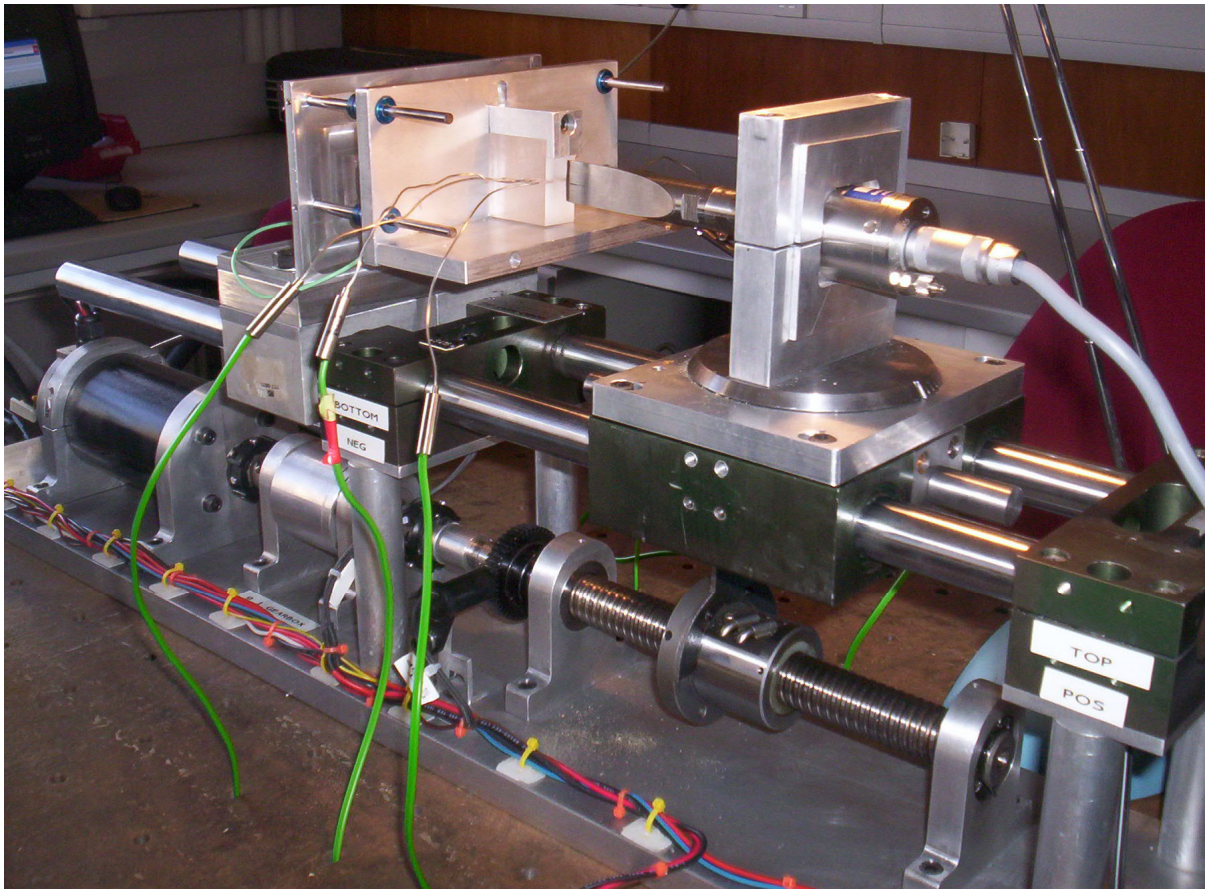

Fig. 5.26: Linear ultrasonic cutting rig.

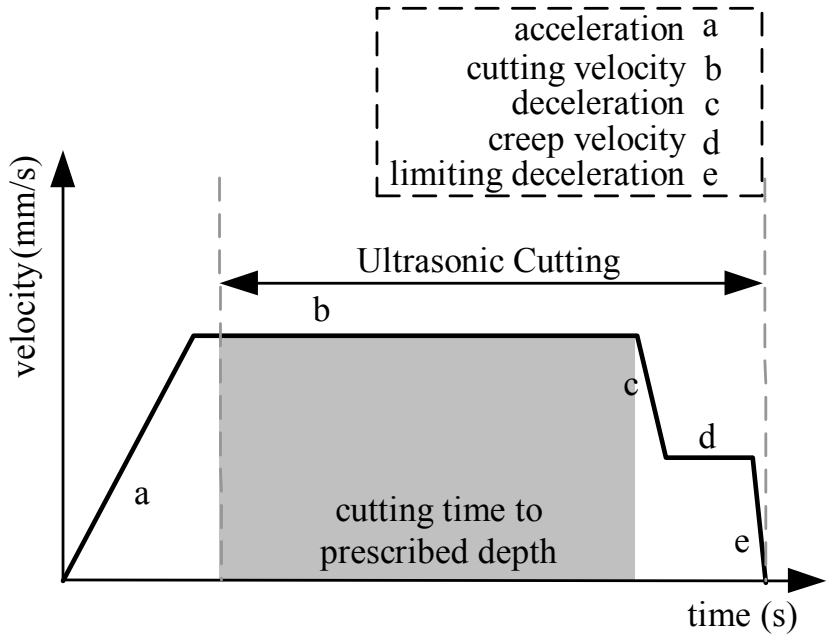

Fig. 5.27: velocity profile used during ultrasonic cutting tests.

5.3.1 Gearbox calculation

The linear axis ultrasonic cutting rig is designed to operate at translational speeds up to 25mm/s and also to be versatile to allow adaptation to a variety of gearboxes if required, to vary the range of cutting speeds. A reduction gearbox reduces the rotational speed of the motor driving the lead screw to ensure that it operates within a safe operational range. When the user specifies the translational velocity of the cutting blade, the motor is driven by supplying the motor with a voltage proportional to the speed of the motor. Similarly, the torque is proportional to the current. The electric motor functions smoothly in the linear region of its operational profile as shown in Fig. 5.28. When the motor operates in the lower region of the graph in Fig. 5.28 jerky rotational motion is often caused as the speeds are very low and thus operating in this region should be avoided. It is more advantageous to operate at higher speeds and reduce the speed through a reduction gearbox.

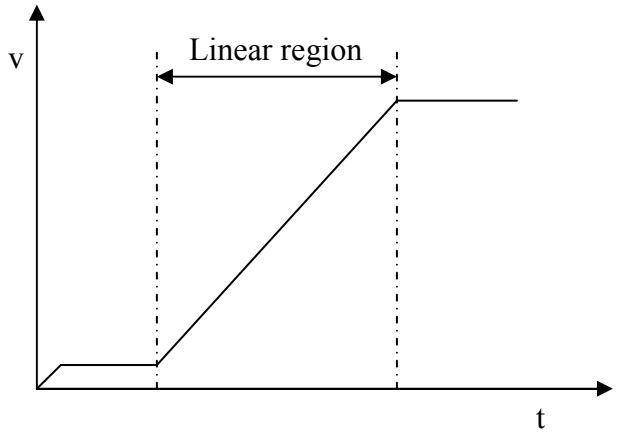

Fig. 5.28: Operational profile of electric motor.

The electric motor when operating at full power produces 3000 rev/min. When coupled to a lead screw with a pitch of 5 mm the translational speed of the plinth is 250 mm/s if the electric motor operates at maximum speed.

The maximum translational speed of the plinth if the motor is connected directly onto the lead screw is extremely high and for control and safety purposes is problematic. The cutting trials in this thesis are aimed at validating the FE models of ultrasonic cutting and high cutting speeds are advantageous for efficient computational run times but within realistic operational requirements. For cutting trials in this thesis the maximum speed of the plinth will be considered to be no more

than 25 mm/s which is realistic for cutting of food products using ultrasonic cutting. As such a gearbox is required to reduce the rotational speed of the motor supplied to the lead screw to ensure the motor is operating in the linear operating region as shown in Fig. 5.28. The one used for the cutting rig was a 9-1 gearbox ratio. The maximum translational velocity of the plinth was calculated to be 27.8 mm/s when operating on full power using this motor, gearbox and lead screw combination.

5.3.2 Specimen test configuration

Cubic material specimens were manufactured for cutting trials. Fig. 5.29 is a diagram of a specimen used in the cutting tests and illustrates the measurement locations proposed for the three K-type thermocouple probes used to monitor cutting temperature. Since it is not possible to monitor temperature at the actual cut site, the temperature probes are inserted in predrilled holes within the specimens at depths of 1 mm from the cut site and at steps of 5 mm along the cut direction as shown in Fig. 5.29.

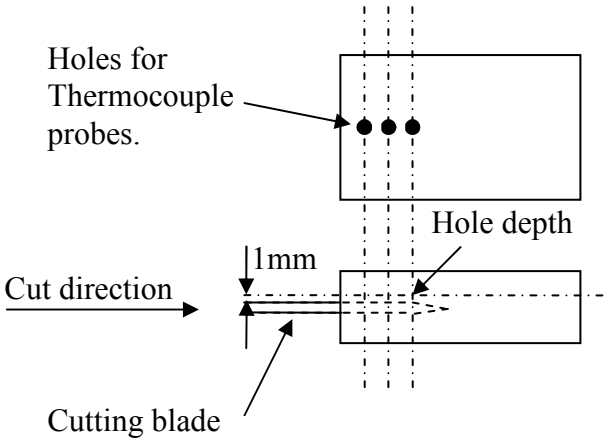

Fig. 5.29: Thermocouple location and cutting orientation in a material specimen.

5.4 Cutting Tests

Several experimental cutting trials were conducted in order to validate the 2D FE models of ultrasonic cutting and to investigate experimentally the effect of varying several ultrasonic cutting parameters namely, cutting speed, frequency and blade tip amplitude had on cutting force and temperature. All the experimental cutting tests conducted in this thesis were performed on the linear axis ultrasonic cutting rig.

5.4.1 Preliminary validation of single and multi-layer 2D element erosion models

Ultrasonic cutting blades usually operate with a uniform blade tip vibration velocity which is maintained during cutting using closed feedback control to adjust power. In many applications the material being cut is inhomogeneous and, although the ultrasonic parameters being used may be optimal for the bulk material, the prescribed vibration velocity may have an adverse effect on localised material of different properties. This study investigates whether it would be advantageous to alter ultrasonic cutting parameters during cutting to account for different materials or whether fixed blade tip vibration conditions are suitable for ultrasonic cutting of multilayer materials.

5.4.1.1 Methodology

It was the aim of this study to advance further the FE modelling technique of ultrasonic cutting using the 2D fully coupled thermo-stress element erosion model developed for single layer materials to incorporate materials with multilayer architectures to allow the effect of adjusting ultrasonic cutting parameters, such as blade tip vibration velocity and cutting speed, during cutting to be investigated. Ultrasonic cutting experiments were performed on three materials; Perspex, toffee and cheese, to determine the effect of cutting speed and blade tip vibration velocity on cutting force and temperature. Perspex is chosen as a material that allows repeatable experimental analysis and can hence be used to validate the FE model. Toffee and cheese are two of the materials being used in studies of ultrasonic cutting of food products. The accuracy of the model is discussed and subsequently used to investigate the effect of altering blade tip vibration velocity during guillotine cutting in multilayered products.

5.4.1.1.1 Finite element analysis of ultrasonic cutting

Ultrasonic cutting has been modelled as a 2D fully coupled thermal-stress element erosion problem using the explicit solver in the finite element package ABAQUS [252] as discussed earlier in this Chapter. Perspex, toffee and cheese were described as elastic-plastic materials using temperature and strain-rate dependent stress-strain curves evaluated previously and documented in Chapter 4 of this thesis. Element erosion can be used to model blade progression through the material to a predefined cut depth. The temperature can then be predicted at and remote from the cut site. The load applied to the blade can also be estimated for the duration of the cut.

5.4.1.2 Ultrasonic Cutting of Perspex

In this study ultrasonic cutting was performed in a guillotine configuration [89, 110] at three cutting speeds, 1, 5 and 10 mm/s, on the linear axis ultrasonic cutting rig using an ultrasonic cutting blade resonant at 35 kHz to investigate the effect of speed on cutting force and specimen temperature. The blade was designed, using finite element analysis (FEA) and experimental modal analysis (EMA) techniques, to oscillate in its first longitudinal mode of vibration with a blade tip vibration velocity in the range 5 – 8.8 ms^{-1}. EMA was used to analyse the surface vibration characteristics of the manufactured blades using a 3D laser Doppler vibrometer to check that cutting blades were tuned and also to ensure that nonlinearities in the form of harmonic generation, amplitude saturation, combination resonances, natural frequency shifting and chaotic motions are avoided.

The effects of the blade tip's ultrasonic vibration velocity and the blade cutting speed on cutting temperature and cutting force were recorded from experiments and compared to predictions from FEA. Fig. 5.30 shows the cutting force measured during ultrasonic cutting experiments. The results show that cutting force is dependent on the cutting speed and the blade tip vibration velocity. The experimental study shows that increasing the cutting speed from 1 – 10 mm/s can increase the load by as much as 1.2 kN at cut depths of up to 2 mm. In Fig. 5.30 the maximum cutting force is similar at cutting speeds of 5 and 10 mm/s as the blade velocity causes the specimen to fail in a brittle manner as opposed to causing a localised melt at lower cutting velocities of 1 mm/s. After a cut depth of approximately 2 mm is reached the cutting force drops quickly at cutting speeds of 5 and 10 mm/s as the specimen has cracked and the measured force is only that required to push the cracked specimen apart. When cutting at 1mm/s the blade is cutting the material and causing a localised melt at the interface of the blade and material and the cutting force continues to increase as the cut depth is increased. Fig. 5.30 shows clearly that as the vibrational velocity of the blade is increased when cutting at 1 mm/s there is a lower cutting force. The change in temperature was also recorded using the three thermocouples. At cutting speeds in excess of 5 mm/s recorded temperatures in the specimen exhibit negligible increases from room temperature. It is expected that, at these high cutting speeds, any point along the cut axis is exposed to frictional heating and a hot blade for a very short time period as the blade passes, and therefore the thermocouple locations, which are 1 mm remote from the cut axis, do not record any measurable change in temperature. At lower cutting speeds ($\leq$ 5 mm/s) an increase in cutting speed is shown to reduce cutting temperature, and an increase in blade tip

vibration velocity also reduces cutting temperature. Temperature measurements are inherently more difficult to perform as a precisely repeatable thermocouple location is hard to achieve.

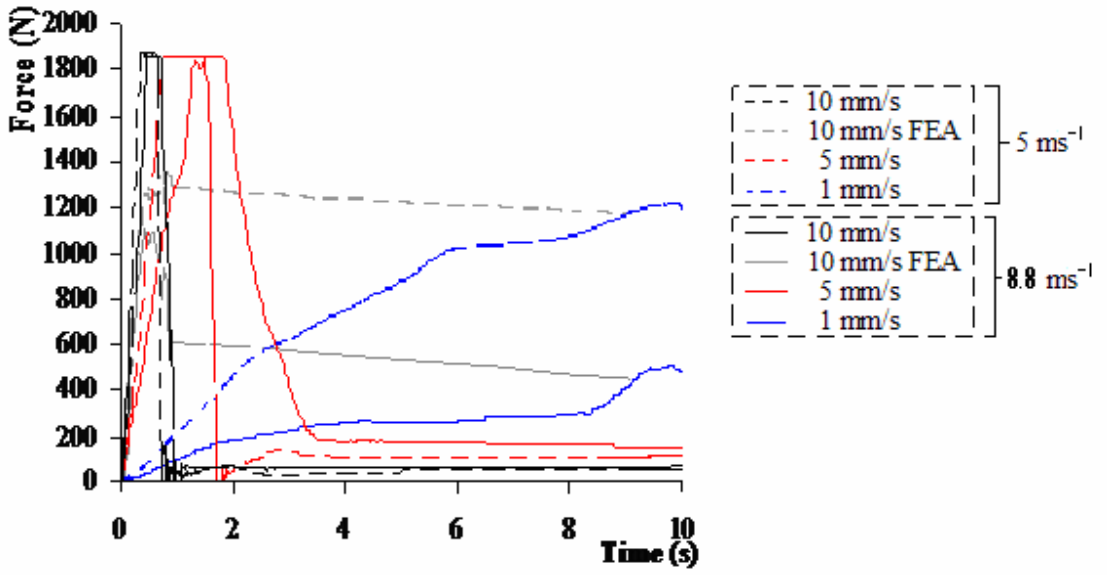

Fig. 5.30: Effect of cutting speed and blade tip vibration velocity on cutting force for ultrasonic cutting of Perspex; vibration velocity of 5 ms^{-1} is represented with dashed lines and 8.8 ms^{-1} is represented using solid lines.

The result from the FEA for a cutting speed of 10 mm/s is included in Fig. 5.30. The predicted cutting force is lower than the force measured experimentally for both of the blade tip vibration velocities. These predicted results could be due to the inaccuracy of the material data included in the FE model. The material data used could be less stiff than the actual material in the cutting tests which, when modelled would require less cutting force to progress the blade through the specimen. Several assumptions were also made in the FE modelling technique. For example when the elements failed due to ultrasonic cutting the material properties of the elements were instantaneously ramped down to zero and removed from the solution which, in reality doesn't occur. A more accurate approach would be to include damage of the element after the element had failed to gradually ramp down the material properties over a larger time period which would allow the ultrasonic blade to experience an increased opposing force as cutting progressed which could account for cut site debris. The FE simulation predicts that an increase cutting speed and blade tip vibration velocity reduces cutting temperature.

5.4.1.3 FEA of multi-layer ultrasonic cutting

The 2D FE model was adapted to investigate ultrasonic cutting of a multilayer product and

evaluate the effect of altering ultrasonic blade vibration parameters during cutting. A multilayer material consisting of 3 mm layers of Perspex, cheese and toffee was used to investigate the effect of material architecture on cutting temperature and cutting force. Fig. 5.31 plots the cutting force during ultrasonic cutting of this multilayer product with fixed blade tip vibration velocities of 5 and 8.8 ms^{-1}. The results show that blade progression from one material layer to another produces a change in measured cutting force. FEA was applied to investigate if varying the blade tip vibration velocity in each layer of material could minimise cutting load. Blade tip vibration velocities of 5 ms^{-1} and 8.8 ms^{-1} were used to cut the layers of Perspex, cheese and toffee in the simulation. The FE investigation found that the cutting force due to cutting is reduced in comparison to an analysis performed at the same cutting speed with a fixed blade tip vibration velocity. The outcome of this study promotes the use of cutting force as a method of controlling ultrasonic cutting blade parameters during cutting to account for layered material architectures. Force feedback could be used to improve system efficiency in ultrasonic food processing applications which typically use systems that are driven continuously with preset operating parameters.

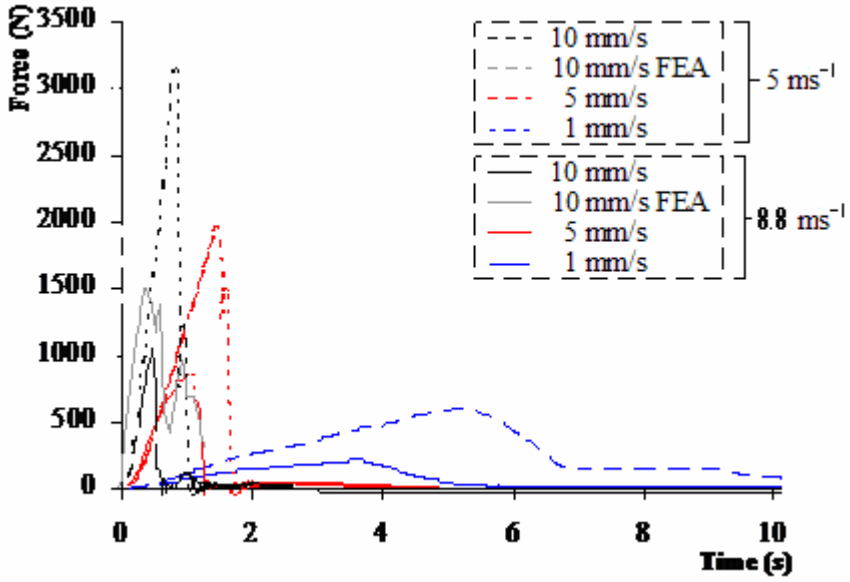

Fig. 5.31: Cutting force in multilayer cutting using a 35 kHz blade at cutting speeds of 1, 5 and 10 mm/s. A vibration velocity of 5 ms^{-1} is represented with dashed lines and 8.8 ms^{-1} is represented using solid lines.

5.4.1.4 Summary

A method of simulating ultrasonic cutting as a 2D fully coupled thermal-stress finite element simulation has been used to predict the effect of blade tip vibration velocity and cutting speed on

cutting force and temperature during ultrasonic cutting of Perspex and a multilayer material.

A parametric study of ultrasonic cutting of Perspex found that cutting force is dependant on cutting speed and vibration velocity. Cutting force has been shown to increase with cutting speed and to increase with decreased blade tip vibration velocity. Temperature was found to decrease if the cutting speed is increased as the time for which specimens are exposed to the ultrasonic cutting blade is minimised. Additionally, temperature is shown to reduce if higher blade tip vibration velocities are adopted. FEA has also been used to show that frequency does not have an effect on the magnitude of the cutting force which agrees with findings from previous experimental investigations. FE predictions for cutting temperature and cutting force were lower than those measured in cutting experiments but within 10%.

The parametric study performed on single layer specimens of Perspex, was used to determine material specific ultrasonic cutting parameters to reduce cutting force and cutting temperature for a given cutting speed. The model was based on a layered product of Perspex, cheese and toffee. It was found that cutting temperature and cutting force could be controlled and reduced, by varying blade tip vibration velocity during cutting to account for the material characteristics of the layer being cut. This result has initiated new research to develop ultrasonic cutting systems that utilise force feedback to determine optimum blade tip ultrasonic parameters and cutting speed specific for the material being cut. This offers opportunities to significantly improve the efficiency and reliability of ultrasonic cutting systems.

5.4.2 Validation of 2D element erosion model against experimental cutting tests for Perspex

Validation of the 2D fully coupled element erosion model was performed by comparing ultrasonic cutting experiments of Perspex in the guillotine configuration performed on a high speed linear axis ultrasonic cutting rig to FE simulations of the ultrasonic cutting experiments. Experimental ultrasonic cutting tests and FE simulations were performed at three different cutting speeds, 1 mm/s, 5 mm/s and 10 mm/s at two different ultrasonic frequencies, 20 kHz and 35 kHz using two different blade tip amplitudes for each cutting blade, 40 μm and 70 μm for the 20 kHz blade and 23 μm and 40 μm for the 35 kHz blade. Perspex was used for the cutting trials due to its abundance and its fairly consistent material properties. Each cutting test was performed to a pre-specified cutting depth of 10 mm. This investigation will consider the effect of cutting speed, blade tip amplitude and excitation frequency on the load applied to material specimens of Perspex represented using the mechanical and thermal material properties presented earlier in this Chapter. The experimental and FE results of ultrasonic cutting are compared to consider validation of the FE modelling approach and an assessment of the results is used to investigate the effect varying cutting speed, ultrasonic frequency and blade tip amplitude has on the cutting force on the specimen.

5.4.2.1 Experimental results and FEA predictions

FE simulations were designed to mimic experimental cutting trials in which a 20 kHz and 35 kHz blade was used to cut specimens of Perspex with two blade tip vibration amplitudes, 23 μm and 40 μm, and at three cutting velocities, 1 mm/s, 5 mm/s and 10 mm/s. Several experimental cutting tests were performed at each cutting speed and blade tip amplitude to determine if ultrasonic cutting produced reproducible cutting force results when cutting through Perspex. Fig. 5.32 and Fig. 5.33 illustrates the average experimental ultrasonic cutting force in blue with the deviation from the mean indicated by the error bars for ultrasonic cutting at 20 kHz and 35 kHz respectively. The corresponding FE predicted results are also presented on the graphs in red for comparison purposes to establish the accuracy of the FE approach. The graphs in Fig. 5.32 and Fig. 5.33 illustrate a small deviation from the mean as indicated by the error bars which gives confidence in the repeatability of the experimental testing technique for ultrasonic cutting on the linear axis ultrasonic cutting rig. In Fig. 5.32 (a) and (b) and Fig. 5.33 (a) and (b) the graphs indicate the simulated ultrasonic cutting force is similar to the experimental cutting force up 0.75 s after cut initiation which is to a cut depth of 3.75 mm. Afterwards the simulated cutting force plateaus at a cutting force lower than the experimental cutting force for both blade tip amplitudes. Similar trends are presented in Fig. 5.32 (c) and (d) and 5.33 (c) and (d) where the

simulated cutting force and the experimental cutting force are approximately equal after 0.3 s of ultrasonic cutting after cut initiation which in for these ultrasonic cutting trials is up to a cut depth of 3 mm.

There are several reasons why the simulated cutting force is lower than the experimental cutting force after these regions. For example in the simulations the blade tip amplitude is always the same whereas the blade tip amplitude in the experiments varies slightly during cutting as the vibrational characteristics of the blade change with cut depth. The generator has an incorporated closed loop feedback function to adjust the power supplied to the transducer to ensure the blade tip amplitude is adjusted during cutting to the predefined setting. However, for faster cutting speeds the generator needs to increase power in order to maintain the blade tip amplitude at this predefined setting. But there is an upper limit for power built into the generator which the generator cannot exceed and if the power supplied reaches this level the generator will cut out.

Due to the highly intensive computational nature of the modelling approach, the mesh density was minimised to allow ultrasonic cutting predictions to be made in reasonable timescales in an attempt to validate the modelling technique. The accuracy of the results could possibly be improved by using a more refined mesh in the cutting region. During cutting the blade tip becomes slightly blunt after prolonged use but the geometry in the simulated model is always unchanged during cutting. This study has provided a solid base for using FE modelling to predict the applied load during ultrasonic cutting but further work is necessary to refine the FE model to allow future predictions about the effect of various cutting parameters on cutting temperature and applied load to be made that are more representative and indicative of the experimental results.

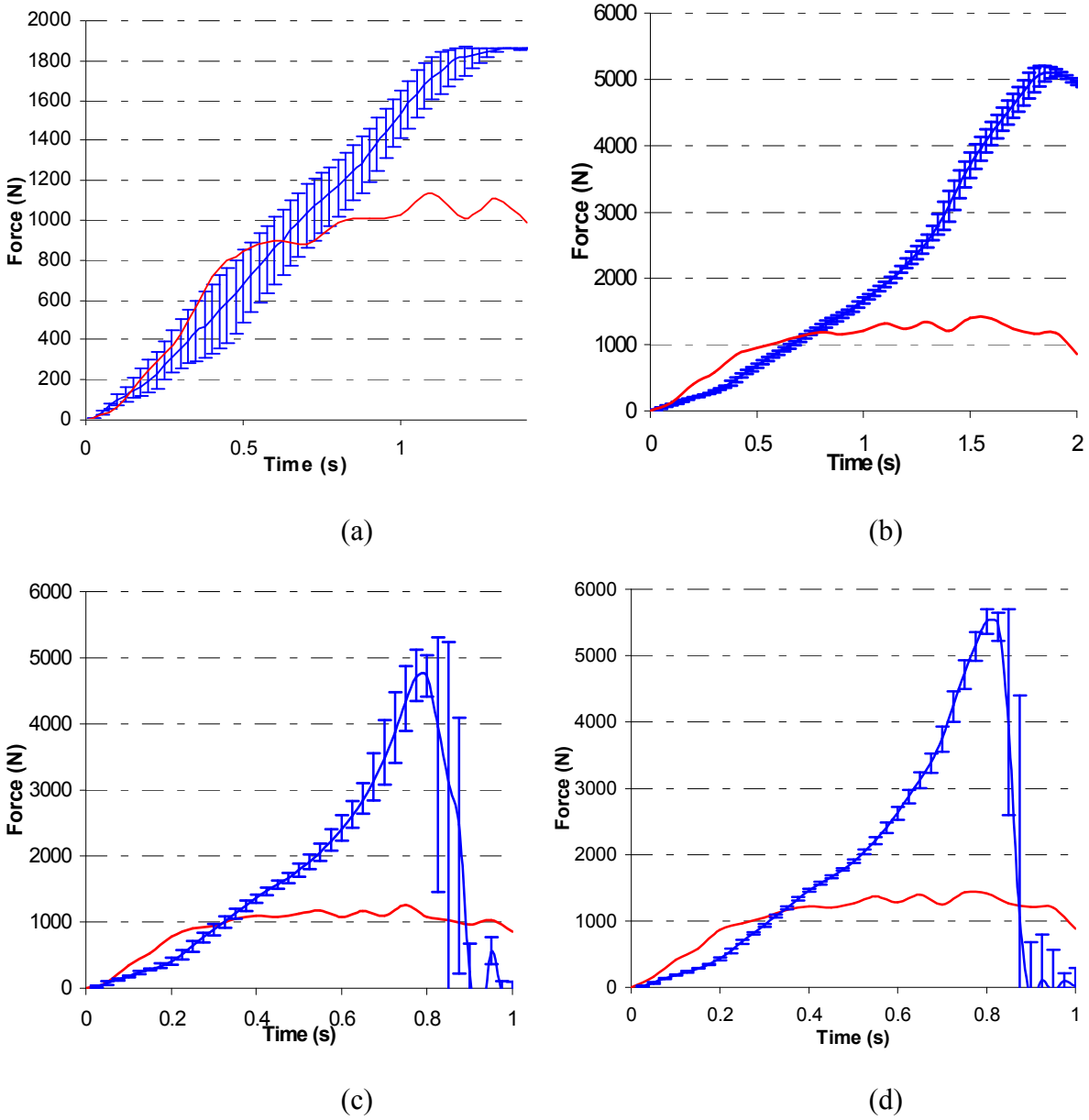

Fig. 5.32: Experimental results and FE predictions of cutting force in ultrasonic cutting of Perspex using a 20 kHz blade at cutting speeds of (a) 5 mm/s at a blade tip amplitude of 70 µm, (b) 5 mm/s at a blade tip amplitude of 40 µm, (c) 10 mm/s at a blade tip amplitude of 70 µm and (d) 10 mm/s at a blade tip amplitude of 40 µm. Experimental cutting tests are illustrated using solid blue lines and the FE predictions are represented using solid red lines.

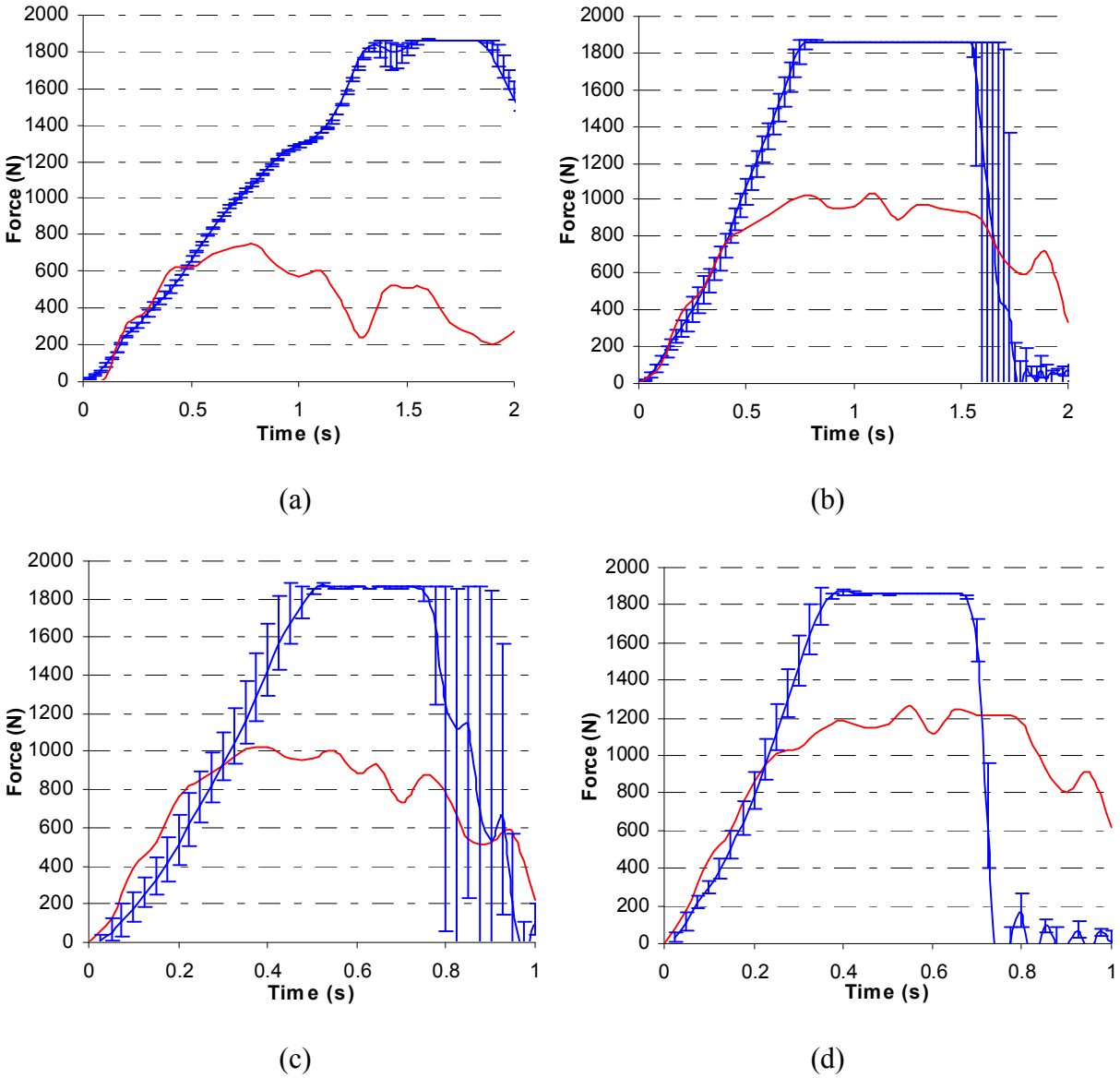

Fig. 5.33: Experimental results and FE predictions of cutting force in ultrasonic cutting of Perspex using a 35 kHz blade at cutting speeds of (a) 5 mm/s at a blade tip amplitude of 40 µm, (b) 5 mm/s at a blade tip amplitude of 23 µm, (c) 10 mm/s at a blade tip amplitude of 40 µm and (d) 10 mm/s at a blade tip amplitude of 23 µm. Experimental cutting tests are illustrated using solid blue lines and the FE predictions are represented using solid red lines.

An experimental investigation on the effect cutting speed and blade tip amplitude have on the cutting force was also studied. Fig. 5.34 (a) and (b) illustrate the mean cutting force and the experimental curves describe that as cutting speed increases the cutting force increases for ultrasonic cutting using a 20 kHz and 35 kHz blade respectively. In Fig. 5.34 (b) the cutting force is approximately the same for cutting speeds of 5 mm/s and 10 mm/s for both blade tip amplitudes due to the generator cutting out during the experimental cutting trials as the power

required to drive the ultrasonic cutting blade was in excess of the maximum power available in the generator. A similar trend is also present in Fig. 5.34 (a) for ultrasonic cutting of Perspex at 10 mm/s for both blade tip amplitudes and for 5 mm/s for the lower blade tip amplitude. Both graphs in Fig. 5.34 illustrate how cutting force decreases with increasing blade tip amplitude for each cutting speed, which is a trend that has been shown by previous researchers [89,110].

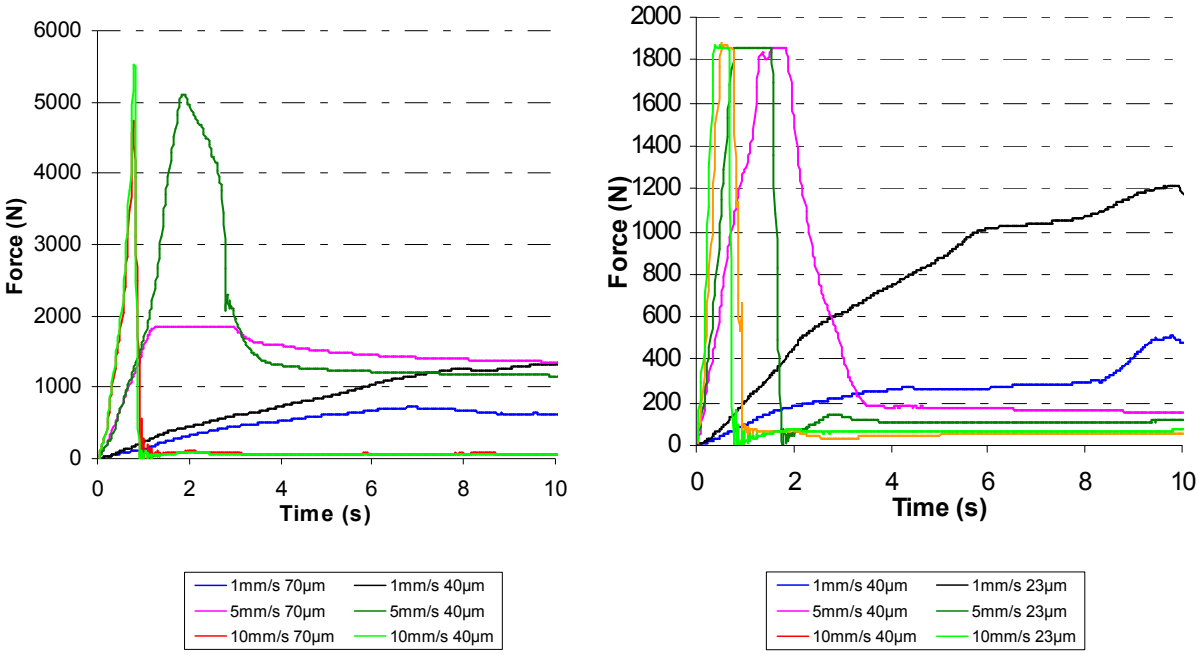

(a) (b)

Fig. 5.34: Average experimental predictions of cutting force in ultrasonic cutting of Perspex using a (a) 20 kHz ultrasonic cutting blade and a (b) 35 kHz ultrasonic cutting blade for cutting speeds of 1, 5 and 10 mm/s at a blade tip amplitude of 40 µm and 70 µm for the 20 kHz blade and 23 µm and 40 µm for the 35kHz blade.

Fig. 5.35 represents mean experimental ultrasonic cutting trials at cutting speeds of (a) 1 mm/s, (b) 5 mm/s and (c) 10 mm/s for comparison purposes. The effect ultrasonic frequency has on the applied cutting force was investigated at blade tip amplitudes of 40 µm and 70 µm for the 20 kHz blade and 23 µm and 40 µm for the 35 kHz blade. Fig. 5.35 (a) indicates that cutting force decreases with increasing ultrasonic frequency especially at higher blade tip amplitudes. For lower blade tip amplitudes the effect of frequency on cutting force is less noticeable but the trend is still apparent. Fig. 5.35 (b) and (c) also illustrates the effect increasing frequency has on decreasing cutting force in the earlier stages of ultrasonic cutting. As the operational time of ultrasonic cutting was increased and subsequently the cut depth was increased, the ultrasonic

generator cut out in all tests in Fig. 5.35 (c) and for ultrasonic cutting at 35 kHz at 5 mm/s at a blade tip amplitude of 70 µm.

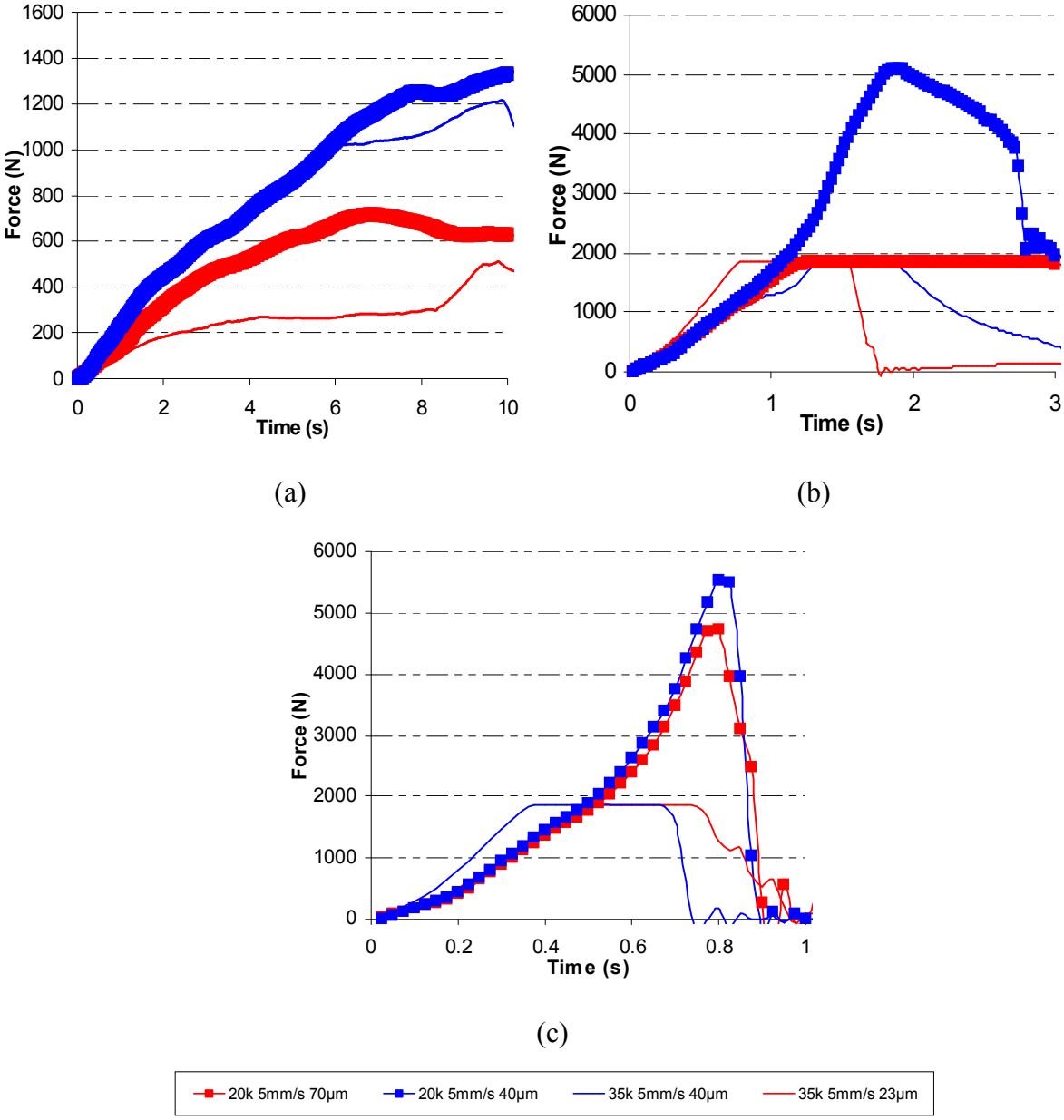

Fig. 5.35: Average experimental results for cutting force in ultrasonic cutting of Perspex using a 20 kHz and 35 kHz blade at cutting speeds of (a) 1 mm/s, (b) 5 mm/s and (c) 10 mm/s.

5.4.2.2 Summary

This investigation presented a comparison of parametric experimental ultrasonic cutting tests performed on Perspex for various cutting speeds, blade tip amplitudes and ultrasonic frequencies and compared these findings with FE simulations mimicking the parametric experimental tests.

The cutting force resulting during ultrasonic cutting of Perspex up to a cut depth of 10 mm was compared for both experimental and FE simulations of ultrasonic cutting in an attempt to validate the 2D model of ultrasonic cutting.

Average experimental cutting force results indicating the spread in results illustrated by error bars for the 20 kHz and 35 kHz ultrasonic cutting blade cutting Perspex on the linear axis ultrasonic cutting rig were compared to the equivalent FE predicted force results from FE models mimicking the experimental tests. The comparison indicates that for the simulated ultrasonic cutting tests performed using the 20 kHz and 35 kHz ultrasonic cutting blade at 5 mm/s the results are similar up to a cut depth of approximately 3.75 mm and for a cut depth exceeding 3.75 mm the predicted FE results are lower than the experimental. A similar trend indicating FE results analogous to the experimental results is also apparent for a cutting speed of 10 mm/s but only up to a cut depth of 3 mm and then afterwards the predicted FE results are lower than the experimental results.

An additional experimental investigation was performed to study the effect of cutting speed and blade tip amplitude on the mean cutting force. Findings showed that as cutting speed increases the mean cutting force increases for ultrasonic cutting at both ultrasonic frequencies tested. The experimental results also indicate for lower cutting speeds the mean cutting force decreases with increasing blade tip amplitude. Further experimental studies investigated the effect ultrasonic operating frequency had on the mean experimental cutting force. The experimental results indicated a decrease in cutting force with increasing ultrasonic frequency more noticeably at higher blade tip amplitudes.

This study investigating ultrasonic cutting of Perspex using an experimental and FE approach in the guillotine configuration was used as a validation exercise to compare actual experimental results with FE predictions in an attempt to use FE modelling of the ultrasonic cutting process as a design tool in the design process for ultrasonic equipment. Initial findings indicate that FE predictions for cutting force are similar to experimental cutting results up to a certain cut depth and the modelling technique can be assumed to be valid for ultrasonic cutting of Perspex but further work needs to be performed to reduce the errors in modelling the ultrasonic cutting process and allow a more accurate response to be predicted especially at higher cutting speeds

and greater cut depths. However, this study has shown there is a possibility of the modelling technique to be used in ultrasonic component and ultrasonic process design and the technique could be further explored to predict cutting force in ultrasonic cutting of food products.

5.4.3 Validation of toffee cutting trials with 2D element erosion model

This study investigates the accuracy of using finite element analysis (FEA) to model ultrasonic food cutting as a material shear failure problem. Ultrasonic cutting experiments are performed on a high speed linear axis ultrasonic cutting rig to allow axial cutting to be performed to pre-specified depths at constant cutting velocities in the range 1 - 25 mm/s. Representation of food products in FEA is usually conducted by using mechanical properties determined from compression tests due to the ease of testing. However, the mechanical properties in tension are different from those in compression and for representing ultrasonic cutting of food products tensile data may be more representative than compressive data.

This study investigates the effect of cutting speed, blade tip amplitude and excitation frequency on the load applied to material specimens of toffee represented using (1) compression data and (2) tensile data. These experimental tests are subsequently replicated using the 2D element erosion model developed in the FE package ABAQUS and the predictions for applied load calculated from the model are compared to experimental measurements. Evaluations of the accuracy of the FE predictions against actual experimental cutting tests on the high speed linear axis ultrasonic cutting rig are discussed with the aim of validating the FE simulation for ultrasonic cutting of toffee and offering the modelling technique as a tool for ultrasonic component design for use in the food industry. This study uses material characterisation data for toffee as documented in Chapter 4 of this thesis and presents a novel method of predicting the effect of various ultrasonic cutting parameters on applied load prior to ultrasonic cutting blade design and manufacture. The overall aim is to reduce cost to manufacturers and consumers.

5.4.3.1 Experimental results and FEA predictions

FE simulations were designed to mimic experimental cutting trials in which 20 and 35 kHz blades were used to cut specimens of toffee with two blade tip vibration amplitudes, 23 μm and 40 μm for the 35 kHz blade and 40 μm and 70μm for the 20 kHz blade at two cutting velocities, 5 mm/s and 10 mm/s. The data for the repeated experimental cutting trials at each cutting speed and blade tip amplitude are then compared with the cutting force results for each simulation

using (1) the tensile material properties for toffee and (2) the compression material properties for toffee, emulating the experimental test to establish the accuracy of the FE approach. The experimental ultrasonic cutting results can then be used in future numerical studies of ultrasonic cutting to refine the FE modelling approach to allow future predictions about the effect of various cutting parameters on applied load to be made.

5.4.3.3 Experimental results

Fig. 5.36 and Fig. 5.37 show a comparison of experimental and simulated ultrasonic cutting force data for experiments performed on toffee with a 20 kHz and 35 kHz ultrasonic cutting blade respectively at two different blade tip amplitudes at a cutting speed of 5 mm/s and 10 mm/s. The experimental cutting forces in Fig. 5.36 (a) and (b) are shown to decrease with increasing ultrasonic amplitude during cutting at a cutting speed of 5mm/s, a trend that is also similar in Fig. 5.37 (a) and (b) at a cutting speed of 5 mm/s and Fig. 5.37 (c) and (d) at a cutting speed of 10 mm/s. The predictions from the FE simulations also represent a reduction in cutting force with increasing ultrasonic blade amplitude as shown in Fig. 5.36 and Fig. 5.37. These findings for ultrasonic cutting of toffee have also been discovered for ultrasonic cutting of other materials including Perspex as illustrated earlier in this Chapter.

At 20 kHz, as shown in Fig. 5.36, a larger scatter of measured cutting force is produced during experimental cutting trials on the linear high speed cutting rig compared to the higher frequency counterpart as shown in Fig. 5.37 for ultrasonic cutting at 35 kHz. This is illustrated by the high deviation of the error bars from the mean. This could be due to the brittle nature of toffee. For cutting brittle materials the higher operating frequency of the ultrasonic cutting blade could be advantageous to produce a more controlled cut and higher quality of surface finish. The large scatter in the experimental results as indicated by the wide spread in the error bars deviating from the mean illustrate the vibro-impact nature of the ultrasonic cutting blade is slowly chipping away the product causing uncontrollable fracture at the cut site. However, the higher frequency causes more oscillations per second and as such the ultrasonic blade is chipping away at the product more times per second which allows the cutting mechanism to be more controllable. In addition, the higher number of oscillations per second causes more heat to be produced at the cut site due to friction as the blade moves back and fore more times per second. This process could alter the local cutting mechanism from a fracture dominated one to a melting process due to the low melting point of toffee. This process could be considered more controllable, as the spread in the experimental cutting force is smaller as illustrated by the small

deviation from the mean of the error bars in Fig. 5.37. A melting process could be considered more advantageous from an operational aspect however. As the material is melting the taste of the product could be chemically changed, rendering the product undesirable for the consumer.

FE simulations of ultrasonic cutting at both operating frequencies and representing all experimental cutting trials as indicated in Fig. 5.36 and Fig. 5.37 illustrate the small difference in cutting force when representing toffee using compressive or tensile data. The FE predicted results for ultrasonic cutting of toffee using both tensile and compression data at 5mm/s and at blade tip amplitudes of 40 µm and 70 µm as shown in Fig. 5.36 represent a slightly lower cutting force than the actual experimental tests however, the results provide confidence that with some refinement of the FE model, prediction of cutting force for food products could be achieved. Fig. 5.37 represents ultrasonic cutting at an operating frequency of 35 kHz for blade tip amplitudes of 23 µm and 40 µm at cutting speeds of 5 mm/s and 10 mm/s. The FE predictions of these cutting trials are even lower than those at the lower operating frequency of 20 KHz, but as stated previously exhibit the same trends of decreasing cutting force with increasing ultrasonic amplitude and these results again emphasise that with further refinement of the FE model an accurate prediction of cutting force could be achieved for ultrasonic cutting of food products.

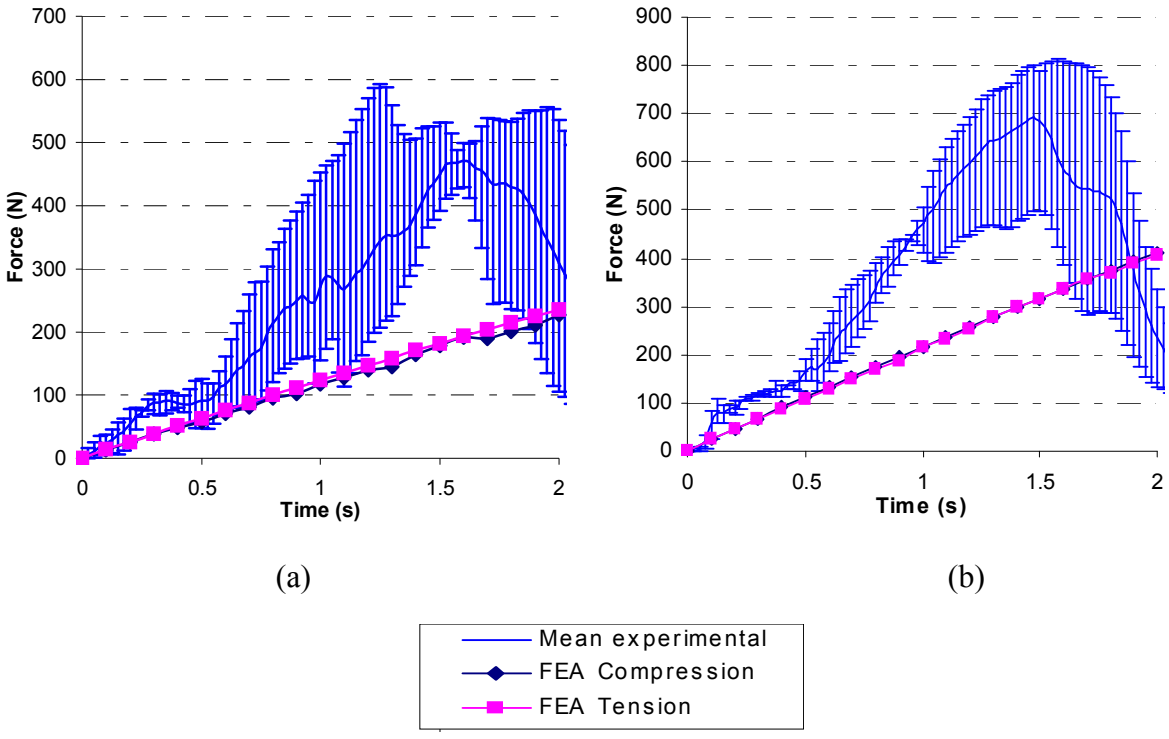

Fig. 5.36: Experimental results and FE predictions of cutting force in ultrasonic cutting of Toffee using a 20 kHz blade at cutting speeds of (a) 5 mm/s at a blade tip amplitude of 70 µm and (b) 5 mm/s at a blade tip amplitude of 40 µm.

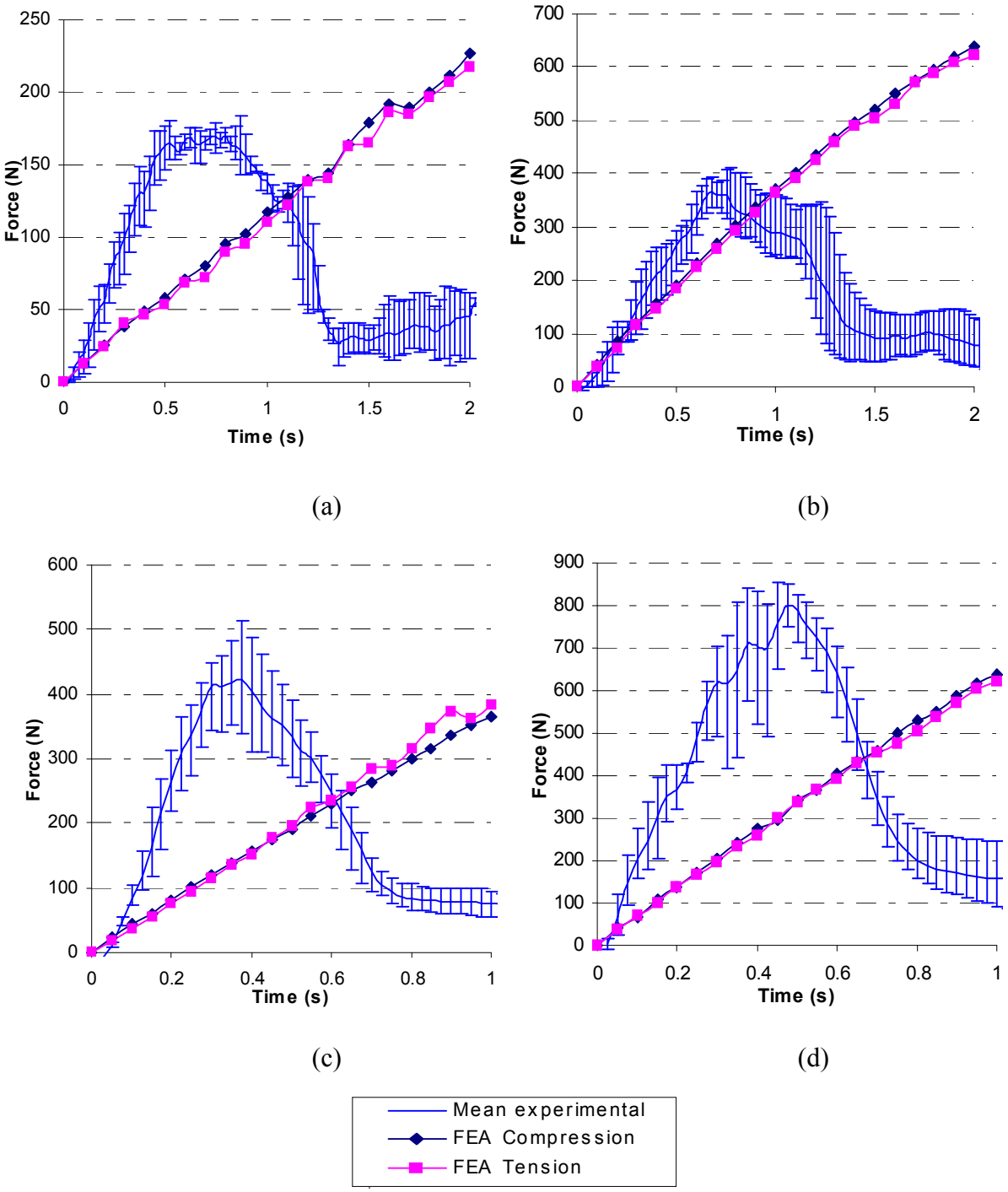

Fig. 5.37: Experimental results and FE predictions of cutting force in ultrasonic cutting of Toffee using a 35 kHz blade at cutting speeds of (a) 5 mm/s at a blade tip amplitude of 40 µm, (b) 5 mm/s at a blade tip amplitude of 23 µm, (c) 10 mm/s at a blade tip amplitude of 40 µm and (d) 10 mm/s at a blade tip amplitude of 23 µm.

Fig. 5.38 depicts average experimental cutting force for ultrasonic cutting of toffee at various cutting speeds and blade tip amplitudes for ultrasonic operating frequencies of 20 kHz and 35

kHz. Both diagrams indicate that as cutting speed increases the cutting force increases during cutting. Also, as the ultrasonic amplitude at all cutting speeds increases the cutting force decreases during ultrasonic cutting. These trends are consistent with findings from other studies of ultrasonic cutting including ultrasonic cutting of Perspex as discussed earlier in this Chapter. These significant finding is that cutting parameters can be optimised to produce a specific cutting force if required to optimise the cut of a particular product. This could be advantageous, resulting in the required cut and surface finish of the product which is desired by the consumer.

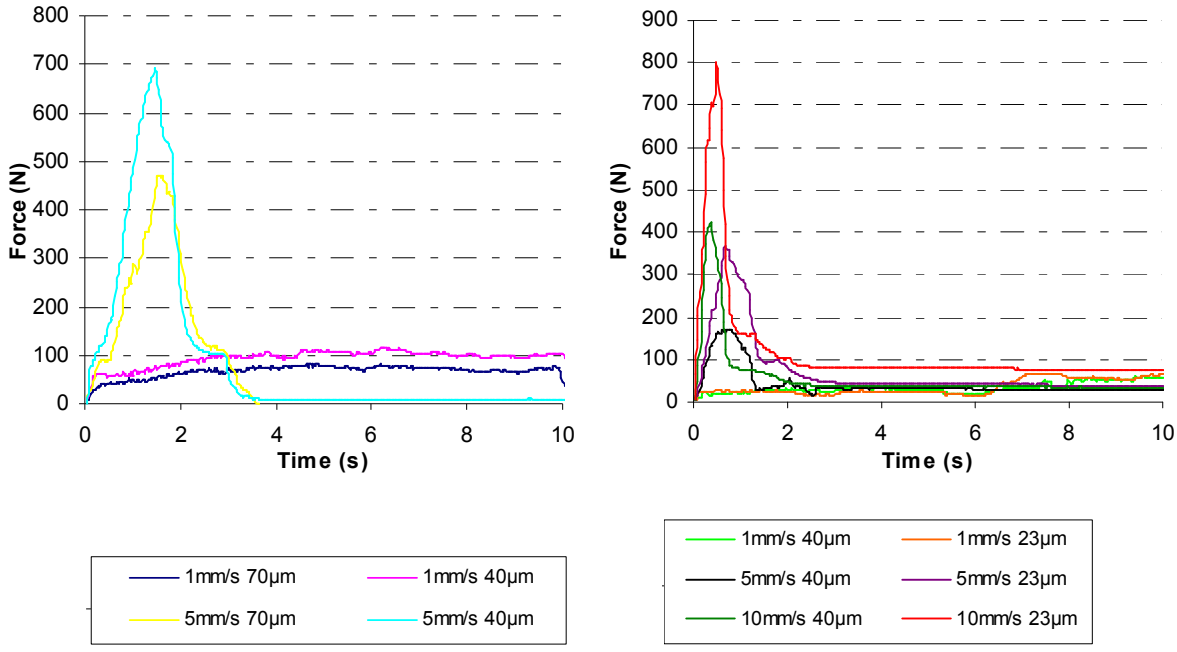

(a) (b)

Fig. 5.38: Average experimental predictions of cutting force in ultrasonic cutting of Toffee using a (a) 20 kHz ultrasonic cutting blade and a (b) 35 kHz ultrasonic cutting blade for cutting speeds of 1, 5 and 10 mm/s at a blade tip amplitude of 40 µm and 70 µm for the 20 kHz blade and 23 µm and 40 µm for the 35 kHz blade.

5.4.3.4 Summary

This study presented experimental and numerical cutting force data for ultrasonic cutting of toffee using ultrasonic cutting blades tuned to an operating frequency of 20 kHz and 35 kHz. Cutting trials were experimentally performed on a linear high speed ultrasonic cutting rig and numerically simulated in the FE code ABAQUS. Experimental and numerical cutting trials for toffee were performed at cutting speeds of 5 mm/s and 10 mm/s for blade tip amplitudes of 40 µm and 70 µm for the 20 kHz blade and 23 µm and 40 µm for the 35 kHz blade. Two simulated FE models for each test were performed (1) representing toffee using tensile data and (2) using

compression data, and compared against experimental cutting in an attempt to validate the modelling technique for ultrasonic cutting of toffee.

The study showed that ultrasonic cutting of toffee, using two cutting blades resonant at different operating frequencies, resulted in a reduction in cutting force with increased ultrasonic blade tip amplitude. The independent simulated FE predictions, using tensile and compression data, both showed similar findings for ultrasonic cutting of toffee at both operating frequencies. These findings are in agreement with other studies of ultrasonic cutting such as the one performed on Perspex earlier in this Chapter. Also, for ultrasonic cutting of toffee using compression material data as opposed to tensile material data, a small difference in predicted cutting force results for all simulated cutting trials, but this can be considered to be negligible.

At lower ultrasonic operating frequencies there is a larger spread in experimental cutting force data compared with cutting trials performed at a higher frequency for ultrasonic cutting of toffee. This could be attributed to various factors such as the higher oscillatory movement of the cutting blade, producing more impacts of the substrate material per second and producing a more controllable fracture event at the cut site which results in a more reproducible cutting force prediction. Alternatively, the higher oscillatory movement of the cutting blade could produce a higher localised temperature rise at the interface between the resonant blade and the material being cut. This effect could increase the temperature of the material at the interface above the melting temperature and instead of producing a fracture event at the cut site the cut mechanism could be a melting process which is more controllable. However, for ultrasonic cutting of food products this could be unwanted as the localised temperature increase could chemically change the material properties, leaving the product with an undesirable taste.

Studies using the average experimental cutting force for toffee at both operating frequencies indicate that an increase in cutting speed produces an increase in cutting force and as blade tip amplitude increases the cutting force decreases during ultrasonic cutting of toffee. These findings are significant as they illustrate how with some refinement of the FE model a set of optimal cutting parameters could be predicted for ultrasonic cutting of a particular product to ensure the cutting force or even localised temperature at the interface remains below or above a certain value allowing a process to be optimised for operational efficiency.

5.5 Conclusions

The research documented in this Chapter presents two novel modelling approaches to simulate ultrasonic cutting of single or multi-layered materials in the guillotine configuration; one using the debond modelling approach and one using the element erosion method. Both models are generic 2D fully coupled thermal-stress representations of the ultrasonic cutting process that allow the temperature and stress distribution at the interface to be investigated numerically to allow predictions of the effects of various blade tip parameters including cutting speed, blade tip amplitude and ultrasonic frequency on the temperature distribution within the cutting blade and material to be cut and also cutting force.

Both models utilise the symmetry condition about the cut axis for computational efficiency and represent both the blade tip and the material being cut as deformable bodies to allow temperature distribution of both to be determined. For further computational efficiency, a rigid body constraint is applied to the blade as the blade is assumed to be significantly more rigid and robust compared to the material being cut and deformation of the blade can be considered negligible. The oscillatory movement of the blade is included in the model by applying a sinusoidal oscillation at the required frequency at a specific blade tip amplitude. The cutting speed is represented in the model by applying a velocity to the specimen and moving the deformable body into the oscillating blade. Frictional contact is specified between the resonant blade and the material to be cut using a Columbic friction model with heat generation to allow the energy generated at the interface to be converted to heat in the simulation. The static and dynamic coefficients of friction were experimentally determined from Columbic friction experiments between the substrate material and a titanium block horn or the same material as used for the cutting blades. These parameters were determined with and without ultrasonic excitation of the block horn for incorporation into the FE models. The materials are represented in the debond model using either elastic-plastic material representations or a hyperelastic material definition. For the element erosion model the materials are represented using only the elastic-plastic material definition.

The debond modelling approach represents a theoretical crack tip in a specimen by tying the nodes on the cut axis to an analytical rigid line. When the blade is progressed onto this theoretical crack tip the nodes fail at the contact interface when the critical stress condition at a predetermined distance ahead of the crack tip has been reached and crack progression and

ultrasonic cutting is simulated. The critical stress and its distance ahead of the crack tip are determined from FE simulations of the SENB test by measuring the stress normal to the crack tip along the theoretical crack path using Irwin's model of crack tip plasticity. The numerical SENB test is validated against experimental SENB tests to provide confidence in the modelling approach for defining the failure criterion for the debond modelling approach.

The element erosion model uses a shear failure criterion specified in the model as a value between 0 and 1 representative of a location in the plastic region of the material definition of the substrate material. In the element erosion simulations an adaptive mesh is used which updates the deformed mesh automatically during the analysis to allow the numerical solution to converge smoothly, for computational efficiency and to minimise run time of the analysis. The models are generic in that by varying material properties of the blade and the substrate material the ultrasonic cutting process can be simulated to cut a variety of products and materials.

A preliminary study investigated ultrasonic cutting of single-layer materials using the 2D debond model for ultrasonic cutting of cheese and studied the effect of varying ultrasonic amplitude and excitation frequency on the cutting force. The preliminary study neglected any temperature effects at the interface between the resonant blade and the material but offered an insight into the suitability of the modelling approach. Results indicated that increasing blade tip amplitude increased the cutting force calculated from the simulations, however the mean cutting force remained unchanged. Also, varying the operating frequency of the simulations had no effect on the cutting force during cutting. These results provided a foundation for further exploration into the modelling technique for single-layer materials and also for incorporating temperature effects in the simulations to capture the process more fully. Exploration of the modelling technique to incorporate multi-layer materials was also explained to try to simulate ultrasonic cutting through complex material architectures.

Due to the highly computational intensive nature of the debond modelling technique and the restriction for expanding the modelling technique into a 3D modelling approach, an alternative modelling technique using the element erosion method was explored which could simulate ultrasonic cutting without requiring to pre-notch the specimen and could offer expansion of the technique into 3D if required. A preliminary study was performed comparing ultrasonic cutting of toffee at several cutting speeds using the debond modelling approach and the element erosion approach to gain confidence in the modelling technique and to investigate if both predicted

similar results for temperature distribution at the cut site. Results indicated similar trends of increasing cutting temperature at the interface as cutting speed is reduced and also similar temperature predictions at the cut site for both modelling techniques, but the element erosion method was more versatile and offered a faster, smoother solution to the problem. In addition to the faster computational time to produce the same solution as the debond modelling technique, the element erosion option could be expanded into 3D and offers the possibility of modelling ultrasonic cutting without needing to pre-notch the specimen. It was concluded that if adaptive meshing was available in the 2D debond model then computational time would be faster for the same solution, offer less convergence issues and offer a useful approach to simulating ultrasonic cutting. However, both these versatile models allow localised temperature distribution at the blade/material interface to be predicted on the surface of the cutting blade or at the material cut site, which is extremely useful to designers of ultrasonic cutting equipment as temperature measurements are currently difficult or impossible to determine as the high oscillatory movement of the cutting blade damages sensors.

A further preliminary investigation was performed using the 2D element erosion model to predict the effect of varying blade tip amplitude and operating frequency on the temperature at the blade tip for ultrasonic cutting of toffee. Findings indicated that as blade tip amplitude and operating frequency increased the blade tip temperature increased. These preliminary studies provided confidence in the modelling technique and offered confidence that the modelling technique could be used in the ultrasonic cutting blade design process to produce accurate predictions of cutting force and cut site temperature at the interface. Further research refined the modelling technique to minimise the mesh density of the 2D element erosion model to optimise computational run time whilst maintaining accuracy of the solution to allow predictions of the effects of varying cutting parameters on the cutting force and temperature distribution in the models.

Exploration of the 2D element erosion modelling technique into a 3D element erosion model was also discussed in detail in this Chapter. The 3D modelling technique offers the user the possibility of varying the same parameters as in the 2D modelling technique, including operating frequency, blade tip geometry, blade tip amplitude, material properties and cutting speed. However, the 3D model offers further flexibility in simulating ultrasonic cutting whereby non-symmetrical blades and blade tips, shaped specimens and complex cutting orientations can be simulated readily. This modelling technique is however very computationally intensive and often

requires a very refined mesh for high accuracy. Due to the high run times, studies of ultrasonic cutting using this model were not considered for this thesis but the modelling technique and advantages of this technique were presented for information and for the possibility of future researchers performing parametric studies using this modelling technique to capture ultrasonic cutting in various cutting configurations.

Validation of the 2D element erosion model was carried out by comparing ultrasonic cutting experiments performed on a specially designed linear axis high speed cutting rig with numerical simulations mimicking the experimental cutting trials. Initially the 2D element erosion model was validated for Perspex, a commonly used material with very stable and reproducible material properties. Determination of the mechanical properties of Perspex in tension at various temperatures was performed by experimental tensile tests using dog bone specimens. The mechanical properties were represented using an elastic-plastic material description at various temperatures and included in the FE simulation. A preliminary study investigated experimentally the effect of varying cutting speed and vibration velocity on ultrasonic cutting of Perspex. Findings indicated that as cutting speed increased the experimental cutting force increased and ultrasonic cutting was a more fracture dominated process at higher cutting speeds as opposed to a melting mechanism at lower speeds. Also, as vibration velocity increased there was a reduction in experimental cutting force. Temperature was also measured remote from the cut site using thermocouples embedded in the specimens and for cutting speeds in excess of 5mm/s there was a negligible increase in temperature above ambient. For lower cutting speeds temperature at the thermocouple was found to increase as cutting speed decreased. Initial comparisons of FE results for Perspex at 10 mm/s were compared with experimental results and were found to be within 10%.

The modelling technique was further explored to investigate multi-layer architectures consisting of Perspex, toffee and cheese and the effect cutting speed and vibration velocity had on cutting force and temperature. The experimental and FE results indicated that as the ultrasonic cutting blade progressed from one material to another a change in cutting force was measured. Varying blade tip vibration velocity during cutting of each layer was investigated using the 2D FE model to explore whether minimising the blade tip vibration velocity could minimise cutting force. The FE results indicated that cutting force was reduced for studies where the vibration velocity was reduced as it translated through different layers compared to an analysis performed using the same cutting speed and vibration velocity for all three layers. The study demonstrated the

possibility of using force feedback as a method of controlling ultrasonic cutting blade parameters during cutting to optimise cutting of multi-layered material architectures and offering improvements in ultrasonic cutting system efficiency.

A more detailed validation was performed for ultrasonic cutting of Perspex in the guillotine configuration for FE ultrasonic cutting simulations. Repeated experimental cutting trials were performed at several cutting speeds, ultrasonic frequencies and blade tip amplitudes to investigate the effect varying each parameter had on the measured cutting force. Cutting force predictions from the FE simulations aping the experimental trials were compared to the experimental cutting force to establish the quality of the comparison against actual tests. Results indicated that an increase in cutting speed produced a higher cutting force, an increase in blade tip amplitude produced a lower cutting force and an increase in ultrasonic operating frequency produced a lower cutting force. FE predictions were found to be similar to experimental cutting tests up to a cut depth of approximately 3mm, then the predicted cutting force was found to be lower than the actual experimental results.

Validation of the 2D element erosion modelling technique was also conducted for ultrasonic cutting of toffee at various cutting speeds, blade tip amplitudes and operating frequencies. Experimental cutting force determined from cutting tests performed on the linear axis ultrasonic cutting rig were compared to cutting force predictions from FE simulations of ultrasonic cutting of toffee, where the toffee was represented using initially tensile material data and subsequently compression material data.

This study presented experimental and numerical cutting force data for ultrasonic cutting of toffee using ultrasonic cutting blades tuned to an operating frequency of 20 kHz and 35 kHz. Cutting trials were experimentally performed on a linear high speed ultrasonic cutting rig and numerically simulated in the FE code ABAQUS. Experimental and numerical cutting trials for toffee were performed at cutting speeds of 5 mm/s and 10 mm/s for blade tip amplitudes of 40 μm and 70 μm for the 20 kHz blade and 23 μm and 40 μm for the 35kHz blade. Two simulated FE models for each test were performed (1) representing toffee using tensile data and (2) using compression data, and compared against experimental cutting in an attempt to validate the modelling technique for ultrasonic cutting of toffee. Findings indicated that increasing ultrasonic blade tip amplitude reduced the experimental and FE predicted cutting force at both operating frequencies, a trend that is similar in ultrasonic cutting of Perspex. The experimental cutting

force data indicated that as cutting speed increased the cutting force increased at both operating frequencies. The FE predicted results using both the compression and tensile material data show a negligible difference in predicting cutting force during the FE simulation and both predict a lower cutting force than actual experimental findings.

This Chapter has introduced two different modelling techniques that can be used to represent ultrasonic cutting. The studies within this thesis illustrate how FE modelling can be used to predict ultrasonic cutting parameters and subsequently can be used to optimise the ultrasonic cutting process. The modelling technique can be incorporated into the blade design process to predict the optimum ultrasonic cutting parameters required to cut a variety of materials to ensure the ultrasonic cutting blades designed are fit for purpose and optimal for cutting a particular material. With further work and refinement, the modelling technique could have a higher accuracy by incorporating more accurate material definitions and more accurate failure criteria to represent the process in more detail. The work described in this Chapter provides a foundation for further refinement of the modelling techniques to continue and for further studies to be researched to enhance this proposed methodology into the design process.

Chapter 6

Conclusions

This thesis reports on a method for including a computation FE model of the ultrasonic cutting process in the cutting blade design process. The inclusion of the FE modelling approach will enhance the cutting blade design process in an attempt to predict the optimum ultrasonic cutting parameters for cutting a substrate material prior to blade design and manufacture. This method could reduce the number of design iterations in the cutting blade design process offering time and cost savings to the blade manufacturer.

Until now there were limited FE representations of the ultrasonic cutting process with the models available restricted to the ultrasonic turning process. The current ultrasonic turning models were restricted to very fast cutting speeds and small cut depths due to the highly intensive computation requirements. Previously there were no specific FE simulations for ultrasonic cutting of single layer or multi layer food products. The research presented in this thesis represents the ultrasonic cutting process in the guillotine configuration using two different FE modelling approaches namely the debond model and the element erosion model. Both models are represented in the FE code ABAQUS as 2D fully coupled thermo stress models where temperature and stress is considered during the simulations. These modelling approaches allow the temperature at the cut site to be predicted using a variety of cutting parameters which are currently unavailable using real life experimental methods as sensors are often damaged at the interface. Knowledge of the temperature at the interface would be advantageous as localised temperature effects can be beneficial in some processes like ultrasonic cutting of food where a localised melt can give a highly attractive product that is appealing to the eye or unattractive in the ultrasonic cutting of bone as the necrosis temperature could be exceeded hindering bone regeneration. The contact conditions at the interface are specified using a Coulombic friction model where all energy generated due to friction is converted to heat and assumes that the temperature generated is equally distributed 50 % into the blade and 50 % into the substrate material. The coefficient of

friction at the interface is included in the models from experimental friction tests conducted on an ultrasonic block horn with and without superimposed ultrasonic oscillations.

Both models are generic and allow ultrasonic cutting to be simulated for a plethora of materials, including foodstuffs, and ultrasonic cutting conditions quickly and easily by adjusting particular variables in the FE simulations. The FE ultrasonic cutting models can be used to represent simple or complex multi-layered material architectures in a variety of orientations. The simulations allow slower cutting speeds and greater cut depths to be simulated in a more realistic timescale than are currently available.

The debond modelling method uses the implicit solver in ABAQUS standard and considers ultrasonic cutting to be a controlled crack propagation simulation through a material. The failure criterion is specified as a critical stress normal to the direction of crack propagation and ultrasonic cutting, at a pre-specified distance ahead of the crack tip. The failure conditions were predicted from FE simulations of the SENB test of the substrate material after comparison of the FE predictions of force and displacement of the simulation with real life experimental SENB tests. This modelling technique is restricted to simulating ultrasonic cutting using an indentation in the specimen and is often sensitive to convergence and mesh quality issues. This technique does not allow expansion of the modelling technique into a 3D simulation but offers an alternative approach to ultrasonic cutting.

The element erosion method uses the explicit solver in the FE package ABAQUS that was specifically designed to simulate high impact contact problems such as ultrasonic cutting. The failure of the substrate material was specified as a shear failure criterion at a location on the plastic region of the elastic-plastic stress-strain diagram for a material at a specific temperature and crosshead velocity. This method allows quicker convergence of the solution than the debond model and doesn't require the specimen to be pre-notched in the simulation. Mesh quality can also be automatically adjusted during the FE simulation offering a smoother simulation and faster run times. Expansion of this modelling technique is also possible to represent ultrasonic cutting as a 3D problem where ultrasonic cutting in the guillotine or slicing configurations can be represented or at complex cutting orientations.

Accurate representation of any simulation in an FE package is highly dependent on accurate material properties. Current availability of food material data is limited and are often represented

in compression due to testing difficulties in tension. This thesis includes mechanical properties data for the food materials toffee, cheese, chocolate and jelly in tension and compression at different environmental temperatures and crosshead velocities which are currently unavailable in the literature. Specially design moulds were designed and manufactured to produce high quality specimens for materials testing. Specially designed testing grips were manufactured to allow these food materials to be tested in tension by pulling dog bone shaped specimens under the radii of the specimens. The experimental testing results were averaged for each material and curve fitted using a polynomial curve fitting expression for inclusion in the elastic-plastic material model in the FE package ABAQUS. Findings indicate that the material properties for foodstuffs in tension are different than in compression and it would be advantageous to represent a food material in an FE package using combined tension and compression data to further increase the accuracy of the simulated process. Using the 3rd order reduced polynomial curve fitting expression for a hyperelastic material, compression and tension data were represented together for cheese. Simulations of the SENB test using the hyperelastic material representation and the elastic-plastic material representation were made to give confidence in the material representations. Preliminary simulations of ultrasonic cutting of cheese were studied using the hyperelastic material definition in the debond model to predict the cutting force during ultrasonic cutting. Thermal properties for the food materials were also included in the simulations such as specific heat capacity and thermal conductivity to allow the temperature distribution to be predicted in the FE simulations. The specific heat capacity was determined for toffee and cheese on a DSC and the thermal conductivity was found by testing using a Fox 50 thermal conductivity machine.

Validation of the 2D element erosion model was attempted by comparing force and temperature results from experimental cutting trials with FE predictions. Experimental cutting trials were performed on a specially designed linear axis ultrasonic cutting rig where cutting force was measured using a load cell and cut site temperature in the substrate specimens could be measured remote from the cut site using thermocouples. Two ultrasonic cutting blades were designed using FEA to resonate in the longitudinal mode at 20 kHz and 35 kHz where the blade tip geometry was the same for both blades to allow a comparison of cutting force at different frequencies to be studied. The ultrasonic cutting blades were designed and tuned to the longitudinal mode using FEA and manufactured using CAD/CAM technology. After manufacture the blades were validated using EMA to check the dynamic response of the manufactured blades where the mode shape and the natural frequencies were compared to those predicted using FEA. The

manufactured blades resonated in the longitudinal mode at natural frequencies similar to those predicted using FEA with errors in the range of 200 to 500 Hz outside the predicted driving frequency.

This document reports on a preliminary investigation using the 2D debond model to simulate ultrasonic cutting of cheese for variable ultrasonic amplitudes and operating frequencies. Temperature effects in the model were neglected and findings indicated as ultrasonic blade tip amplitude increased the cutting force increased and the adjusting the operating frequency had no effect on the predicted cutting force.

Further studies compared the temperature results produced for ultrasonic cutting of toffee at various cutting speeds using the debond model and the element erosion model. Findings indicated similar temperature results and temperature distribution in the ultrasonic cutting blade and the cut material in addition to similar trends of increasing cutting temperature at the interface as cutting temperature is reduced which provided confidence in both of the modelling approaches and the element erosion model was further pursued due to the faster run times and smoother convergence of the solution.

Other studies documented in this thesis used the 2D element erosion model to predict the effect that varying the blade tip amplitude and operating frequency had on the temperature at the blade tip for ultrasonic cutting of toffee. Results indicated that as the blade tip amplitude and driving frequency of the cutting blade increased the temperature increased at the cutting blade tip.

Validation of the 2D element erosion model was performed by comparing ultrasonic cutting trials executed on the linear axis ultrasonic cutting rig using the two ultrasonic cutting blades designed using FEA with FE simulations mimicking the experimental cutting trials. Prior to validation of the 2D element erosion model simulating ultrasonic cutting of foodstuffs, validation was attempted using ultrasonic cutting of Perspex. For FE modelling purposes determination of the mechanical properties of Perspex in tension at different environmental test temperatures and crosshead velocities were required. Experimental tensile tests were performed at testing temperatures up to 110°C and the stress-strain curves produced from the experiments were curve fitted using the polynomial curve fitting representation and implemented in the FE package using the elastic-plastic material definition. Experimental findings for ultrasonic cutting on Perspex indicated that as cutting speed and vibration velocity increased the cutting force increased. At

higher cutting speeds the cutting mechanism was more fracture dominated compared to a combination of cutting and melting at lower cutting speeds. As vibration velocity increased the experimental cutting force decreased at each cutting speed and frequency tested. Temperature measured remote from the cut site for cutting speeds in excess of 5 mm/min produced a negligible temperature rise in the material. Findings indicated that as cutting speed decreased the temperature in the material increased. Initial comparisons of the experimental cutting force with the cutting force predicted from FEA illustrated simulated cutting force predictions in the region of 10 % lower than the actual experimental results.

Ultrasonic cutting of multi-layer material architectures consisting of Perspex, cheese and toffee was investigated to explore the effect cutting speed and vibration velocity had on cutting force. Both the FE simulations and experimental cutting trials indicated a change in cutting force as the blade progressed from one layer to another. Possible variation of vibration velocity during cutting of a particular material was explored using the 2D element erosion model to investigate if adjusting blade tip vibration velocity could minimise cutting force during ultrasonic cutting and also if force feedback could be used to control ultrasonic cutting blade parameters when cutting through multi-layer material architectures to optimise the cutting process. FE predictions indicated that cutting force was reduced compared to simulations performed using the same cutting speed and a fixed vibration velocity for each layer.

Further validation of ultrasonic cutting of Perspex was performed comparing the cutting force from experimental cutting trials at different cutting speeds, blade tip amplitudes and operating frequencies with FE simulations. Experimental and FE predictions indicated that as cutting speed increased cutting force increased, as blade tip amplitude increased the cutting force decreased. The FE predictions for cutting force were similar to the experimental cutting force up to a cut depth of approximately 3mm then the predicted cutting force was lower than the experimental results.

Validation of the FE simulations for ultrasonic cutting of toffee was also performed where the toffee was represented in the FE package ABAQUS using either tensile or compression data. As the blade tip amplitude was increased the cutting force predicted using FE simulations and experimentally decreased at both operating frequencies. Also, as cutting speed increased the cutting force decreased in both the experimental and FE simulations. Using either tensile or compression data in the FE package to simulate ultrasonic cutting produced a negligible

difference in cutting force and FE predictions for cutting force were lower than the actual experimental findings.

Further exploration of simulating ultrasonic cutting in 3D was also discussed in this thesis to allow predictions for ultrasonic cutting in different cutting orientations such as slicing. Due to the highly intensive computational nature of the modelling technique and subsequently long run times studies using the 3D element erosion model were not included in this thesis but the model creation is discussed to allow other researchers possibly to pursue studies of ultrasonic cutting in the future.

The research documented in this thesis provides a basis for the inclusion of FE simulations of the ultrasonic cutting process to be included in the cutting blade design process which could predict optimum cutting parameters for the cutting tool prior to tool design. The studies described in this thesis provide the foundation work for validation of the ultrasonic cutting simulations and provide confidence that with further refinement of the modelling techniques described in this thesis the FE simulations would be an advantageous tool to add to the ultrasonic tool designer's arsenal.

Chapter 7

Future Work

The research conducted in this thesis has considered integrating a modelling concept of ultrasonic cutting into the ultrasonic cutting blade design process to enhance blade design and performance. Several distinct areas of research have been incorporated in this thesis and have provided a stable platform for which further exploration of the modelling of ultrasonic cutting using the finite element method and on the determination of the thermal and mechanical properties of foodstuffs can be progressed.

Investigating the mechanical and thermal properties of a larger variety of food products using the experimental testing techniques discussed in this thesis could allow a database of properties to be collated for use in a variety of engineering problems or for modelling problems involving food products such as cutting or mastication. Conducting the experimental tests on foods using a non contact strain measuring device would provide more accurate results for the mechanical properties that could be used in the FE simulations.

Future research considerations should include expanding the debond modelling approach of ultrasonic cutting to include automatic adaptive meshing which has just became available in the new version of ABAQUS 6.7. This will allow the mesh to adapt automatically during the solution which could reduce solver iteration problems and provide a faster more flexible solution to modelling ultrasonic cutting.

The 2D modelling approach using the element erosion method could be used to study the effect of horn material on the temperature at the interface between the blade and the material to be cut. Also, the effect blade tip geometry and various blade tip angles have on the reaction force and temperature at the cut site could also be investigated.

Further refining of both 2D modelling approaches of ultrasonic cutting would provide an accurate representation of cutting force at deeper cut depths and also enhance the temperature prediction remote from the cut site to give a more detailed representation of temperature distribution in the specimen and on the blade.

Further exploration of the 3D modelling approach to ultrasonic cutting would allow cutting to be captured in the through-thickness direction, which would be a great benefit. This will allow complex non-symmetrical blade and specimen shapes to be investigated numerically and offer the possibility to study ultrasonic cutting at various cutting angles also. Studies of ultrasonic cutting in the slicing configuration could be explored using this 3D model.

Incorporating not only single or multi-layered food products in the FE modelling technique but investigating cutting of porous, non-homogenous food products would also be advantageous as most products being cut have very complex material architectures.

For all FE modelling techniques of ultrasonic cutting, using a larger number of frames during the cutting process would allow a more detailed and more accurate capture of the force and temperature distribution during cutting. This currently is restricted to time for the solution to be completed but further refinement of the modelling technique and the mesh in addition to advances in computational power could allow faster run times of the analysis.

Appendix I: References

[1] Abramov O.V., High Intensity Ultrasonics Theory and Industrial Applications: Gordon and Breach Science Publishers (1998).

[2] Povey M.J.W., Mason T.J., editors, Ultrasound in Food Processing, London: Blackie Academic (1998)

[3] Povey M.J.W., Determination of Food Materials. In: Povey M.J.W., Mason T.J., editors, Ultrasound in Food Processing, London: Blackie Academic (1998) 30-56

[4] McClements D.J., Particle Sizing of Food Emulsions Using Ultrasonic Spectrometry: Principals, Techniques and Applications. In: Povey M.J.W., Mason T.J., editors, Ultrasound in Food Processing, London: Blackie Academic (1998) 85-103

[5] Robins M.M., Ultrasonic Monitoring of Shelf Life in Food Emulsions. In: Povey M.J.W., Mason T.J., editors, Ultrasound in Food Processing, London: Blackie Academic (1998) 219-233

[6] http://en.wikipedia.org/wiki/Doppler_Effect; 26/4/07

[7] http://en.wikipedia.org/wiki/Nondestructive_testing; 26/4/07

[8] Ridgway J., Henthorn K.S., Hull J.B., Controlling Overfilling in Food Processing. In: Povey M.J.W., Mason T.J., editors, Ultrasound in Food Processing, London: Blackie Academic (1998) 1-16

[9] Benedito J., Carcel J.A., Gonzalez R., Mulet A., Application of Low Intensity Ultrasonics to Cheese Manufacturing Processes, Ultrasonics Vol. 40, (2002), 19-23.

[10] http://www.suhr.dk/anglecuttingmachines.html, 15/3/05

[11] http://www.amgas.com/sonpage2.htm, 15/3/05

[12] http://www.agfm.com/Cutting3D/intro.htm, 15/3/05

[13] http://www.ultrasonic-eng.co.uk/default.htm, 15/3/05

[14] http://www.matiss.com/eg/matissonic/ultrasonic-cutting-speed.htm, 15/3/05

[15] http://www.gildemeister.com; 26/4/07

[16] http://www.branson-plasticsjoin.com/applications_food.asp; 26/4/07

[17] http://www.dukcorp.com/us/products/thermo/fabfilm/cutting.htm; 26/4/07

[18] http://www.dukcorp.com/us/products/food/whatisFP.htm; 26/4/07

[19] http://www.ethiconendo.com/ultrasonic.jsp; 26/4/07

[20] http://en.wikipedia.org/wiki/HIFU; 26/4/07

[21] http://www.freepatentsonline.com/5359996.html, 15/3/05

[22] http://www.wchstv.com/newsroom/healthyforlife/1926.shtml, 21/6/05

[23] Earnshaw R.G., Ultrasound: A New Opportunity for Food Preservation. In: Povey M.J.W., Mason T.J., editors, Ultrasound in Food Processing, London: Blackie Academic (1998) 183-192

[24]http://www.foodmanufacture.co.uk/news/fullstory.php/aid/1238/The_tender_sound_of_ultrasonics.html, 2/8/05

[25] Gallego-Juarez J.A., Some Applications of Air-Borne Power Ultrasound to Food Processing. In: Povey M.J.W., Mason T.J., editors, Ultrasound in Food Processing, London: Blackie Academic (1998) 127-143

[26] Tarleton E.S., Wakeman R.J., Ultrasonically Assisted Separation Processes. In: Povey M.J.W., Mason T.J., editors, Ultrasound in Food Processing, London: Blackie Academic (1998) 193-217

[27] Mason T.J., Power Ultrasound in Food Processing – The Way Forward In: Povey M.J.W., Mason T.J., editors, Ultrasound in Food Processing, London: Blackie Academic (1998) 105-125

[28] Rawson F.F., An Introduction to Ultrasonic Food Cutting. In: Povey M.J.W., Mason T.J., editors, Ultrasound in Food Processing, London: Blackie Academic (1998) 254-269

[29] Quartly-Watson T., The Importance of Power Ultrasound in Cleaning and Disinfection in the Poultry Industry – A Case Study. In: Povey M.J.W., Mason T.J., editors, Ultrasound in Food Processing, London: Blackie Academic (1998) 144-150

[30] Leighton T.G., The Principals of Cavitation. In: Povey M.J.W., Mason T.J., editors, Ultrasound in Food Processing, London: Blackie Academic (1998) 151-178

[31] http://www.healthsonics.com/houke.htm, 21/6/05

[32] http://www.foodscience.afisc.csiro.au/pressure-processes.htm, 2/8/05

[33] Hunter G., Lucas M., Watson I., Parton R., A Radial Mode Ultrasonic Horn for the Inactivation of Escherichia Coli K12, Ultrasonics Sonochemistry, (2007), In Press

[34] Rayleigh J.W.S., Lindsay R.B., The Theory of Sound, Dover Publications (1976).

[35] Savart F., Translated in Lindsay (1974). Annals of Physical Chemistry, vol. 20, (1830), 290

[36] Galton F., Nature, vol. 27, I3, (1883)

[37] Koenig R., Annals of Physical Chemistry, Vol. 69, (1899) 626, 721.

[38] Curie J.-P, Curie P., Translated in Lindsay (1973), Académie des sciences Paris, vol..91, (1880), 294.

[39] Graff K.F., Physical Acoustics – Chapter 1. A History of Ultrasonics, Academic Press (1981).

[40] Mason W.P., Piezoelectricity, its History and Applications, Journal of the Acoustic Society of America, Vol. 70, (1981) 1568-95.

[41] Berlincourt D., Piezoelectric Ceramics: Characteristics and Applications, Journal of the Acoustic Society of America, Vol. 70, (1981), 1561-6.

[42] Damjanovic D., Ferroelectric, Dielectric and Piezoelectric Properties of Ferroelectric Thin Films and Ceramics, Rep. Prog. Phys., Vol. 61, (1998) 1267-1324.

[43] Grupp D.E., Goldman A.M., Giant Piezoelectric Effect in Strontium Titanate at Cryogenic Temperatures, Science, Vol. 276, (1997), 392-4.

[44] Sokolov S., Means for Indicating Flaws in Materials, No.US 2, 164, 125, (1939).

[45] Nepiras E.A., Report on Ultrasonic Machining, Metalworking Production, Vol. 100, (1956), 1283-8.

[46] Astashev V.K., Babitsky V.I., Ultrasonic Cutting as a Nonlinear (Vibro-Impact) Process, Ultrasonics 36 (1998) 89-96

[47] Liu K., Li X.P., Rahman M., Liu X.D., Study of Ductile Mode Cuttign in Grooving of Tungsten Carbide With and Without Ultrasonic Vibration Assistance, International Journal of Manufacturing Technology Vol.24 (2004) 389-394

[48] Neugebauer R., Stoll A., Ultrasonic Application in Drilling, Journal of Materials Processing Technology 149 (2004) 633-639

[49] Pei Z.J., Ferreira P.M., An Experimental Investigation of Rotary Ultrasonic Face Milling, International Journal of Machine Tools and Manufacture 39 (1999) 1327-1344

[50] Zhao B., Liu C.S., Zhu X.S., Xu K.W., Research on the Vibrating Cutting Performance of Particle Reinforced Metallic Matrix Composites SiCp/Al, Journal of Materials Processing Technology 129 (2002) 380-384

[51] Thoe T.B., Aspinwall D.K., Wise M.L.H., Review on Ultrasonic Machining, Journal of Machine Tools and Manufacture Vol. 38 No 4 239-255 (1998)

[52] Churi N.J., Pei, Z.J., Treadwell C., Rotary Ultrasonic Machining of Titanium Alloy: Effects of Machining Variables, Machining Science and Technology (2006) Vol. 10 301-321

[53] Balamuth L., Method of Abrading (1948) no.602801

[54] http://www.gildemeister.com; 26/4/07

[55] Pei Z.J., Ferreira P.M., Kapoor S.G., Haselkorn M., Rotary Ultrasonic Machining for Face Milling of Ceramics, International Journal of Machine Tools and Manufacture, Vol. 35 No. 7 (1995) 1033-1046

[56] Suzuki N., Nakamura A., Shamoto E., Harada K., Matsuo M., Osada M., Ultraprecision Micromaching of Hardened Steel by Applying Ultrasonic elliptical Vibration Cutting, International Symposium on Micromechatronics and Human Science (2003)

[57] Huang H., Zhang H., Zhou L., Zheng H.Y., Ultrasonic Vibration Assisted Electro-discharge Machining of Microholes in Nitinol, Journal of Micromechanics and Microengineering Vol. 13 (2003) 693-700

[58] Wansheng Z., Zhenlong W., Shichun D., Guanxin C., Hongyu W., Ultrasonic and Electric Discharge Machining to deep and Small Hole in Titanium Alloy, Journal of Materials Processing Technology Vol. 120 (2002) 101-106

[59] Jin M., Murakawa M., Development of a Practical Ultrasonic Vibration Cutting Tool System, Journal of Materials Processing Technology Vol. 113 (2001) 342-347

[60] Japitana F.H., Morishige K., Takeuchi Y., Six-Axis Controlled Ultrasonic Vibration Cutting in Fabrication of a Sharp Corner, International Journal of Advanced Manufacturing Technology, Vol. 21 (2003) 564-570

[61] Guzzo P.L., Rasian A.A., De Mello J.D.B., Relationship Between Quartz Crystal Orientation and the Surface Quality Obtained by Ultrasonic Machining, Joint Meeting EFTF-IEEE IFCS (1999) 792-795

[62] Xiao M., Sato K., Karube S., Soutome T., The Effect of Tool Nose Radius in Ultrasonic Vibration Cutting of Hard Metal, International Journal of Machine Tools and Manufacture Vol. 43 (2003) 1375-1382

[63] Zhao B., Liu C.S., Zhu X.S., Xu K.W., Research on the Vibration Cutting Performance of Particle Reinforced Metallic Matrix Composites SiCp/Al, Journal of Materials Processing Technology Vol. 129 (2002) 380-384

[64] Zhang C., Rentsch R., Brinksmeier E., Advances in Micro ultrasonically Assisted Lapping of Microstructures in Hard-Brittle Materials: A Brief Review and Outlook, International Journal of Machine Tools and Manufacture Vol. 45 (2005) 881-890

[65] Ichida Y., Sato R., Morimoto Y., Kobayashi K., Material Removal Mechanisms in Non-Contact Ultrasonic Abasive Machining, Wear, Vol. 258 (2005) 107-114

[66] Wang X., Zhou M., Gan G.K., Ngoi B., Theoretical and Experimental Studies of Ultraprecision Machining of Brittle Materials with Ultrasonic Vibration, International Journal of Advanced Manufacturing Technology, Vol. 20 (2002) 99-102

[67] Zeng W.M., Li Z.C., Pei Z.J., Treadwell C., Experimental Observation of Tool Wear in Rotary Ultrasonic Machining of Advanced Ceramics, International Journal of Machine Tools and Manufacture Vol. 45 (2005) 1468-1473

[68] Wiercigroch M., Neilson R.D., Player M.A., Material Removal Rate Prediction for Ultrasonic Drilling of Hard Materials Using an Impact Oscillator Approach, Physics Letters A Vol. 259 (1999) 91-96

[69] Lee T.C., Chan C.W., Mechanism of the Ultrasonic Machining of Ceramic Composites, Journal of Materials Processing Technology Vol. 71 (1997) 195-201

[70] Schmutz J., Brinksmeier E., Bischoff E., Sub-Surface Deformation in Vibration Cutting of Copper, Journal of the International Societies for Precision Engineering and Nanotechnology Vol. 25 (2001) 218-223

[71] Babitsky V.I., Astashev V.K., Kalashnikov A.N., Autoresonant Control of Nonlinear Mode in Ultrasonic Transducer for Machining Applications., Ultrasonics 42 (2004) 29-35

[72] Miller G.E., Special Theory of Ultrasonic Machining, Journal of Applied Physics, Vol. 28, No. 2, (1957), 149 – 156

[73] Sinn G., Zettl B., Mayer H., Stanzl-Tschegg S., Ultrasonic-Assisted Cutting of Wood, Journal of Materials Processing Technology Vol. 170 (2005) 42-49

[74] Sinn G., Zettl B., Mayer H., Stanzl-Tschegg S., Surface Properties of Wood and MDF after Ultrasonic-assisted Cutting, Journal of Materials Science Vol.40 (2005) 4325-4332

[75] Volkov S.S., Sannikov D.V., Ultrasonic Cutting of Polymeric Materials Svarochnoe Proizvodstvo Vol. 10 (2001) 31-34

[76] Kuriyama Y., Kikura K., Sajima T., Cutting and Dividing Device for Timber, Wood Material and Plastic Using an Ultrasonic Vibration Cutting Tool Patent No JP2004243425 (2004)

[77] Kim J.D., Choi I.H., Micro Surface Phenomenon of Ductile Cutting in the Ultrasonic Vibration Cutting of Optical Plastics, Journal of Materials Processing Technology Vol.68 (1997) 89-98

[78] Zhou M., Wang X.J., Ngoi B.K.A., Gan J.G.K., Brittle-Ductile Transition in the Diamond Cutting of Glasses With the Aid of Ultrasonic Vibration, Journal of Materials Processing Technology Vol.121 (2002) 243-251

[79] Giraud J.Y., Villemin S., Darmana R., Cahuzac J.P.H., Autefage A., Morucci J.P., Bone Cutting, Clinical Physics and Physiological Measurement, Vol.12 no.1 (1991) 1-19

[80] Lal A., White R.M., Silicon Micromachined Ultrasonic Micro-Cutter, Ultrasonics Symposium IEEE (1994) 1907-1911

[81] Lal A., White R.M., Micromachined Silicon Needle for Ultrasonic Surgery, Ultrasonics Symposium IEEE (1995) 1593-1596

[82] Lal A., White R.M., Optimisation of Silicon Longitudinal Mode Ultrasonic Actuators, with Application to Surgery, Transducers '97 IEEE, International Conference on Solid-State Sensors and Actuators (1997) 57-60

[83] Arai F., Amano T., Fukuda T., Satoh H., Microknife Using Ultrasonic Vibration, 2000 International Symposium on Micromechatronics and Human Science, (2000) 195-200

[84] Arai F., Amano T., Fukuda T., Satoh H., Mechanical Micro-Dissection by Microknife Using Ultrasonic Vibration and Fine Touch Probe Sensor, Proceedings of the 2001 IEEE International Conference on Robotics and Automation Seoul, Korea, 2001 139-144

[85] Sun D, Zhou Z.Y., Liu Y.H., Development and Application of Ultrasonic Surgical Instruments, IEEE Transactions on Biomedical Engineering Vol. 44 (1997)

[86] Williams A.R., Walmsley A.D., Experimentry of Low-Frequency Ultrasonic Dental Devices, IEEE Trans Ultrasonic Vol. 35 (1998)

[87] Waplington M., Blunt L., Walmsley A.D., Lumley P.J., Dental Hard Tissue Cutting Characteristics of an Ultrasonic Drill, International Journal of Machine Tools Manufacture, Vol. 35, No 2., (1995), 339-343.

[88] Kirk W.B., A Quarter Century of Ultrasound Technology, Ultrasound Medical Biol, Vol. 18 (1992)

[89] MacBeath A., Ultrasonic Bone Cutting, Department of Mechanical Engineering University of Glasgow, (2006), 17

[90] Zahn S., Schneider Y., Zucker G., Rohm H., Impact of Excitation and Material Parameters on the Efficiency of Ultrasonic Cutting of Bakery Products, Journal of Food Science Vol. 70 No.9 (2005) 510-513

[91] Cardoni A., Lucas M., Strategies for Reducing Stress in Ultrasonic Cutting Systems, Strain Vol. 41 (2005) 11-18

[92] Knorr D., Zenker M., Heinz V., Lee D.U., Applications and Potential of Ultrasonics in Food Processing, Trends in Food Science and Technology Vol. 15 (2004) 261-266

[93] Schneider Y., Zahn S., Linke L., Qualitative Process Evaluation for Ultrasonic Cutting of Food, Engineering Life Sciences Vol. 2 (2002) 153-157

[94] Rawson F.F., An Introduction to Ultrasonic Food Cutting. In: Povey M.J.W., Mason T.J., editors, Ultrasound in Food Processing, London: Blackie Academic (1998) 254-269

[95] Henning A., Cutting With High-Pressure Jet in the Food Industry, Fleischwirtschaft, Vol. 78, No. 1, (1998), 43-46.

[96] Alitavoli M., McGeough J.A., An Expert Process Planning System For Meat Cutting by High Pressure Water Jet, Journal of Materials Processing Technology, Vol. 76, (1998), 146-152.

[97] de Silva C.W., Gu J.H., On-line Sensing and Modelling of Mechanical Impedance in Robotic Food Processing, IEEE, (1995), 1693-1698.

[98] An Innovative Machine for Automated Cutting of Fish, IEEE/ASME Transactions on Mechatronics, Vol. 2, No. 2, (1997), 1083-4435.

[99] Cartmell M.P., Lim F.C.N., Cardoni A., Lucas M., Optimisation of the Vibrational Response of Ultrasonic Cutting Systems, Journal of Applied Mathematics Vol.70 (2005) 645-656

[100] Lucas M., Cardoni A., Cartmell M.P., Lim F.C.N., Controlling the Effects of Modal Interactions in Ultrasonic Cutting Devices, World Congress on Ultrasonics, Paris, France, (2003)

[101] Cardoni A., Lucas M., Cartmell M.P., Lim F.C.N., A Novel Multiple Blade Ultrasonic Cutting Device, Ultrasonics, Vol. 42, (2004), 69-74

[102] Cardoni A., Lucas M., Enhanced Vibration Performance of Ultrasonic Block Horns, Ultrasonics, (2002), Vol. 40, No. 1-8, 365-369

[103] Graham G., Petzing J.N., Lucas M., Modal Analysis of Ultrasonic Block Horns by ESPI, Ultrasonics, Vol. 37, (1999), 149-157

[104] Lucas M., Smith A.C., Redesign of Ultrasonic Block Horns for Improved Vibration Performance, Transactions of the ASME, Journal of Vibration and Acoustics, Vol. 119, No. 3, (1997), 410-414

[105] Lucas M., Petzing J.N., Cardoni A., Smith L., Design and Characterisation of Ultrasonic Cutting Tools, Annals of CIRP, Vol. 50, (2001), 149-152

[106] Lucas M., Graham G., Smith A.C., Enhanced Vibration Control of an Ultrasonic Cutting Process, Ultrasonics, Vol. 34, No. 2-5, (1996), 205-211

[107] Lim F.C.N., Cartmell M.P., Cardoni A., Lucas M., A Preliminary Investigation into Optimising the Response of Vibrating Systems Used for Ultrasonic Cutting, Journal of Sound and Vibration, Vol. 272, No.3-5, (2004), 1047-1069

[108] Cardoni A., Lucas M., Design of Ultrasonic Block Horns by Finite element Analysis, 18th International Cape Conference, Edinburgh, UK, (2003)

[109] Lucas M., Cardoni A., Lim F.C.N., Cartmell M.P., Effects of Modal Interactions on Vibration Performance in Ultrasonic Cutting, CIRP Annals, Vol.52, No.1, (2003), 193-196

[110] Lucas M., Cardoni A., MacBeath A., Temperature Effects in Ultrasonic Cutting of Natural Materials, CIRP Annals, Vol. 54, No.1, (2005), 195-198

[111] Cardoni A., Lucas M., Cartmell M.P., Lim F.C.N., Nonlinear and Parametric Vibrations in Ultrasonic Cutting Systems, Materials Science, Vol. 440-441, (2003), 397-404

[112] Lucas M., Chapman G.M., Vibration Analysis at Ultrasonic Frequencies, American Society of Mechanical Engineers, Design Engineering Division, Montreal, Vol. 18, (1989), 235-240

[113] Chapman G.M., Lucas M., Frequency Analysis of an Ultrasonically Excited Thick Cylinder, International Journal of Mechanical Sciences, Vol. 32, No. 3, (1990), 205-214

[114] Graham G., Petzing J., Lucas M., Tyrer J.R, Qualitative Modal Analysis Using Electronic Speckle Pattern Interferometry, Optics and Lasers in Engineering, Vol. 31, No. 2, (1999), 147-161

[115] Graham G., Petzing J., Lucas M., Tyrer J.R., Whole-Field Modal Analysis Using Electronic Speckle Pattern Interferometry, Proceedings of SPIE – The International Society for Optical Engineering, Washington, Vol. 2868, (1996), 352-361

[116] Lucas M., Vibration Sensitivity in the Design of Ultrasonic Forming Dies, Ultrasonics, Vol. 34, No.1, (1996), 35-41

[117] Merkulov L.G., Design of Ultrasonic Concentrations, Soviet Physical Acoustics, Vol. 3, (1957), 230-238

[118] Ensminger D., Solid Cone in Longitudinal Half-Wave Resonance, The Journal of the Acoustical Society of America, Vol. 32, No. 2, (1960), 194-196

[119] Neppiras E., Mechanical Transformers for Producing Very Large Motion, Acoustica, Vol. 13, (1963), 368-370

[120] Belford J.F., The Stepped Horn, Proceedings of the National Electronics Conference, Chicago, (1960), 814-822

[121] Amza G., Drimer D., The Design and Construction of Solid Concentrators for Ultrasonic Energy, Ultrasonics, Vol. 9, (1976), 223-226

[122] Satyanarayana A., Krishna R.B.G., Design of Velocity Transformers for Ultrasonic Machining, Electrica India, (1984), 11-20

[123] Muhlen S.S., Design of an Optimized High-Power Ultrasonic Transducer, Ultrasonics Symposium, Brazil, (1990), 1631-1634

[124] Derks P.L.L.M., The Design of Ultrasonic Resonators with Wide Output Cross-sections, Eindhoven University of Technology, (1984)

[125] Pis P., Balaz I., Minarik M., Design of an Ultrasonic Concentrator, Journal of Electrical Engineering, Vol. 48, No. 5-6, (1997), 131-139

[126] Amin S.G., Ahmed M.H.M., Youssef H.A., Computer-Aided Design of Acoustic Horns for Ultrasonic Machining Using Finite Element Analysis, Journal of Materials Processing Technology, Vol. 55, (1995), 254-260

[127] Lin S., Sandwiched Piezoelectric Ultrasonic Transducers of Longitudinal-Torsional Compound Vibrational Modes, IEEE Transactions on Ultrasonics, Ferroelectrics and Frequency Control, Vol. 44, No. 6, (1997), 1189-1197

[128] Zhou G., Zhang Y., Zhang B., The Complex-Mode Vibration of Ultrasonic Vibration Systems, Ultrasonics, Vol. 40, No. 1-8, (2002), 907-911

[129] Tsujino J., Ihara S., Harada Y., Kasahara K., Sakamaki N., Characteristics of Coated Copper Wire Specimens Using High Frequency Ultrasonic Complex Vibration Welding Equipments, Ultrasonics, Vol. 42, (2004), 121-124

[130] Hongoh M., Yoshikuni M., Hashi H., Ueoka T., Tsujino J., Welding Characteristics of 67kHz Ultrasonic Plastic Welding System Using Fundamental and Higher-Resonance-Frequency Vibrations, Japanese Journal of Applied Physics, Part 1: Regular Papers and Short Notes and Review Papers, Vol. 42, No. 5B, (2003), 2981-2985

[131] Ueoka T., Tsujino J., Welding Characteristics of Aluminium and Copper Plate Specimens Welded by a 19 kHz Complex Vibration Ultrasonic Seam Welding System, Japanese Journal of Applied Physics, Part 1: Regular Papers and Short Notes and Review Papers, Vol. 41, No. 5B, (2002), 3237-3242

[132] Tsujino J., Ueoka T., Sano T., Welding Characteristics of 27 kHz and 40 kHz Complex Vibration Ultrasonic Metal Welding Systems, Proceedings of the IEEE Ultrasonics Symposium, Caesars Tahoe, USA, Vol. 1, (1999), 773-778

[133] Tsujino J., Harada Y., Sano T., Ultrasonic Complex Vibration Welding Systems of 100 kHz to 200 kHz with Large Welding Tip Area for Packaging in Microelectronics, Proceedings of the IEEE Ultrasonics Symposium, Atlanta, Vol. 1, (2001), 665-668

[134] Sherrit S., Askins s.A., Gradziol M., Dolgin B.P., Bao X., Chang Z., Bar-Cohen Y., Novel Horn Designs for Ultrasonic/Sonic Cleaning, Welding, Soldering, Cutting and Drilling, Smart Structures and Materials, Proceedings of SPIE, Vol. 4701, (2002), 353-360

[135] Wakako R., Hashimoto M., Development of Ultrasonically Activated Bending Scalpel for Endoscopic Surgery, Proceedings of the 2002 IEEE/RSJ International Conference on Intelligent Robots and Systems, (2002), 1415-1420

[136] Schneider Y., Zahn S., Hofmann J., Wecks M., Rohm H., Acoustic Cavitation Induced by Ultrasonic Cutting Devices: A Preliminary Study, Ultrasonics Sonochemistry, Vol. 13, (2006), 117-120

[137] Nesvadba P., Thermal and Other Physical Properties of Foods: Needs for Data and For Standards, Letter to the Editor: International Journal of Food Science and Technology, Vol. 31, (1996), 295-296.

[138] Nesvadba P., Houska M., Wolf W., Gekas V., Jarvis D., Sadd P.A., Johns A.I., Database of Physical Properties of Agro-Food Materials, Journal of Food Engineering, Vol. 61, (2004), 497-503.

[139] Ogunjimi L.A.O., Aviara N.A., Aregbesola O.A., Some Engineering Properties of Locust Bean Seed, Journal of Food Engineering, Vol. 55, (2002), 95-99.

[140] Singh K.K., Goswami T.K., Mechanical Properties of Cumin Seed (Cuminum Cyminum Linn) Under Compressive Loading, Journal of Food Engineering, Vol. 36, (1998), 311-321.

[141] Ozguven F., Vursavus K., Some Physical, Mechanical and Aerodynamic Properties of Pine (Pinus Pinea) Nuts, Journal of Food Engineering, Vol. 68, I2, (2005), 191-196.

[142] Omobuwajo T.O., Akande E.A., Sani L.A., Selected Physical, Mechanical and Aerodynamic Properties of African Breadfruit (Treculia Arficana) Seeds, Journal of Food Engineering, Vol. 40, (1999), 241-244.

[143] Baryeh E.A., Physical Properties of Millet, Journal of Food Engineering, Vol. 51, (2002), 39-46.

[144] Zhang Q., Yang W., Sun Z., Mechanical Properties of Sound and Fissured Rice Kernels and their Implications for Rice Breakage, Journal of Food Engineering, Vol. 68, (2005), 65-72.

[145] Vursavus K., Ozguven F., Mechanical Behaviour of Apricot Pit Under Compression Loading, Journal of Food Engineering, Vol. 65, (2004), 255-261.

[146] Eves A., Kilcast D., The Texture of Confectionary, Chemistry and Industry, (1992), 95-97.

[147] Aguilera J.M., Materials and Structures of Foods, Design and Nature, Vol. 57, (2002), 391-400.

[148] Ross K.A., Scanlon M.G., A Fracture Mechanics Analysis of the Texture of Fried Potato Crust, Journal of Food Engineering, Vol. 62, (2004), 417-423.

[149] Vincent J.F.V, Saunders D.E.J., Beyts P., The use of the Critical Stress Intensity Factor to Quantify ‘Hardness’ and ‘Crunchiness’ objectively, Journal of Texture Studies, Vol. 33 (2002), 149–159.

[150] Vincent J.F.V., The Quantification of Crispness, Journal Science Food Agriculture, Vol. 78, (1998), 162–168.

[151] Vincent J.F.V., Application of Fracture Mechanics to the Texture of Food, Journal Science Food Agriculture, Vol. 78, (1998), 162–168.

[152] Mancini M., Moresi M., Rancini R., Mechanical Properties of Alginate Gels: Emperical Characterisation, Journal of Food Engineering, Vol. 39, (1999), 369-378.

[153] Tang J., Tung M.A., Lelievre J., Zeng Y., Stress-Strain Relationships for Gellan Gels in Tension, Compression and Torsion, Journal of Food Engineering, Vol. 31, (1997), 511-529.

[154] Liu CC., Tellez-Garay A.M., Castell-Perez M.E., Physical and Mechanical Properties of Peanut Protein Films, Lebensmittel-Wissenschaft Und -Technologie - Food Science And Technology,Vol. 37, I. 7, 731-738.

[155] Sothornvit R., Krochta J.M., Plasticizer Effect on Mechanical Properties of β-lactoglobulin Films, Journal of Food Engineering, Vol. 50, (2001), 149-155.

[156] Jagannath J.H., Nadanasabapathi S., Bawa A.S., Effect of Starch on Thermal, Mechanical, and Barrier Properties of Low Density Polyethylene Film, Journal of Applied Polymer Science, Vol. 99, (2006), 3355-3364.

[157] Caner C., Hernandez R.J., Pascall M.A., Riemer J., The Use of Mechanical Analyses, Scanning Electron Microscopy and Ultrasonic Imaging to Study the Effects of High-Pressure Processing on Multilayer Films, Journal of the Science of Food and Agriculture, Vol. 83, (2003), 1095-1103.

[158] Ettelaie R., Computer Simulation and Modelling of Food Colloids, Current Opinion in Colloid and Interface Science, Vol. 8, (2003), 415-421

[159] Boakye K., Mittal G.S., Changes in Textural Properties of Beef Longissimus Dorsi Muscle During Aging, Lebensmittel-Wissenschaft Und -Technologie - Food Science And Technology, Vol. 26, (1993), 145-150.

[160] Awonorin S.O., Rheological and Mechanical Properties, B-Vitamin Retention and Sensory Characteristics of Smoked Sausage Made from Mixtures of Broiler Chicken and Guinea fowl, Lebensmittel-Wissenschaft Und -Technologie - Food Science And Technology, Vol. 26, (1993), 291-300.

[161] Awonorin S.O., Quality of smoked chicken-Guinea fowl sausage as affected by processing conditions and cold storage, Lebensmittel-Wissenschaft Und -Technologie - Food Science And Technology, Vol. 26, (1993), 285-290.

[162] Tocci A.M., Mascheroni R.H., Characterisations of Differential Scanning Calorimetry Determinations of Thermophysical Properties of Meats, Lebensmittel-Wissenschaft Und - Technologie - Food Science And Technology, Vol. 31, (1998), 418-426.

[163] Tocci A.M., Flores E.S.E., Mascheroni R.H., Enthalpy, Heat Capacity and thermal conductivity of bone less mutton between -40 and +40 C, Lebensmittel-Wissenschaft Und - Technologie - Food Science And Technology, Vol. 30, (1997), 184-191.

[164] Scanlon M.G., Lamb J., Fracture Mechanisms and Particle shape formation during size reduction of a model food material, Journal of Materials Science, Vol. 30, (1995), 2577-2583.

[165] Scanlon M.G., Lamb J., A viscoelastic material for fracture studies of food materials, Journal of Materials Science Letters, Vol. 4, (1985), 1296-1297.

[166] Langley K.R., Martin A., Ogin S.L., The Effect of Filler Volume Fraction on The fracture toughness of a model food composite, Composites Science and Technology, Vol. 50, (1994), 259-264.

[167] Pham Q.T., Bail A.L., Hayert M., Tremeac B., Stresses and Cracking in Freezing Spherical Foods: A Numerical Model, Journal of Food Engineering, Vol. 71, (2005), 408-418.

[168] Watanabe H., Tang C.Q., Mihori T., Fracture Stress of Frozen Food Analysed by a Two-Component Model Consisting of Pure Water Ice and Concentrated Amorphous Solution, Journal of Food Engineering, Vol. 24, (1995), 113-122.

[169] Jha S.N., Kingsly A.R.P., Chopra S., Physical and Mechanical Properties of Mango During Growth and Storage for Determination of Maturity, Journal of Food Engineering, Vol. 72, (2006), 73-76

[170] Chiralt A., Martinez-Navarrete N., Martinez-Monzo J., Talens P., Moraga G., Ayala A., Fito P., Changes in Mechanical Properties Throughout Osmotic Processes Cryoprotectant effect, Journal of Food Engineering, Vol. 49, (2001), 129-135.

[171] Lewicki P.P., Jakubczyk E., Effect of Hot Air Temperature on Mechanical Properties of Dried Apples, Journal of Food Engineering, Vol. 64, (2004), 307-314.

[172] Pepi M., Aliya D., Food for Thought, Practical Failure Analysis, Vol. 3, No. 6, (2003), 6-9.

[173] Schantz B., Linke L., Rohm H., Effects of Different Emulsifiers on Rheological and Physical Properties of Chocolate, 3rd International Symposium on Food Rheology and Structure, 329-333

[174] Brunello N., McGauley S.E., Marangoni A., Mechanical properties of cocoa butter in relation to its crystallization behaviour and microstructure, Lebensmittel-Wissenschaft Und - Technologie - Food Science And Technology, Vol. 36, (2003), 525-532.

[175] Kachru R.P., Kotwaliwale N., Balasubramanian D., Physical and Mechanical Properties of Green Banana (Musa Paradisiaca) Fruit, Journal of Food Engineering, Vol. 26, (1995), 369-378.

[176] Bahnasawy A.H., El-Haddad Z.A., El-Ansary M.Y., Sorour H.M., Physical and Mechanical Properties of Some Egyptian Onion Cultivars, Journal of Food Engineering, Vol. 62, (2004), 255-261.

[177] Paoletti F., Moneta E., Bertone A., Sinesio F., Mechanical Properties and Sensory Evaluation of Selected Apple Cultivars, Lebensmittel-Wissenschaft Und -Technologie - Food Science And Technology, Vol. 26, (1993), 264-270.

[178] Toole G.A., Parker M.L., Smith A.C., Waldron K.W., Mechanical Properties of Lettuce, Journal of Materials Science, Vol. 35, (2000), 3553-3559.

[179] Hayakawa K., Akiyama T., Tensile Fracture Stress of a Pasta Product at Temperatures From 293 to 343K, Lebensmittel-Wissenschaft Und -Technologie - Food Science And Technology, Vol. 27, (1994), 93-94.

[180] Cuq B., Goncalves F., Mas J.F., Vareille L., Abecassis J., Effects of Moisture Content and Temperature of Spaghetti on their Mechanical Properties, Journal of Food Engineering, Vol. 59, (2003), 51-60.

[181] Zhang J., Datta A.K., Mukherjee S., Transport Processes and Large Deformation During Baking of Bread, Bioengineering, Food, and Natural Products, Vol.51, No. 9, (2005), 2569-2580.

[182] Matuda T.G., Parra D.F., Lugao A.B., Tadini C.C., Influence of Vegetable Shortening and Emulsifiers on the Unfrozen Water Content and Textural Properties of Frozen French Bread Dough, Lebensmittel-Wissenschaft Und -Technologie - Food Science And Technology, Vol. 38, No. 3, (2005), 275-280.

[183] Williams J.G., Charalambides M.N., Wanigasooriya L, Chakrabarti S., Biaxial Deformation of Dough Using the Bubble Inflation Technique, Rheologica Acta, Vol. 41, (2002), 532-540.

[184] Charalambides M.N., Food Research at Mechanical Engineering Department Imperial Collage London, Food Engineering Newsletter, (2005), 1-3.

[185] Charalambides M.N., Goh S.M., Wanigasooriya L, Williams J.G., Effect of Friction on Uniaxial Compression of Bread Dough, Journal of Materials Science, Vol. 40, (2005), 3375-3381.

[186] Clubbs E.A., Vittadini E., Shellhammer T.H., Vodovotz Y., Changes in the Mechanical Properties of Corn Tortillas Due to the Addition of Glycerol and Salt and Selective High

Pressure Treatments, Innovative Food Science and Emerging Technologies, Vol. 6, (2005), 304-309.

[187] Maache-Rezzoug Z., Bouvier J.M., Alaf K., Patras C., Effect of Principal Ingredients on Rheological Behaviour of Biscuit Dough and on Quality of Biscuits, Journal of Food Engineering, Vol. 35, (1998), 23-42.

[188] Saleem Q., Wildman R.D., Huntley J.M., Whitworth M.B., Material Properties of Semi-Sweet Biscuits for Finite Element Modelling of Biscuit Cracking, Journal of Food Engineering, Vol. 68, (2005), 19-32.

[189] Kim M.H., Okos M.R., Some Physical, Mechanical and Transport Properties of Crackers Related to the Checking Phenomenon, Journal of Food Engineering, Vol. 40, (1999), 189-198.

[190] Gormley T.R., Fracture Testing of Cream Cracker Biscuits, Journal of Food Engineering, Vol. 6, (1987), 325-332.

[191] Foegeding E.A., Brown J, Drake MA, Daubert C.R., Sensory and Mechanical aspects of cheese texture, International Dairy Journal, Vol. 13, (2003), 585-591.

[192] Buchin S., Martin B., Dupont D., Bornard A., Achilleos C., Influence of the Composition of Alpine Highland Pasture on the Chemical, Rheological and Sensory Properties of Cheese, Journal of Dairy Research, Vol. 66, (1999), 579-588.

[193] Williams J.G., Charalambides M.M., Goh S.M, Mechanical properties and sensory texture assessment of cheese, Journal of Texture Studies, Vol. 34, (2003), 181-201.

[194] Luginbuhl W., The Effect of Stress Correction on Fracture Point Coordinates in Uniaxial Compression Tests of Cheese, Lebensmittel-Wissenschaft Und -Technologie - Food Science And Technology, Vol. 29, (1996), 433-437.

[195] Williams J.G., Charalambides M.M., Goh S.M, Lim S.L., The Analysis of the Frictional Effect on Stress-strain Data from Uniaxial Compression of Cheese, Journal of Materials Science, Vol. 36, (2001), 2313-2321.

[196] Ak M.M., Gunasekaran, Stress-Strain Curve Analysis of Cheddar Cheese Under Uniaxial Compression, Journal of Food Science, Vol. 57, No. 5, (1992), 1078-1081.

[197] Fife R.L., McMahon D.J., Oberg C.J., Test for Measuring the Stretchability of Melted Cheese, Journal of Dairy Science, Vol. 85, (2002), 3539-3545.

[198] Goh S., Charalambides M.N., Williams J.G., Characterisation of Non-Linear Viscoelastic Foods by the Indentation Technique, Rheologica Acta, Vol. 44, No. 1, (2004), 47-54.

[199] Williams J.G., Charalambides M.M., A Study on the Influence of Aging on the Mechanical Properties of Cheddar Cheese, Journal of Materials Science, Vol. 30, (1995), 3959-3967.

[200] Goh S., Charalambides M.N., Williams J.G., Fracture Mechanics of Food Products, 2nd International Symposium on Food Rheology and Structure, (2000), 259-263.

[201] Goh S.M., Charalambides M.N., Williams J.G., Determination of the Constitutive Constants of Non-linear Viscoelastic Materials, Mechanics of Time Dependent Materials, Vol. 8, (2004), 255-268.

[202] Williams J.G., Charalambides M.M., Goh S.M, Large Strain Time Dependent Behaviour of Cheese, Journal of Rheology, Vol. 47, No. 3, (2003), 701-716.

[203] Goh S.M., Charalambides M.N., Williams J.G., On the Mechanics of Wire Cutting of Cheese, Engineering Fracture Mechanics, Vol. 72, (2005) 931-946.

[204] Goh S.M., Charalambides M.N., Williams J.G., Rheological Characterisation of Cheese, 3rd International Symposium on Food Rheology and Structure, (2003), 267-271.

[205] Kamyab I., Chakrabarti S., Williams J.G., Cutting Cheese With Wire, Journal of Materials Science, Vol. 33, (1998), 2763-2770.

[206] Goh,S.M., Charalambides, M.N., Williams, J.G., Experimental and Numerical Investigation of the Wire Cutting of Cheese, 9th International Congress on Engineering and Food, Montpellier, France, 7 - 11 March 2004, 2004, Pages: 228 – 233.

[207] Atkins A.G., Xu X, Jeronimidis G., Cutting by 'Pressing and Slicing' of Thin Floppy Slices of Materials Illustrated by Experiments on Cheddar Cheese and Salami, Journal of Materials Science, Vol. 39, (2004), 2761-2766.

[208] Lei, S., Shin, Y.C., Incropera, F.P., Thermo-mechanical modelling of orthogonal machining process by finite element analysis, International Journal of Machine Tools and Manufacture 39 (1999) 731-750

[209] Ohbuchi, Y., Obikawa, T., Finite Element Modelling of Chip Formation in the Domain of Negative Rake Angle Cutting, Journal of Engineering Materials Technology Vol. 125 (2003) 324-332

[210] Ceretti, E., Lucchi, M., Altan, T., FEM Simulation of Orthogonal Cutting: Serrated Chip Formation, Journal of Materials Processing Technology 95 (1999) 17-26

[211] Giorleo, G., Teti, R., Prisco, U., D'addona, D., Merging Neural Network Material Rheological Behaviour Modelling with FEM Simulation of Orthogonal Metal Cutting, Machining Science and Technology, Vol. 7 No. 3 (2003) 401-417

[212] Mitrofanov, A.V., Babitski, V.I., Silberschmidt, V.V., Finite Element Analysis of Ultrasonically Assisted Turning of Inconel 718, Journal of Materials Processing Technology 153-154 (2004) 233-239

[213] Sasahara, H., Obikawa, T., Shirakashi, T., FEM Analysis of Cutting Sequence Effect on Mechanical Characteristics in Machined Layer, Journal of Materials Processing Technology 62 (1996) 448-453

[214] Yen, Y.C., Sohner, J., Weule, H., Schmidt, J., Altan, T., Estimation of Tool Wear of Carbide Tool in Orthogonal Cutting Using FEM Simulation, Machining Science and Technology Vol. 6 No. 3 (2002) 467-486

[215] Lin, Z.C., Lin, Y.Y., Three-dimensional elastic-plastic finite element analysis for orthogonal cutting with discontinuous chip of 6-4 brass, Theoretical and applied Fracture mechanics 35 (2001) 137-153

[216] Flocke, F., Raedt, H.W., Hoppe, S., 2D-FEM Simulation of the Orthogonal High Speed Cutting Process, Machining Science and Technology, 5 No.3 (2001) 323-340

[217] Ahmed N., Mitrofanov, A.V., Babitski, V.I., Silberschmidt, V.V., Analysis of Material Response to Ultrasonic Vibration Loading in Turning Inconel 718, Materials Science and Engineering A 424 (2006) 318-325

[218] Li Z.C., Liang-Wu Cai, Pei Z.J., Treadwell C., Edge-chipping Reduction in Rotary Ultrasonic Machining of Ceramics: Finite Element Analysis and Experimenatal Verification, International Journal of Machine Tools and Manufacture 46 (2006) 1469-1477

[219] Maudlin P.J., Stout M.G., Metal Cutting Simulation of 4340 Steel Using an Accurate Mechanical Description of Metal Strength and Fracture, Materials Issues in Machining III (1996) 29-41

[220] Sandstrom D.R., Hodowany J.N., Modelling The Physics of Metal Cutting in High speed Machining, Machining Science and Technology Vol. 2 I2 (1998) 343-353

[221] Marusich T.D., Ortiz M., A Finite Element Study of Chip Formation in High Speed Machining, Manufacturing Science and Engineering ASME Vol. 3-1 (1995) 245-257

[222] Lin Z.C., Lin Y.Y., Elastic-Plastic Finite Element Analysis for Oblique Cutting with a Discontinuous Chip of 6-4 Brass, Journal of Strain Analysis Vol. 36 No.6 (2001) 579-594

[223] Shirakashi T., Obikawa T., Recent Progress and Some Difficulties in Computational Modelling of Machining, Machining Science and Technology Vol.2 I.2 (1998) 277-301

[224] Obikawa T., Sasahara H., Shirakashi T., Usui E., Application of Computational Machining Method to Discontinuous Chip Formation, Journal of Manufacturing Science and Engineering Vol. 119 (1997) 667-674

[225] Obikawa T., Usui E., Computational Machining of Titanium Alloy-Finite Element Modelling and a Few Results Transactions of the ASME Vol.118 (1996) 208-215

[226] Camacho G., Marusich T., Ortiz M., Adaptive Meshing Methods for the Analysis of Unconstrained Plastic Flow, Advanced Computational Methods for Material Modelling ASME 1993 Vol. 180 71-83

[227] Jiao Y., Liu W.J., Pei Z.J., Xin X.J., Treadwell C., Study on Edge Chipping in rotary Ultrasonic Machining of Ceramics: An Integration of Designed Experiments and Finite Element Analysis Transactions of the ASME Vol. 127 (2005) 752-758

[228] Flocke F., Raedt H.W., Hoppe S., 2D-FEM Simulation of the Orthogonal High Speed Cutting Process, Machining Science and Technology Vol.5 I.3 (2001) 323-340

[229] Lin Z.C., Lin Y.Y., Elastic-Plastic Finite Element Analysis for Orthogonal Cutting with a Discontinuous Chip of 6-4 Brass, Theoretical and Applied Fracture Mechanics Vol. 35 (2001) 137-153

[230] Yen Y.C., Sohner J., Weule H., Schmidt J., Altan T., Estimation of Tool Wear of Carbide Tool in Orthogonal Cutting Using FEM Simulation, Machining Science and Technology Vol.6 No.3 (2002) 467-486

[231] Sasahara H., Obikawa T., Shirakashi T., FEM Analysis of Cutting Sequence Effect on Mechanical Characteristics in Machined Layer, Journal of Materials Processing Technology Vol. 62 (1996) 448-453

[232] Lin. J., Lee. S.L., Weng. C.I., Estimation of Cutting Temperature in high Speed Machining, Journal of Engineering Materials Technology Vol. 114 (1992) 289-295

[233] Tay O.A., Stevenson M.G., de Vahl Davis G., Using the Finite Element Method to Determine Temperature Distribution in Orthogonal Machining, Proceedings of IMechE Vol. 188 (1974) 627-638

[234] Tay O.A., Stevenson M.G., de Vahl Davis G., Oxley P.L., A Numerical Method for Calculating Temperature Distributions in Machining from Force and Shear Angle Measurements, International Journal of Machine Tool Design Vol. 16 (1976) 335-349

[235] Strenkowski J.S., Carroll J.T., A Finite Element Model of Orthogonal Metal Cutting, Journal of Engineering Industry Vol. 107 (1985) 349-354

[236] Konvopoulos K., Erpenbeck S.A., Finite Element Modelling of Orthogonal Metal Cutting, Journal of Engineering Industry Vol. 113 (1991) 253-267

[237] Vasilash G.S., Cutting Tools, Production Engineering Magazine (1992) 40-44

[238] Sehkon G.S., Chenot J.L., Numerical Simulation of Continuous Chip Formation During Non-Steady Orthogonal Cutting, Engineering Computations Vol. 10 (1993) 31-48

[239] Shinozuka J., Obikawa T., Shirakashi T., Chip Breaking Process Simulation by Thermo-Elastic Plastic Finite Element Method, Journal of Japan Society for Precision Engineering Vol. 62 I.8 (1996) 1161-1166

[240] Sasahara H., Obikawa T., FEM Simulation on Cutting process of Two phase alloys, Journal of Japan Society for Precision Engineering Vol. 64 I.7 (1998) 1083-1087

[241] Baker M., Rosler J., Siemers C., A Finite Element model of High Speed Metal Cutting with Adiabatic Shearing, Computers and Structures Vol. 80 (2002) 495-513

[242] Smith A., Nurse A., Graham G., Lucas M., Ultrasonic Cutting a Fracture Mechanics Model, Ultrasonics Vol. 34 (1996) 197-203

[243] Smith L., Lucas M., Fracture Model of Ultrasonically Assisted Osteotomy, 9th International Congress in Experimental Mechanics (2000) 571

[244] Astashev V.K., Babitsky V.I., Ultrasonic Cutting as a Nonlinear (Vibro-Impact) Process, Ultrasonics Vol. 36 (1998) 89-96

[245] Mitrofanov A.V., Babitsky V.I., Silberschmidt V.V., Finite Element Simulations of Ultrasonically Assisted Turning, Computational Materials Science Vol. 28 (2003) 645-653

[246] Babitsky V.I., Kalashnikov A.N., Molodtsov F.V., Autoresonant Control of Ultrasonically Assisted Cutting, Mechatronics Vol. 14 (2004) 91-114

[247] Babitsky V.I., Kalashnikov A.N., Meadows A., Wijesundara A. A. H. P. ,Ultrasonically Assisted Turning of Aviation Materials, Journal of Materials Processing Technology Vol. 132 (2003) 157-167

[248] Babitsky V.I., Mitrofanov A.V., Silberschmidt V.V Ultrasonically Assisted Turning of Aviation Materials, Simulations and Experimental Study, Ultrasonics Vol. 42 (2004) 81-86

[249] Mitrofanov A.V., Babitsky V.I., Silberschmidt V.V., Thermomechanical Finite Element Simulation of Ultrasonically Assisted Turning, Computational Materials Science Vol. 32 (2005) 463-471

[250] McCarthy, C T; Hussey, M; Gilchrist, M D, An Investigation into Scalpel Blade Sharpness using Cutting Experiments and Finite Element Analysis**,** Key Engineering Materials. Vol. 293-294, (2005) 769-776.

[251] Ahmed N., Mitrofanov A.V., Babitsky V.I., Silberschmidt V.V., 3D Finite Element Analysis of Ultrasonically Assisted Turning, Computational Materials Science Vol. 39 (2007) 149-154

[252] ABAQUS User's Manual Version 6.6.2, Hibbitt, Karlsson & Sorensen, Inc. (2006)

[253] ANSYS Hyperelasticity lecture notes, unknown.

[254] Marlow R.S., A General First Invariant Hyperelastic Constitutive Model, Constitutive Models for Rubber III, edited by Busfield and Muhr, (2003), 157-160

[255] Anderson T.L., Fracture Mechanics Fundamentals and Applications, Ewalds H.L., Wanhill R.J.H.

[256] http://www.matweb.com/Matweb; 26/4/07

[257] Littmann W., Storck H., Wallascheck J., Sliding Friction in the Presence of Ultrasonic Oscillations: Superposition of Longitudinal Oscillations, Archive of Applied Mechanics, Vol. 71, (2001), 549

[258] Ewins D.J., Modal Testing Theory, Practice and Application Second Edition, Research Studies Press LTD, (2000)

[259] Avitabile P., Experimental Modal Analysis – A Simple Non-Mathematical Overview, Sound and Vibration Magazine, Jan (2001)

[260] Avitabile P., Modal Space – Back to Basis, Experimental Techniques SEM, Feb (1998) to Aug (2006)

[261] Beer F.P., Johnston E.R., Mechanics of Materials Second Edition, McGraw-Hill (1992)

[262] Griffith A.A., The Phenomena of Rupture and Flow in Solids, Philosophical Transactions, Series A, Vol. 221, (1920), 163-198

[263] Inglis C.E., Stresses in a Plate due to the Presence of Cracks and Sharp Corners, Transactions of the Institute of Navel Architects, Vol. 55, (1913), 219-241

[264] Irwin G.R., Fracture Dynamics, Fracturing of Metals, American Society for Metals, Cleveland, (1948), 147-166

[265] Orowan E., Fracture and Strength of Solids, Reports on Progress in Physics, Vol.12, (1948), 185

[266] Westergaard H.M., Bearing Pressures and Cracks, Journal of Applied Mechanics, Vol. 6, (1939), 49-53

[267] Irwin G.R., Analyses of Stresses and Strains near the End of a Crack Traversing a Plate, Journal of Applied Mechanics, Vol. 24, (1957), 361-364

[268] Williams M.L., On the Stress Distribution at the Base of a Stationary Crack, Journal of Applied Mechanics, Vol.24, (1957) 109-114

[269] Markov A.I., Kinematics of the Dimensional Ultrasonic Machining Method, Machines and Tooling, Vol. 30 I. 10, (1959), 28-31

[270] Rozenberg L.D., Kazantsev V.F., Ultrasonic Cutting, Consultants Bureau, New York, (1964)

[271] Kainth G.S., Nandy, Amitav and Singh, Kuldeep, On the Mechanics of Material Removal in Ultrasonic Machining, International Journal MTDR, Vol. 19, (1979), 33-41

[272] Kops L., Investigation into the Influence of the Wear of the Abrasive Powder on the Technological Indices of Ultrasonic Machining, CIRP Annal, Vol. 12, I.3, (1964), 151-157

[273] Kazantsev V.F., The Relationship between Output and Machining Conditions in Ultrasonic Machining, Machines and Tooling, Vol. 34, (1963), 14-17

[274] Pentland E.W., Ektermanis J.A., Improving Ultrasonic Machining Rates – Some Feasability Studies, J. Engg for India, Transcripts of the ASME, Vol. 87B, (1965), 39-46

[275] Goetze D., Effect of Vibration Amplitude, Frequency and Composition of the Abrasive Slurry on the Rate of Ultrasonic Machining in Ketos Tool Steel, The Journal of The Acoustic Society of America, Vol. 28, I.6, (1956), 1033-1037

[276] Komariah M., Reddy P., Narashima, Rotary Ultrasonic Machining – A New Cutting Process and its Performance, International Journal Production, Vol. 29, I. 11, (1991), 2177-2187.

[277] Prabhakar D., Haselkorn M., An Experimental Investigation of Material Removal Rates in Rotary Ultrasonic Machining, Transcripts of NAMRI/SME, Vol. 20, (1992), 211-218

[278] Venkatesh V.C., Machining of Glass by Impact Processes, Journal of Mechanical Working Technology, Vol. 8, (1983), 247-260

[279] Adithan M., Tool Wear Studies in Ultrasonic Drilling, Wear, Vol. 29, (1974), 81-93

[280] Clouser H.A., New Techniques for Electrode Forming, Research and Technological Devices in non-traditional Machining Presented at the Winter Annual Meeting of the ASME, (1988), 75-88

[281] Kennedy D.C., Grieve R.J., Ultrasonic Machining –A Review, The Production Engineer, Vol. 54, I. 9, (1975), 481-486

[282] Koval'chenko M.S., Paustovskii A.V., Perevyazko V.A., Influence of Properties of Abrasive Materials on the Effectiveness of Ultrasonic Machining of Ceramics, Soviet Powder Metallurgy and Metal Ceramics, Vol. 25, I. 7, (1986), 560-562

[283] Shaw M.C., Ultrasonic Grinding, Microtechnic, Vol. 10, I.6, (1956), 257-265

[284] Kremer D., Bazine G., Moison A., Ultrasonic Machining Improves EDM Technology, Electromachining, Proceedings of the 7th International Symposium, Edited by Professor Crookall, Birmingham UK, (1983), 67-76

[285] Hartmann J., Construction, Performance and Design of the Acoustic Air Generator, Journal of Scientific Instruments, Vol. 16, (1939), 140-149

[286] Allen C.H., Rudnick I., A Powerful High Frequency Siren, Journal of Acoustic Society of America, Vol. 19, (1947), 857-865

[287] Thomson W.T., The Theory of Vibration with Applications fourth Edition, Prentice Hall (1993)

[288] http://www.sv.vt.edu/classes/MSE2094_NoteBook/97ClassProj/num/widas/history.html, 15/3/05

[289] Measurement solutions made possible by Laser Vibrometry, Polytec LM INFO Special, Issue 1/2003, Poltec Gmbh. D-Waldronn

Appendix II: Publications

[1] LUCAS, M., MCCULLOCH, E., MACBEATH, A., CARDONI, A. A finite element model for ultrasonic cutting, World Congress on Ultrasonics, Beijing (China), September 2005, (invited paper).

[2] LUCAS, M., MCCULLOCH, E., MACBEATH, A., CARDONI, A. A finite element model for ultrasonic cutting, Ultrasonics, Vol. 44/1, pp 503-509, 2006, doi: 10.1016/j.ultras.2006.05.115

[3] MCCULLOCH, E., MACBEATH, A., LUCAS, M. A finite element model for ultrasonic cutting of toffee, Proc. Modern Practice in Stress and Vibration Analysis, Applied Mechanics and Materials, Vol. 5-6, pp 519-526, 2006.

[4] MACBEATH, A., MCCULLOCH, E., LUCAS, M. Optimising ultrasonic cutting of multi-layered materials, International Congress on Ultrasonics, Vienna (Austria), April 2007.

[5] MCCULLOCH, E. Simulating ultrasonic cutting using finite element models, Proc. 36th Ultrasonic Industry Association (UIA) Annual Symposium, Graduate Paper Competition Winner, London (UK), 2007.